THE QUANTUM MONTE CARLO METHOD: APPLICATION TO PROBLEMS IN STATISTICAL PHYSICS

by

David Frederick Coker

A thesis submitted to the
Australian National University
for the degree of Doctor of Philosophy

July 1985

STATEMENT

Except where acknowledgements are made in the text, all the material contained in this thesis is the work of the candidate.

D.F. Coker

ACKNOWLEDGEMENTS

I would like to thank my supervisor, Dr R.O. Watts, for his help and encouragement. His unbounded scientific curiosity has been a great inspiration for me.

I am indebted to Dr R.W. Crompton for allowing me to work in the Electron and Ion Diffusion Unit and I greatly appreciate the support and assistance of the members of the unit.

I have greatly benefited from many informative discussions with Dr A. Ding, Dr D.J. Evans, Dr R.E. Miller and Dr J.R. Reimers. My fellow PhD students; Mr C.V. Boughton, Mr G. Bryant, Dr R.A. Cassidy, Mr H.J. Gardner, Mr I. Morey, Mr M.J. Norman, Dr Z.Lj. Petrovic, Mr R.K. Porteous and Mr P.F. Vohralik also deserve many thanks for putting up with my "ravings" over the years.

I wish to thank Professor J.H. Carver for giving me the opportunity to travel to West Germany and Dr J. Schaefer who made it possible for me to visit the Max Planck Institute for Physics and Astrophysics and to use their CRAY I computer. I am also grateful to CSIRONET for their generous grant of CYBER 205 time.

Special thanks must also go to the operators, programmers and other members of staff of the A.N.U. Computer Services Centre who have provided an exceptional computing service.

I greatly appreciate the detailed comments and criticisms of the early drafts of this thesis which were made by Dr K.G.H. Baldwin and Dr R.O. Watts.

I gratefully acknowledge the financial assistance of a Commonwealth Postgraduate Award.

Finally I must thank my parents and family for their tremendous support and especially my wife Traudel, for her patience whilst typing this "Never Ending Story".

ABSTRACT

The diffusion Monte Carlo method for performing quantum calculations on many body systems is extended and applied to a number of areas of chemical physics. An ab initio quantum Monte Carlo procedure for simulating wave functions with nodal surfaces is presented. Some few Fermion problems are treated using this technique.

A method for using the ground state wave function obtained from a diffusion Monte Carlo calculation to determine the vibrational spectrum of a molecular cluster is presented. Very accurate vibrational spectra can be obtained with this approach. Results of quantum Monte Carlo calculations on the water dimer and trimer using an improved intramolecular potential and the intermolecular potential of Reimers, Watts and Klein (1981) have been used to assign cluster spectra obtained from molecular beam experiments. It is demonstrated that the vibrational predissociation spectrum of a molecular cluster is sensitive to the details of the intermolecular potential and different surfaces may be tested by comparing calculated spectra with experimental results.

The diffusion Monte Carlo method is applied to calculate the thermodynamic and structural properties of liquid ^{4}He and solid molecular hydrogen. Importance sampling must be used if efficient bulk phase calculations are to be performed. When the spherical part of the interaction potential due to Buck et al. (1983) is used in diffusion Monte Carlo calculations on solid H_2 good agreement with experiment is found. Anisotropy may be important for this system at higher densities.

Methods for using the diffusion Monte Carlo method to study the behaviour of systems at non-zero temperatures are developed. Improved high temperature approximations must be employed as initial conditions when systems with mixed "classical" and "quantum" degrees of freedom are considered. The properties of neon gas and the water dimer are studied with this method.

The work presented in Chapter 3 has been published in

"The Infrared Predissociation Spectra of Water Clusters" by D.F. Coker, R.E. Miller and R.O. Watts (1984), J. Chem. Phys 82, 3554.

CONTENTS

FIGURE CAPTIONS

6.2 (a) Solid curves give the position distributions for a harmonic oscillator obtained at different temperatures along the random walk trajectory (T_{in} = 1000°K). Points are exact results obtained from equation (6.3). (b) Solid curves are the momentum distributions calculated at the same points along the trajectory. Crosses are the predictions of classical theory. PAGE 159a

6.3 Upper solid curve gives the temperature dependence of the total energy of the O-H Morse oscillator obtained by summing over the analytic bound states. Lower solid and long dashed lines are respectively the potential and kinetic energies of the oscillator. Short dashed curves are classical results. Various coloured symbols are the results of quantum Monte Carlo calculations using different initial temperatures. Classical initial distributions were used.

Colour	T_{in}(°K)
black	10000
red	7500
blue	5000

PAGE 160a

6.4 Comparison of analytic results for the harmonic oscillator with values obtained from a quantum simulation using the exact position and momentum distributions at 100°K as the initial condition.

PAGE 162a

6.5 Same as Figure 6.3 except the improved high temperature approximation in Equation (6.9) is used to give the initial distributions. PAGE 165a

CHAPTER 1 AN OVERVIEW OF QUANTUM SIMULATION

Classical computer simulation methods have been used extensively to study both equilibrium and non-equilibrium behaviour of many body systems. The physical behaviour of a assembly of particles, however, is determined by quantum theory. Recently, a variety of quantum simulations methods have been developed and applied to studies of many body systems in which quantum effects are important. The algorithms can be divided into two categories: zero temperature methods for considering the individual quantum states of many body systems and non-zero temperature procedures in which a thermal distribution of quantum states is important. In this thesis we explore a stochastic numerical method which is useful for performing both zero and finite temperature calculations.

At zero temperature, quantum Monte Carlo methods have been used to study bulk systems such as the crystal and liquid phases of helium (Whitlock *et al.* (1979), (1980); Lee *et al.* (1981)), the electron gas (Ceperley and Alder (1980)), metallic hydrogen (Ceperley and Alder (1981)) and a variety of other important systems (Ceperley and Kalos (1979)). The zero temperature quantum Monte Carlo methods have also been extended to the realm of molecular quantum mechanics where they are now becoming competitive in both speed and accuracy with the more conventional CI techniques (Ceperley and Alder(1984)). Quantum Monte Carlo methods provide numerically exact solutions of the many body Schrödinger equation. The results are not dependent on the choice of a basis set and so the answers are not influenced by the input of "chemical intuiton". In principle the quantum Monte Carlo methods can provide completely *ab initio* results (Öksüz

(1984)).

The basic "diffusion Monte Carlo" method which was first presented by Anderson (1975) and which is used throughout this thesis is developed and studied in detail in Chapter 2. The method involves using a "finite time step" approximation to solve a multidimensional diffusion equation. Results obtained using this approximation depend on the step size and in the limit as $\Delta\tau \to 0$ exact values are obtained.

Diffusion Monte Carlo methods have been used mainly in studying electronic systems where the particle interactions vary relatively slowly with distance. Thus the finite time step approximation is expected to be valid. The most significant problem in using quantum Monte Carlo methods to study electronic systems is the treatment of identical particle statistics (Kalos (1984)). In most of the electronic applications of the zero temperature quantum Monte Carlo methods, approximate information about nodal surfaces in the Fermion wave function is used to provide boundary conditions for the random walks. Wave functions obtained from variational calculations are often used for this purpose. With the fixed node approximate methods (Reynolds et al. (1982)) the random walk results are dependent on the nodal surfaces used in the calculation. Methods for "relaxing" the nodes have been developed (Ceperley and Alder (1984)) and essentially exact solutions which are antisymmetric with respect to particle inerchange may be obtained.

In Chapter 2 we present an alternative procedure which does not require any prior knowledge of the nodal surfaces. Results of ab initio random walk calculations performed on the ground and excited states of small electronic systems using this approach are presented.

Identical particle statistics are not important in the ground state of

an assembly of Bosons so exact quantum Monte Carlo calculations can be performed using Boltzmann statistics. This simplification is exploited in Chapters 3 and 4 where we discuss the application of zero temperature quantum Monte Carlo methods to the study of the ground state properties of molecular clusters and Boson solids and liquids.

Recently there has been a great deal of interest both theoretically and experimentally in the study of clusters of atoms and molecules. With molecular beam techniques, well defined clusters can be prepared in a collision free enviroment. The internal degrees of freedom of clusters produced by these methods are strongly "cooled" so experimental results can be compared with ground state calculations. In Chapter 3 we describe the result of some ground state quantum Monte Carlo calculations performed on small clusters of water molecules. A method for studying the intramolecular vibrations of molecules in clusters using the wave function obtained from a ground state quantum Monte Carlo calculation is presented. Calculated vibrational spectra are compared with molecular beam results. The input to these calculations is a potential surface and we demonstrate that comparing the vibrational spectra obtained from ground state quantum Monte Carlo calculations with the results of molecular beam experiments provides a sensitive test for the potential surface.

Comparison of bulk phase thermodynamic data obtained from classical simulation studies with experimental results provides a further means of testing intermolecular potential surfaces (Barker, Fisher and Watts (1971)). However, when quantum behaviour is important in determining the properties of bulk phase systems quantum simulation methods must be used. Variational calculations on liquid ^{4}He have been performed to test different pair potentials for this system (Murphy and Watts (1970), Murphy

(1972)). These methods provide an upper bound on the energy of the system and hence approximate ground state thermodynamic properties are obtained. Thus comparison with experiment is ambiguous. With the quantum Monte Carlo methods, however, different interaction potentials can be reliably tested (Whitlock et al. (1980)).

In Chapter 4 we consider applying the diffusion Monte Carlo method to study bulk phase quantum systems with strongly repulsive interactions. The basic algorithm is not useful for these studies and improvements in the efficiency and accuracy of the method are necessary. Importance sampling techniques, in which approximate many body wave functions are used to guide the diffusion Monte Carlo procedure to sample the more important regions of configuration space, greatly reduce the statistical fluctuations during the simulation. With these improvements efficient bulk phase quantum calculations can be performed.

The finite time step approximation is expected to be most severe in dense systems with strongly repulsive interactions. By using different time steps in bulk phase calculations the significance of this approximation is considered. At higher densities smaller time steps are used and over the range of step sizes considered in our work, little time step dependence is observed.

We have used the spherical part of a semiempirical intermolecular pair potential due to Buck et al. (1983) in diffusion Monte Carlo calculations on solid H_2. The ground state energies obtained from these calculations are generally about 10% lower than the results of variational calculations and are in closer agreement with experiment. Inadequacies in the variational wave function are highlighted by comparing predicted structural properties with the results of the full quantum simulation.

As mentioned earlier, the quantum Monte Carlo methods provide a general means for solving multidimensional diffusion equations. In the case of the zero temperature methods, stationary solutions of the Schrödinger equation are obtained. Quantum Monte Carlo methods can also be used to give "time" evolving solutions of diffusion equations. The behaviour of a system at non-zero temperatures is governed by the density matrix which evolves as a function of the inverse temperature, $\beta = {}^{1}/k_B T$, according to a diffusion equation known as the Bloch equation. The non-zero temperature quantum Monte Carlo procedure described in Chapter 5 uses the methods employed with the zero temperature techniques to solve the Bloch equation. From the evolution of the solution, information at different temperatures is obtained.

The formulation of the non-zero temperature method presented here is different from the path integral Monte Carlo procedures which have been developed recently but the methods are equivalent. Finite temperature path integral techniques have been used to study a variety of interesting problems. The properties of liquid ^{4}He (Pollock and Ceperley (1984)) and Neon (Thirumalai et al. (1984)) at non-zero temperatures have been explored. Solvation of electrons in fused salts (Parrinello and Rahman (1984)), the physical properties of clusters of Argon atoms (Freeman and Doll (1985)), solvation of H atoms and muonium in classical water (De Raedt et al. (1984)) as well as the calculation of electronic and vibrational spectra of molecules (Thirumalai and Berne (1983), (1984)) are some of the problems which have been explored recently using path integral methods.

The method developed in Chapter 5 uses a classical distribution at some high temperature as the initial condition for the solution of the Bloch equation. A diffusion Monte Carlo procedure is then applied to "propagate"

the distribution through β and the Bloch equation is simulated. This approach provides a means of obtaining results at a number of different temperatures during a single calculation. Information about quantum position and momentum distributions may be obtained using this approach as well as thermodynamic data.

In Chapter 6 the use of the non-zero temperature diffusion Monte Carlo method is demonstrated by considering some representative problems, including the one dimensional Morse and harmonic oscillators, quantum effects in neon gas and finally the quantum behaviour of the water dimer as a function of temperature. More accurate high temperature approximations must be used as the initial condition for the intramolecular vibrations of the cluster but classical results may be employed to give initial conditions for the intermolecular degrees of freedom.

Many classical simulations of systems of water molecules have been performed. It is not obvious that the assumptions of classical mechanics are valid for systems of light molecules which are able to bond strongly to one another. The results presented here complement those of Wallquist and Berne (1985) and we are able to study the onset of quantum behaviour for the intermolecular degrees of freedom of the water dimer as a function of temperature.

CHAPTER 2 BASIC QUANTUM MONTE CARLO, DEVELOPMENT AND SIMPLE APPLICATIONS

Introduction

In this chapter the quantum random walk method is developed and applied to some simple illustrative problems. The methods described are employed in subsequent chapters to study some important many body quantum problems.

Chapter 2 is organised as follows: After a brief description of basic quantum theory we consider the analogy between the Schrödinger equation and a diffusion process modified by chemical reaction. The analogy is used to develop a numerical model of the Schrödinger equation based on a "short time" approximation. The method produces an ensemble distributed according to the wave function and the number of systems in the ensemble decays at a rate proportional to the eigenvalue.

In Section 2.) the question of symmetry and the generation of nodal surfaces in the wave function is considered. A feedback mechanism for maintaining a stable ensemble is discussed. The stabilizing method provides an efficient means for estimating the eigenvalue but it allows only the ground state distribution to be sampled. Next, a procedure for forcing the distribution to remain orthogonal to the ground state is described. With this technique a stable excited state distribution can be sampled. After studying the excited vibrational states of molecular hydrogen we consider extending the approach to many dimensions, using the S and P states of the hydrogen atom as an example.

In Section 3.) we present a method for calculating expectation values

of various operators from a quantum random walk calculation. We also consider importance sampling methods which are used to improve the efficiency of quantum Monte Carlo calculations.

Finally in Section 4.) we consider the question of identical particle statistics. After discussion of some techniques which have been used for treating Fermi systems we consider generalising the method for generating nodal surfaces described in Section 2.) so that an antisymmetric distribution is obtained. With this procedure systems containing a few fermions can be simulated. As examples, different spin states of atomic helium and lithium are modeled.

1.) The Basic Quantum Monte Carlo Algorithm

a) Formal Preliminaries

In quantum mechanics, the behaviour of a system is determined by the wave function $\psi(\underline{r},t)$. For a non-relativistic system, $\psi(\underline{r},t)$ obeys the Schrödinger equation (Merzbacher (1970)) which takes the following form

$$i\hbar\frac{\partial}{\partial t}\psi(\underline{r},t) = \hat{H}\,\psi(\underline{r},t) \qquad (2.1)$$

$$= \sum_{k}^{N} \frac{-\hbar^2}{2m_k}\nabla_k^2\,\psi(\underline{r},t) + \left(V(\underline{r})-V_{ref}\right)\psi(\underline{r},t)$$

Here the $\hat{H}$ is the Hamiltonian operator, the vector $\underline{r}$ describes the position of the N particles in the system and m_k are the particle masses. The function $V(\underline{r})$ gives the interaction energy and the quantity V_{ref} is an arbitrary reference on the energy scale whose introduction will prove useful in later discussion.

There are an infinite number of solutions to equation (2.1). The set of solutions which are products of separate functions of time and space

$$\psi(\underline{r},t) = f(t)\ \phi(\underline{r}) \tag{2.2}$$

are of particular physical importance. Substituting (2.2) into equation (2.1) and separating variables we find that

$$f(t) = e^{\frac{-it}{\hbar}(E-V_{ref})} \tag{2.3}$$

and

$$\sum_{k=1}^{N} \frac{-\hbar^2}{2m_k} \nabla_k^2\ \phi(\underline{r}) + \left(V(\underline{r})-V_{ref}\right)\phi(\underline{r}) = \left(E-V_{ref}\right)\phi(\underline{r}) \tag{2.4}$$

Where $(E-V_{ref})$ is the separation constant.

Equation (2.4), the time independent Schrödinger equation, is an eigenvalue equation

$$\hat{H}\ \phi(\underline{r}) = \left(E-V_{ref}\right)\phi(\underline{r})$$

Since $\hat{H}$ is a hermitian operator its eigenvalues, $(E-V_{ref})$, are real. Thus f(t) is a purely oscillatory function of time.

For particular solutions of the form

$$\psi(\underline{r},t) = e^{-it/\hbar(E-V_{ref})}\phi(\underline{r}) \tag{2.5}$$

the probability density, $\psi^*(\underline{r},t)\psi(\underline{r},t)$, is independent of time. For this reason such solutions are said to represent "stationary states" of the system.

In a stationary state the expectation value of a time independent physical property represented by an operator, A, depends only on the time independent part of the solution and

$$\langle A \rangle = \int \psi^*(\underline{r},t)\, A\psi(\underline{r},t)\, d\underline{r} = \int \phi^*(\underline{r})\, A\phi(\underline{r})\, d\underline{r} \qquad (2.6)$$

General solutions of the Schrödinger equation can be constructed by superposition of particular stationary solutions. Thus, if the time independent Schrödinger equation yields a set of eigenfunctions $\phi_n(\underline{r})$ which are complete in the sense that any initial state, $\psi(\underline{r},0)$, may be expanded in terms of them

$$\psi(\underline{r},0) = \sum_n a_n\, \phi_n(\underline{r}) \qquad (2.7)$$

then the solution for all later times will be of the form

$$\psi(\underline{r},t) = \sum_n a_n e^{-it/\hbar(E_n - V_{ref})}\, \phi_n(\underline{r}) \qquad (2.8)$$

In this chapter we describe a computational method for solving the eigenvalue problem presented in the time independent Schrödinger equation. The procedure involves simulating the time dependent Schrödinger equation by making use of the analogy between (2.1) and an equation which describes a combined diffusion and chemical reaction process. In this section we shall present the basic technique used to obtain ground state properties. The questions of identical particle statistics and wave function symmetry will be considered in later sections.

b) <u>The Diffusion Equation Analogy, a Numerical Model of the Schrödinger Equation</u>

Defining the "imaginary time" variable $\tau = it/\hbar$ enables the wave equation given in (2.1) to be transformed into the following

$$\frac{\partial\psi(\underline{r},\tau)}{\partial\tau} = \sum_k \frac{\hbar^2}{2m_k} \nabla_k^2\psi(\underline{r},\tau) - \left(V(\underline{r}) - V_{ref}\right)\psi(\underline{r},\tau) \qquad (2.9)$$

Equation (2.9) can be considered in terms of two separate processes. The

first term on the right hand side has the form of an equation describing the diffusion of a concentration profile through a fluid. The second term resembles an equation which models exponential growth and decay or a first order chemical rate process. Thus the Schrödinger equation in imaginary time is analogous to an equation describing diffusion which is modified by a chemical reaction whose rate changes with position. In this analogy the wave function is treated as the density of diffusers.

In the absence of the "birth/death" term, the solution of the diffusion part of equation (2.9) with the initial condition

$$\psi(\underline{r},\tau=0) = \delta(\underline{r}-\underline{r}_o)$$

is well known

$$\psi(\underline{r},\tau) = \prod_k^N (4\pi D_k\tau)^{-\frac{1}{2}} e^{-(\underline{r}_k-\underline{r}_{ko})^2/4D_k\tau} \qquad (2.10)$$

Here $\underline{r}_k$ is the position of particle k in three dimensional space and D_k is the diffusion coefficient of the particle and depends on its mass

$$D_k = \hbar^2/2m_k$$

By interpreting the wave function as a density, equation (2.10) is treated as the distribution function for an ensemble of free particle systems moving in imaginary time. The evolution of the ensemble can be modeled on a computer. First a set of systems is established at $\underline{r}_o$. In a time $\Delta\tau$, each particle should sample a three dimensional Gaussian distribution centred on $\underline{r}_{ko}$ with variance $\Delta x_k = (2D_k\Delta\tau)^{\frac{1}{2}}$. The distribution may be sampled numerically by displacing the particles in every system of the ensemble by distances $\Delta x_k\xi$ in each dimension. Here ξ are random variables chosen from a standard normal distribution. If this procedure is repeated many times the

ensemble distribution will spread out as the wave function given in equation (2.10).

A numerical model for simulating the effects of the potential term in equation (2.9) can be devised using the analogy between this term and a phenomenological rate equation. The model involves replicating or removing systems from an ensemble depending on the potential energy.

Ignoring the diffusion term, equation (2.9) gives that the amplitude of the wave function at some point $\underline{r}$ changes in time as follows

$$\frac{d\psi(\underline{r})}{d\tau} = -(V(\underline{r})-V_{ref})\psi(\underline{r})$$

Rearranging and integrating for a finite time, $\Delta\tau$, we have

$$\int_{\psi}^{\psi+\Delta\psi} \frac{d\psi}{\psi} = -\int_{\tau}^{\tau+\Delta\tau}(V-V_{ref})d\tau$$

Thus the change in amplitude of the wave function at $\underline{r}$ during $\Delta\tau$ is

$$\Delta\psi(\underline{r}) = \psi(\underline{r})(e^{-(V(\underline{r})-V_{ref})\Delta\tau}-1)$$

Consequently at time $\tau + \Delta\tau$ we have

$$\begin{aligned}\psi(\tau+\Delta\tau) &= \psi(\tau) + \Delta\psi \\ &= \psi(\tau)\, e^{-(V-V_{ref})\Delta\tau}\end{aligned} \qquad (2.11)$$

The population of the ensemble can be made to grow or decay according to equation (2.11) by defining the birth probability as

$$P_b = e^{-(V-V_{ref})\Delta\tau}-1 \qquad (2.12)$$

If a particular system is in a configuration for which $V < V_{ref}$ then the system itself, as well as P_b replicas, will be continued into the next time step. In general P_b will be a positive number with integer and fractional

parts.

$$P_b = \text{int}(P_b) + \text{frac}\,(P_b)$$

The necessary births can be accomplished by producing $\text{int}(P_b)$ replicas together with an extra replica included with a probability $\text{frac}(P_b)$. When the energy of a system is such that $V > V_{ref}$, there is a probability $P_d = -P_b$ that the system will "die" and be removed from the ensemble.

The numerical methods for treating the separate terms in the Schrödinger equation which were discussed above are exact independent of the size of the time step. Anderson (1975, 1976) has presented an approximate procedure for simulating the Schrödinger equation which involves combining the diffusion and birth/death processes by making a short time approximation. Thus it is assumed that the potential is approximately constant over the short distances through which systems move as a result of diffusion for a finite time $\Delta\tau$.

The idea of studying quantum problems using the analogy between the time dependent Schrödinger equation and a diffusion and birth/death process has been attributed to Fermi (Metropolis and Ulam (1949)). In the 1950's several workers discussed various Monte Carlo methods based on this idea and Anderson (1975) presents a summary of these early references. Most of the quantum Monte Carlo methods which have been devised involve using a finite time step approximation. The Green's function Monte Carlo method which was developed by Kalos and his coworkers (Kalos (1970), Kalos Levesque and Verlet (1974), Ceperley and Kalos (1979)) is a related technique which does not require the short time approximation and is essentially exact. In Chapter 4 we present a brief description of this rather complicated procedure.

The algorithm given by Anderson is particularly simple and is summarised as follows:

1) Establish an ensemble of systems in some initial distribution.

2) Increament time by $\Delta\tau$ and allow each ensemble member to diffuse by giving its particles random cartesian displacements, the components being chosen from Gaussian distributions of appropriate width.

3) Calculate the potential energy of each displaced system and, depending on this value, allow the system to replicate or "die".

Repeating steps 2) and 3) enables the imaginary time evolution of the initial ensemble to be followed and, if a sufficiently small time step is used, the ensemble motion models the evolution of the wave function.

The initial distribution can be expanded in terms of the eigenfunctions of the Hamiltonian and the time evolution is thus determined by equation (2.8), which can be written in imaginary time as

$$\psi(\underline{r},\tau) = \sum_n a_n e^{-(E_n - V_{ref})\tau} \phi_n(\underline{r}) \qquad (2.13)$$

As $\tau \to \infty$ the sum will be dominated by the lowest energy eigenstate contained in the initial expansion. Thus in the long time limit, the simulation algorithm summarised above will produce an ensemble of systems distributed in space according to the eigenstate, ϕ_o and since

$$\lim_{\tau\to\infty} \psi(\underline{r},\tau) = a_o e^{-(E_o - V_{ref})\tau} \phi_o(\underline{r}) \qquad (2.14)$$

the asymptotic population decay rate will give an estimate of the eigenvalue E_o.

To illustrate how the algorithm behaves, in Figure 2.1 we present the results for a simulation of the Schrödinger equation describing a one

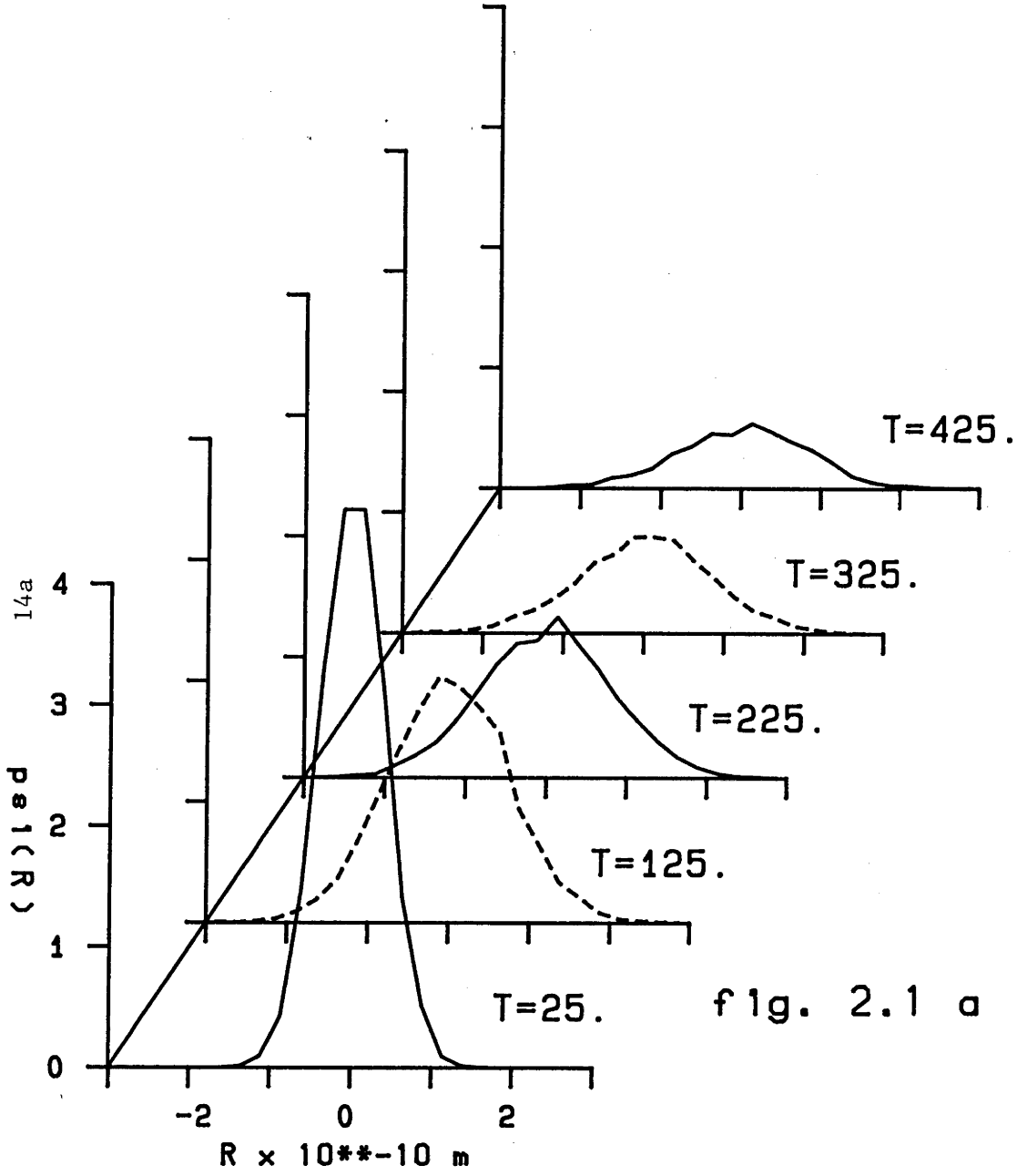

fig. 2.1 a

fig. 2.1 b

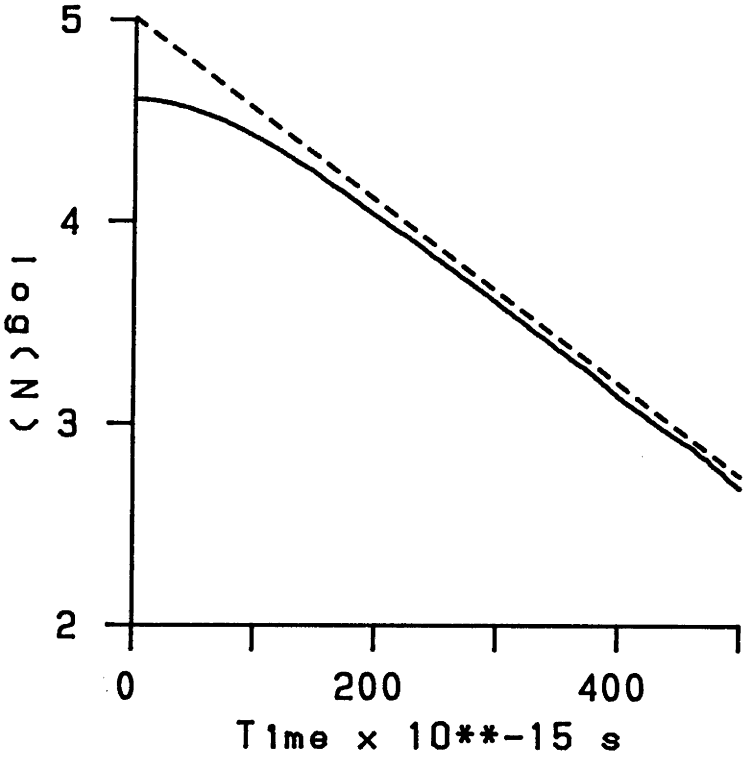

dimensional harmonic oscillator. Parameters are chosen to model a proton in a harmonic well $V(x) = \frac{1}{2}kx^2$ with force constant $k = 100\ \mathring{A}^{-2}$. The initial condition was an ensemble of 100 systems, all with zero displacement. Figure 2.1a shows the evolution of this ensemble in imaginary time. Here, histograms of the ensemble displacements have been accumulated at various times along the trajectory. The curves are the result of averaging over 100 such trajectories all having the same initial condition. At short times the ensemble distribution undergoes some initial spreading following which a stable Gaussian distribution of constant width is obtained. The amplitude of the distribution decays along the trajectory. In Figure 2.1b we plot the logarithm of the ensemble population as a function of time. After some transient behaviour, associated with the spreading of the initial distribution, a constant exponential decay rate is established. The asymptotic slope of this line gives the ground state energy of the oscillator.

There are several problems with the simple minded algorithm described in this section. The birth/death step causes exponential growth or decay of the ensemble population. Thus at long times, if the population is decaying there will be problems with small sample sizes while if population growth occurs the available computer storage will be exceeded. Time step dependence must also be considered. In the limit as $\Delta\tau \to 0$ the separation of the diffusion and birth/death processes is justified. For a finite time step, however, it is an approximation which can lead to numerical errors. Finally, the crude algorithm simulates states for which the wave function is everywhere positive so that only the ground state of a system of Bosons can be studied. In general, wave functions have regions of both positive and negative density and a procedure for handling more general problems

must be developed.

2.) Extension of the Basic Algorithm

a) Wave Function Symmetry

The Monte Carlo method for modeling the Schrödinger equation discussed in Section 1.) dealt only with simulating terms in the Hamiltonian. So far we have said nothing about boundary conditions or wave function symmetry. We confine ourselves to considering only real wave functions. In general such wave functions have positive and negative regions. Consequently a technique for generating nodal surfaces in the sampled distribution must be devised.

Anderson and Freihaut (1979) discussed a random walk method for sampling the difference, $\delta = \psi - \psi_T$, between the ground state wave function ψ and a trial function ψ_T. In general the function δ will have nodes and their random walk involves positive and negative systems which cancel when opposite signed systems entered the same region of space. The method was applied to several one dimensional problems and when used iteratively gave a series of successive corrections to the trial function which improved the efficiency and accuracy of ground state calculations.

We have considered using this idea for treating wave functions with nodes. An ensemble containing positive and negative weighted components is established. Members of the ensemble diffuse and replicate in the manner described in Section 1.). By allowing opposite signed systems to annihilate when they enter the same region of space, a node may be generated. With the algorithm described in Section 1.) "death" could only occur as the random

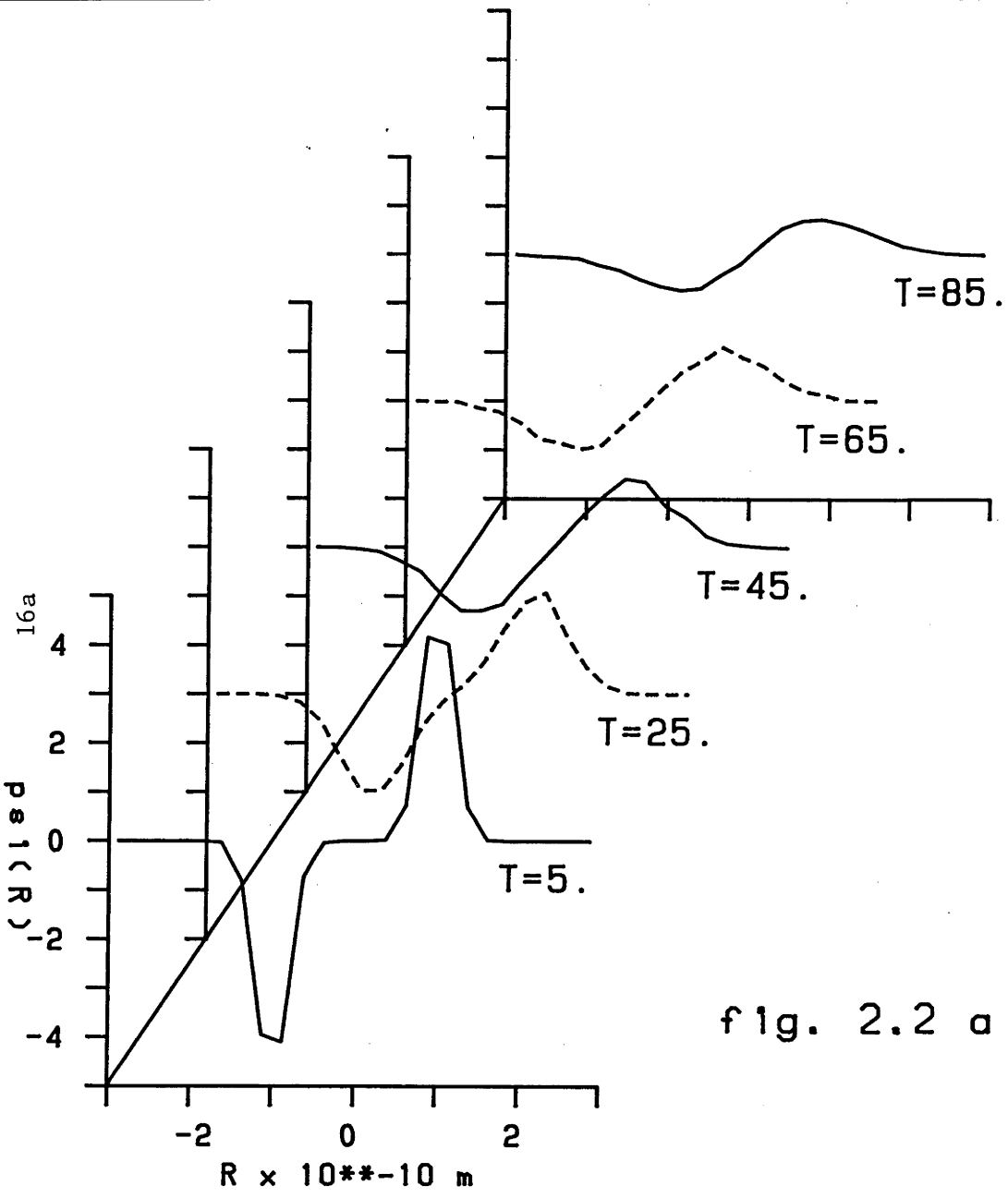

fig. 2.2 a

fig. 2.2 b

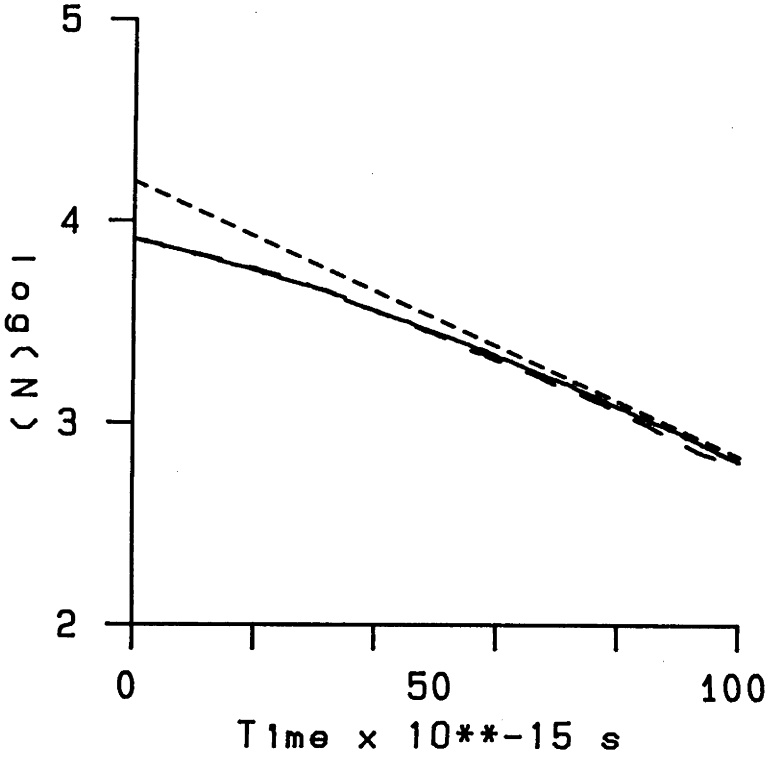

walkers climbed up the walls of the potential surface. When opposite signed systems are introduced and annihilation occurs, the boundary conditions on the wave function also give the possibility for "death".

Figure 2.2 again shows results from a quantum simulation of a harmonic oscillator. Now however the initial condition was 50 positive random walkers placed at +a and an equal number of negative systems at -a. The annihilation step was included at the end of each time step after the systems had diffused and replicated. Two systems of opposite sign were allowed to annihilate if they were separated by a distance less than some small value. From the figure we see that the ensemble distribution propagates to the first excited state wave function after some transient behaviour. Figure 2.2b demonstrates that the asymptotic population decay rate gives the first excited state eigenvalue. Later in this section we consider extending the annhilation procedure to more than one dimension and in Section 4.) we discuss the question of annihilation of systems with many identical particles.

b) Producing a Stable Ensemble

From equation (2.14) a stable ground state population may be obtained by setting the value of the reference in the energy scale, V_{ref}, equal to the ground state energy E_o. To use this method requires prior knowledge of the ground state energy. We might consider setting V_{ref} to some guess at E_o and monitoring the population as the simulation proceeds. Adjusting V_{ref} so that on average the population neither grows nor decays gives a means of estimating E_o.

A dynamic adjustment procedure used by Anderson (1975) provides an effective means of stabilising the population. We require a stable ensemble

with average population N_c. At the end of each time step a new value for V_{ref} is chosen according to the following expression

$$V_{ref_{\tau+\Delta\tau}} = \langle V\rangle_\tau - \alpha(N_\tau - N_c) \tag{2.15}$$

Here N_τ is the instantaneous total number of systems in the ensemble and $\langle V\rangle_\tau$ is the average potential energy. The parameter α is a positive energy which controls the size of the population fluctuations. As $\tau\to\infty$ the spatial distribution will be approximately constant and $\langle V\rangle_\tau$ will not change appreciably with time. Choosing $V_{ref_{\tau+\Delta\tau}}$ according to (2.15), gives an energy reference which is appropriately larger or smaller than $\langle V\rangle_\tau$ so that on average the births or deaths in the next time step will correct any discrepancey between N_τ and N_c. If the parameter α is too large, the feed back mechanism may become unstable.

An understanding of the influence of the feed back mechanism described above can be obtained by expanding the distribution in terms of the eigenfunctions $\{\phi_n\}$

$$\psi(\underline{r},\tau) = \sum_n a_n(\tau)\ \phi_n(\underline{r}) \tag{2.16}$$

Here the exponential decay factors appearing in equation (2.13) have been replaced by time varying expansion coefficients $a_n(\tau)$. When V_{ref} is varied with time the coefficients no longer exhibit decoupled exponential decay.

To proceed we consider the Schrödinger equation in which the reference energy varies

$$\frac{\partial\psi(\underline{r},\tau)}{\partial\tau} = \left[\frac{\hbar^2}{2m}\nabla^2 - \left(V(\underline{r}) - V_{ref}(\tau)\right)\right]\psi(\underline{r},\tau) \tag{2.17}$$

By substituting the expansion (2.16) into (2.17), using the fact that the ϕ_n are eigenfunctions of $\hat{H}$ and form an orthonormal set, and integrating

over all space we find that the coefficients satisfy the following differential equations

$$\frac{da_n(\tau)}{d\tau} = -(E_n - V_{ref}(\tau))\, a_n(\tau) \qquad (2.18)$$

These equations are coupled through the function $V_{ref}(\tau)$. The explicit form of the coupling can be found by writing the expression for the V_{ref} adjustment (equation (2.15)) in terms of the eigenfunction expansion.

When opposite signed systems annihilate one another, the total number of systems in the ensemble at time τ is proportional to the area under the function $|\psi(\underline{r},\tau)|$ thus we can write

$$N_\tau = \int \left|\sum_n a_n(\tau)\, \phi_n(\underline{r})\right| d\underline{r}$$

Similarly, the average of the potential energy at time τ can be written as

$$\langle V\rangle_\tau = \frac{\int \left|\sum_n a_n(\tau)\, \phi_n(\underline{r})\right| V(\underline{r})\, dr}{\int \left|\sum_n a_n(\tau)\, \phi_n(\underline{r})\right| d\underline{r}}$$

Substiting these results into (2.15) gives the following expression for the time evolving energy reference

$$V_{ref}(\tau) = \frac{\int \left|\sum_n a_n(\tau)\, \phi_n(\underline{r})\right| V(\underline{r})\, d\underline{r}}{\int \left|\sum_n a_n(\tau)\, \phi_n(r)\right| d\underline{r}} - \alpha \left[\int \left|\sum_n a_n(\tau)\, \phi_n(\underline{r})\right| d\underline{r} - N_c\right] \qquad (2.19)$$

Equations (2.18) and (2.19) constitute a set of coupled differential equations which describe how the amplitudes of the different eigenfunction components change when V_{ref} is adjusted according to (2.15). A qualitative understanding of the effects of adjusting V_{ref} can be obtained by

considering the behaviour of the solutions of (2.18) and (2.19) for a problem where the eigenvalues and eigenfunctions are known.

Harmonic oscillator eigenvalues and eigenfunctions have been used, and equations (2.18) and (2.19) solved numerically to give the solutions shown in Figure 2.3a. The initial distribution was dominated by the first excited state eigenfunction and contained small components of the ground and other excited states. Through the nature of the couplings introduced in $V_{ref}(\tau)$, the lowest lying state contained in the initial distribution is amplified at the expense of the other states. Further, at long times the amplitude of the lowest energy initial state attains a constant value and the excited state contributions decay to zero.

Behaviour similar to this can be observed in a random walk simulation using the V_{ref} adjusting algorithm. The wave function is represented by an ensemble of positive and negative systems and can be written in the following form

$$\psi(\underline{r},\tau) = \sum_p \delta(\underline{r}-\underline{r}_p(\tau)) - \sum_m \delta(\underline{r}-\underline{r}_m(\tau)) \qquad (2.20)$$

Here $\underline{r}_p(\tau)$ and $\underline{r}_m(\tau)$, respectively, give the positions of positive and negative systems at time τ. When $\psi(\underline{r},\tau)$ is written in terms eigenfunction expansion in (2.16), the expansion coefficients are obtained from the overlap between ψ and the eigenfunctions so that

$$\begin{aligned} a_n(\tau) &= \int \psi(\underline{r},\tau)\, \phi_n(\underline{r})\, d\underline{r} \\ &= \sum_p \phi_n(\underline{r}_p(\tau)) - \sum_m \phi_n(\underline{r}_m(\tau)) \end{aligned} \qquad (2.21)$$

The second equality is obtained by substituting (2.20) and using the properties of integrals over δ distributions.

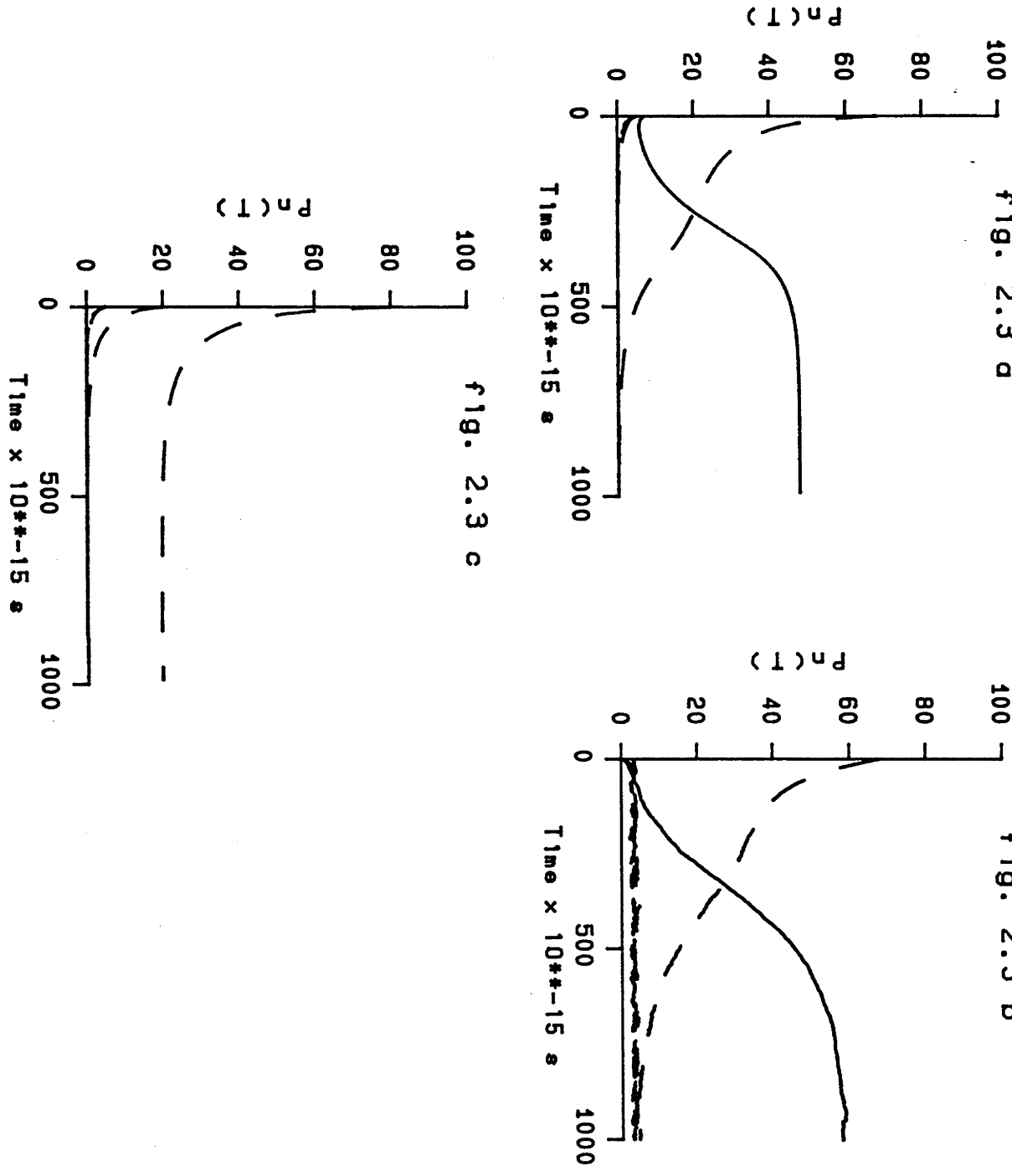

fig. 2.3 a

fig. 2.3 b

fig. 2.3 c

Equation (2.21) can be used to resolve the ensemble distribution into its eigenfunction components. Figure 2.3b shows the evolution of the first five expansion coefficients calculated, using equation (2.21), during a simulation of the harmonic oscillator in which V_{ref} was adjusted according to equation (2.15). The initial condition was an ensemble of fifty positive systems at +a and fifty negative systems at -a. An annihilation step was included in the algorithm. The ensemble is dominated by the ground state distribution at long times.

It is interesting to note that the initial distribution for the random walk calculation considered above contains no component of the ground state. If the system of differential equations (2.18) and (2.19) is solved with this initial condition the results shown in Figure 2.3c are obtained. The first excited state establishes itself with constant amplitude while the other excited states decay. Throughout the calculation the ground state remains with zero amplitude. The qualitative difference between the behaviour of the solutions of equations (2.18), (2.19) and the results of the simulation is due to the fact that the equations do not include the statistical fluctuations which occur in the simulation algorithm. Thus in Figure 2.3b we see a component of the ground state enter the ensemble distribution through statistical noise which is amplified and dominates the asymptotic ensemble distribution.

We have seen that the V_{ref} adjustment algorithm can produce a stable ensemble distributed according to the ground state eigenfunction. The algorithm also provides a means of estimating the ground state eigenvalue obtained as the average of V_{ref} which holds the population approximately constant in the long time limit.

c) Orthogonal Filtering and Stable Excited State Distributions

In order to use the V_{ref} adjusting algorithm to obtain a stable excited state distribution we need to devise a scheme to remove ground state components which may build up as a result of statistical noise. From equation (2.21) the overlap between the ensemble distribution and the ground state wave function is given by

$$a_o(\tau) = \sum_p \phi_o\left(\underline{r}_p(\tau)\right) - \sum_m \phi_o\left(\underline{r}_m(\tau)\right) \qquad (2.22)$$

By forcing $a_o(\tau)$ to remain approximately zero, ground state components can be filtered from the distribution. To use equation (2.22), the ground state wave function must be known in advance.

One procedure that ensures orthogonality is summarised as follows: At the end of each time step we calculate the overlap with the ground state. If $a_o(\tau)$ is greater than some tolerence δ then the overlap must be reduced. By removing a positive system or introducing a negative system, $a_o(\tau)$ can be changed appropriately. If necessary the overlap can be increased in a similar fashion. The total number of systems should not be directly altered by the orthogonalisation step, rather, only the shape of the distribution should be changed. In this way the rate of change of the population is not directly influenced by the orthogonalization. By replicating and removing opposite signed systems the relative numbers of positive and negative components can be adjusted so that $a_o(\tau)$ is forced to fluctuate around zero.

Figure 2.4 shows the eigenstate decomposition of a harmonic oscillator simulation which uses a V_{ref} adjusting algorithm together with the ground state filtering scheme described above. The maximum amplitude of the ground state wave function was used as the tolerance for the orthogonalisation. An

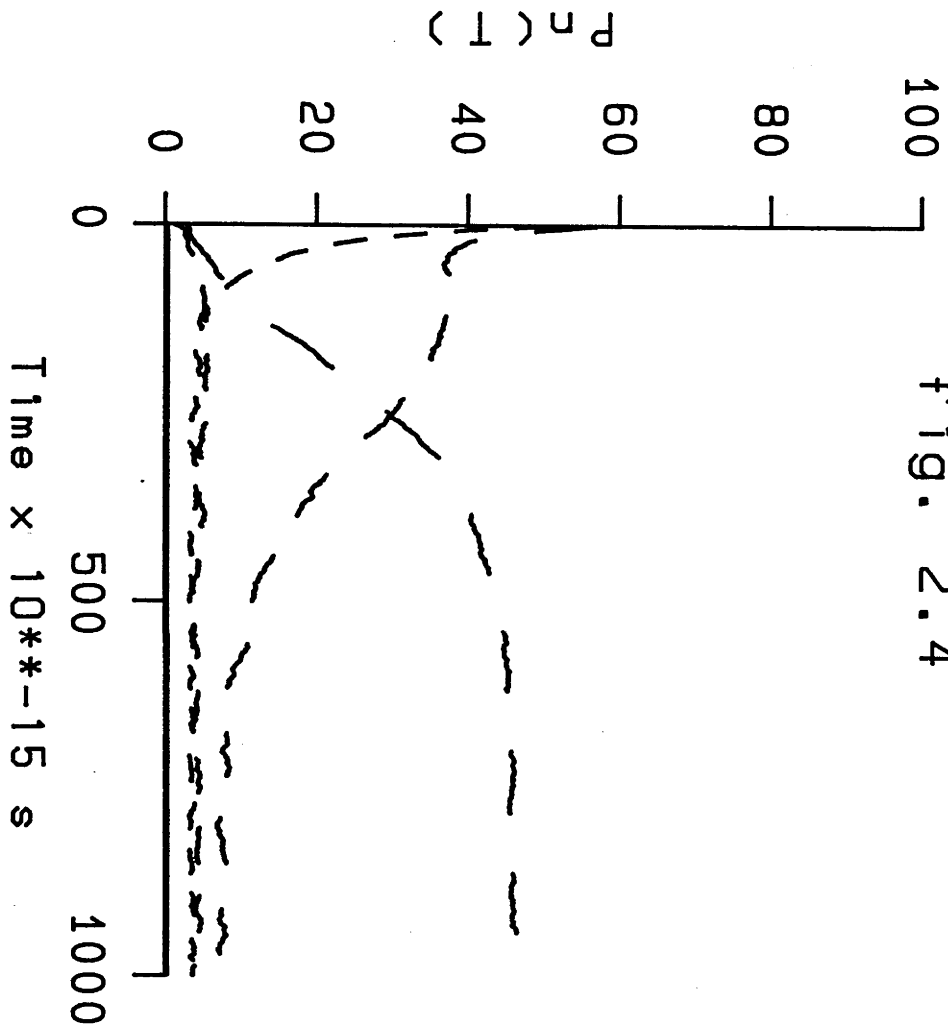

fig. 2.4

initial ensemble consisting of fifty negative systems at both +a and -a and one hundred positive systems at the origin was used. This condition resembles the second excited state of the oscillator. We see from the figure that there is also an initial component of the fourth excited state. As time is advanced the contributions from ϕ_2 and ϕ_4 decay and the first excited state component grows and stabilizes, dominating the asymptotic distribution. The ground state noise level does not build up during the calculation indicating that the orthogonalization procedure effectively filters ground state components from the ensemble. There are, however, significant components of the higher excited states which do not decay to zero and which perturb the stable excited state distribution.

The procedure discussed above can be used to simulate higher excited states. With such calculations, all the lower energy eigenfunctions must be known and the ensemble distribution is held orthogonal to these states. As an example consider the second excited state so there are two orthogonality conditions to be satisfied.

$$a_0(\tau) = \sum_p \phi_0 \left(\underline{r}_p(\tau)\right) - \sum_m \phi_0 \left(\underline{r}_m(\tau)\right) = 0 \qquad (2.23)$$

$$a_1(\tau) = \sum \phi_1 \left(\underline{r}_p(\tau)\right) - \sum \phi_1 \left(\underline{r}_m(\tau)\right) = 0 \qquad (2.24)$$

The situation is now complicated because ϕ_1 can have both positive and negative values. There are a number of possible alternatives which are summarised in Table 2.1.

Table 2.1 Procedure for Maintaining Orthogonality to the ground and first exited states

Tolerence Condition		Corrective Action	
		insert	withdraw
$a_0 > \delta_0$	$a_1 > \delta_1$	m^+	p^+
$a_0 > \delta_0$	$a_1 < \delta_1$	m^-	p^-
$a_0 < \delta_0$	$a_1 > \delta_1$	p^-	m^-
$a_0 < \delta_0$	$a_1 < \delta_1$	p^+	m^+

In the table, the notation m^+ represents a negative system which is in a region of space where the value of the first excited state eigenfunction is positive. Thus for example, if $a_0 > \delta_0$ and the excited state overlap $a_1 > \delta_1$, the action which will correct these discrepancies and leave the total population unaltered is to introduce an extra negative system and withdraw a positive system. Both changes should occur in regions where ϕ_1 is positive. An alternative to the replication and removal of opposite signed systems is to change the sign of a single system. We have used this alternative in applications only when there are no systems available for replication in the appropriate region of space.

The excited state method detailed in this section has been used to simulated the first few vibrational eigenstates of the H_2 molecule. The vibrational potential surface presented by Kolos and Wolniewicz (1975) was used. A ground state calculation was first performed and a histogram of the ensemble distribution accumulated. Fitting a piece wise cubic polynomial through this data gave a form for the ground state wave function which could be used for the orthogonalization step in the excited state calculations. Eigenfunctions for the ground, first, and second excited

fig. 2.5

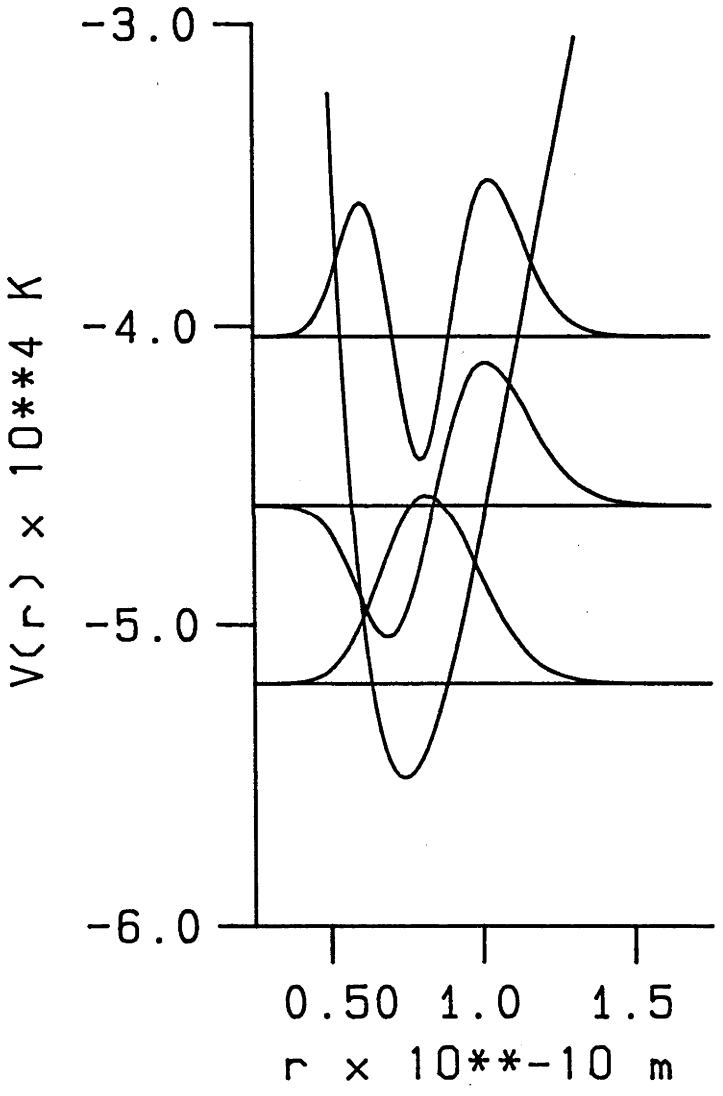

vibrational states obtained in this way are presented in Figure 2.5. In Table 2.2 we give the corresponding eigenvalues which were calculated from the average value of V_{ref} required to hold the population approximately constant. The ground state energy agrees with the result of Kolos and Wolniewicz and the excited state energies are slightly too high. The discrepancy probably results because of higher eigenstate impurities (Figure 2.4) which may arise through noise introduced by the orthogonalization procedure.

Table 2.2. Vibrational Energies of the H_2 Molecule (in 10^4°K)

ν	Random Walk	Kolos and Wolniewcz (1975)
0	-5.19	-5.20
1	-4.58	-4.60
2	-3.97	-4.03

d) System Annihilation in Many Dimensions

For multidimensional systems the annihilation step becomes complicated. When the system contains many indistinguishable particles, comparing two systems requires all possible permutations of the particle labels to be considered. With such systems the problem of identical particle statistics becomes important. This question will be discussed in more detail in Section 4.). A second problem stems from the difficulty in defining the region of space occupied by a member of the ensemble. If a system occupies only a single point and is thus represented by a multidimensional delta distribution, the probability of two systems annihilating one another is vanishingly small. In this case an ensemble with an extremely large number

of members would be required otherwise the opposite signed systems could never find one another, no annhilations would occur, and two opposite signed ground state distributions would result. If the members of the ensemble occupy a non-infinitessimal volume of the configuration space, a finite ensemble can be used.

The simplest means for giving the systems a finite size is to use a 3N dimensional rectangular grid to define the configuration space. Instead of being represented by a multidimensional delta distribution, each system now occupies a small hypercube. Results obtained using this procedure will depend on the size of grid and on the number of systems in the ensemble. If the grid were too fine and the ensemble population to small to fill the space then opposite signed systems could easily avoid one another and positive and negative ground state distributions would again result. The problem can be remedied by increasing the number of systems in the ensemble, which increases the computational effort involved with the calculation. Alternatively, we may use a coarser spatial grid. Adopting the latter measure means that the resolution of the spatial features of the wave function, such as the nodal surfaces, will be poorer and the accuracy of the eigenvalue effected. Ideally, the number of systems in the ensemble may be increased till a particular spatial grid becomes "saturated". Beyond this point, any increase in the number of systems will have no effect on the calculation and the results will depend only on the spatial resolution.

A more effective scheme for dividing the configuration space is to allow systems of opposite sign to penetrate the same regions without annhilating one another completely. The positions of the systems are now considered as the centres for a local wavefunction density which may take a Gaussian form for example. In this case the width of the Gaussian is

analogous to the grid size. The nodes of a wave function are generaly curved sufaces in hyperspace. Using a local Gaussian density should provide a better representation of these surfaces than the rectangular grid. Thus fewer systems occupying larger volumes should give comparable accuracy.

When represented by a Gaussian density profile, the spatial extent of system i is given by

$$\rho_i(\underline{r}) = \left(\frac{a}{\pi}\right)^{3N/2} e^{-a(\underline{r}-\underline{r}^i)^2} \tag{2.25}$$

The overlap of the density profiles for systems i and j is then

$$\begin{aligned} S(|\underline{r}^i-\underline{r}^j|) &= \int \rho_i(\underline{r})\rho_j(\underline{r})d\underline{r} \\ &= \left(\frac{a}{2\pi}\right)^{3N/2} e^{-a/2(\underline{r}^i-\underline{r}^j)^2} \end{aligned} \tag{2.26}$$

When represented as delta distributions the annihilation probability for opposite signed systems was zero if their respective infinitessimal volume elements did not overlap and one if there was any overlap at all. A consistent definition for the annihilation probability is thus

$$P_a(|\underline{r}^i-\underline{r}^j|) = 2 \int_{|\underline{r}^i-\underline{r}^j|}^{\infty} S(t)dt \tag{2.27}$$

For system with Gaussian density the annihilation probability becomes

$$\begin{aligned} P_a(|\underline{r}^i-\underline{r}^j|) &= 2\left(\frac{a}{2\pi}\right)^{3N/2} \int_{|\underline{r}^i-\underline{r}^j|}^{\infty} e^{-a/2s^2} ds \\ &= 1-\mathrm{erf}\left(\frac{a}{2}|\underline{r}^i-\underline{r}^j|\right) \end{aligned} \tag{2.28}$$

An efficient scheme for implementing the annihilation step involves first using a coarse rectangular grid to find the systems which are close

to one another. We then evaluate the probabilities and perform the annihilation. If several cancellations are possible we proceed in order of probability.

e) The Hydrogen Atom

To demonstrate the use of the techniques described in this section the lowest energy S and P states of the hydrogen atom have been considered. Despite its analytic solution, this example presents a non-trivial numerical problem. Grimm and Storer (1969) developed an iterative method for solving the Schrödinger equation which employed a short time approximation to the Green's function. The approach is useful for problems which can be reduced to one dimension and as an example they studied the S-states of the hydrogen atom. Anderson and Freihaut (1979) studied the lowest energy S-state using a diffusing random walk in three dimensions and as a starting point we have repeated this calculation.

In atomic units and imaginary time the Schrödinger equation for the hydrogen atom is

$$\frac{\partial \psi}{\partial \tau} = \tfrac{1}{2}\nabla^2\psi - \left(V(r)-V_{ref}\right)\psi$$

where $$V(r) = -1/r$$

The nuclear attraction term gives an infinite birth rate at the nucleus, thus sampling small distances may lead to uncontrollable growth of the ensemble population. To prevent problems caused by the nuclear attraction we have used the method suggested by Anderson (1976). Any electrons entering a small sphere of radius r_c about the nucleus experience an averaged nuclear attraction given by

$$V_{nuc}(r<r_c) = -3/2\ Z\ r_c^{-1}$$

here Z is the charge of the nucleus. If r_c is of the order of the diffusion step size then the error in using the integrated nuclear attraction will be of similar magnitude to the finite time step error.

The initial ensemble in our calculation on the ground electronic state was a set of 200 positive systems. In each system the electron was placed randomly within a cube centered on the nucleus having a side length of 5 a.u.. We used a time step of 0.01 a.u. and allowed the systems to diffuse and replicate throughout the three dimensional configuration space. Adjusting V_{ref} maintained a stable ensemble. After equilibration, averages were accumulated for 200 a.u.. The average value of V_{ref} gave an eigenvalue estimate of $E_{1s} = -.504 \pm 0.005$ a.u. which is in good agreement with the value obtained by Anderson and close to the analytic result (-0.5 a.u.).

To test the methods for simulating excited states which have been developed in this section we now consider modelling the degenerate 2p state of the hydrogen atom. The different p states have nodes in their angular distributions and an ensemble containing opposite signed members which may annihilate one another must be used. In our studies we let each system represent a centre of Gaussian density as described in the previous subsection and the annihilation probability for opposite signed systems is given in equation (2.28).

A V_{ref} adjusting algorithm was used to maintain a stable ensemble and the ground state components were removed from the calculation by the orthogonalization procedure described earlier in this section. To obtain a stable 2p state, the ensemble distribution must also be held orthogonal to the degenerate 2s state. Thus at the end of each time step the overlap between the ensemble distribution and both the 1s and 2s wave functions was

evaluated using the analytic forms for these functions. The positive and negative populations were adjusted as outlined in Table 2.1 to keep the overlap between the sampled distribution and the 1s and 2s states small.

We have performed calculations using different values of the Gaussian width parameter and also considered the effects of changing the number of systems in the ensemble. A time step of $\Delta\tau = 0.01$ a.u. was used in all these calculation. In Figure 2.6a we present the eigenvalue estimate as a function of the width parameter a. When a is increased the Gaussian profile narrows. For systems which occupy larger volumes of configuration space (low values of a), we see that the eigenvalue is over estimated by the quantum Monte Carlo calculation. These higher energies result because the larger systems annihilate one another too rapidly in the region of the node. As a is increased, the cancellation of opposite signed systems is less effective and the eigenvalue estimate falls. When a finite ensemble is used, the eigenvalue estimate tends to the ground state result in the limit as $a \to \infty$.

As discussed earlier in the section, fixing the "size" of the systems determines the spatial resolution of the calculation. For a given resolution, we may increase the number of systems in the ensemble, N, and the eigenvalue estimate is seen to increase. This can be understood in terms of packing more ensemble members into the finite volume of configuration space sampled by the wave function. Eventually the total volume to be sampled will be adequately filled by systems of a given size and beyond this point the eigenvalue estimate will not change as N is increased. The energy obtained in the limit as $N \to \infty$ will be the best eigenvalue estimate for a given spatial resolution. Further, this asymptotic estimate should be an upper bound for the energy since poorer

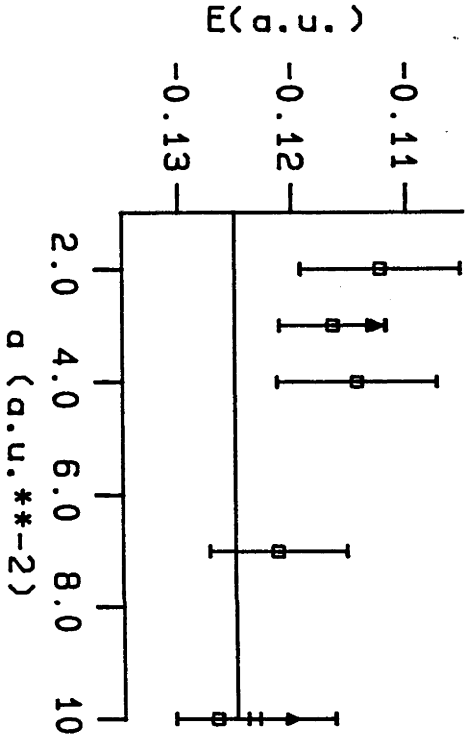

fig. 2.6 a

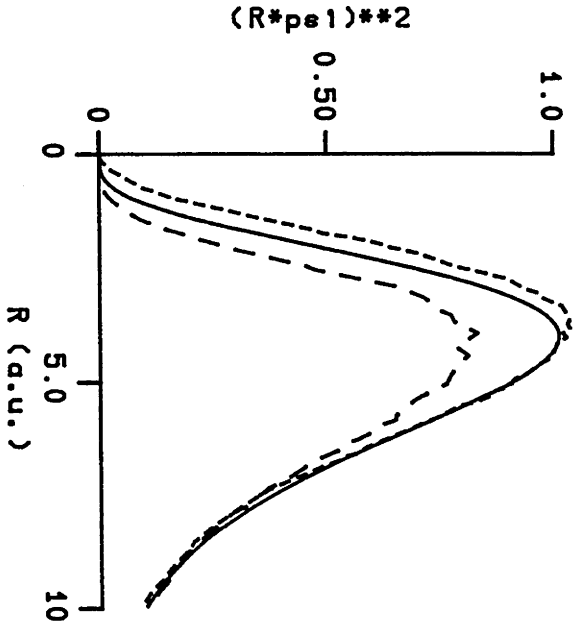

fig. 2.6 b

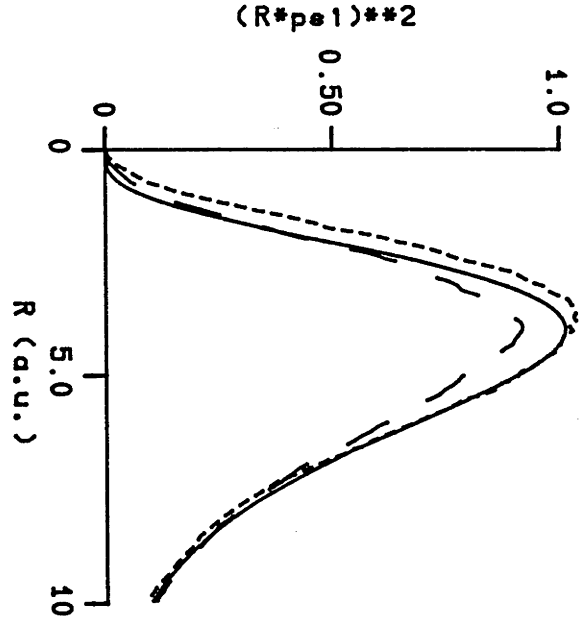

fig. 2.6 c

nodal resolution causes excessive annihilation in the region of the node.

Figure 2.6b shows how the calculated electron distribution for the p state is influenced by changes in the nodal resolution whilst holding the number of systems fixed. We accumulated separate histograms of the distance of the electron from the nucleus for the positive and negative systems. These two distributions were always found to be identical within the statistical uncertainty. In the figure we present the radial electron density obtained from the average of the positive and negative distributions. For comparison, the analytic 2p electron density is also given. We see that as the size of the systems is increased the maximum in the electron density shifts to larger r. Electron density is depleated within the region of the node (r=0) due to the excessive annihilation of the large systems. When the systems are too small and there are insufficient numbers to fill the space, the electron density penetrates too close to the nucleus due to ineffective annihilation. Figure 2.6c shows that increasing the number of systems for a given nodal resolution pushes the electron density out since annihilation becomes more effective as the space is filled.

Since the 2p state is degenerate our ensemble distribution will be a linear combination of the $2p_0$, $2p_{+1}$ and $2p_{-1}$ functions and the distribution on average is isotropic. To demonstrate that the orthogonalization and annihilation procedures are effective in producing a stable node in the orientation space we must construct a coordinate system which rotates with the sampled distribution and project the wave function onto this reference frame. We have done this by using the vector defined by the average position of the positive systems as the x-axis in a coordinate system which is now fixed to the moving ensemble. By projecting the ensemble

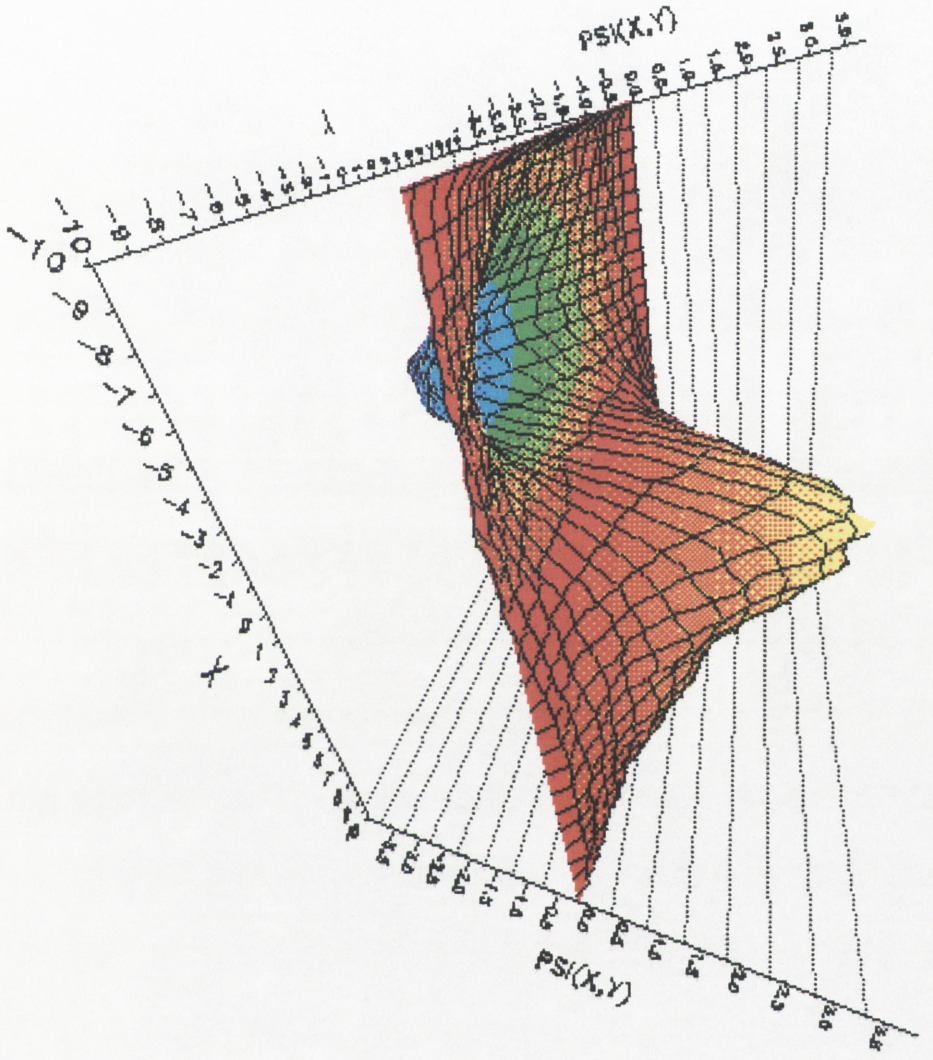

fig. 2.7

distribution onto the x-y plane in this coordinate system and accumulating a two dimensional histogram, the angular resolved distribution presented in Figure 2.7 was obtained. The two opposite signed lobes of the $2p_x$ wave function are seen, indicating that a stable excited state distribution can be simulated.

Anderson (1976) has performed quantum random walk calculations on the 2p state of hydrogen but his method requires prior knowledge of the nodal surface. If a random walker crosses the node then its walk is terminated. Anderson restricted his random walks by terminating those which crossed the plane $x = 0$ and in this way he modeled the positive lobe of the $2p_x$ function. The fixed node method is discussed in more detail in Section 4.) where we consider simulating wave functions describing systems of identical Fermions. The nodal surfaces of such wave functions are not known exactly so the fixed node approach can only be applied approximately.

It should be noted that the 2p state is particularly difficult to simulate using systems which annihilate one another. The reason for this difficulty is that the wave function changes very rapidly in the region of the node. Due to these large changes in density over very short distances, high resolution of the configuration space is required. For this reason large numbers of systems occupying very small volumes must be used. Resolution of the wave function at short distances is very important with an attractive coulomb potential as the energy is very large in this region. The eigenvalue estimates presented in Figure 2.6a could be improved by using many smaller systems but the calculation soon becomes intractable.

Fortunately, for other interesting systems, the wave function does not change so rapidly at the node and the behaviour around the nodal region is not so important for determining the energy. Consequently coarser

resolution of the configuration space can be used and accurate results obtained. We shall see in the final section of this chapter that the nodal surfaces in the wave functions of systems containing a few fermions are adequately described using relatively coarse resolution and excellent estimates of the eigenvalues are obtained.

3.) Expectation Values and Importance Sampling

a) Expectation Values

So far we have described a scheme for producing a stable ensemble distributed according to a particular eigenstate of a system. A method for estimating of the eigenvalue has also be obtained. Expectation values of other operators may be calculated using the ensemble. In this section we consider calculating the expectation value of a time independent non-differential operator A.

If the wave function is real, equation (2.6) gives that the expectation value of A is

$$\langle A \rangle = \int \phi^2(\underline{r})\ A(\underline{r})\ d\underline{r}$$

Integrals of this form can be evaluated numerically using a Monte Carlo method in which the function $A(\underline{r})$ is averaged over an ensemble which samples the distribution $\phi^2(\underline{r})$. The random walk method, however, only produces an ensemble distributed according to $\phi(\underline{r})$. A $\phi^2(\underline{r})$ distribution may be sampled by appropriately weighting the contributions of each system in the ensemble. Once a stable ensemble distributed according to $\phi(\underline{r})$ is established, systems replicate most rapidly in the regions of highest wave

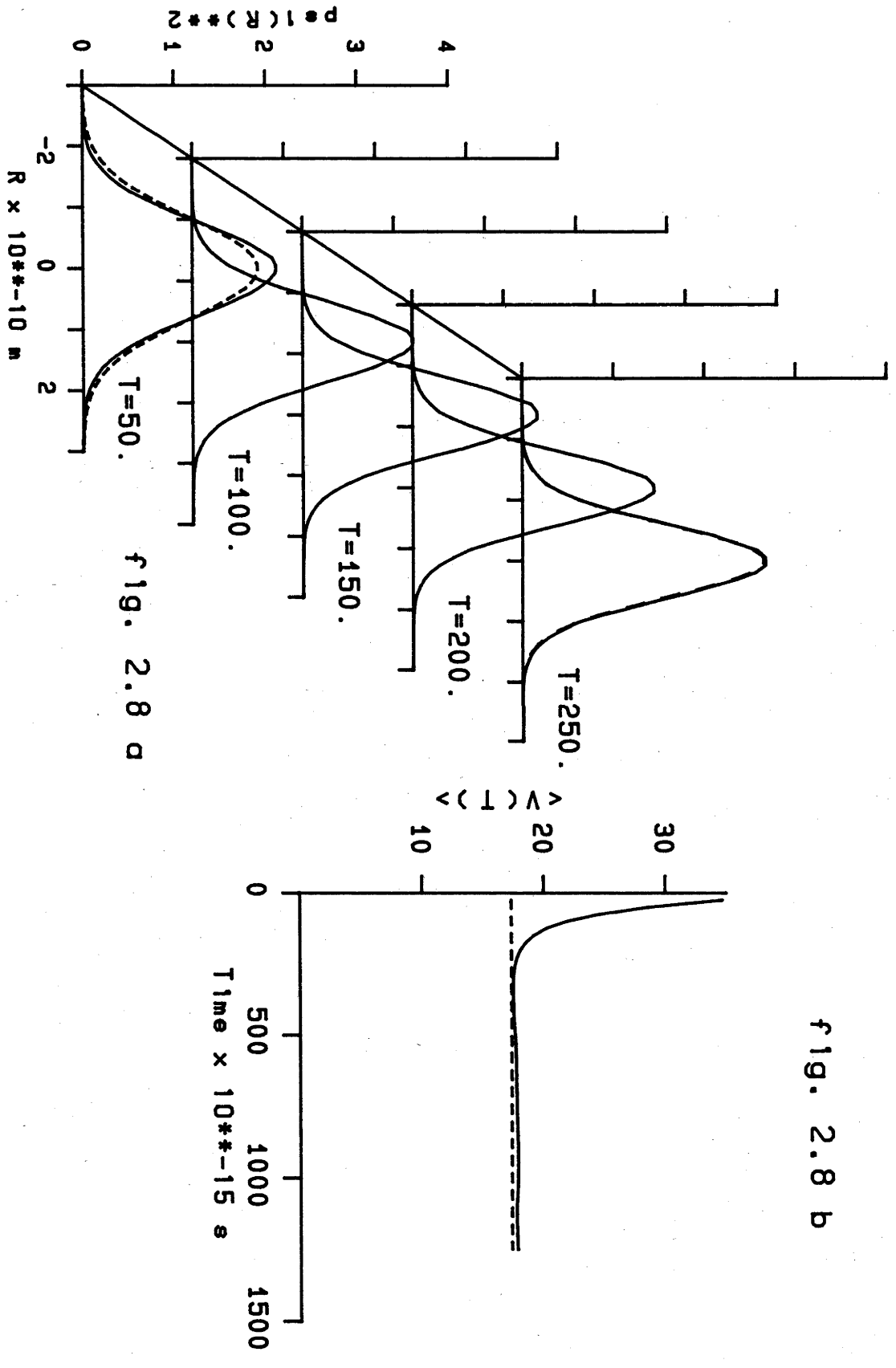

fig. 2.8 a

fig. 2.8 b

function density. Due to this feature of the random walk method, the asymptotic number of descendents of a particular system is proportional to the wave function in the region sampled by the parent. Thus weighting the contributions of each system by the number of descendents it produces at long times, enables a $\phi^2(\underline{r})$ distribution to be sampled. Kalos (1967, 1970) has described a similar procedure for calculating expectation values from the Green's function Monte Carlo method.

The behaviour described above is demonstrated for the one dimensional harmonic oscillator in Figure 2.8. Figure 2.8a shows the ensemble distribution weighted by the descendent numbers for different delay times. It is seen that the product distribution converges to $\phi^2(r)$ in the long time limit.

The curves are the result of averaging over many segments of the random walk trajectory. Since its distribution is stationary, the ensemble at any time can be used as a parent distribution and the history of its descendents monitored. An efficient sampling cycle can be devised in which each ensemble is used as both a parent distribution and when determining the descendent weights for a previous parent ensemble.

Figure 2.8b shows that when the weighted ensemble distribution relaxes to ϕ^2, the expectation value of the potential energy may be estimated. This estimate is plotted as a function of delay time to show the asymptotic convergence. The ϕ^2 distribution is more strongly peaked around the minimum than ϕ so smaller values of the potential energy make more important contributions. Consequently the potential energy estimate decays as the ϕ distribution is modified.

b) Importance Sampling

The Quantum Monte Carlo algorithm can be made more efficient if an approximate form for the wave function is known. Importance sampling involves using an approximate wave function to guide the random walk into the important regions of space. Kalos, Levesque and Verlet (1974) successfully used the idea to perform Green's function Monte Carlo calculations on a hard sphere quantum fluid. Ceperly derived an equation of motion for the importance sampled distribution and Anderson (1980) used a drifting and diffusing random walk method to simulate it. The importance sampling function may be the wave function obtained from a variational calculation or some functional form concocted from physical intuition.

Suppose the wave function, $\psi(\underline{r},\tau)$, is peaked in some region and that an approximate form or trial wave function $\psi_T(\underline{r})$ is known. The function $f = \psi\psi_T$ will be very strongly peaked in the important regions of configuration space. An equation of motion for f can be derived as follows: We use a trial function which is independent of τ so that

$$\frac{\partial\psi}{\partial\tau} = \frac{1}{\psi_T}\frac{\partial f}{\partial\tau} \qquad (2.29)$$

Now consider the quantity $\nabla^2 f$. By some simple manipulations of vector calculus summarised below

$$\nabla^2 f = \nabla.(\nabla\psi\psi_T) = \psi_T\nabla^2\psi + 2\nabla\psi.\nabla\psi_T + \psi\nabla^2\psi_T$$

and since $$\nabla.(\psi\nabla\psi_T) = \nabla\psi.\nabla\psi_T + \psi\nabla^2\psi_T$$

we find $$\nabla^2 f = \psi_T\nabla^2\psi + 2\nabla.(\psi\nabla\psi_T) - \psi\nabla^2\psi_T$$

Rearrangeing gives

$$\nabla^2\psi = \frac{1}{\psi_T}\left[\nabla^2 f - 2\nabla.\left(\frac{f\nabla\psi_T}{\psi_T}\right) + \frac{f\nabla^2\psi_T}{\psi_T}\right] \qquad (2.30)$$

Substituting equations (2.29) and (2.30) into (2.9) and multiplying throughout by ψ_T we obtain the following equation of motion for f

$$\frac{\partial f}{\partial \tau} = \sum_k \frac{\hbar^2}{2m_k} \nabla_k{}^2 f - \sum_k \frac{\hbar^2}{m_k} \nabla_k . (f \nabla_k \ln \psi_T) - \left(\frac{\hat{H}\psi_T}{\psi_T} - V_{ref}\right) f \qquad (2.31)$$

The first term on the right hand side describes the familiar diffusion process while the last term resembles a population growth or decay term. The second term has a form similar to an equation which describes how the density changes due to drift which is induced by an applied velocity field $\underline{v}(\underline{r})$.

$$\frac{\partial \rho(\underline{r}, \tau)}{\partial \tau} = - \nabla . (\rho \underline{v})$$

A finite difference scheme for simulating a drift process involves incrementing time by $\Delta\tau$ and moving each system in the ensemble through a vector displacement determined by the product of the drift velocity at the point sampled by the ensemble member and the time step so that the drift displacements are $\Delta\underline{r} = \underline{v}(\underline{r})\Delta\tau$.

Assuming the different terms operate indepentently over a small enough time step, equation (2.31) is modeled by a diffusion and reaction procedure together with a drift step. The drift velocities are determined by the importance sampling function and

$$\underline{v}_k = \hbar^2/m_k \nabla_k \ln \psi_T \qquad (2.32)$$

As a result of the drift term, systems move out of regions where ψ_T has its minima and towards the regions where the function is a maximum.

With the basic quantum Monte Carlo procedure the birth rate was determined by the potential function $V(\underline{r})$. Generally the potential energy is a rapidly varying function of position particularly for systems

characterised by harsh repulsive core interactions. Rapid variations in the potential surface pose two related problems for the basic quantum Monte Carlo method: First, large fluctuations in the population may occur resulting in poor statistical properties. Secondly, the separation of the diffusion and birth/death processes is only valid if the potential does not change substantially during the diffusion step. For this conditon to be met, very small time steps must often be employed.

A useful feature of the importance sampling equation of motion (2.31) is that the birth rate is determined by the quantity $\hat{H}\psi_T/\psi_T$ where $\hat{H}$ is the Hamiltonian operator. If the trial function were the exact wave function, the birth rate for the importance sampling algorithm would be the eigenvalue $E = \hat{H}\psi/\psi$. In this case the birth rate becomes independent of position, thus a perfectly stable ensemble is obtained. If ψ_T approximates ψ, the birth rate is no longer be a constant but will be a slow varying function of position. With a reasonable choice for ψ_T the population fluctuations are thus reduced.

Use of the short time approximation presents a somewhat different problem in the importance sampling random walk. Since the birth rate is now a slow varying function of position, the separation of the birth/death term from the drift and diffusion processes in the limit as $\Delta\tau \to 0$ should be a very good approximation. However, the separation of drift and diffusion may present a significant source of error. Importance sampling trial functions often involve pair correlation terms (Jastrow (1956)) which take the form

$$e^{-\tilde{u}(r)}$$

where $\tilde{u}(r)$ is an effective pair potential. The drift velocity will depend on the derivative of this potential and may have a rapid variation with

position. Consequently using the drift displacement, $\Delta r = v\Delta\tau$, in which the drift velocity is assumed constant over the small step may introduce an error in the random walk path. Anderson (1985) has recently considered this problem and finds that large time steps may be used without introducing significant errors by employing an average drift velocity.

The drifting random walk described above gives an ensemble distributed according to $f = \psi\psi_T$. An estimate of the exact eigenvalue can be obtained directly with the f distribution by averaging the "local energy" $\hat{H}\psi_T/\psi_T$. This result is proved by considering the average

$$\langle \hat{H}\psi_T/\psi_T \rangle_f = \int \psi\psi_T \frac{\hat{H}\psi_T}{\psi_T} \, d\underline{r} \Big/ \int \psi\psi_T d\underline{r}$$

$$= \int \psi \hat{H}\psi_T d\underline{r} \Big/ \int \psi\psi_T d\underline{r}$$

Due to the fact that the Hamiltonian is an hermitian operator, the above expression can be written as

$$\langle \hat{H}\psi_T/\psi_T \rangle_f = \int \psi_T \hat{H}\psi dr \Big/ \int \psi\psi_T d\underline{r}$$

Finally, since $\hat{H}\psi = E\psi$ we obtain the result

$$E = \langle \hat{H}\psi_T/\psi_T \rangle_f \qquad (2.33)$$

The expectation values of other quantities can only be obtained approximately using the importance sampled distribution. Averaging quantities over the distribution $\psi\psi_T$ will give approximate expectation values accurate to order $\delta = (\psi - \psi_T)$. We can improve the estimate of the expectation value by noting that

$$\delta^2 = \psi^2 - 2\psi\psi_T + \psi_T^2$$

Thus, to order δ^2, we can use the following result, to extrapolate

importance sampled averages

$$\langle A\rangle_{\psi^2} \sim 2\langle A\rangle_{\psi\psi_T} - \langle A\rangle_{\psi_T^2} \qquad (2.34)$$

The quantity $\langle A\rangle_{\psi_T^2}$ can be obtained from variational calculations which will be discussed in Chapter 4.

4.) Identical Particle Statistics

Particle indistinguishability has been ignored in our development of the quantum Monte Carlo method. Consequently the procedure is only applicable to systems of identical particles obeying Boltzmann statistics, that is the particles are distinguished by labels. The ground state wave function of a system of labeled, identical particles is symmetric with respect to particle interchange and thus identical to the Boson ground state. In later chapters we use this feature and employ the basic quantum Monte Carlo method together with importance sampling to study the ground state properties of assemblies of Bosons including liquid ^4He, solid H_2 and some small clusters of water molecules.

This section, however, considers methods for incorporating Fermi statistics in quantum Monte Carlo calculations. Fermion wave functions must be antisymmetric under particle exchange. Further, the particles may have different spins. We first review some methods for handling Fermi statistics in quantum random walk calculations. The method described in Section 2.) for generating spatial nodes in the ensemble distribution is then extended, enabling systems of indentical particles to be modelled. For systems of Fermions the modifications involve including spin variables in the

coordinate space and introducing a Monte Carlo procedure for sampling the permutation operators. In principle the method is exact, however practical approximations including finite time steps and approximate methods for handling the annihilation of opposite signed systems must be used. We demonstrate that the method can be employed to model systems of a few Fermions by considering the lowest energy spin states of atomic helium and lithium.

a) The Fixed Node Approximation

A ground state solution of the Schrödinger equation which is antisymmetric with respect to particle interchange will result if the configuration space available to each pair of identical particles is divided symmetrically by a nodal surface. The spatial distribution on either side of the surface will differ by exchange of the two particle labels. Due to this antisymmetry we need only consider random walks which sample one side of each nodal surface. Thus the nodes may be treated as boundary conditions which require $\psi = 0$ outside these surfaces.

Consider the example of three identical fermions each moving in three dimensions. One choice of nodes which symmetrically divide the space are the surfaces

$$x_1 = x_2,\ x_1 = x_3 \text{ and } x_2 = x_3 \tag{2.35}$$

By restricting our quantum random walk to sample only those regions in which

$$x_1 > x_2 > x_3 \tag{2.36}$$

we will generate the wave function distribution on one side of each nodal

surface. The nodes are treated as hard absorbing walls thus if a system diffuses out of the region defined by equation (2.36) it is killed. The full antisymmetric wave function is constructed by reflecting the random walk distribution in the nodal surfaces and changing its sign.

Solutions generated in the manner described above are antisymmetric however there is no guarantee that they will be the lowest energy, physical solutions. There are an infinite number of possible nodal surfaces which could be used to give an antisymmetric distribution, equation (2.35) is but one example. In general the nodes of the physical solution are unknown and they will be complicated by the particle interactions. If the actual nodes could be used as input to the calculation described above, exact results would be obtained. Anderson (1976) suggested that the nodal surfaces of wave functions obtained from variational calculations could be used as boundary conditions for random walks and this idea provides the basis of the fixed node approximation.

The fixed node approximation reduces the problem of treating an antisymmetric wave function having regions of both positive and negative density to a problem involving a positive definite distribution sampling a confined region of space. Positive definite distributions are easily interpreted as probability densities for random walks.

Importance sampling methods can be used to improve the efficiency of the fixed node random walk procedure. The antisymmetric trial function, ψ_T, obtained from variational calculations may involve Slater determinants together with electron correlation factors. Ensemble members drift, diffuse and replicate in the manner described in Section 3.). Now, however, the random walk of a system is terminated when a move causes ψ_T to change sign. Consequently the importance sampled, fixed node procedure samples a

distribution $f = \psi_T\psi$ where ψ is not the exact Fermion ground state wave function, ψ_F, but rather it is best antisymmetric wave function having the nodal surfaces of ψ_T.

It can be shown that the energy estimated from an importance sampled, fixed node quantum Monte Carlo calculation is an upper bound to the Fermion ground state energy (Ceperley (1981) see also Reynolds et al. (1982)). Thus a variational approach could be used to improve the fixed node results. In principle the trial function could contain variational parameters which adjust the positions of the nodal surfaces. In practice, however, nodal sufaces in many dimensions are difficult to parameterise. Kalos (1984) has considered using an idea of Reatto (1984) to optimise nodal surfaces in fixed node calculations.

The basic fixed node approximation has been used by Anderson to study a number of small molecular systems (J.B. Anderson (1976), (1979)) and he and his coworkers have also used importance sampling methods (J.B. Anderson (1980), F. Mentch and J.B. Anderson (1981), J.B. Anderson (1985)). A detailed description of the importance sampled, fixed node procedure has been given by Reynolds et al. (P.J. Reynolds, D.M. Ceperly, B.J. Alder and W.A. Lester, Jr. (1982)) who also considered several small molecules. The method has been applied to study the properties of metallic hydrogen (D.M. Ceperley and B.J. Alder (1981)) and was used as the starting point in a study of the ground state properties of the one component plasma (D.M. Ceperley and B.J. Alder (1980)). The fixed node approximation has been used in connection with the Green's function Monte Carlo approach to calculate the potential energy surface of a small molecule (J.W. Moskowitz, K.E. Schmidt, M.A. Lee and M.H. Kalos (1982)).

b) Nodal Relaxation and Transient Estimation

Ceperley and Alder (1981) devised a means of relaxing the nodal surfaces of an importance sampled fixed node distribution. If the diffusion process begins in an antisymmetric distribution then in principle the antisymmetry should be maintained by an importance sampling random walk which permits diffusion across nodes of the trial function. Since the initial distribution is antisymmetric, it is orthogonal to all states with energy lower than the Fermi ground state and consequently this state should dominate the asymptotic distribution. The ensemble members must now carry a sign so that systems which diffuse across the nodes of ψ_T an even number of times have positive weight, while an odd number of nodal crossings result in negative weights. Changing the sign in this way antisymmetrises the wave function. Asymptotically, the distribution sampled by this process will be $\psi_T\psi_F$, with ψ_F the exact fermion ground state.

There is a serious stability problem with the method described above. In Section 2.) it was observed that a component of the lowest energy state could enter an excited state distribution through fluctuations. Amplification of this noise caused the excited state signal to be buried beneath the ground state at long times. In the same way, a fluctuation of the Boson ground state will grow, and in the long time limit, dominate the distribution sampled by the Fermion random walk outlined above. The rate at which the symmetric noise can build up over the antisymmetric signal will depend on the difference between the Bose and Fermi ground state energies, E_B and E_F respectively. Following Schmidt and Kalos (1984) the evolving wave function containing Fermi and Bose components can be written as

$$\psi(\underline{R}, \tau\to\infty) = e^{-E_F\tau}[a_F\psi_F(\underline{R}) + a_B\psi_B(\underline{R})\ e^{-(E_B-E_F)\tau}] \qquad (2.37)$$

In Section 3.) we saw that with an importanced sampling calculation the energy estimate is obtained from the following

$$E_F(\tau) = \int \psi_T(\underline{R})\hat{H}\ \psi(\underline{R},\tau)d\underline{R} \ / \int \psi_T(\underline{R})\ \psi(\underline{R},\tau)d\underline{R} \qquad (2.38)$$

Since ψ_T, the antisymmetric trial function, and ψ_B are orthogonal, the Bose component in equation (2.37) will not contribute to the energy estimate and $E_F(\tau\to\infty) = E_F$. The symmetric components however will contribute to the variance (Kalos (1981)) which will grow exponentially as $e^{-(E_B-E_F)\tau}$. Provided the inital distribution obtained from the fixed node calculation is close to the true fermion ground state, the nodes may have sufficient time to relax to their actual positions and give an estimate of the true Fermion energy before the noise becomes too severe. For this reason the method is refered to as "transient estimation".

As mentioned earlier Ceperley and Alder (1980) obtained an estimate of the ground state energy of the electron gas using nodal relaxation from a fixed node calculation. Lee, Schmidt, Kalos and Chester (1981), used transient estimation with Green's function Monte Carlo to obtain the ground state energy of liquid ^{3}He. With their approach the energy estimate is always an upper bound of the Fermion ground state energy.

c) System Annihilation for Identical Particles

In Section 2.) we described a procedure for simulating a wave function with nodes. The random walk involved different signed systems which annihilate one another if they enter the same region of space. With many particles, the problem of determining whether two systems occupy the same region of space is complicated if the particles are indistinguishable. For distinguishable particles we may allow two systems of opposite sign to

annihilate if the two sets of labeled coordinates coincide within some tolerence. Thus if systems i and j are of opposite sign they annihilate one another if

$$|\underline{r}_1{}^i - \underline{r}_1{}^j| < \delta, \; |\underline{r}_2{}^i - \underline{r}_2{}^j| < \delta, \ldots, \; |\underline{r}_N{}^i - \underline{r}_N{}^j| < \delta$$

which we can summarize as

$$|\underline{r}^i - \underline{r}^j| < \Delta \tag{2.39}$$

When a system of indistinguishable particles is considered however, the comparison of two configurations must ignore the particle labels. Thus in order to decide whether two systems are in the same region of space we must compare a labeled configuration of one system with all possible configurations of the other system, obtained by permuting the particle labels. Consequently if two systems of indistinguishable particles are of opposite sign they can annihilate one another if a permutation ,P, can be found so that the following condition is satisfied

$$|\underline{r}^i - P\underline{r}^j| < \Delta \tag{2.40}$$

Here the permutation operator ,P, permutes the particle labels in the configuration. The procedure outlined above could in principle be applied directly to simulating a system of identical Bosons.

For systems of Fermions the question of annihilation is more complicated. Fermions may exist in different spin states and further the Fermion wave function must be antisymmetric with respect to the interchange of a pair of identical particles. The first of these features of Fermion systems may be incorporated into the system annihilation step by extending the coordinate space to include spin variables. Spin variables do not

appear in the Hamiltonian so they will be uneffected by the diffusion and birth/death processes in the random walk. With the extended coordinate space, the comparison of two systems is now based on both the spatial configuration and the set of spins of each system. Thus, systems i and j will be in the same region of the extended coordinate space if a permutation operator can be found which causes both the following conditions to be satisfied simultaneously

$$|\underline{r}^i - P\underline{r}^j| < \Delta$$

and (2.41)

$$\underline{s}^i - P\underline{s}^j = 0$$

With a random walk calculation, the wave function is the distribution function for the ensemble of positive and negative systems. Thus the antisymmetry of the Fermion wave function requires that an odd permutation of the particle labels in a particular system should change the sign of the system and an even permutation will leave the sign unchanged. Consequently the antisymmetry requirement determines which systems are able to annihilate one another. Two opposite signed systems will annihilate if an even permutation can be found which causes the conditions in equations (2.41) to be satisfied. Systems of the same sign can also annihilate provided an odd permutation is found which satisfies these conditions.

Since the wave function is antisymmetric, on average there will be equal numbers of positive and negative systems in the ensemble. Suppose that the average total number of systems is n. On average the total number of like and unlike system comparisons which must be made in order to determine all possible system annihilations is thus n(n-1)/2. If there are N particles in each system there will be N!/2 even or odd permutations

which must be considered in each of the above comparisons. The comparison with a particular permutation involves only the evaluation of the square of a distance in 3N dimensional space. Due to the $n^2 \times N!$ dependence, there will be a very large number of these computations for only a modest number of particles.

We have considered a Monte Carlo procedure for sampling the permutation operators and in this way we reduce the N! dependence. The method involves diffusion and replication in the usual way. At the end of each time step all possible cancelations are considered. Spin coordinates are included and the particles must be distinguished by labels. Thus opposite signed systems i and j can annihilate if

$$|\underline{r}^i - \underline{r}^j| < \Delta$$

and

$$\underline{s}^i - \underline{s}^j = 0$$

The particle indistinguishability is accounted for by including an antisymmetrization procedure at the end of each time step. In this procedure a randomly selected permutation operator is applied to each system. The labels on both the space and spin coordinates are permutated and, depending on the parity of the applied operator, the sign of the system is appropriately changed.

The procedure outlined here assumes that the time scale for the diffusion and birth/death processes is slow. Thus systems which are capable of annihilation remain in the same volume long enough for the necessary permutation operator to be sampled by the Monte Carlo method. The assumption is very reasonable for systems containing a few particles and may prove useful with larger systems.

d) Spin States of Atomic Helium and Lithium

The method for treating systems of Fermions described above has been applied to the lowest energy states with different spin multiplicity in helium and the ground state of the lithium atom. We assume a nucleus with charge Z and infinite mass fixed at the origin so in atomic units the Hamiltonian for the N electron system can be written as follows

$$\hat{H} = -\tfrac{1}{2} \sum_{i=1}^{N} \nabla_i^2 + V(\underline{r})$$

with

$$V(\underline{r}) = \sum_{i<j}^{N} \frac{1}{r_{ij}} - \sum_{i=1}^{N} \frac{Z}{r_i}$$

Here $r_i = (x_i^2+y_i^2+z_i^2)^{\frac{1}{2}}$ and $r_{ij} = \left((x_i-x_j)^2+(y_i-y_j)^2+(z_i-z_j)^2\right)^{\frac{1}{2}}$. The electrons were allowed to diffuse in 3N dimensional space and each system replicated or died depending on its potential energy, $V(\underline{r})$. Electrons entering a small sphere about the nucleus experienced the averaged nuclear attraction discussed in Section 2.). A V_{ref} adjusting procedure was used to keep the total number of positive and negative systems approximately constant.

The position of each system represented a centre of Gaussian density in 3N dimensions as described in Section 2.) and the error function annihilation probability given in equation (2.28) was used. Pairs of opposite signed systems could only annihilate if they also had the same sets of labeled spins. At the end of each time step the Monte Carlo antisymmetrization process described in the previous subsection was implemented. For helium there are only two permutation operators to be considered: The identity, an even operator which leaves the particle labels unchanged, and the odd operator which exchanges the particle labels. The

Monte Carlo antisymmetrization for the two electron system thus involves exchanging the particle labels in half the systems of the ensemble at the end of each time step.

The singlet state of helium involves a pair of identicle particles having different spins. Thus the singlet state could be studied by considering the particles as distinguished by their spins. This approach is equivalent to performing a fixed node calculation. For the singlet state the node is in the spin part of coordinate space and its position is known exactly, $s_1 = s_2$. Rather than using this simplifying feature of the singlet state and performing a random walk with only positive systems on one side of the node, we have used opposite signed systems as described above.

An equal number of positive and negative systems were used as the initial condition for our simulation. The particles in each system were positioned at random within a cube centered on the origin. Initially all systems had particle 1 with spin up and particle 2 with spin down.

Figure 2.9 shows projections of the singlet state wave function obtained from this calculation. Two dimensional histograms of the distributions of distances of the two labeled electrons from the nucleus are presented. After equilibration, separate histograms for positive and negative systems were accumulated and appear as Figures 2.9a and 2.9b respectively. The histograms represent the different signed lobes of the function

$$\psi_o(r_1,r_2)\ r_1^2 r_2^2.$$

An examination of the distribution of labeled spins in several instantaneous equilibrated ensembles indicated that all the positive systems had particle 1 with spin up and particle 2 with spin down. All the

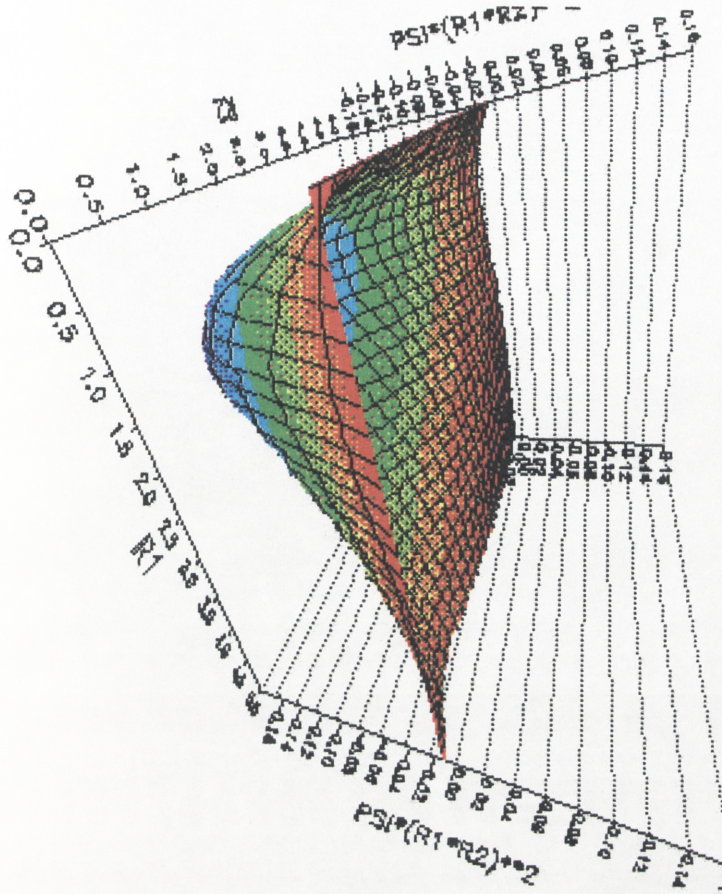

fig. 2.9 a

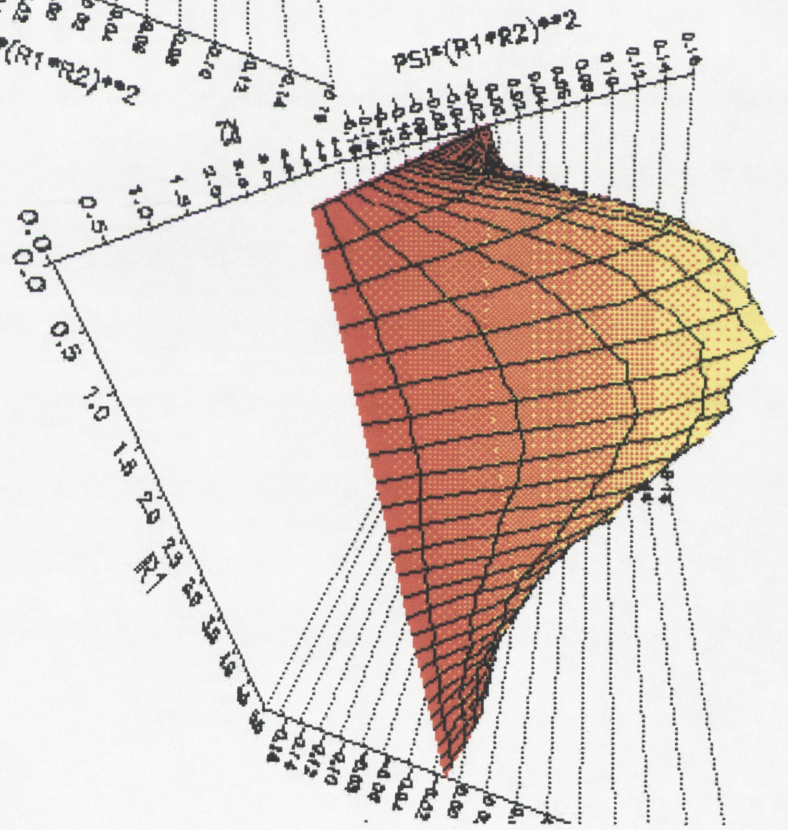

fig. 2.9 b

fig. 2.10 b

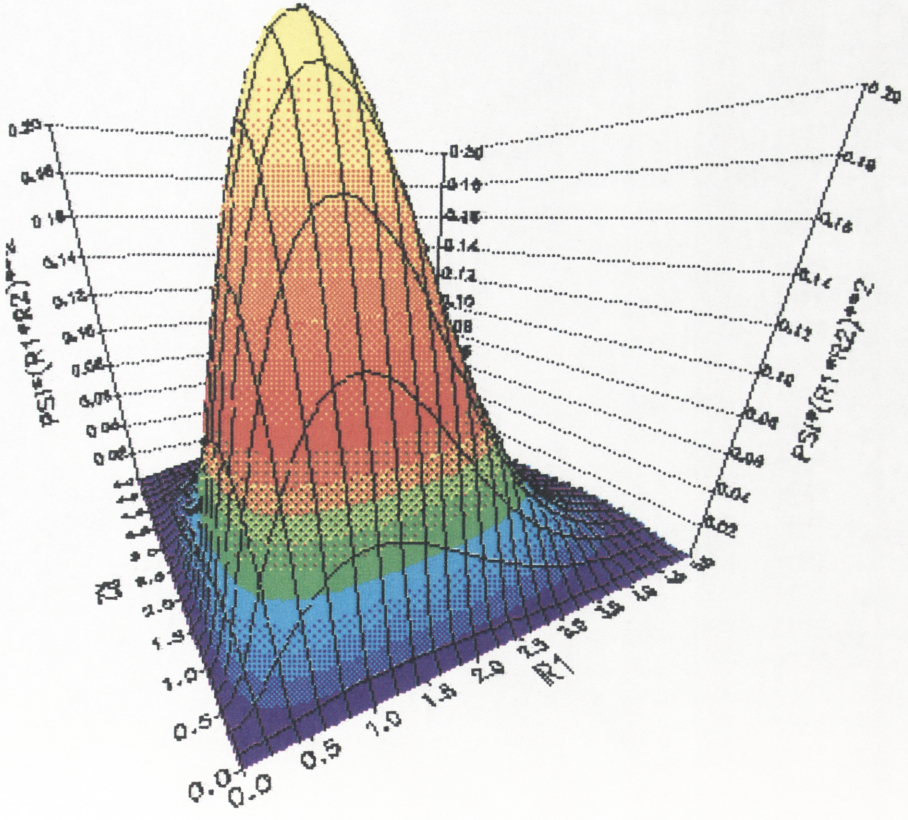

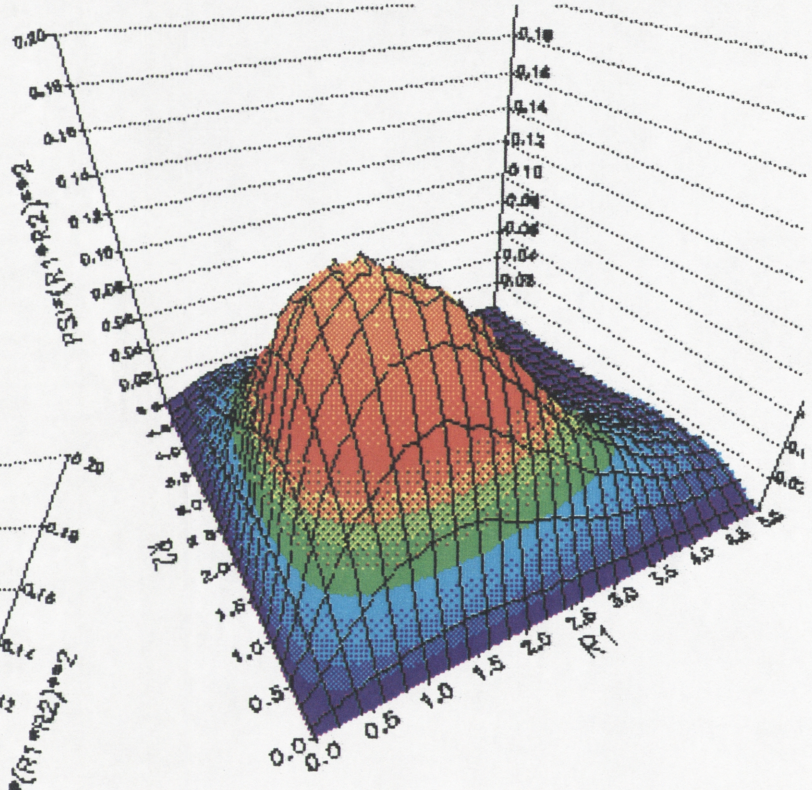

fig. 2.10 a

negative systems were found to have the permuted set of labeled spins. In this way the positive and negative systems could exist in the same region of configuration space without annihilating one another. Once this situation is established, no more annihilations can occur since a label permutation will change the sign of the ensemble member. The result is thus the propagation of two independent, opposite signed, ground state distributions.

Within the independent electron approximation the antisymmetrized singlet state eigenfunction for the helium atom can be written in terms of the hydrogenic wave function as follows

$$1s(1)1s(2)\ \left[\alpha(1)\beta(2)-\beta(1)\alpha(2)\right]$$

Here α and β are the spin eigenfunctions and the 1s wave function has the form

$$1s(r) = e^{-Zr}$$

The opposite signed terms in the above result approximate the two lobes of the ensemble distribution. Effects of electron interaction can be estimated within the independent electron approximation by variational calculations which use the nuclear charge as a parameter. The best variational wave function using hydrogenlike orbitals is compared with the quantum random walk result in Figure 2.10. The differences between the variational (Figure 2.10b) and quantum Monte Carlo (Figure 2.10a) wave functions result from the fact that correlations between the motions of the electrons are ignored in the assumed variational form. The quantum Monte Carlo calculations include the electron correlation exactly.

In Table 2.3 we summarize the singlet state energy predicted by

different approximations and compare these values with the best quantum Monte Carlo result. The essentially exact result of Pekeris (1959) was obtained using a variational form which allowed for electron correlation. The quantum Monte Carlo value is lower than the results obtained using the independent electron approximation.

Tabel 2.3 Ground State Energies of Helium Atom

Wave function	Energy (au)
Product of He^+ orbitals	-2.7501[1]
Product of hydrogenlike orbitals optimized by SCF method	-2.8425[1]
Best independent electron wave function	-2.8619[1]
Random Walk	-2.8770
Pekeris (1959)	-2.9037

[1]These values are taken from Lowe (1978)

The triplet state of the helium atom may be simulated in a similar fashion. Now, however, both particles are given the same spin and systems should thus annihilate more often. For the singlet state we saw that the annihilation step was only effective in modifying the initial condition so that two non-interacting ground state distributions could be established. With the triplet state, however, annihilations will continue in the equilibrated ensemble and the extra deaths which occur at the spatial node will contribute to the eigenvalue estimate.

In Figure 2.11 we present the eigenvalue, calculated from the average

fig. 2.11

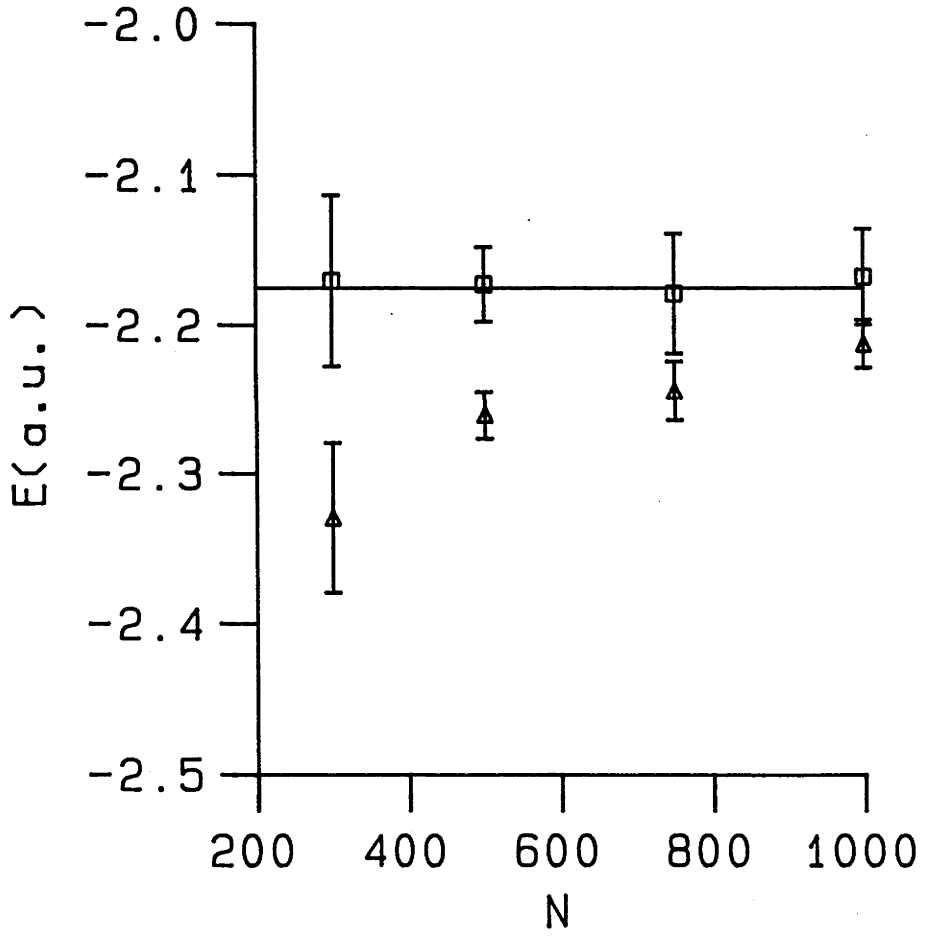

of V_{ref}, as a function of the total number of systems in the ensemble. The two curves are the results obtained with different values of the Gaussian width parameter. Opposite signed systems may avoid one another when the systems occupy only small volumes of configuration space (a = 5 a.u.$^{-2}$ for example) and there are too few systems in the ensemble. Under these circumstances annihilation at the nodes will be ineffective and the eigenvalue obtained from the death rate of the population, is underestimated. As the number of systems in the ensemble is increased the calculated eigenvalue tends asymptotically to an estimate of the energy of the system.

The accuracy of the asymptotic estimate is determined by the size of the volume element occupied by each system. With larger systems the asymptotic convergence with increasing number of systems is faster. For a = 2 a.u.$^{-2}$ the energy estimated is converged at 300 systems. Beyond this point the eigenvalue estimates obtained with different numbers of systems are consistently about 0.5% higher than the value of -2.175 a.u. reportedly Pekeris (1959). This systematic error results from the coarse resolution of the configuration space due to the finite volume occupied by the systems.

The triplet state wave function obtained from the quantum Monte Carlo calculation is presented in Figure 2.12a. Separate two dimensional histograms for the positive and negative ensembles were again accumulated. In the figure we present the full triplet state wave function constructed as the sum of the positive and negative ensemble distributions. From Figure 2.12a it is apparent that the annihilation procedure has successfuly established a nodal surface corresponding to $r_1 = r_2$.

In the independent electron approximation the triplet state has the following form

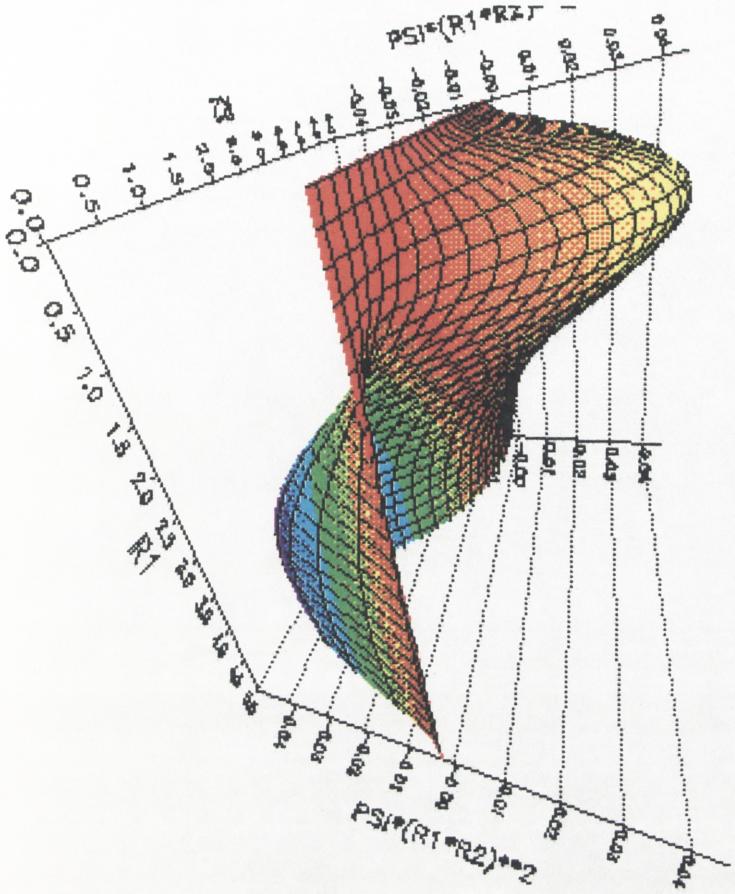

fig. 2.12 b

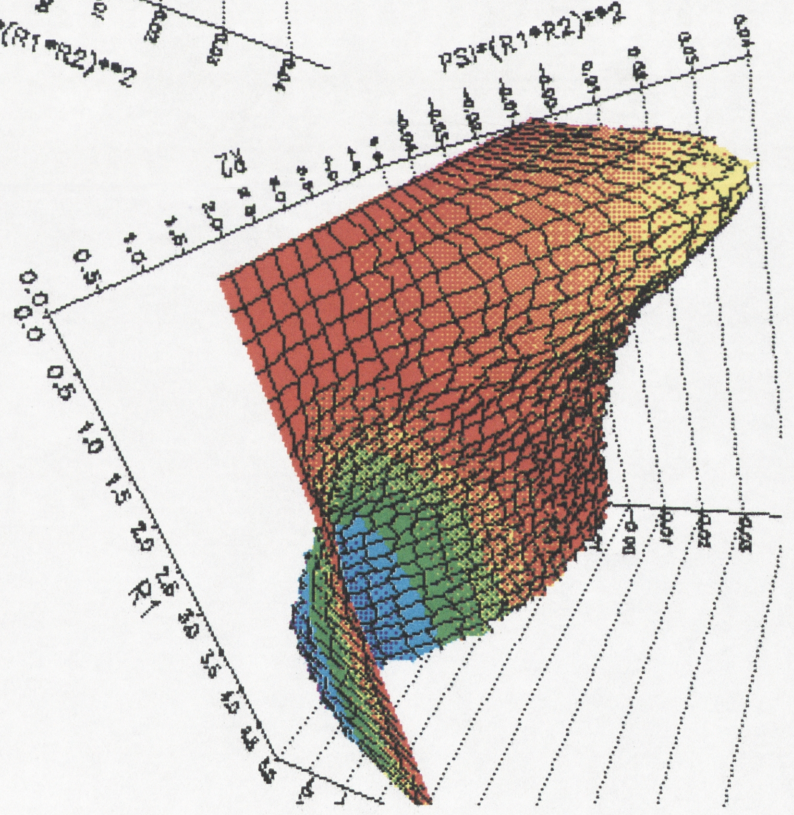

fig. 2.12 a

$$\left(1s(1)2s(2) - 1s(2)2s(1)\right)\alpha(1)\alpha(2)$$

Here the 2s hydrogenic function is

$$2s(r) = (2-r)e^{-Zr/2}$$

The best SCF approximate triplet state eigenfunction having this form is presented in Figure 2.12b. Comparing this function with the exact quantum Monte Carlo generated distribution we see that the neglect of electron correlation gives a wave function which is too strongly peaked.

As a final example which demonstrates how the permutation operator sampling scheme works for more complicated systems we have considered simulating the lithium atom.

There are six different permutation operators for the three particle system which are summarized in Table 2.4

Table 2.4

operator	exchange decomposition	result
P_1	1	123
P_2	(12)(13)	312
P_3	(12)(13)	231
P_4	(12)	213
P_5	(13)	321
P_6	(23)	132

P_1 is the unit operator which leaves the particle lables unchanged. The

parity of a permutation operator is determined by the number of exchanges into which the permutation can be decomposed. If there are an even number of exchanges the operator is even. Thus in Table 2.4 P_1, P_2 and P_3 are even operators while P_4, P_5 and P_6 are odd. When each of the above operators is applied from the left to the ordered triple 123 the result indicated is obtained.

The procedure for simulating the lithium atom is identical to that described above for helium. Now, however, after the systems of labeled particles have diffused, replicated and annihilated, we permute the particle labels in each system by applying one of the six operators selected at random and change the sign of the system depending on the parity of the operator.

In Figure 2.13 we present some preliminary results obtained for the lowest energy doublet state of the lithium atom. The figure shows the convergence of the eigenvalue estimate as a function of the number of time steps. Relaxation from the initial uniform cube of electron density is demonstrated. The points are the results of averaging V_{ref} over each block of 5000 time steps. Fairly coarse resolution ($a = 2$ a.u.$^{-2}$) and an ensemble of 1000 systems were used in this calculation the eigenvalue estimate obtained by averaging over the last 100 a.u. of the quantum Monte Carlo run is -7.488 ± 0.045 a.u. in excellent agreement with the observed value -7.4820 a.u. obtained from the sum of the ionization energies (Weast (1983)).

fig. 2.13

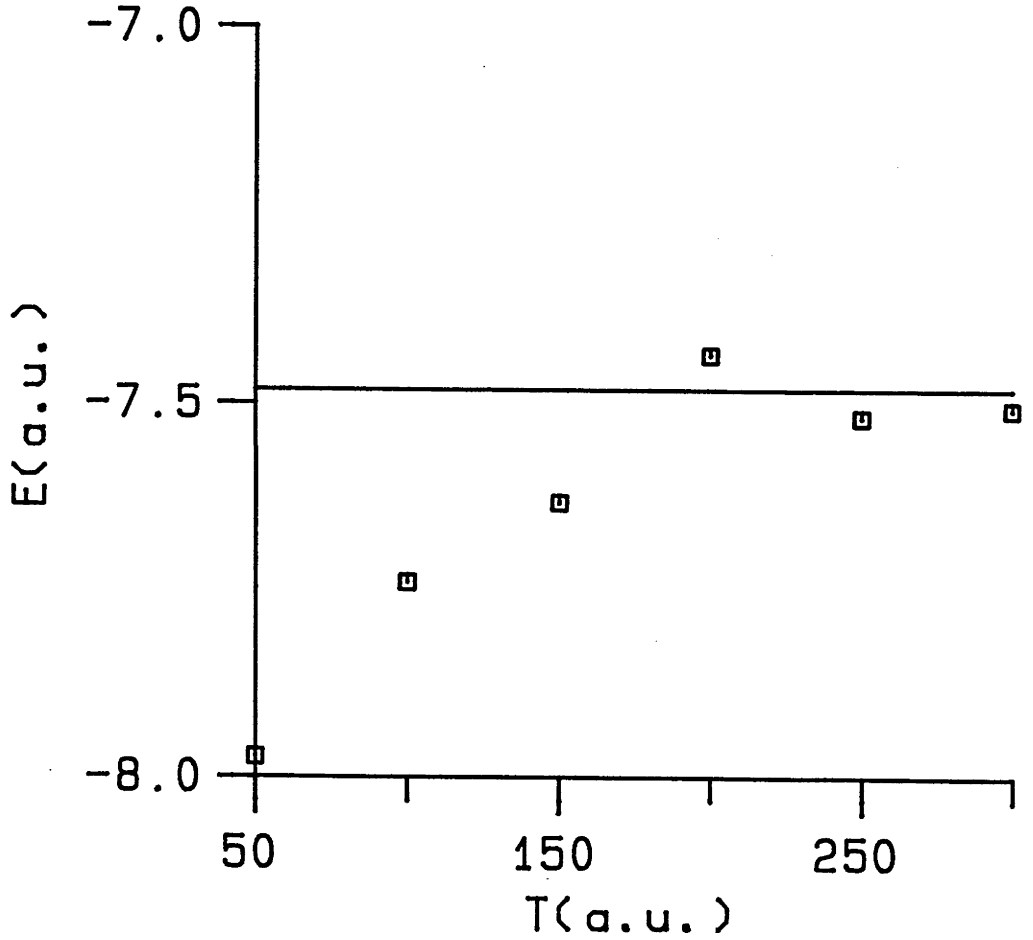

Conclusion

In this chapter we have described the basic random walk methods which will be employed in subsequent chapters to study the ground state properties of small molecular clusters and bulk phase quantum systems including solid H_2 and liquid ^4He. The random walk approach discussed in this chapter will also be extended to treat quantum systems at finite temperatures in the final chapters of the thesis.

The important development presented in this chapter is the method for treating many body wave function having nodal surfaces. We have seen that accurate energies can be calculated for systems involving a few Fermions. These calculations are completely ab initio and do not require the input of a trial wave function. Nodal surfaces are generated by the approach and a stable Fermion wave function may be obtained.

In the form presented here the method is probably restricted to treating only a few Fermions. When a large number of permutation operators must be considered, comparing systems in order to determine annihilation probabilities will become excessively time consuming. Sampling the permutation operators with a Monte Carlo procedure may be useful for many electron problems.

Wave functions having nodal surfaces which require high resolution due to rapid changes in the wave function density in the region of the node also present significant problems for our approach. Systems occupying very small volumes of configuration space must be used in these calculations and the asymptotic eigenvalue estimate can only be obtained with a very large number of small systems.

Arnow, Kalos, Lee and Schmidt (1982) have described an extension to the

Green's function Monte Carlo method which enables systems of a few Fermions to be treated exactly. The method involves sampling from a "pair Green's function" which produces positive and negative components in the ensemble. This method also seems to have problems with extension to systems of more particles.

Recently Öksüz (1984) has presented a related method which involves performing a random walk using an antisymmetrized position basis and this approach may over come some of the problems described above.

CHAPTER 3 VIBRATIONAL SPECTROSCOPY OF MOLECULAR CLUSTERS OBTAINED FROM QUANTUM RANDOM WALKS

1.) Conventional Vibrational Spectroscopy of Isolated Molecules, Normal and Local Modes

Intramolecular vibrations in general must be studied using quantum methods (Wilson, Decius and Cross (1955)). It should be possible to use the quantum Monte Carlo methods described in Chapter 2 to obtain information about molecular vibrations. In the later sections of this chapter we develop such a method and use it to calculate the intramolecular vibrational spectra of the water dimer and trimer. Before considering the development of this method, however, it is instructive to outline the more conventional techniques for studying the vibrations of molecules.

The most widely used procedures of vibrational analysis are the normal and local mode methods (Wilson, Decius and Cross (1955), Reimers and Watts (1984a)). These techniques approximate the molecular Hamiltonian by a reference system which can be solved analytically. The approximations are taken into account by variational or perturbation calculations which use the eigenfunctions of the reference state.

The logical starting point for both techniques is the Born Oppenheimer approximation. It is assumed that the rapid electronic motions produce an average potential surface over which the slower nuclear motions occur and the resulting Hamiltonian depends only on nuclear coordinates. Translational degrees of freedom are removed by transforming to the centre-of-mass frame. The final simplification common to both methods is

the rigid rotor approximation in which coriolis and centrifugal couplings between the vibrations and rotations are ignored. Using this approximation the Hamiltonian can be written as a sum of vibrational and rotational parts.

$$H = H^v + H^r \tag{3.1}$$

H^v contains relative coordinates of the atoms, while H^r has only angular variables which describe how the rigid rotor tumbles about its principle axes. Both methods now proceed by approximating the potential operator and it is at this point that the normal and local mode theories begin to differ. We shall consider first the approach taken in normal mode analysis.

In normal mode theory the potential is expanded as a Taylor series in small cartesian displacements about the minimum energy geometry. Quadratic terms in this expansion, together with the kinetic energy terms, are used to define a harmonic oscillator reference Hamiltonian for the vibrational part of the problem, H_o^v. This Hamiltonian is easily diagonalized; the eigenvalues are related to the squares of the normal mode vibrational frequencies, ω_k, and the eigenvectors define the normal mode coordinates, Q_k, which give the direction of the vibrational distortion of the molecule. In these coordinates the vibrational reference Hamiltonian describes a set of 3N-6 decoupled harmonic oscillators

$$H_o^v = \tfrac{1}{2} \sum_k^{3N-6} \left(\frac{\partial^2}{\partial Q_k^2} + \omega_k^2 Q_k^2 \right) \tag{3.2}$$

Here N is the number of atoms in the molecule. The eigenfunctions of this Hamiltonian are products of the hermite polynomials in the normal mode coordinates and we shall represent these eigenfunctions as $|\underline{n}_v\rangle$ where $\underline{n}_v$ is a vector of quantum numbers describing the vibrational excitation of the

different normal modes.

In a similar fashion, if we assume that the molecule can be represented as a rigid symmetric top the reference Hamiltonian for the rotational part of the problem, H_o^r, also has analytic eigenvalues and the eigenfunctions are the spherical harmonics which we shall represent as $|\underline{n}_r\rangle$. The total Hamiltonian of the reference problem is now written as

$$H_o = H_o^v + H_o^r$$

and the eigenfunctions and eigenvalues of this Hamiltonian are respectively

$$|\underline{n}\rangle = |\underline{n}_v\rangle|\underline{n}_r\rangle$$

and

$$\varepsilon_{\underline{n}} = \varepsilon_v + \varepsilon_r$$

The complete molecular vibration-rotation problem is solved by using the analytic solutions of the reference problem as a basis for a variational calculation (Whitehead and Handy (1975)). The total Hamiltonian is written as a sum of the reference system Hamiltonian and a perturbation operator

$$H = H_o + \Delta H, \qquad \Delta H = T_{cc} + \Delta V$$

Here ΔH contains the terms which were ignored in simplifying the Hamiltonian, such as the coriolis and centrifugal couplings, T_{cc}, and the anharmonic terms in the Taylor series expansion of the potential $\Delta V = V - \frac{1}{2}\sum\omega_K{}^2 Q_K{}^2$. An accurate approximation for the coriolis and centrifugal coupling terms which was given by Darling and Dennison (1940) is often used and the full Hamiltonian matrix in the reference system basis is calculated

$$H_{\underline{mn}} = \langle\underline{m}|H|\underline{n}\rangle = \delta_{\underline{mn}}\varepsilon_{\underline{m}} + \langle\underline{m}|\Delta H|\underline{n}\rangle$$

and, in principle, may be diagonalized to give the eigenvalues. The integrals of the hermites with many different functions are analytic but numerical integration procedures for more complicated perturbation operators can be devised (Whitehead and Handy (1975)).

The major problem with the approach outlined above is that the matrix elements of the perturbation operator must be small compared with the eigenvalues of the reference system otherwise the variational calculation may not converge. For molecular systems the anharmonic terms in ΔH are often large and convergence problems are encountered.

With local mode theory an attempt is made to include a major part of the potential anharmonicity in the reference Hamiltonian so the perturbation operator will be small and the variational calculation will converge rapidly. To proceed the local coordinates must first be chosen as in general there is no unique set of coordinates which will completely describe anharmonic vibrations. This is contrasted by the situation in normal mode theory where a unique set of normal modes result because of the assumed harmonic form of the potential operator. When a molecule vibrates it distorts so as to stretch its bonds and bend its bond angles. Thus the curvilinear coordinate system consisting of the set of bond lengths and bond angles which describe the equilibrium geometry (the valence coordinates) is probably the best coordinate system for specifying the intramolecular potential surface. The Hamiltonian can be written in a curvilinear coordinate system (Wallace (1975)), however the kinetic operator becomes very complicated. To alleviate this problem a rectilinear coordinate system which approximates the curvilinear coordinates is used. A set of rectilinear coordinates which is often used (Wilson, Decius and Cross (1955)) is defined by the first term in the multidimensional Taylor

series expansion of the valence coordinates $\underline{R}$ in cartesian displacements $(\underline{r}-\underline{a})$ about some reference geometry $\underline{a}$.

$$\underline{R} = \underline{B} \cdot (\underline{r}-\underline{a}) + C : (\underline{r}-\underline{a})\,(\underline{r}-\underline{a}) + \ldots$$

The rectilinear coordinates, $\underline{S}$, are thus defined by the following expression

$$\underline{S} = \underline{B} \cdot (\underline{r}-\underline{a}) \qquad (3.5)$$

The reference configuration is chosen subject to the Eckart conditions (Eckart (1935)) so that the coordinate frame rotates with the molecule and its origin is on the centre of mass.

In these coordinates the vibrational kinetic operator can be expressed in a matrix form due to Wilson (1939) and the rotational kinetic operator in the $\underline{S}$ coordinates may also be derived (Reimers and Watts (1984a)). The full Hamiltonian is thus written in the following form

$$H = \tfrac{1}{2} \sum_{i,j} G_{ij} P_i P_j + T_{rot} + T_{cc} + V(\underline{R}) \qquad (3.6)$$

Here the Wilson $\underline{G}$ matrix contains the particle masses and reference geometry while the operator $\underline{P}$ is the momentum conjugate to the $\underline{S}$ coordinates.

In local mode theory the kinetic operator in the above Hamiltonian is simplified in two ways: first, the rigid rotor approximation is made and second, the off diagonal elements of the G matrix are ignored so that the kinetic operator of the vibrational reference system is diagonal in the $\underline{S}$ coordinates. Next, the potential operator must be simplified and this is done by assuming that the full potential in the valence coordinates can be approximated by a set of decoupled anharmonic oscillators in the

rectilinear coordinates. Thus local mode theory uses a more accurate, anharmonic, functional form for the potential energy and in this way the important anharmonic terms may be included in the reference Hamiltonian. The potential function due to Morse (1929) (see also ter Haar (1946)) is a very useful form for this purpose as its eigenvalues and eigenfunctions are analytic and it models the anharmonic intramolecular interactions rather well. The vibrational reference Hamiltonian in local mode theory is thus

$$H_o^V = \sum_{j=1}^{3N-6} \left(\tfrac{1}{2}G_{jj}P_j^2 + V_j(S_j)\right) \qquad (3.7)$$

If the Morse potential is used to approximate anharmonic interactions the potential term in equation (3.7) takes the form

$$V_j(S_j) = D_j\left(e^{-\alpha_j S_j} - 1\right)^2 \qquad (3.8)$$

The eigenvalues of the vibrational reference Hamiltonian are analytic (Morse (1929)) and the vibrational eigenfunctions, $|\underline{n}_V\rangle^{(m)}$, are products of generalized Laguerre polynomials in each of the 3N-6 S coordinates. Now the vector quantum number, $\underline{n}_V$, describes the excitation of the local modes of the molecule.

The complete reference system is defined by the Hamiltonian

$$H_o = H_o^{V(m)} + H_o^r$$

and the eigenfunctions and eigenvalues

$$|\underline{n}\rangle = |\underline{n}_V\rangle^{(m)}|\underline{n}_r\rangle \qquad \varepsilon_{\underline{n}}^m = \varepsilon_{\underline{n}_V}^m + \varepsilon_{\underline{n}_r}$$

are used as the basis of a variational calculation. As with normal mode theory the matrix elements of the full Hamiltonian become

$$H_{\underline{mn}} = \langle \underline{m}|H|\underline{n}\rangle = \langle \underline{m}|H_o+\Delta H|\underline{n}\rangle$$

$$= \delta_{\underline{mn}}\varepsilon_{\underline{m}}^{(m)} + \langle \underline{m}|\Delta H|n\rangle$$

Now, however, the perturbation operator contains the vibration-rotation coupling, the off diagonal elements of the kinetic operator in the rectilinear coordinates, and the difference between the intramolecular potential in the valence coordinates and the assumed diagonal form in the rectilinear coordinates so that

$$\Delta H = T_{cc} + \tfrac{1}{2}\sum_{i\neq j} G_{ij}P_iP_j + V(\underline{R})-\sum_{\ell}V_{\ell}(S_{\ell}) \qquad (3.9)$$

To obtain the Hamiltonian matrix it is necessary to evaluate the integrals of the various terms in the perturbation operator with the Morse oscillator basis set. The integrals of the off diagonal terms in the kinetic operator are analytic (Watson, Henry and Ross (1981)). In general, however, integrals of the coriolious and centrifugal coupling operator and other complicated functions of the $\underline{S}$ coordiantes must be performed numerically. Reimers and Watts (1984a) have developed a useful numerical procedure for performing these integrals with the Laguerre basis set.

2.) Application of Conventional Vibrational Spectroscopy: An Improved Potential Surface for the Water Monomer

Reimers and Watts (1984) have described in detail how local mode variational calculations can be used to determine a potential surface for the intramolecular interactions of the water monomer. The procedure is simple; a parameterised form for the potential surface $V(\underline{R})$ is chosen, and

this is used in a local mode variational calculation to obtain a model vibrational spectrum. The potential parameters are adjusted to give good agreement between the model spectrum and that obtained from experiment.

Reimers and Watts used this procedure to fit a potential surface which was designed to show rapid convergence of the local mode basis for the water molecule. Their potential takes the form of a sum of three Morse potentials in the radial and tangential components of the valence coordinates of the water molecule so that

$$V(s_1,s_2,s_3) = \sum_{i=1}^{3} V_i(s_i) \tag{3.10}$$

where the Morse potential V_i is the two parameter form given in equation (3.8) and the s coordinates and defined as

$$\begin{aligned} s_1 &= R_1 \cos\left[\tfrac{1}{2}(\theta-\theta_0)\right] - R_0 \\ s_2 &= R_2 \cos\left[\tfrac{1}{2}(\theta-\theta_0)\right] - R_0 \\ s_3 &= \left(\frac{R_1+R_2}{R_0}\right) \sin\left[\tfrac{1}{2}(\theta-\theta_0)\right] \end{aligned} \tag{3.11}$$

Here R_0 and θ_0 are equilibrium bond length and bond angle respectively while R_1, R_2 and θ are the instantaneous values of these variables. The s_1 and s_2 coordinates describe motions resembling stretches of the two O-H bonds in the water molecule. Distortions along the s_3 coordinate are similar to angle bending motions. As the s_1 and s_2 coordinates are equivalent there are two unique Morse potentials and the model potential surface contains only four parameters $D_1 = D_2$, D_3, $\alpha_1 = \alpha_2$ and α_3. Reimers and Watts determined these parameters by fitting to 37 observed vibrational band origins for H_2O, 9 for D_2O and 10 for HDO. It was found that overall a

good representation of these levels could be obtained, but that the splitting between the symmetric and antisymmetric bond stretching vibrations was incorrectly described.

For the reference system, the two decoupled OH stretch motions are degenerate. The perturbation operator contains terms which couple the stretching coordinates. When the variational calculations are performed the degeneracy is lifted and it is found (Coker, Reimers and Watts (1982)) that the coupled stretching motions are best represented by almost pure symmetric and antisymmetric combinations of the local O-H stretch basis functions. Thus the degeneracy in the reference problem is split by the perturbations. The situation is analogous to that found in normal mode calculations on the water monomer. In this case symmetric and antisymmetric normal modes arise naturally as the coordinates in which the kinetic and harmonic potential operators are simultaneously diagonalised. The failure of the potential form used by Reimers and Watts to reproduce the experimentally observed splittings results because the form neglects explicit coupling between the local mode oscillators.

As a starting point for the present calculations, a harmonic coupling interaction between s_1 and s_2 has been introduced, specifically to account for the incorrect splitting of the O-H stretching modes. Thus the modified potential surface takes the form

$$V(s_1,s_2,s_3) = \sum_{i=1}^{3} V_i(s_i) + f_{12}s_1s_2 \qquad (3.12)$$

The coupling term can be easily included in the perturbation operator. Integrals of the form $\langle \underline{n}|s_1s_2|\underline{m}\rangle$ are analytic and a general expression for these terms has been given by Heaps and Herzberg (1952).

In order that the modified potential has the correct dissociation

behaviour the coupling term was multiplied by a switching function similar to that used by Ben-Naim and Stillinger (1972) which has the following form

$$S(r) = 1 - \begin{cases} 0 & r<R_1 \\ \dfrac{(r-R_1)^2(3R_2-R_1-2r)}{(R_2-R_1)^3} & R_1 \leq r<R_2 \\ 1 & R_2 \leq r \end{cases}$$

where $r = (s_1+s_2)^{\frac{1}{2}}$, $R_1 = 2$ a.u. and $R_2 = 3$ a.u.

The monomer analysis of Reimers and Watts has been repeated, and the Morse parameters, and f_{12}, adjusted to give a good fit to experimental band origins for the H_2O and D_2O monomers. A basis set with 120 morse oscillator eigenfunctions corresponding to up to 5 quanta of excitation in the molecule was used and gave well converged eigenvalues. Results from the analysis are compared with experiment and the values obtained by Reimers and Watts in Table 3.1 and Figures 3.1 and 3.2. From Figure 3.1 it is seen that there is a much improved representation of the splitting between the symmetric and antisymmetric stretching modes when coupling between the stretches is introduced. In Figure 3.2 we present the difference between the calculated and observed frequencies as a function of frequency for the Reimers-Watts potential and the modified form. Generally as the frequency is increased the divergence between the calculated and observed results becomes larger. This indicates that the Morse potential provides the best representation around the minimum. The range of deviations for the Reimers-Watts surface is about 100 cm^{-1} and the modified potential form seems to overestimate the frequencies, by about 40 cm^{-1} at worst.

Parameters used in the modified potential are

fig. 3.1

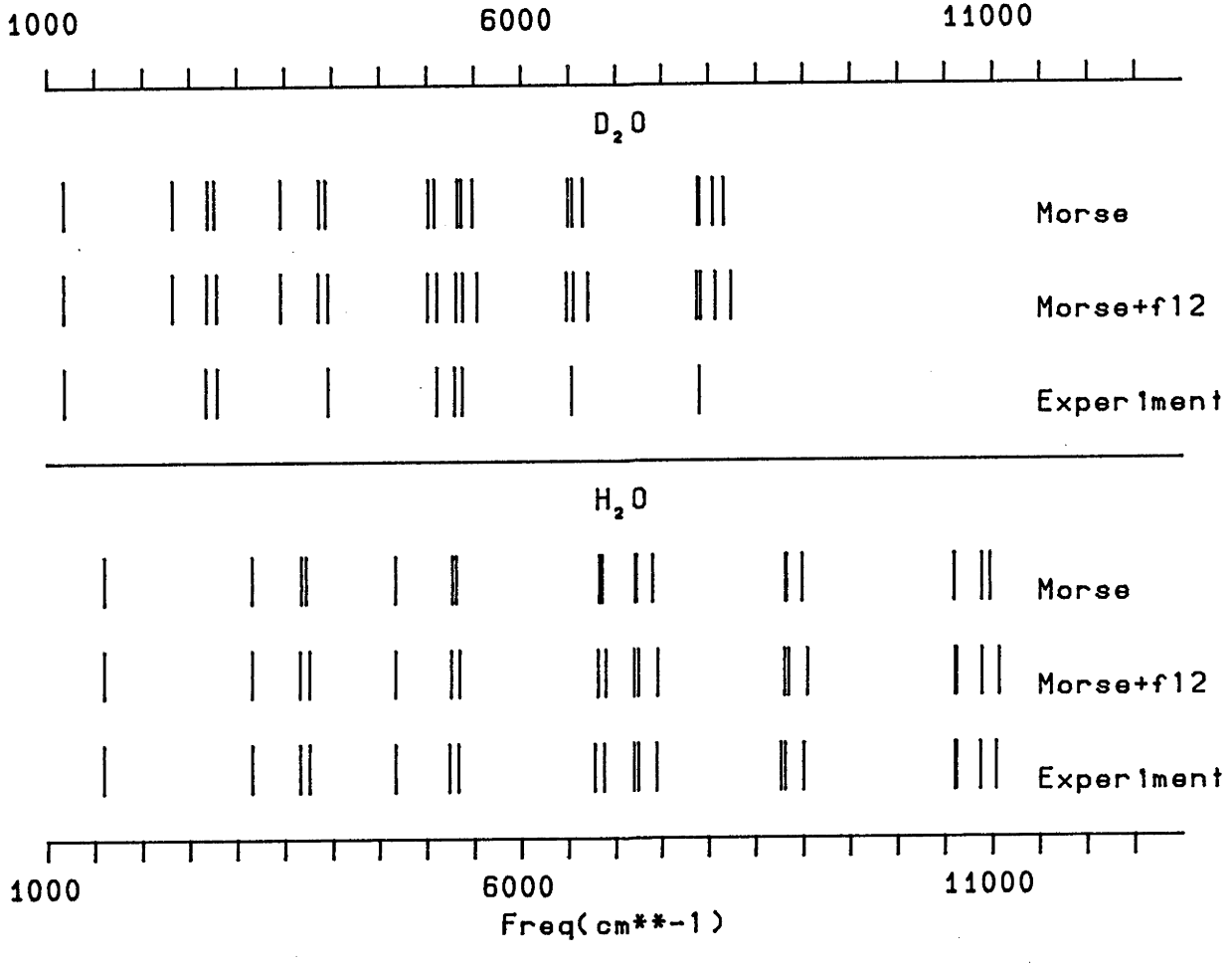
1000
6000
11000
D2O
Morse
Morse+f12
Experiment
H2O
Morse
Morse+f12
Experiment
1000
6000
11000
Freq(cm**-1)

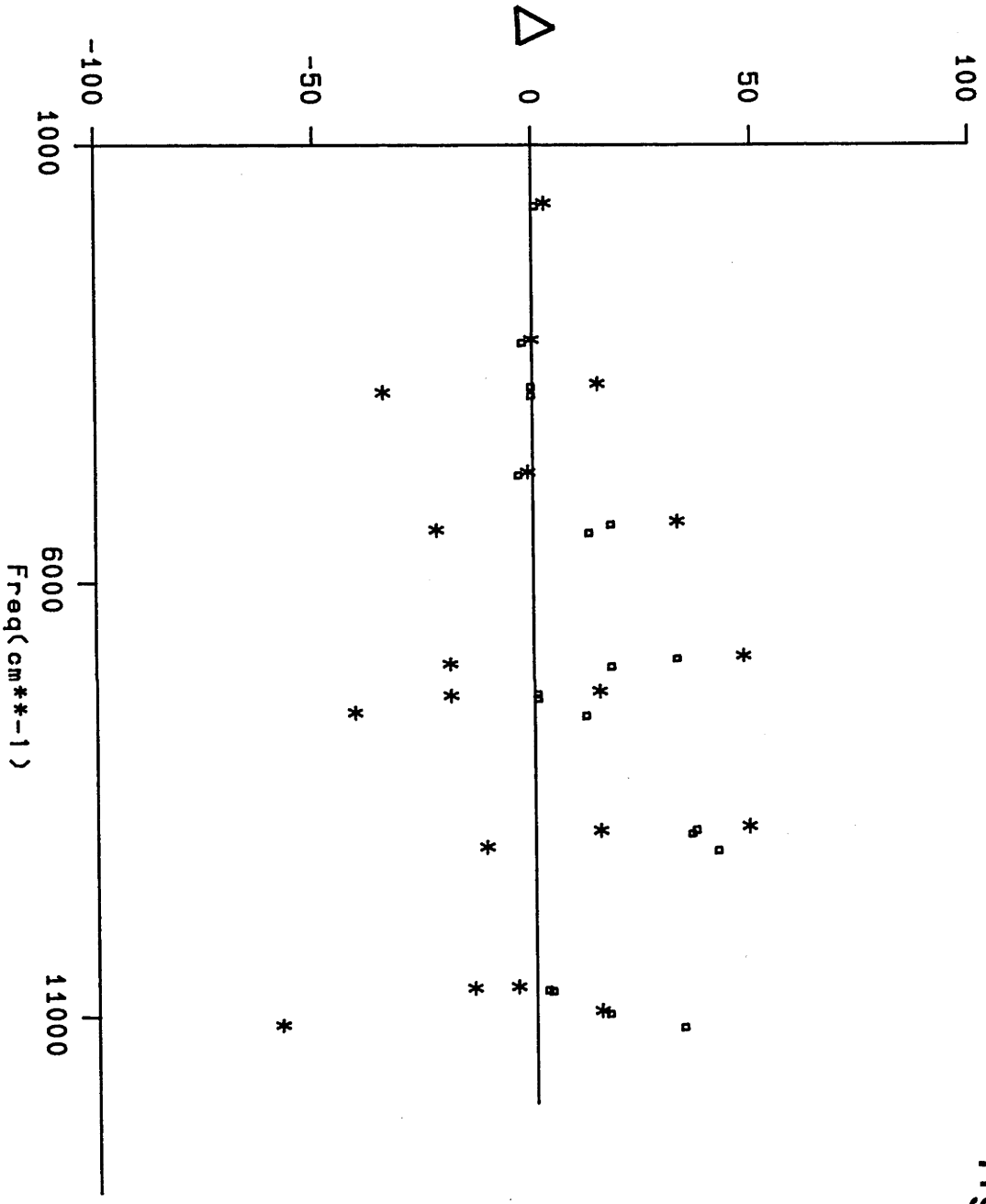

fig.3.2

$D_1 = D_2 = 549.5196$ kJ mole^{-1}

$D_3 = 411.4368$ kJ mole^{-1}; $f_{12} = -63.444$ kJ mole^{-1} Å^{-2}

$\alpha_1 = \alpha_2 = 2.14125$ Å^{-1}; $\alpha_3 = 0.70600$

It should be noted that the value for the f_{12} constant which couples the s_1 and s_2 local modes is similar to the normal mode force constant obtained by Kuchitsu and Morino (1965), (1966). Their value for the constant $k_{rr'}$ which couples the two O-H bond extensions is -60.8323 kJ mole^{-1}Å^{-2}.

Table 3.1 Vibrational frequencies (in cm^{-1}) for the H_2O and D_2O monomers predicted by the Reimers-Watts and present potential surfaces. Assignment is based on local mode quantum numbers described by Reimers and Watts (1984a). The experimental values were taken form this paper.

	H_2O			D_2O		
Assignment	Experiment	Present	R.-W.	Experiment	Present	R.-W.
001	1595	1595	1595	1178	1173	1173
002	3152	3149	3149		2324	2324
100s	3657	3656	3669	2672	2679	2688
100a	3756	3755	3719	2788	2785	2758
003	4667	4663	4663		3456	3453
101s	5235	5252	5265		3852	3861
101a	5331	5343	5306	3956	3956	3929
102s	6775	6807	6820		5004	5013
102a	6872	6889	6850	5105	5106	5076
200s	7201	7201	7213	5292	5307	5322
200a	7250	7250	7228	5374	5380	5363
110	7445	7456	7401		5533	5583
201s	8762	8798	8808		6481	6496
201a	8807	8842	8819	6533	6552	5634
111	9000	9041	8986		6703	6652
300s	10600	10602	10593		7875	7887
300a	10613	10616	10596	7900	7915	7902
210s	10869	10885	10881		8071	8045
210a	11032	11065	10971		8237	8162

With the present potential the zero point energy for H_2O is 4623.0 cm^{-1} and for D_2O 3381.4 cm^{-1}.

3.) Application of Conventional Vibrational Analysis to the Study of Clusters of Molecules

In this section we explore the possibilities of extending the methods of normal and local mode analysis to studying the vibrations of small clusters of molecules. A detailed account of the application of conventional spectroscopic theory to studying the vibrations of molecular clusters has been presented by Reimers and Watts (1984b). This section only outlines the approximations that must be made and the difficulties encountered when applying conventional methods to studying cluster systems.

The vibrational spectrum of a molecular cluster will differ from that of an isolated molecule due to the intermolecular interactions. Vibrational frequencies of the individual molecules will change through coupling with the rest of the cluster. The major influence of the intermolecular interactions is to distort the internal geometry of each molecule. If the intramolecular potential is anharmonic, the distorted molecules will vibrate on a region of potential surface with different curvature from molecules in their equilibrium geometries. The normal mode vibrational frequencies are related to the local curvature of the potential so intramolecular vibrational frequencies different from those of the isolated molecules will result. Another effect of clustering is the formation of intermolecular bonds. The entire cluster is able to establish modes of vibration in which molecules move relative to one another in a periodic fashion. Intermolecular vibrations occur at lower frequencies than the intramolecular modes because the intermolecular potential is usually weaker and longer ranged.

In principle, normal mode theory is easily applied to studying cluster

vibrations. The combined inter- and intramolecular potential is used and the cluster as a whole is treated in the same fashion as discussed in Section 1.). In practice however, this calculation is usually slowly convergent (Reimers and Watts (1984b)) since the intermolecular potential allows large zero point motions and the surface is anharmonic.

The procedure to be used when applying local mode analysis to the problem of vibrations in molecular clusters is not so obvious. Generally intermolecular bonds are rather loosly defined structures, so there are no local coordinates which will give a simple description of the intermolecular modes. The situation for the intramolecular modes, however, is more promising. In a cluster the motions involved in intramolecular vibrations are usually localized on the particular molecule. Thus it is likely that the local coordinates used in local mode calculations on the isolated molecules probably still provide a good representation of the intramolecular vibrations of the cluster. This idea forms the basis of an effective potential, or "frozen field", local mode method for studying how intramolecular motions are perturbed by clustering. The method was developed and applied to water clusters by Reimers and Watts (1984b) and has since been used by Miller, Watts and Ding (1984) to interpret the intramolecular vibrational spectra of nitrous oxide clusters.

We now present a brief description of the frozen field local mode method. In this approach the intermolecular potential acts as a perturbation which can be included by fitting an effective Morse oscillator surface in the intramolecular coordinates to the full inter/intramolecular potential. The equilibrium geometry of the molecular cluster is first found by minimising the full potential surface. Holding all other molecules fixed in this geometry, each molecule in turn is internally distorted along its

local coordinates. The centre of mass of the distorted molecule is maintained. The total potential energy for several distortions of the molecule is calculated and an effective Morse surface in the local coordinates is fitted to the results. The effective potential obtained using this approach includes the influence of the stationary intermolecular field provided by the rest of the cluster. Each molecule in the cluster is considered as an isolated entity moving on its own effective potential surface which includes the influences of its environment. The intramolecular vibrational spectrum of the cluster is thus regarded as a superposition of the spectra associated with the different molecules. Local mode theory is employed to calculate the spectra of the molecules and basis sets constructed from the eigenfunctions of the effective Morse oscillators are used to perform the variational calculations.

There are two major approximations with frozen field local mode analysis. First, the method ignores correlations between the inter- and intramolecular motions since it is assumed that each molecule vibrates in the stationary field of its neighbours. Secondly, any correlations between the intramolecular motions of different molecules are ignored.

The effects of the approximations described above can be estimated using normal mode analysis, as has been done by Reimers and Watts (1984) for water clusters. In their treatment, they set the appropriate elements of the normal mode force constant matrix to zero and were able to estimate the importance of the different terms using harmonic approximations. As noted earlier, the intermolecular potential is appreciably anharmonic so the harmonic treatment can give only qualitative information about the magnitudes of the couplings. In the next section we describe a procedure in which the many body wave function obtained from a quantum Monte Carlo

calculation is used to determine the intramolecular vibrational spectrum of a molecular cluster. The couplings and correlations which are ignored in the effective potential local mode approach can be treated by the quantum simulation method.

4.) Application of the Quantum Monte Carlo Method to Molecular Clusters

The quantum Monte Carlo procedure, which was described in Chapter 2, may be used to study the ground state of a molecular cluster. A collection of replica systems is established, each member of the ensemble being a single molecular cluster. At every time step the simulation algorithm consists of the usual Gaussian diffusion step, modelling the kinetic energy operator, followed by a birth/death process which accounts for the potential term in the Hamiltonian.

The time step used must be sufficiently small to ensure that the separation of the diffusion and birth/death processes is an accurate approximation. A rapidly varying potential surface demands the use of very small time steps. In a cluster of water molecules the intramolecular potential varies more rapidly than the intermolecular surface and a time step which gives small intramolecular displacements must be used. An adequate sample of the distribution of intermolecular geometries can only be obtained with very long runs using short time steps.

The different atoms in the molecules have different diffusion coefficients, $D_i = \hbar^2/2m_i$. In water for example, the diffusion coefficient for the motion of the hydrogen atoms approximately sixteen times greater than that associated with the motions of the oxygen atoms. Since the width

of the Gaussian distribution of displacements depends on the square root of the diffusion coefficient, in a single time step the oxygen atoms will diffuse through distances that are about four times smaller than those of the hydrogen atoms. Thus the distribution of intermolecular geometries will take a long time to equilibrate.

We now describe the method which has been used to calculate the vibrational spectrum of a molecular cluster from a quantum random walk calculation. As discussed in Chapter 2, the basic quantum Monte Carlo procedure produces an ensemble of systems distributed according to the ground state wave function. The ensemble can be used to obtain the intramolecular vibrational spectrum of the molecular cluster providing certain assumptions are made. The basic idea behind our approach involves fitting an analytic form to the "exact" ground state wave function obtained from the quantum Monte Carlo calculation. If a convenient form is chosen the vibrational frequencies can be obtained using conventional vibrational analysis.

The ground state wave function of the cluster is assumed to have the form of a product of an intermolecular part and a set of separate intramolecular functions, $\Phi_i(\underline{R}_i)$, each of which describes the vibrations of a single molecule thus

$$\Psi = \psi_{inter} \prod_i \Phi_i(\underline{R}_i)$$

Analytic functions of this form are fitted to the quantum Monte Carlo wave function and provide the basis set for variational calculations.

We restrict ourselves to studying only those motions of the cluster which are approximately localised on single molecules. The frozen field local mode method of Reimers and Watts (1984b) assumes that the effective

potential in which a molecule in a cluster vibrates can be constructed as a sum of Morse oscillators in the local coordinates of the molecule. Following this approach we assume that the intramolecular wave functions are written as products of Morse oscillator eigenfunctions in the local coordinates and the effective wave function for a molecule takes the following model form

$$\Phi(\underline{R}) = \prod_j \phi_j(s_j) \qquad (3.13)$$

Here the ground state Morse oscillator eigenfunction is given by

$$\phi_j(s_j) = N^{-\frac{1}{2}} e^{-x/2} x^{K-\frac{1}{2}}$$

where $$K = A D_j^{\frac{1}{2}} \quad , \quad x = 2K e^{-\alpha_j(s_j - s_{jo})} \qquad (3.14)$$

and A is related to the diagonal elements of the G matrix by

$$A = 2^{\frac{1}{2}} / (\alpha_j h G)$$

The normalising constant for the ground state wave function is

$$N = \frac{\Gamma(2K)}{(2K-1)^2}$$

An ensemble generated by a quantum Monte Carlo calculation is distributed according to the many body ground state wave function. A multidimensional distribution obtained in such a form may be projected onto the intramolecular coordinates of interest by accumulating histograms of these coordinates averaged over all systems in the ensemble. Histograms generated as outlined above include the influences of both the intermolecular zero point motions and the intramolecular motions of the other molecules. By fitting the functional form for the model wave function

projections given in equation (3.14) to the exact wave function projections we obtain effective independent Morse oscillator eigenfunctions. Functions obtained by the method are used as a basis set for a conventional local mode analysis and estimates of the intramolecular vibrational frequencies may be calculated. The fitting is performed by varying the parameters D_j, α_j and s_{jo} in equation (3.14).

The major assumption in the approach considered above is that the many body wave functions describing the intramolecular vibrational states of the cluster can be written as products of effective independent Morse oscillator eigenfunctions in the local coordinates. Any possibility of direct coupling between the local modes on a particular molecule is neglected by the assumption. In Section 2.) we found that such couplings were important for giving the correct splitting between the symmetric and antisymmetric combinations of the equivalent O-H stretch motions. The couplings are properties of the isolated molecules and as such should not be strongly effected by clustering. Thus it is reasonable to approximate these terms by the isolated molecule values. Couplings of this form are included in the variational calculations performed with the effective oscillator basis set. The off diagonal elements of the vibrational kinetic energy operator must also be included in a variational calculation.

When isolated molecules are brought together to form a cluster, their rotational degrees of freedom are perturbed by binding with the other molecules in the cluster. Such motions manifest themselves as librational modes of the cluster. The influences of these "hindered rotations" are included in the effective oscillators which were fitted to the many body ground state wave function. Effects of coriolis and centrifugal couplings which exist between the inter- and intramolecular modes are included in the

effective oscillators and need not be considered in variational calculations.

5.) Quantum Monte Carlo Local Mode Vibrational Analysis of Water Clusters

Procedures discussed in the previous section have been applied to intramolecular vibrations of the water dimer and trimer. In these calculations we used the improved intramolecular potential presented in Section 2.) combined with the RWK2 intermolecular potential of Reimers, Watts and Klein (1981).

Quantum random walks were performed for the water dimer with ensembles of both 200 and 400 systems and the energies and vibrational frequencies obtained from these calculations were found to agree within the statistical fluctuations. The results of finite time step calculations converge to the true ground state values in the limit as $\Delta\tau \to 0$ (Anderson (1976)). To test convergence we performed calculations with imaginary time steps of $\Delta\tau = 0.004$ and 0.002 fs and the results obtained were again in agreement within the statistical uncertainties. Thus in the range of operating conditions considered, time step and ensemble size dependence effects were negligible. To test the accuracy of the random walk method under these conditions we first performed a simulation of the water monomer. A value of 4615 ± 15 cm^{-1} for the ground state energy of the monomer was obtained in excellent agreement with the results of the variational calculations summarized in Table 3.1. All the results reported in this section were obtained from a simulation based on an ensemble of 400 systems and a time step of $\Delta\tau = 0.004$ fs. Runs of 100 000 time steps or more were necessary to

fig. 3.3

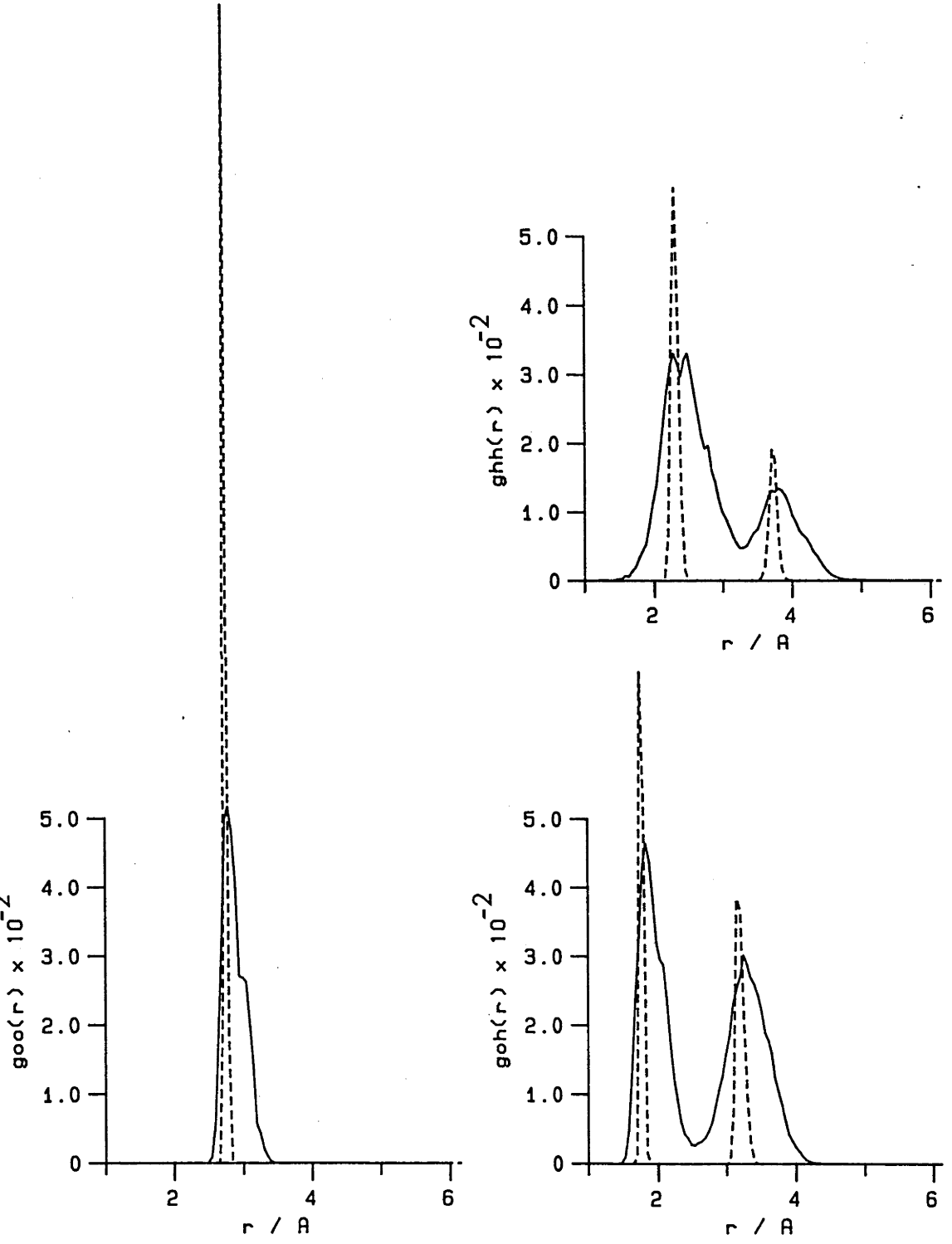
goo(r) x 10^-2
5.0
4.0
3.0
2.0
1.0
0
2
4
6
r / A
ghh(r) x 10^-2
5.0
4.0
3.0
2.0
1.0
0
2
4
6
r / A
goh(r) x 10^-2
5.0
4.0
3.0
2.0
1.0
0
2
4
6
r / A

obtain reasonable convergence of the intermolecular distribution functions.

The expectation values of various quantities including structural properties of the ground state cluster were obtained using the descendent weighting procedure for generating a ϕ_o^2 distribution which was described in Chapter 2.

Expectation values of the potential and kinetic operators were obtained with the ϕ_o^2 distribution. The average kinetic energy was calculated using the quantum virial theorem which gives that, in the absence of external forces, the kinetic energy of a system can be obtained from the following relation

$$\int \psi^*(\underline{r}) \left(\sum_i \frac{-\hbar^2}{2m_i} \nabla_i^2 \right) \psi(\underline{r}) \, d\underline{r} = -\frac{1}{2} \int \psi^*(\underline{r}) \, \psi(\underline{r}) \, \nabla V(\underline{r}) \, d\underline{r}$$

Thus by averaging the gradient of the potential over the ϕ_o^2 distribution we can evaluate the kinetic engery.

As discussed in Chapter 2, the total energy is obtained from the average value of the energy reference which holds the population of the ensemble approximately fixed. Comparing the ground state energy calculated using this approach with the sum of the potential and kinetic energy components gives a selfconsistent check of our calculation.

In Figure 3.3 we present the atom-atom pair distributions for the water dimer obtained from the ϕ_o^2 distribution. For comparision we also present the distribution functions obtained by Reimers (1982) who performed a classical Monte Carlo calculation on the water dimer at 10 °K. Inadequacy of the low temperature classical Boltzman distribution is rather apparent. The classical distribution does not allow for zero point motions of the cluster and this neglect gives rise to extremely sharp, unphysical structural features. On the other hand the exact quantum distributions show

fig. 3.4

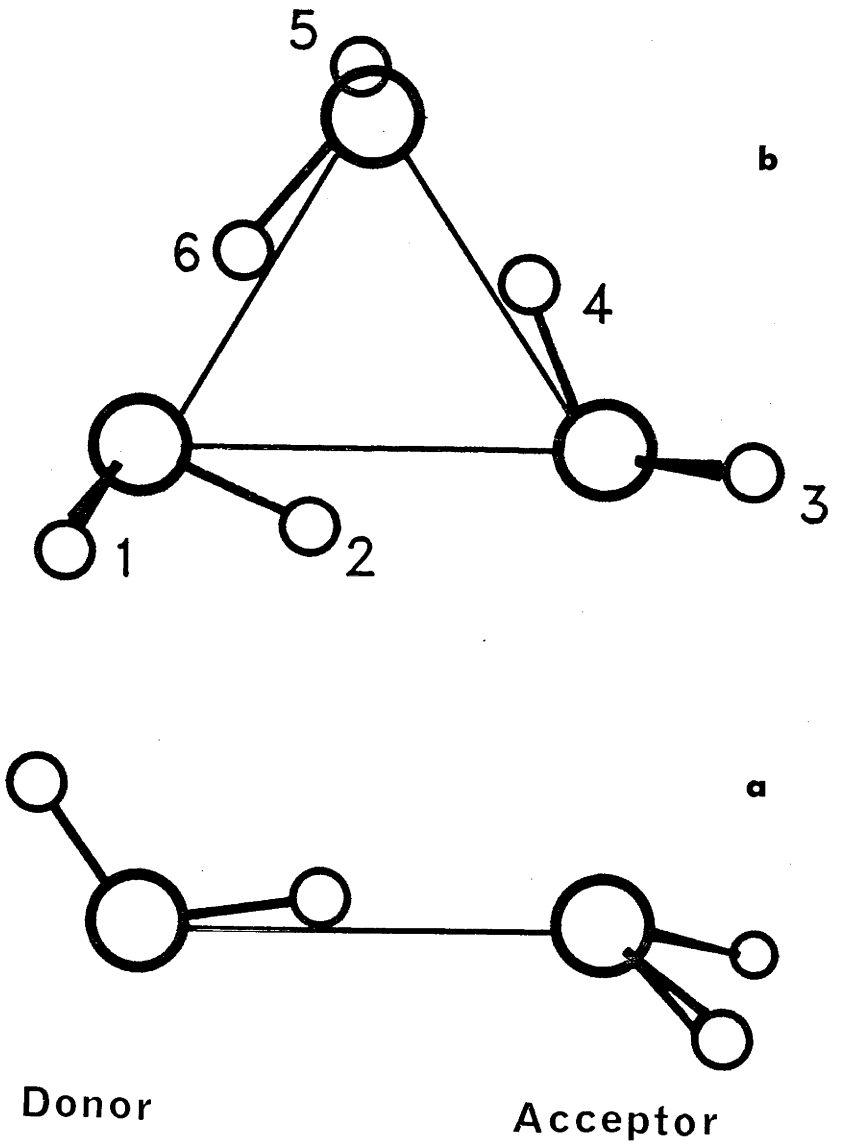

broader structural features due to large amplitude zero point motions.

Figure 3.3 also highlights the differences between the frozen field local mode method for calculating the intramolecular vibrational spectrum of a cluster and the quantum Monte Carlo projection method. In the latter, we obtain an effective wave function for the intramolecular degrees of freedom which has been averaged over the full quantum distribution of intermolecular enviroments. With the frozen field local mode method however, we hold the rest of the cluster in its minimum energy geometry and sample only the zero temperature classical distribution of intermolecular geometries.

Figure 3.4a presents the minimum energy dimer structure predicted by the RWK2 potential, the energy of this geometry is -3093 K. Intermolecular distances involving the hydrogen bonded atom give rise to the sharp first peaks in both the g_{OH} and g_{HH} distributions presented in Figure 3.3. Other hydrogens being less strongly bound give more diffuse structural features.

Calculation of the intermolecular distributions is rather noisy for two reasons: first, since fairly small time steps are used so that an accurate separation of the diffusion and birth/death processes can be made, very long runs are necessary to obtain good statistics for the slower intermolecular degrees of freedom. Secondly, the procedure for generating the ϕ_0^2 distribution involves large fluctuations since two fluctuating quantities must be folded together.

Figure 3.5 demonstrates how the descendent weighting procedure is used to calculate the average kinetic and potential energies in the ground state of the water dimer. We plot the potential energy and the virial, both averaged over the ensemble distribution and weighted by the descendent numbers after a time τ. The procedure used here was described in

fig. 3.5

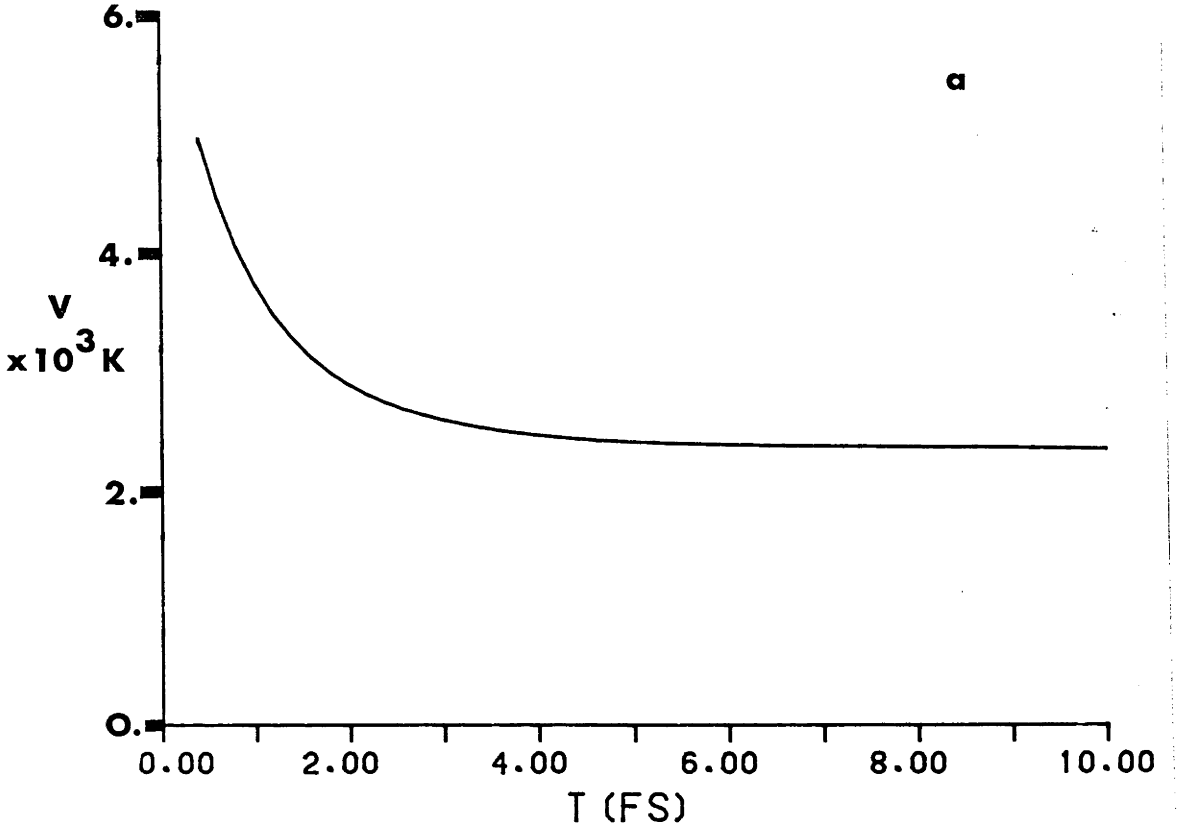
a
6.
4.
2.
0.
V
x10^3 K
0.00
2.00
4.00
6.00
8.00
10.00
T (FS)

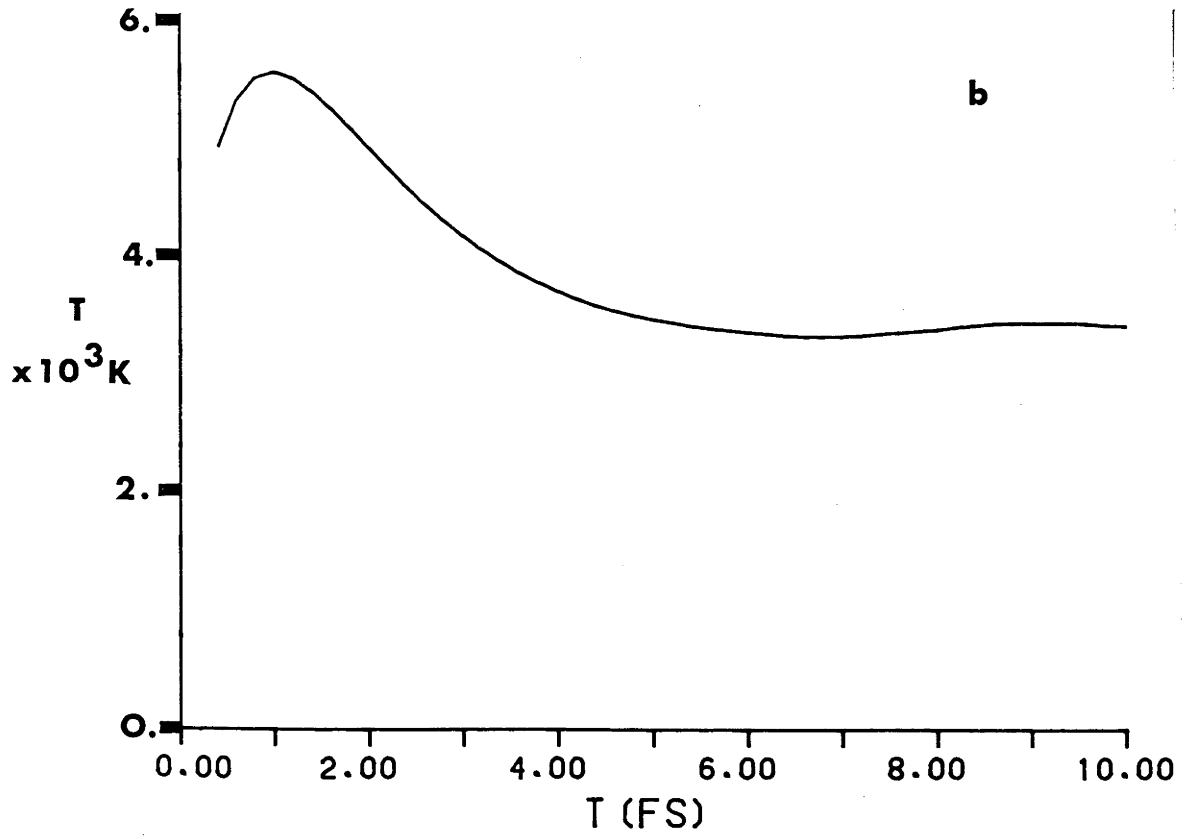
b
6.
4.
2.
0.
T
x10^3 K
0.00
2.00
4.00
6.00
8.00
10.00
T (FS)

Section 3.) of Chapter 2 and the curves presented in Figure 3.5 are the results of superimposing many segments of the random walk trajectory. As discussed in Chapter 2, estimates of the expectation values of the potential and kinetic energy can be obtained from the asymptotic behaviour of the curves presented in Figures 3.5. The values of these quantities are $\langle V \rangle = 2370 \pm 50$ K/molecule and $\langle T \rangle = 3400 \pm 100$ K/molecule giving the total ground state energy of the water dimer as $\langle E_o \rangle = 5770 \pm 100$ K/molecule. To within the statistical fluctuations inherent in these calculations this agrees with the average value of V_{ref} $\langle V_{ref} \rangle = 5730 \pm 20$ K/molecule obtained during the run. As discussed earlier, this agreement provides a self-consistent check of the quantum Monte Carlo method and indicates that the Virial Theorem is satisfied. The eigenvalue estimate calculated from the average energy reference has less statistical uncertainty than the value obtained from the sum of the potential and kinetic energies since the evaluation does not rely on the ϕ_o^2 generation procedure.

In Table 3.2 we compare the ground state energies of the water dimer predicted by various calculations.

Table 3.2 Comparison of different calculations of the ground state energy (in cm^{-1}) of the water dimer.

Calculation	Eo	Intra	Inter
Random Walk	10115	9130	985
Local mode (Reimers-Watts (1984b))	10113	9093	1020
Normal mode (Reimers-Watts (1984b))	10193	9172	1020
Slania (1981)	10225	9456	769
Curtiss and Pople (1975)	10626	9838	788

The results of Curtiss and Pople (1975) were obtained by performing normal mode analysis on an ab initio potential surface calculated using LCAO-SCF theory with a limited basis set. Slania (1981) also employed normal mode analysis with the improved ab initio potential surface of Matsuoka et at. (1976) who used CI methods. The results of Reimers and Watts can be compared with the random walk values since there are only slight differences in the potentials used in these two calculations. As discussed earlier the major effect of the modifications which have been made to the Reimers-Watts surface is to split the degenerate stretch motions and the changes have little influence on the total ground state energy. The local mode results which include normal mode estimates of the intermolecular energy are close to the ground state energy obtained from the random walk calculation. Both these values are lower than the results obtained from normal mode analysis. The total energy obtained from the random walk calculation has been separated into inter- and intramolecular contributions by using the intramolecular vibrational frequencies obtained from the projection method.

The intramolecular energy calculated from the random walk is slightly higher than the results of the local mode calculations while the intermolecular component is lower than, but surprisingly close to the normal mode result. It is difficult to make more detailed comparisons with any certainty due to the differences in the potential surfaces and the statistical error in the random walk results.

We now consider using the ensemble obtained from the random walk calculation, together with the projection method described in the previous section to obtain the intramolecular vibrational spectrum of the water dimer. Histograms of the local mode coordinates , defined in equation

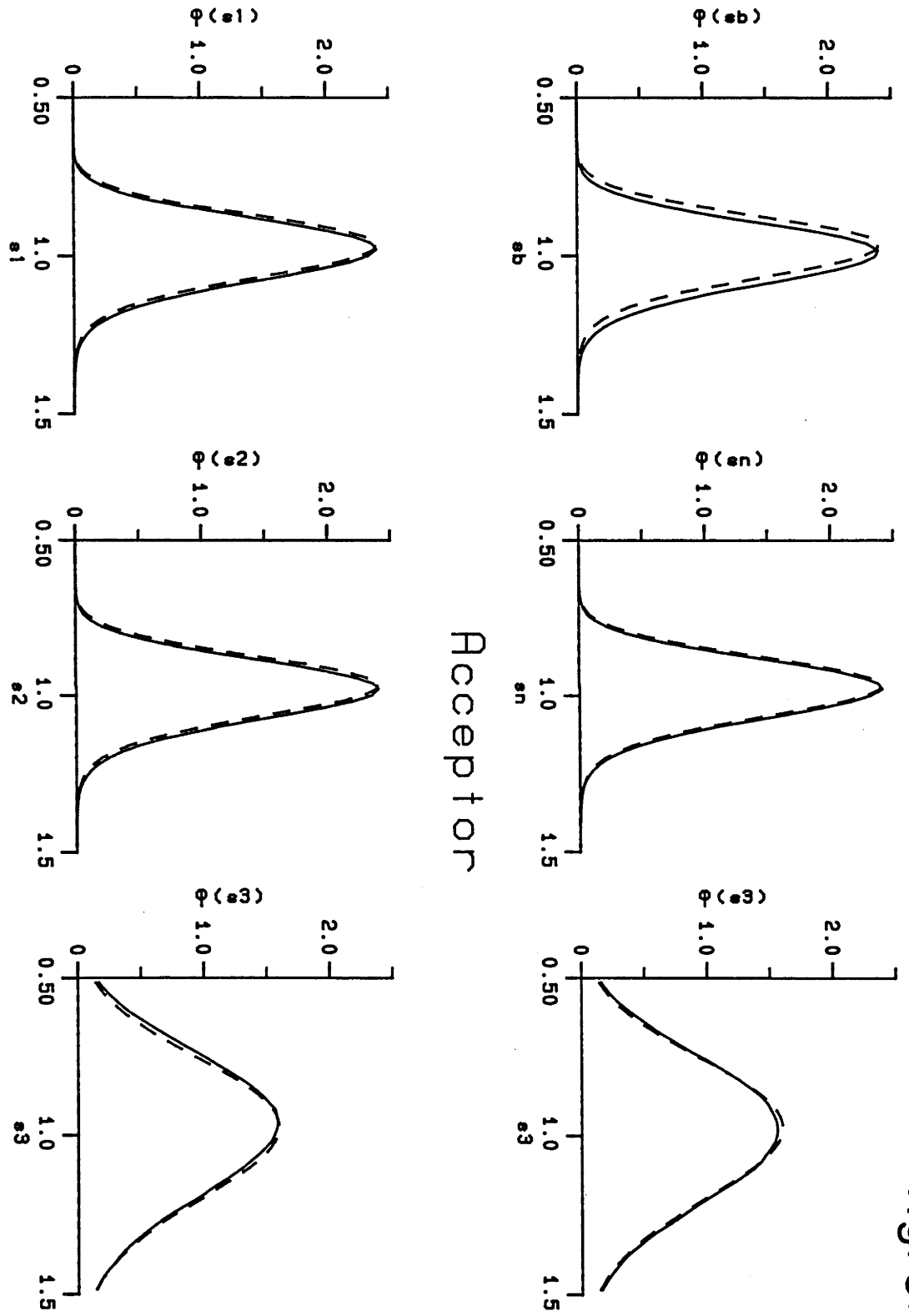
Donor
Acceptor
φ(eb)
φ(en)
φ(e3)
φ(e1)
φ(e2)
φ(e3)
0
1.0
2.0
0.50
1.0
1.5
eb
en
e3
e1
e2
e3

fig. 3.6

(3.11), were averaged over the ensemble distribution and these projections are presented in Figure 3.6. The dashed curves in the figure are the ground state Morse basis functions for the water monomer. Differences between the dashed and solid curves demonstrate the effects of clustering on the various intramolecular modes. The slight distortions of the intramolecular wave functions apparent in Figure 3.6 have a significant effect on the vibrational frequencies. A frequency shift of more than 200 cm^{-1} is associated with the largest distortion.

For each dimer in the ensemble the shortest O-H intermolecular distance was used to define the bonded hydrogen atom. Separate histograms for the bonded and non-bonded local coordinates on the donor and also for the s_1 and s_2 coordinates on the acceptor molecule were accumulated. The two hydrogen atoms on the acceptor are equivalent and so their motions should take place in the same averaged field. From Figure 3.6 we see that the projected wave function describing the motion of the hydrogen bonded atom on the donor is significantly perturbed from the monomer wave function. Attraction by the oxygen atom on the acceptor molecule distorts the local coordinate distribution for the donor atom. The projections onto other intramolecular stretching and bending coordinates differ only slightly from the monomer wave functions describing these motions.

As discussed in the previous section, a least squares method was used to fit an effective Morse oscillator basis set to the histograms of intramolecular local coordinates. For the moment we confine our attention to the O-H stretch motions in the dimer. Figure 3.7a shows the $v = 0 \rightarrow 1$ excitation energies of the various Morse basis oscillators obtained by fitting to the quantum Monte Carlo generated wave function projections. The lowest frequency corresponds to the projection onto the hydrogen bonded O-H

fig. 3.7

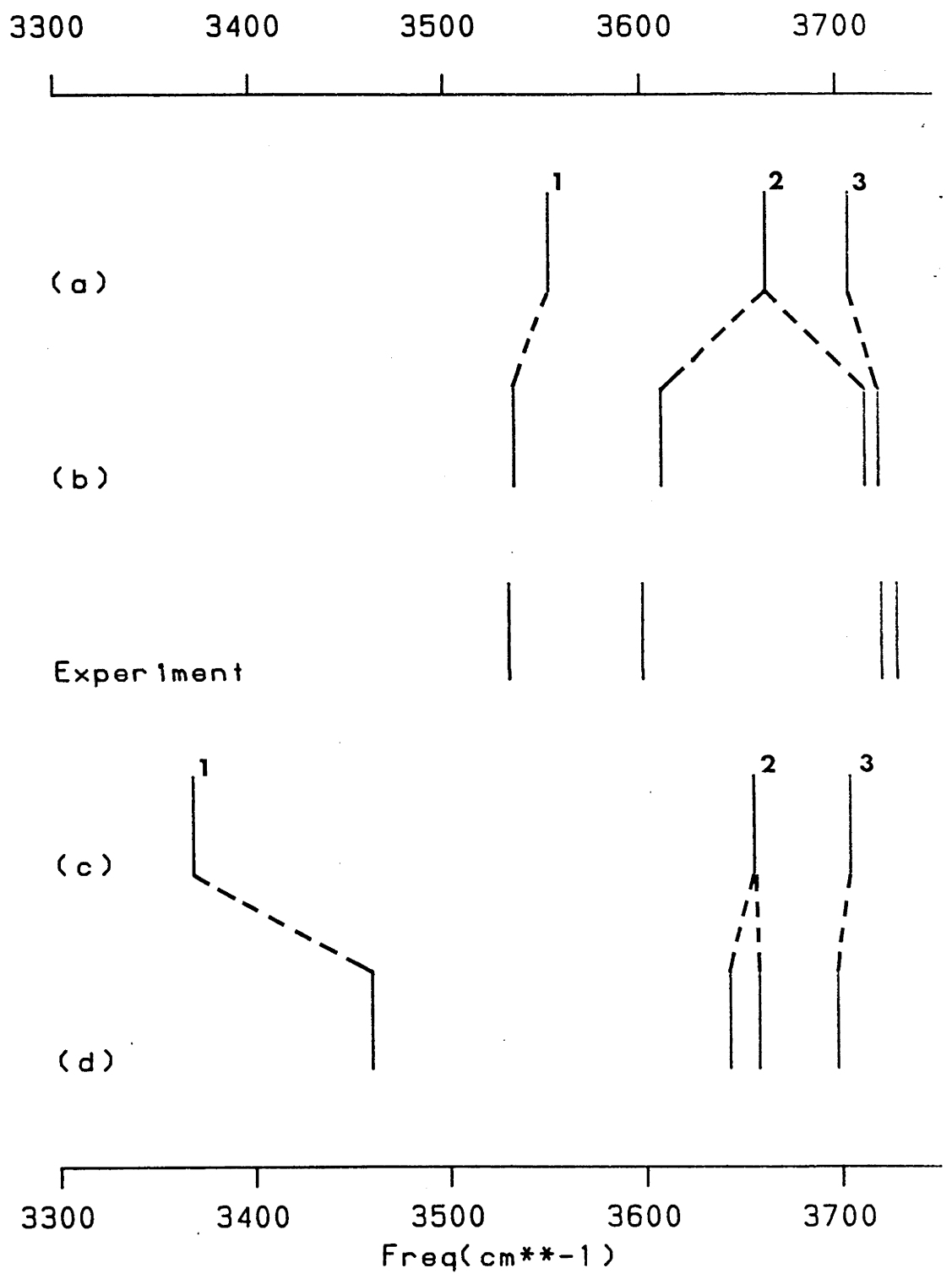
3300
3400
3500
3600
3700
1
2
3
(a)
(b)
Experiment
1
2
3
(c)
(d)
3300
3400
3500
3600
3700
Freq(cm**-1)

stretch motion while the highest frequency band is associated with the non-hydrogen bonded oscillator on the donor molecule (refere to Figure 3.4a for the dimer structure). The band in between these two corresponds to the two degenerate stretches of the acceptor. Frequencies obtained from the s_1 and s_2 projections of the acceptor molecule differed slightly as a result of the fluctuations inherent in the calculation. During the 100 000 time steps over which the steady state averages were accumulated these two frequencies were never separated by more than 25 cm^{-1}. This value gives a reasonable estimate of the statistical error for the frequencies predicted by our calculation. The degenerate frequency presented in Figure 3.7a was obtained by fitting to the average of the s_1 and s_2 histograms.

Figure 3.7c shows the excitation energies of the basis oscillators obtained by Reimers and Watts from fitting to the frozen field potential surface. The two bands associated with the non-hydrogen bonded stretch on the donor and the degenerate stretches on the acceptor occur at similar frequencies to those obtained from the quantum Monte Carlo wave function projections. This indicates that these intramolecular motions are not strongly influenced by the zero point motion of the rest of the cluster and that the approximations made in frozen field local mode analysis are quite reasonable for these modes. However, this is not the case for the hydrogen bonded stretch. The frozen field basis oscillator representing this mode is some 200 cm^{-1} lower in frequency than the basis oscillator obtained from the quantum Monte Carlo projection method. A reason for the difference is that the bonded O-H stretch is probably strongly coupled to the intermolecular mode which represents stretching of the dimer O-O bond. Since these motions are approximately colinear, any change in dipole moment associated with one stretch must influence the other. The two oxygens and

the bridging hydrogen can be thought of as a linear triatomic. Coulson and Robertson (1974), (1975) have used this model to perform a theoretical study of the combination bands expected in strongly hydrogen bonded systems.

Figures 3.7b and 3.7d respectively show how the basis oscillators obtained from the quantum Monte Carlo projections and the frozen field fitted potentials are perturbed when variational calculations are performed. In Figure 3.7b we have taken the quantum Monte Carlo Morse basis and performed a variational calculation, using excitations up to 5 quanta to include the off diagonal elements of the kinetic operator and the coupling between the s_1 and s_2 coordinates. As with the monomer the major effect of these terms is to split the degenerate stretches on the acceptor giving symmetric and antisymmetric modes. Basis oscillators of the donor molecule are only perturbed slightly by these couplings since they are already non-degenerate. In Figure 3.7d we present the results obtained by Reimers and Watts (1984b) who performed variational calculations to include only the off diagonal elements of the G matrix and also approximate harmonic couplings between the inter- and intramolecular modes.

As in their monomer calculations, the off-diagonal kinetic energy terms result in only a small splitting between the acceptor stretches. The major influence of the harmonic couplings between the intramolecular modes and the motions of the rest of the cluster is to shift the hydrogen bonded stretch to higher frequencies by about 100 cm^{-1}. The predicted band, however, still falls well below the frequency obtained from the quantum Monte Carlo results.

Also presented in this figure are the results of molecular beam experiments in the region of the O-H stretch vibration reported by Coker,

Miller and Watts (1985). The frequencies obtained from the quantum Monte Carlo simulation with couplings included by variational calculations are seen to agree with the experimental values to within the statistical uncertainties of the calculations (± 25 cm^{-1}).

The nature of the enviroment in a molecular beam is such that the individual clusters find themselves in collision free conditions. Rotational temperatures are extremely low and both the inter- and intramolecular degrees of freedom should be very strongly cooled. Due to the conditions in a molecular beam it is reasonable to expect good agreement between the results of the ground state calculations and molecular beam data.

6.) Comparisons of Theories and Experiment

Figures 3.8 and 3.9 present in more detail the experimental findings of Coker, Miller and Watts (1985). Molecular beams containing clusters of water molecules are formed by expanding mixtures of water vapour in helium through a small nozzle and skimmer arrangement into an evacuated chamber. By adjusting the conditions of pressure, temperature and composition, the dominent size of cluster produced in the beam can be controlled. When infrared radiation from a colour centre laser is absorbed by the intramolecular vibrations of the cluster, the excitation rapidly migrates into the intermolecular modes and causes the cluster to dissociate. The dissociation fragments are sent tumbling out of the molecular beam and the intramolecular absorption is detected as a decrease in beam intensity. Figures 3.8, 3.9 and 3.10 show the attenuation of the energy of the

fig.3.8

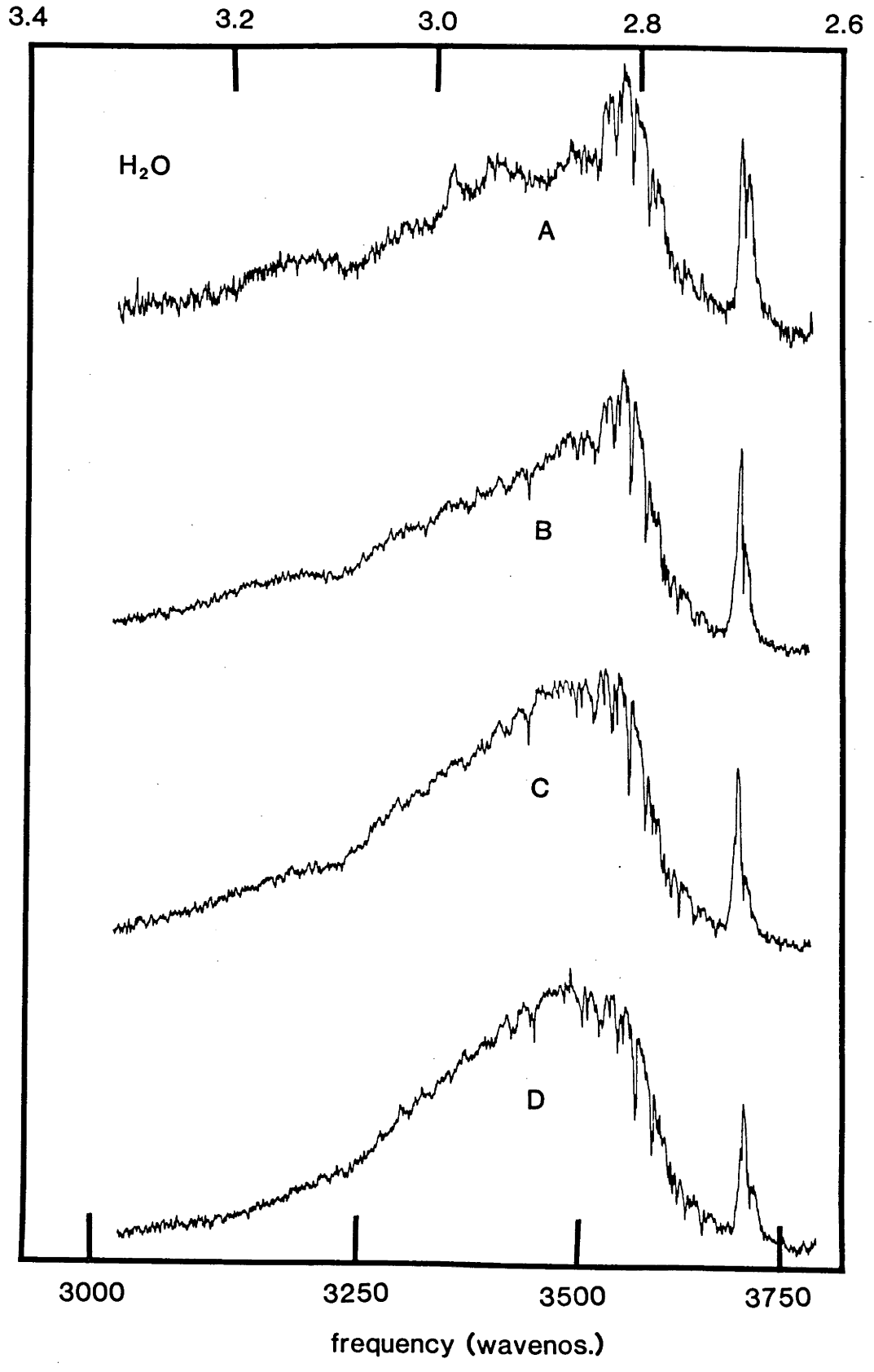
wavelength (microns)
3.4
3.2
3.0
2.8
2.6
H_2O
A
B
C
D
3000
3250
3500
3750
frequency (wavenos.)

molecular beam, measured by a bolometer, as a function of laser frequency for a range of different beam conditions.

Figure 3.8 indicates that as the water concentration is reduced, the broad feature reminiscent of the spectrum of liquid water (Robertson and Williams (1971)), though shifted to the blue by about a hundred wave numbers, gives way to several strong features which emerge from the envelope. There is also evidence of a small band which persists in the low frequency tail near 3200 cm^{-1}. The sharp band above 3700 cm^{-1} is evident in all spectra and grows in relative intensity as the concentration is reduced. This band consists of at least two distinct peaks. Figure 3.9 shows that at least six strong features are apparent in the spectrum at very low concentrations and that the weak band at near 3200 cm^{-1} is possibly resolved into two peaks. Examination of the pressure dependence of these absorptions, together with mass spectrometry, indicates that these low concentration spectra are most likely associated with the water dimer and trimer. Figure 3.10 compares the experimental results with the values obtained from the random walk projection method. The values are in very close agreement.

fig.3.9

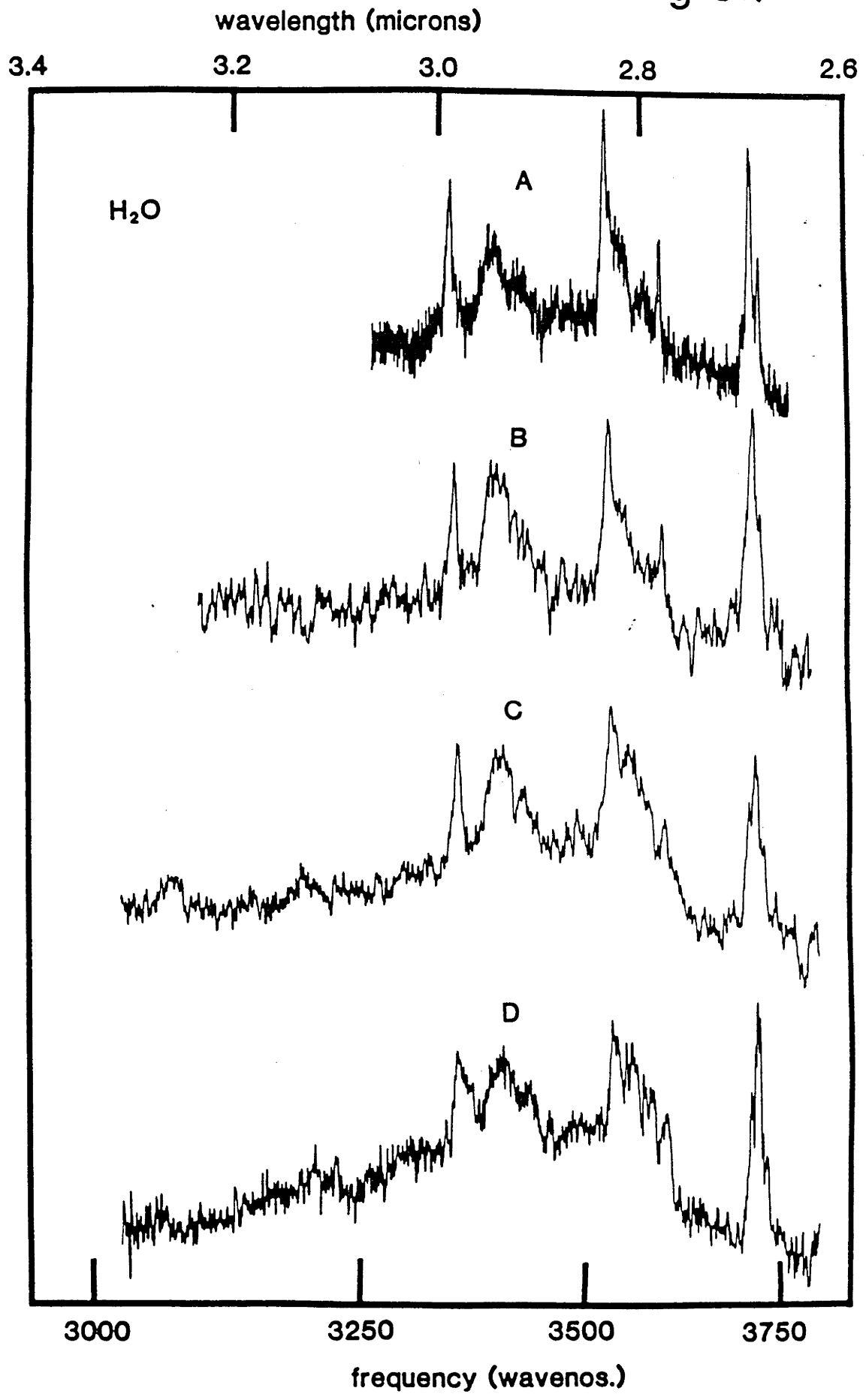
wavelength (microns)
3.4
3.2
3.0
2.8
2.6
H_2O
A
B
C
D
3000
3250
3500
3750
frequency (wavenos.)

fig. 3.10

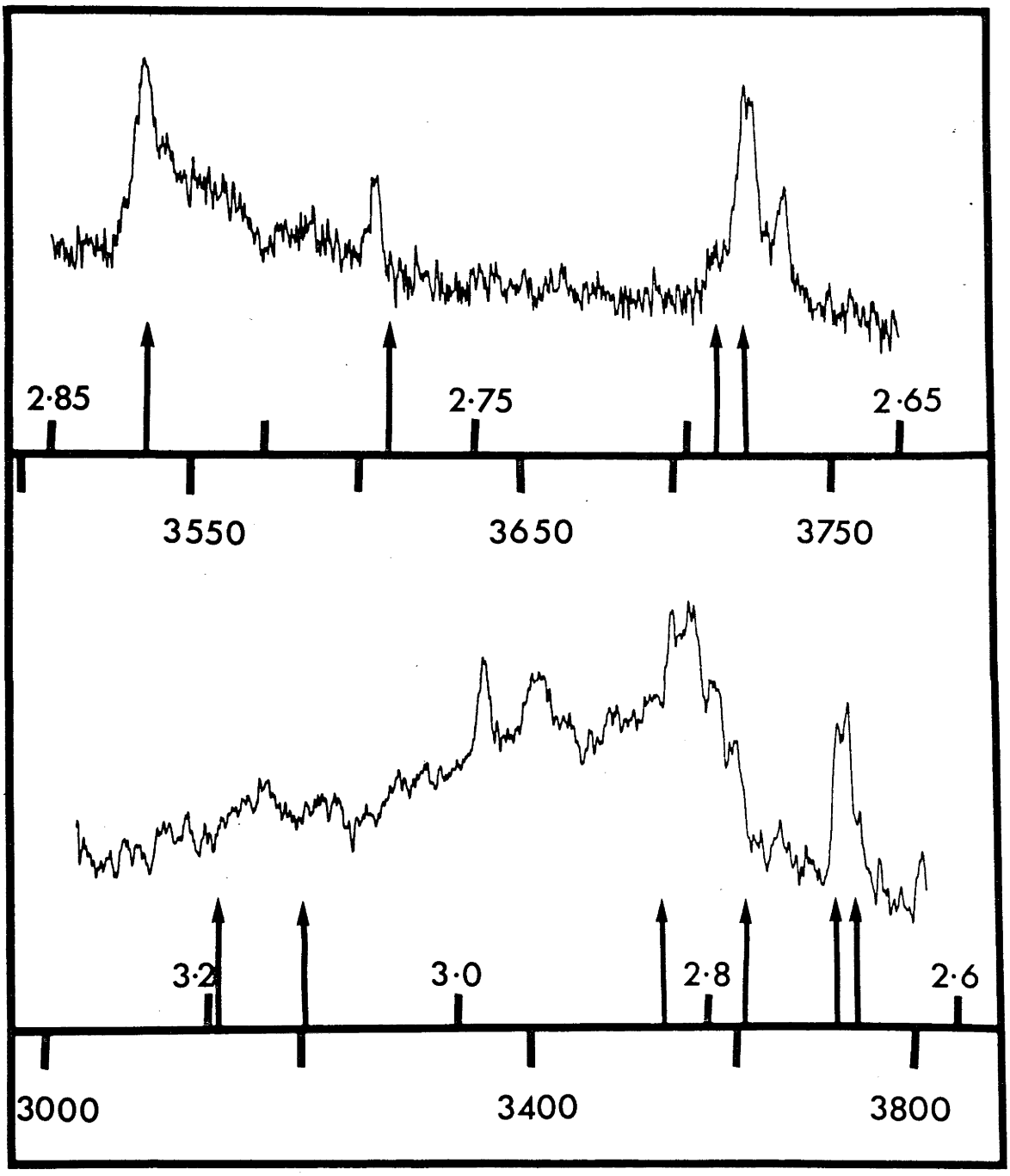
wavelength (microns)
2·85
2·75
2·65
3550
3650
3750
3·2
3·0
2·8
2·6
3000
3400
3800
frequency (cm⁻¹)

Table 3.3 Absorption bands observed at low H_2O concentrations in helium. Also given are molecular beam results of Page et al. (1984) and matrix isolation results of Bentwood et al. (1980) for the dimer and predictions of dimer frequencies from quantum simulation theory. All frequencies are in cm^{-1}.

Present Experiment	Page et al.	Ar Matrix	N_2 Matrix	Theory	Dimer Assignment
3730 ± 3	3730	3726	3715	3721	Donor Stretch
3722 ± 3	3714	3709	3699	3714	Acceptor asymmetric Stretch
3600 ± 3	3600	3634	3627	3610	Acceptor symmetric Stretch
3532 ± 3	3545	3574	3550	3535	Donor Stretch
3400 ± 5				3430	Trimer
3357 ± 3				3380	Trimer
3215 ± 5				3201	Donor bend overtone
3170 ± 5	3186			3130	Acceptor bend overtone

In Table 3.3 the frequencies of all the absorptions found in these lowest concentration spectra are summarised and compared with the results obtained from matrix isolation studies (Bentwood et al. (1980)) and another molecular beam experiment (Page et al. (1984)). Also presented are the results of the quantum Monte Carlo calculations which enable a detailed assignment of the experimental spectra to be made. As discussed earlier, in descending order of frequency, the four sharp bands at higher frequencies correspond to the non-hydrogen bonded stretch on the donor, the asymmetric stretch on the acceptor, the symmetric stretch on the acceptor and finally

the hydrogen bonded stretch on the donor. The quantum Monte Carlo wave function was also projected onto the bending coordinates of the molecules and the calculated bend overtones are close to the two broad, weak absorptions observed in the experimental spectrum near 3200 cm^{-1}. The low intensities of these bands are consistent with such an assignment.

The two remaining strong absorptions in the experimental spectrum, observed at 3357 cm^{-1} and 3400 cm^{-1}, are difficult to assign as vibrations of the dimer. It is likely that the broader band at 3400 cm^{-1} is in fact associated with the trimer. Such an assignment is supported by the beam experiments of Vernon et al. (1982) in which a poorly resolved trimer spectrum indicates a very broad absorption centred near 3400 cm^{-1}. Their results for the tetramer show a similar feature while for the pentamer they find a band at approximately 3350 cm^{-1}. The sharp feature at 3357 cm^{-1} in the molecular beam results of Coker, Miller and Watts is, however, unlikely to be associated with such a large cluster for, as stated earlier, the mass spectra of the low concentration cluster beams indicates the presence of predominently dimers and trimers. Though there are difficulties in interpreting the mass spectra due to fragmentation as the clusters are detected.

An alternative assignment is that the peak at 3357 cm^{-1} is associated with a dimer difference band. Suppose that the water dimer is formed in the beam in an excited intermolecular vibrational state. For example there may be significant population in the vibrationally excited O...O stretching mode. It is thus possible, in principle, to observe the difference frequency absorption corresponding to the de-excitation of this mode and the simultaneous excitation of the hydrogen bonded O-H stretch on the donor molecule. Evidence for the existence of such a mode in hydrogen bonded

systems has been considered by Coulson and Robertson (1974), (1975).

The quantum simulation method has been used to estimate the vibrational frequency of the O...O stretch mode. A histogram of O...O separations was accumulated from the ground state ensemble. By fitting a Morse oscillator eigenfunction to this projection of the dimer wave function we obtained an effective Morse function whose eigenvalues approximate the O...O stretch vibrational frequencies. As discussed earlier, very small time steps had to be used in our calculations to accurately represent the intramolecular vibrations. The intermolecular distributions obtained from our studies are fairly noisy. The frequency of the O...O stretch determined from this calculation is 150 ± 50 cm^{-1}. The error estimate is based on the standard deviation of a number of independent determinations performed during the averaging run. Microwave studies of the water dimer (Dyke, Mack and Muenter (1977)) have assigned a band at 150 cm^{-1} to the O...O stretching mode.

In principle the procedure described above could be applied to study other intermolecular modes but in general the choice of coordinates for this calculation is complicated. Projection onto the intermolecular normal modes might be considered but due to the anharmonicities in the intermolecular potential, the normal coordinates probably give a poor description of the actual intermolecular motions of the cluster. For this reason and because of the poor statistics in our calculation of the intermolecular distributions we have not persued these studies.

With the O...O stretch frequency at about 150 cm^{-1}, the dimer difference frequency expected is approximately 3380 cm^{-1}, which is within 50 cm^{-1} of the dimer band in question. Furthermore, calculations similar to those of Coulson and Robertson (1974), (1975) indicate that if the internal temperature of the dimer is around 70° K, the O...O stretch mode may be

significant populated. It is unlikely however that a combination band of this type would be as intense as the fundamentals.

A much more plausable explaination of the two bands at 3400 cm^{-1} and 3357 cm^{-1} is that they are associated with the trimer. To verify this assignment, a quantum simulation calculation on the trimer was performed. Details of the simulation were similar to those of the dimer calculations and the most stable equilibrium geometry for the RWK2M trimer (Reimers and Watts (1984b)) which is presented in Figure 3.4 b was used as the initial condition in our calculations. The three oxygens sit at the corners of an approximately isosceles triangle. As seen in Figure 3.4b, molecules B and C form definite hydrogen bonds and molecule A is more loosely bound. Thus all six hydrogens in the molecular cluster experience different enviroments so their intramolecular vibrations should occur at different frequencies.

Generally it is found that bonded hydrogens vibrate at lower frequencies than "free" O-H oscillators. With this in mind, together with the geometrical considerations outlined above, we expect that the intramolecular vibrational spectrum of the trimer should include two bands at lower frequencies characteristic of bonded O-H oscillators and four bonds at higher frequencies. When a vibrational analysis of the wave function projections obtained from the quantum simulation is performed the general spectral features outlined above are observed. The calculated O-H vibrational frequency associated with atom 1 is 3740 cm^{-1}, that for atom 2 is 3630 cm^{-1}, for atom 3 is 3725 cm^{-1}, for atom 4 is 3380 cm^{-1}, for atom 5 is 3620 cm^{-1} and for atom 6 is 3430 cm^{-1}. Two of these frequencies, those associated with the hydrogen bonded stretches, are close to the observed bands at 3357 cm^{-1} and 3400 cm^{-1}, two more lie near the two lower frequency dimer O-H absorptions, and the other two are consistent with the bands near

3720 cm^{-1}. It is reasonable to suppose that the shoulders observed on the two dimer absorptions at 3532 cm^{-1} and 3600 cm^{-1} probably result from trimer or larger cluster absorptions while the congestion around the base of the peak above 3700 cm^{-1} is of similar origin.

Figure 3.11 presents a summary of the results obtained from a number of different experimental measurements of the intramolecular vibrational spectrum of small water clusters and also the frequencies obtained from the various calculations which have been discussed in this chapter. The results of the matrix isolation studies of the dimer spectrum (Bentwood et al. (1980)) reported in the bottom section of the figure are in reasonable agreement with the molecular beam results of Page et al. (1984) and those of Coker, Miller and Watts (1985) labeled "Present Beam". This agreement indicates that the influence of the matrix on the intramolecular vibrations of the dimer is not so strong and the results of matrix isolation studies are reasonably reliable for this system.

In the top portion of the figure a summary of the normal and local mode results obtained by Reimers and Watts (1984b) is presented. The "Normal Mode Dimer" results bare little resemblence to experiment indicating that the approximate treatment of the potential anharmonicity by the normal mode variational method requires making severe approximations which are not justified with a realistic model potential for a water cluster. As discussed in the previous section, the effective potential local mode method takes account of the potential anharmonicity very successfully. There are two problems with the "Local Mode Dimer" results of Reimers and Watts. Use of an intramolecular potential surface which does not include coupling between the local O-H oscillators causes the splitting of the symmetric and antisymmetric stretches of the acceptor molecule to be

fig. 3.11

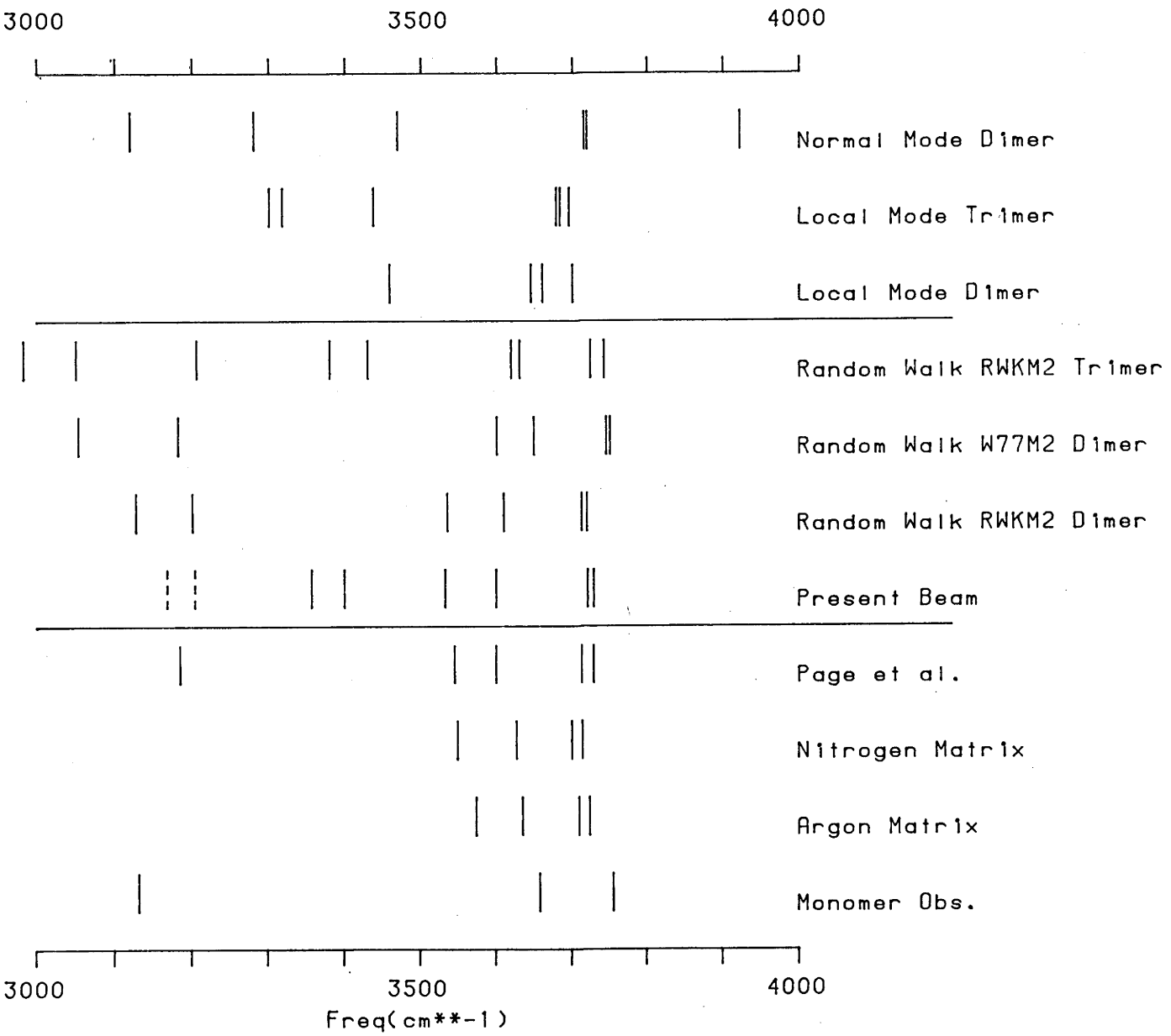
3000
3500
4000
Normal Mode Dimer
Local Mode Trimer
Local Mode Dimer
Random Walk RWKM2 Trimer
Random Walk W77M2 Dimer
Random Walk RWKM2 Dimer
Present Beam
Page et al.
Nitrogen Matrix
Argon Matrix
Monomer Obs.
3000
3500
4000
Freq(cm**-1)

underestimated. Secondly, including the couplings between the inter- and intramolecular degrees of freedom by a harmonic approximation causes the frequency of the bonded O-H stretch on the donor to be underestimated by about 100 cm^{-1}.

The results presented in the central section of the figure demonstrate the good agreement between the spectra of the dimer and trimer calculated using the quantum Monte Carlo projection technique and the molecular beam results of Coker, Miller and Watts.

Finally in Figure 3.11 we present the results of a quantum simulation calculation in which a different intermolecular potential was used. The spectrum labelled "Random Walk W77M2 dimer" reports a dimer simulation which used the intermolecular potential for water proposed by Watts (1977) together with the coupled Morse intramolecular potential surface discussed in Section 2.). The O-H stretch frequencies calculated with this model potential are all shifted to higher frequencies by about 50 cm^{-1} when compared with the molecular beam results. On the other hand the bend overtones predicted by the W77M2 potential occur at frequencies which are too low. This result suggests that the shape of the RWK2 pair potential in the region of its minimum gives an accurate representation of the true water potential surface. Furthermore, as the two model potentials are quite similar (Reimers, Watts and Klein (1981)), the infrared spectrum of the dimer provides a sensitive test of the intermolecular potential surface, at least in the region of the potential minimum.

In Figures 3.12 the two potential surfaces used in the calculations described above are compared. Figure 3.12 a shows the potential energy of the dimer as a function of O...O distance. For each separation the energy was minimised as a function of relative orientation and internal geometry.

Figure 3.12 b shows how the potential energy varies as a function of "donor angle", with the O...O separation and intramolecular geometry fixed to those values giving the most stable dimer. Figure 3.12 c shows the corresponding dependence of the potential energy on the "acceptor angle". These two angles are defined as the angle between the symmetry axes on the two molecules and the O...O axis (Reimers and Watts (1984b)). It is clear that the two surfaces are quite similar.

7.) Conclusions

In this chapter we have demonstrated that wave functions obtained from quantum simulation studies can be used to calculate very accurate vibrational spectra of model molecular systems. When realistic potentials are used, the normal mode variational approach has significant problems due to the large anharmonicities and local mode methods are more useful. The approximations concerning correlations between the inter- and intramolecular degrees of freedom, which must be made to implement local mode methods, can be significant, particularly for systems like the hydrogen bonded molecular cluster. Quantum simulation calculations include the effects of these couplings exactly and when the projection technique described in this chapter is used very accurate intramolecular vibrational frequencies of complicated molecular systems may be obtained. The general approach may also be applied to study intermolecular motions but statistical fluctuations and specification of coordinates present significant problems in more complicated systems.

Due to the accuracy of the quantum simulation and projection approach,

calculated vibrational spectra of Van der Waals clusters can be reliably compared with experimental results. Differences between spectra calculated using our procedure and those obtained from experiment are largely due to the inadequacies of the model interaction potential used in the calculation. We have shown that the intramolecular vibrational spectrum of a molecular cluster is quite sensitive to the details of the intermolecular potential and with the current level of statistical accuracy our approach can detect the differences between two reasonably similar intermolecular potential forms.

Importance sampling procedures discussed in Chapter 2 provide a means of performing quantum random walk calculations with greatly reduced statistical uncertainty. We speculate that the use of importance sampling together with projection methods similar to that described in this chapter may provide a very powerful tool for determining accurate emperical potential surfaces from vibrational spectroscopy of Van der Waals clusters.

CHAPTER 4 SOLID H_2 AND LIQUID ^4He

Introduction

In the previous chapter we saw that the diffusion Monte Carlo method developed in Chapter 2 could be applied succesfully to studying the ground state properties of small molecular clusters. In this chapter the method is used to study the ground states of bulk phase systems. The quantum Monte Carlo method, together with variational quantum techniques, will be employed to consider the ground state theromodynamic and structural properties of liquid ^4He and solid molecular hydrogen.

In the first two sections of this chapter we describe the variational and Green's function Monte Carlo techniques which have been used extensively in the study of bulk phase quantum systems. Variational calculations give only approximate solutions but the Green's function Monte Carlo method is essentially exact. Comparing the results of diffusion Monte Carlo calculations with Green's function Monte Carlo results gives a means of testing the finite time step approximation for bulk phase systems with harsh repulsive core interactions. We find that there are serious problems with the unbiased diffusion Monte Carlo method when applied to a system of 32 helium atoms in a periodic box interacting with Lennard-Jones forces. Large fluctuations are observed and the results obtained depend on the average ensemble size. Kalos (1970) found that the unbiased Green's function Monte Carlo iteration procedure could give useful results for liquid ^4He. Our studies indicate that this is not the case with the unbiased diffusion Monte Carlo method.

The problem outlined above can be overcome by using knowledge of the ground state wave function which is obtained from approximate variational calculations. Importance sampling methods were first used with the Green's function Monte Carlo method in bulk phase calculations by Kalos, Levesque and Verlet (1974). When importance sampling was used a great enhancement in the efficiency of the Green's function Monte Carlo method was reported. For the diffusion Monte Carlo method importance sampling involves including a drift term which forces the random walk into the regions of space which are more important. The approximate variational wave function determines the important regions. We find that the results of importance sampled diffusion Monte Carlo calculations on a system of 32 Lennard-Jones ^{4}He atoms are rather independent of time step and when a system of 108 particles is considered quantitative agreement with the Greens function Monte Carlo calculations of Whitlock et al. (1979) is obtained.

The drifting random walk procedure has been applied to study the ground state properties of solid H_2. A different form of importance sampling or trial wave function must be used with solid state calculations. We have considered solid H_2 over a range of densities. An accurate spherical pair potential due to Buck et al. (1983) has been used in this work. Reasonable agreement with experiment is found when this potential is used. Generally, the ground state energies obtained from the diffusion Monte Carlo calculations are on the order of 10% lower than the variational results indicating that variational calculations are useful only for obtaining qualitative information about quantum solids. The quantitative detail necessary to test the accuracy of an interaction potential can only be obtained from a full quantum calculation.

1.) Variational Calculations

The variational principle gives that the expectation of the total ground state energy is a minimum with respect to variations in the wave function so

$$\frac{\delta}{\delta\psi} \int \ldots \int \psi^* \hat{H} \psi d\underline{r} = 0 \qquad (4.1)$$

Variational calculations involve assuming a parameterised form for ψ and calculating the total energy as a function of the parameters. The set of parameters for which the total energy is a minimum give the best ground state wave function having the assumed form and the minimum energy is an upper bound for the ground state energy.

The variational procedure outlined above has been applied to bulk phase systems by many workers and the systems most often studied are the liquid and solid phases of ^{4}He where quantum effects dominate the behaviour. A variational form proposed by Mott (1949) and employed by Dingle (1949) and Jastrow (1955) has been widely used in these variational calculations. With the so-called Bijl-Jastrow form, the many body wave function is written as a product of pair functions

$$\psi = \prod_{i<j} f(r_{ij}) \qquad (4.2)$$

The function f contains the variational parameters and it depends only on the distance $r_{ij} = |\underline{r}_i - \underline{r}_j|$ between particles i and j. With this form ψ has the correct symmetry to describe the ground state of a system of interacting Bosons. The pair function f(r) can be chosen to vanish rapidly as $r \to 0$. This is an important property for systems with strongly repulsive core interactions.

The Lennard-Jones potential

$$V_{LJ}(r) = 4\varepsilon\left[\left(\frac{\sigma}{r}\right)^{12}-\left(\frac{\sigma}{r}\right)^{6}\right] \tag{4.3}$$

with the deBoer, Michels (1938) parameters

$$\varepsilon/k_B = 10.22^{\circ}K$$

$$\sigma = 2.556\ \mathring{A}$$

has been used in variational calculation to model the helium interaction. A pair function which has proved particularly useful for the Lennard-Jones system is based on the WKB approximate solution for the repulsive part of the potential. The pair function thus takes the following form

$$f(r) = e^{-\left(\alpha/r\right)^{5}} \tag{4.4}$$

and α is used as the variational parameter. A variety of alternative functions have been proposed (Reatto and Chester (1966), Murphy (1972), McGee and Murphy (1972) and De Michelis and Reatto (1974) are a few examples) but equation (4.4) provides the simplest, realistic single parameter variational form.

A number of different methods may be used to evaluate the multidimensional integrals which must be performed in order to determine the energy expectation value. The probability distribution which must be sampled in order to calculate the energy of the N body system is

$$P_N(\underline{r}) = \psi^2(\underline{r}) = \prod_{i<j} f^2(r_{ij}) / \int \prod f^2 \tag{4.5}$$

Since the form of $P_N(\underline{r})$ is identical to the probability distribution for a classical fluid of particles interacting with pair wise additive forces, ($f^2(r_{ij})$ replacing the classical Boltzmann factor $e^{-\beta V(r_{ij})}$), the methods

of classical statistical mechanics may be applied to evaluate the multidimensional integral.

In their work on the quantum hard sphere gas Jastow (1955) and later Aviles (1958) partially summed the Ursell-Mayer cluster development (Hirschfelder, Curtiss and Bird (1964)) of the energy expectation integral in powers of the density. Their results were only valid at low densities due to the slow convergence of the cluster expansion. Murphy and Watts (1970) used the Percus-Yevick and Hypernetted Chain integral equation theories (Watts and McGee (1976)) to perform variational calculations on ^{4}He modeled with the Lennard-Jones potential. They compared the results of the approximate theories with Monte Carlo calculations.

The Monte Carlo method of Metropolis et al. (1953) provides a numerically exact means of evaluating the energy expectation integral. McMillan (1965) first used this method in a variational study of Lennard-Jones ^{4}He. When the pair product wave function of equation (4.2) is used, the energy expectation integral appearing in equation (4.1) can be written as

$$\int \psi^* \hat{H} \psi d\underline{r} = \int \left[\sum_{i<j} \frac{h^2}{2m} \nabla_i^2 \ln f(r_{ij}) + V(r_{ij}) \right] \psi^2(\underline{r}) d\underline{r} \qquad (4.6)$$

Equation (4.6) can be rewritten in terms of the probability distribution defined in equation (4.5).

$$\langle F \rangle = \int F(\underline{r}) P_N(\underline{r}) d\underline{r} \qquad (4.7)$$

Here $F(\underline{r})$ is the quantity in square brackets in equation (4.6). The Monte Carlo method relies on the fact that the distribution, P_N, has the following properties

$$P_N(\underline{r}) \geq 0 \qquad \forall\, \underline{r}$$

$$\int P_N(\underline{r})d\underline{r} = 1 \tag{4.8}$$

With the Monte Carlo method, the integral in equation (4.7) is estimated by interpreting it as an average of the function $F(\underline{r})$ over the distribution $P_N(\underline{r})$. The integral is evaluated by performing an ensemble average over a finite sample of configurations of the N particles. Thus, after n configurations, $\{\underline{r}^i\}$, have been sampled from the distribution $P_N(\underline{r}^i)$, the integral is approximated as

$$\langle F_n \rangle = \frac{1}{n} \sum_{i=1}^{n} F(\underline{r}^i)$$

and (4.9)

$$\langle F \rangle = \lim_{n\to\infty} \langle F_n \rangle$$

The Monte Carlo scheme of Metropolis et al. (1953) involves generating configurations sampled from P_N by using a Markov chain. Each successive configuration, $\underline{r}^{i+1}$, is generated from the previous configuration $\underline{r}^i$ by accepting or rejecting a uniform random displacement of one of the particles. By choosing the transition probability appropriately (Watts and McGee (1976)) the limiting distribution of the chain can be made to equal $P_N(\underline{r})$.

McMillan used the pair function given in equation (4.4) in his Monte Carlo calculations so the classical Boltzmann factor was replaced as follows

$$e^{-V(r)/k_BT} \rightarrow e^{-2(\alpha/r)^5}$$

Once a value of α is found for which the quantity in equation (4.6) is a

minimum the quantum calculation becomes equivalent to a classical calculation with a fictitious potential and temperature which determine the distribution function. When evaluating the energy the actual interparticle potential must be averaged over the distribution.

Classical molecular dynamics provides an alternative method for sampling a distribution. Schiff and Verlet (1967) used the equilibrium molecular dynamics method to perform variational calculations on liquid ^{3}He and ^{4}He. With this approach the fictitious potential described above determines pseudo forces which are used, together with classical equations of motion to move the particles in such a way as to sample the approximate quantum distribution. Systems of Fermions such as ^{3}He can be studied with variational methods by use of an antisymmetric trial function. A Jastrow form multiplied by a Slater determinent is often used. Ceperley (1978) has considered such a form in variational calculations on the electron gas.

Variational procedures provide only an upper bound for the energy. The quantum Monte Carlo method in principle, however, does not have this constraint. In the next section we discuss an exact method known as Greens Function Monte Carlo which is closely related to the diffusion Monte Carlo method described in Chapter 2.

2.) Greens Function Monte Carlo

The Greens Function Monte Carlo method is an essentially exact numerical procedure for solving diffusion equations. It was developed by Kalos and his co-workers (Kalos (1970), Kalos, Levesque and Verlet (1974) and Ceperley and Kalos (1979)) and involves iterating an equivalent

integral equation many times. Unlike the diffusion quantum Monte Carlo method described in Chapter 2, the Green's Function Monte Carlo (GFMC) procedure does not require the finite time step approximation. The GFMC method however is significantly more complicated.

In this section we present a brief description of the GFMC method. Most of the published non-variational quantum calculations performed on bulk phase systems have used the GFMC method and relatively little bulk phase work has been done with the diffusion Monte Carlo procedure.

The GFMC method is useful for solving the Schrödinger equation

$$\hat{H}\psi = \left[-\sum_i \frac{\hbar^2}{2m_i} \nabla_i^2 + V(\underline{r})\right]\psi = E\psi \qquad (4.10)$$

to obtain the lowest energy solution, ψ_o, and the corresponding eigenvalue E_o. The Green's function, $G(\underline{r},\underline{r}')$, for the Hamiltonian is defined as the solution of the following equation

$$\hat{H}\, G(\underline{r},\underline{r}') = \delta(\underline{r}-\underline{r}') \qquad (4.11)$$

Boundary conditions for G must be appropriatly specified for the problem of interest (Ceperley and Kalos (1979)). Using (4.11) in (4.10) we find that the wave function is related to the Green's function by the following integral equation

$$\psi(\underline{r}) = E \int G(\underline{r},\underline{r}')\psi(\underline{r}')d\underline{r}' \qquad (4.12)$$

An equation of this form can be solved iteratively starting with a trial solution, $\psi^{(o)}$, in the following recurrence relation

$$\psi^{(n+1)}(\underline{r}) = E \int G(\underline{r},\underline{r}')\psi^{(n)}(\underline{r}')d\underline{r}' \qquad (4.13)$$

When $\psi^{(o)}$ is substituted in (4.13) and the integral performed a new

solution $\psi^{(1)}$ results. The function $\psi^{(1)}$ may be used to start the next interation and the procedure is repeated till convergence.

For a multidimensional system the integral in (4.13) is most efficiently performed by a Monte Carlo technique. For the ground state of a system of Bosons both $G(\underline{r},\underline{r}')$ and $\psi(\underline{r}')$ are everywhere positive. Consequently $\psi(\underline{r}')$ can be treated as a probability density function for sampling a system in a configuration $\underline{r}'$. Similarly, $EG(\underline{r},\underline{r}')$, can be considered as a conditional probability density for generating a set of new systems $\{\underline{r}\}$ given an old system at $\underline{r}'$. Thus the basic iteration for the GFMC method proceeds as follows: A population of points $\{\underline{r}'\}$ is sampled from a distribution $\psi^{(o)}(\underline{r}') = \psi_T(\underline{r}')$ where ψ_T is some trial function and E_T is a trial eigenvalue. A new set of points $\{\underline{r}\}$ must now be selected from the conditional probability density $E_TG(\underline{r},\underline{r}')$ for each $\underline{r}'$. According to equation (4.13) the new set of points obtained from this iteration will be distributed as $\psi^{(1)}(\underline{r})$. The new "generation" of systems may be used directly to iterate the process again.

By writing the distribution after each iteration in terms of an eigenfunction expansion Kalos (1962) showed that the iteration procedure would converge to the lowest energy eigenstate contained in the initial guess. In a similar fashion to the diffusion Monte Carlo method the rate of charge of the ensemble population with iteration gives an estimate of the eigenvalue.

The major requirement of the basic GFMC iteration described above is the ability to produce a new generation of systems from the old by treating the Green's function as a conditional probability density. Consequently the Greens function for the problem must be known in advance. Generally, the Greens function is unknown and the success of the GFMC method depends

on a procedure for sampling $G(\underline{r},\underline{r}')$ without knowing its form explicitly.

With the diffusion Monte Carlo method an approximate Greens function is used. Systems are established in an initial distribution and an iteration procedure similar to that described above is employed to alter the distribution. As discussed in Chapter 2, each system is allowed to undergo free diffusion, followed by replication or death. An iteration consisting of these steps is equivalent to using the following "short time" approximation for the Green's function

$$G(\underline{r},\underline{r}';\Delta\tau) = e^{\frac{-m}{2h^2\Delta\tau}(\underline{r}-\underline{r}')^2} e^{-V(\underline{r}')\Delta\tau} \qquad (4.14)$$

Thus the time steps of diffusion Monte Carlo are equivalent in a sence to the iterations of GFMC.

We now present a brief description of the elaborate procedure which Kalos and his co-workers have devised for sampling the exact Green's function. For our purposes, only a qualitative understanding of the approach is necessary. A more detailed description of the method can be found in the following references: Kalos, Leversque and Verlet (1974) and Ceperley and Kalos (1979).

The sampling scheme involves using another iteration process to solve an integral equation which relates the Green's function on the full domain of configuration space, D, to a known "partial" Green's function, G_U, defined on a subdomain, $D_o(\underline{r}^o) \varepsilon D$ by the following

$$(-\nabla^2+U_o)\, G_U(\underline{r}^1,\underline{r}^o) = \delta(\underline{r}^1-\underline{r}^o) \quad \forall\, \underline{r}^1,\underline{r}^o \varepsilon D_o \qquad (4.15)$$

Here we use atomic units and U_o is chosen so that $U_o \geq V(\underline{r})\ \forall\ \underline{r} \varepsilon D_o$. The boundary condition for G_U is

$$G_U(\underline{r}^1,\underline{r}^o) = 0 \quad \forall \ \underline{r}^1,\underline{r}^o \notin D_o$$

It can be shown (Ceperley and Kalos (1979)) that the full Green's function is related to this partial Green's function by the following integral equation

$$G(\underline{r},\underline{r}^o) = G_U(\underline{r},\underline{r}^o) + \int_{\partial D_o(\underline{r}^o)} [-\nabla_{n_1} G_U(\underline{r}^1,\underline{r}^o)]\, G(\underline{r},\underline{r}^1)\, dr^1 \tag{4.16}$$

$$+ \int_{D_o(\underline{r}^o)} \{\frac{U_o - V(r^1)}{U_o}\}\, U_o\, G_U(\underline{r}^1,\underline{r}^o)\, G(\underline{r},\underline{r}^1)\, d\underline{r}^1$$

Here $\partial D_o(\underline{r}^o)$ is the boundary of the subdomain and $\nabla_{n_1} G_U(\underline{r}^1,\underline{r}^o)$ is the normal derivative of G_U on the boundary. When equation (4.15) is integrated over $D_o(\underline{r}^o)$ we find that

$$\int_{\partial D_o(\underline{r}^o)} -\nabla_{n'} G_U(\underline{r}',\underline{r}^o)\, dr' + U_o \int_{D_o(\underline{r}^o)} G_U(\underline{r}',\underline{r}^o)\, dr' = 1$$

and since $U_o G_U(\underline{r}',\underline{r}^o)$ and $-\nabla_{n'} G_U(\underline{r}',\underline{r}^o)$ are non-negative they are interpreted as probability densities for moves in a random walk which sample either the interior of the subdomain or its boundary respectively. Equation (4.16) can be iterated in the same way as equation (4.13) and a new generation of points distributed around $\underline{r}^o$ acording to $G(\underline{r},\underline{r}^o)$ may be produced. The iteration involves a random walk which includes moves from $\underline{r}^{n-1}$ to $\underline{r}^n$ chosen either on the boundary of $D_o(\underline{r}^{n-1})$ or in its interior. Moves to points on the boundary are chosen with a density $-\nabla_n G_U(\underline{r}^n,\underline{r}^{n-1})$ while points in the interior are sampled according to $G_U(\underline{r}^n,\underline{r}^{n-1})$ and accepted with a probability $(U_o - V(\underline{r}^n))/U_o$. According to equation (4.16) $G(\underline{r},\underline{r}^o)$ is the expected value of the sum of all the $G_U(\underline{r},\underline{r}^n)$ for the $\underline{r}^n$ sampled by the random walk outlined above.

Importance sampling can also be incorporated in the GFMC method and the algorithm must be modified to sample $\psi_T(\underline{r})\ G(\underline{r},\underline{r}^o)/\psi_T(\underline{r}^o)$. As with the diffusion quantum Monte Carlo method, these modifications greatly improve the sampling efficiency and reduce the fluctuations in the algorithm.

The Green's Function Monte Carlo method has been used to perform bulk phase calculations on solid and liquid ^{4}He using the Lennard-Jones potential (Whitlock et al. (1979), (1980)) and more accurate model potentials have been tested by comparing GFMC results with experiment (Kalos, Lee, Whitlock and Chester (1981)). Variational calculations can only be used to set a bound on the potential well depth (Murphy (1972)). Since GFMC provides the exact ground state energy for a given potential, comparison with experiment gives an unambiguous test of the model interaction.

In the next section we demonstrate that when the importance sampled diffusion Monte Carlo method is used accurate results for systems with repulsive forces may also be obtained.

3.) The Diffusion Monte Carlo Method and Condensed Phase Calculations

As discussed in Chapter 2, the diffusion Monte Carlo method has been widely used in electronic calculations where the particle interactions, governed by the Coulomb potential, vary relatively slowly as a function of distance compared with typical intermolecular interactions. The only bulk phase calculations which have been reported using the diffusion Monte Carlo method have involved particles interacting with Coulomb forces (Ceperley and Alder (1980), (1981)). In this section we present the results of some

diffusion Monte Carlo calculations studying the liquid ^{4}He system modeled with hard core Lennard-Jones forces. As discussed in the previous sections this system is well characterised by both variational and Green's function Monte Carlo results so the significance of the finite time step approximation for dense systems with harsh repulsive interactions may be tested.

Infinite systems are usually modelled using a finite number of particles in a cube of side L together with periodic boundary conditions (Watts and McGee (1976)) and the wave function describing the bulk phase system is thus regarded as multiply periodic. The interactions must be truncated at some distance $r_c \leq L/2$. McMillan (1965) found, with variational calculations on liquid ^{4}He, that using as few as 32 particles in the basic cell gave good qualitative information. We have employed a 32 particle system to study the characteristics of the finite time step method. The size of the cell was chosen so that the reduced density in all our calculations was $\rho\sigma^3 = 0.4$ which is about 10% higher than the equilibrium density of the fluid ($\rho_o\sigma^3 = 0.3648$).

The basic diffusion Monte Carlo method which was successfully employed in the previous chapter to study the ground state properties of small molecular clusters was used in our early bulk phase calculations. Thus only diffusion and replication steps were included in the algorithm. We chose a time step of 0.1×10^{-15}s which gave diffusion displacements of the order of typical distance steps used in classical molecular dynamics simulation studies of fluids at triple point densities. Figure 4.1 shows the instantaneous values of the reference energy as a function of time during several calculations in which different size ensembles were considered. A face centred cubic lattice was used as the initial condition in each

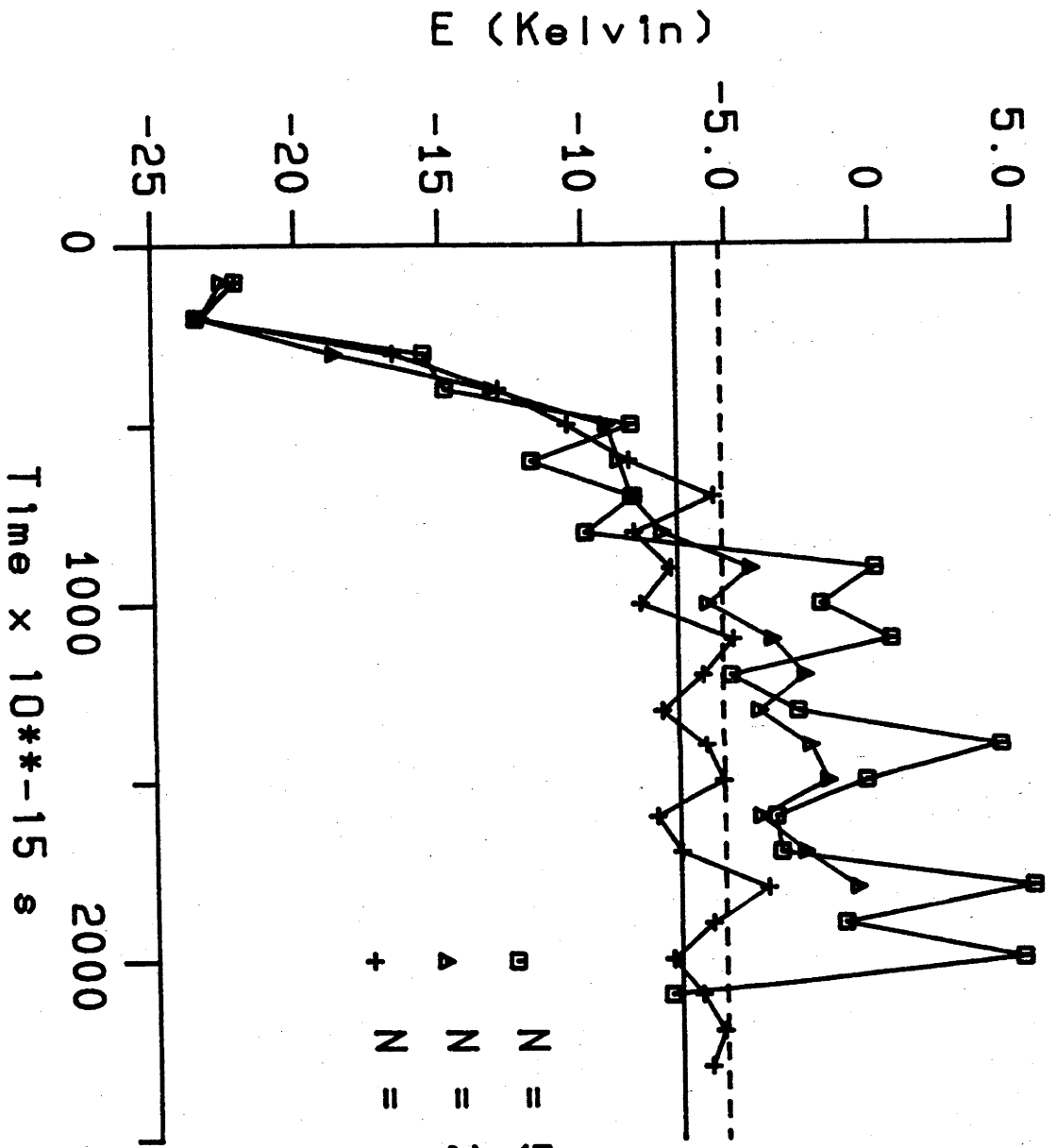
E (Kelvin)
5.0
0
-5.0
-10
-15
-20
-25
0
1000
2000
Time x 10**-15 s
N = 50
N = 200
N = 1000

fig.4.1

calculation. The values have been approximately corrected for long range interactions by assuming the radial distribution function , g(r), is unity beyond the cut off and integrating the potential. For the Lennard-Jones interaction the long range potential correction is approximately

$$V_{lr} = {}^{-8}/_{3}\ \pi\ \rho^{*}\ \varepsilon\ \left(\frac{\sigma}{r_c}\right)^{3}$$

The asymptotic behaviour of the calculations using small ensembles give energies which are too high compared with either the variational or Green's function Monte Carlo results and large fluctuations are observed. By increasing the ensemble size the fluctuations are reduced and the eigenvalue estimate is lowered but the calculation becomes extreamly time consuming. These rather severe problems, of over estimating the eigenvalue and very large fluctuations, probably result from several related factors:

First, the finite time step approximation may be partly responsible for the problems described above. If the time step used was not short enough for the separation of the diffusion and birth-death processes to be accurate, a systematic error in the eigenvalue estimate would be expected. However, the fact that the asymptotic energies presented in Figure 4.1 tend to the GFMC result as the ensemble size is increased indicates that use of a finite step is not the major cause of the difficulties we have observed. With a purely diffusive random walk through a high dimensional space, very large ensembles are necessary to give an adequate sample of the configurations. The over-estimation of the eigenvalue may be related to poor sampling of the multidimensional space. As the initial fcc lattice relaxes systems may diffuse into higher energy geometries. With a small ensemble, the average potential energy will be dominated by these high energy fluctuations. Since the V_{ref} adjustment scheme uses the average

potential energy of the ensemble to set the energy reference for the next time step, such fluctuations may cause the energy estimate to drift.

Another related problem with the free diffusion algorithm is that barriers between potential wells may cause the random walkers to be trapped in a metastable geometry. Trapping can be understood by considering the double square well potential. When the two wells are separated by a long or high potential barrier, an ensemble distribution which starts out on one side of the barrier may rarely sample the other well due to the termination of random walks which enter the barrier. Thus a calculation of finite duration and ensemble size may result in an inadequate sampling of configuration space and incorrect ground state behaviour will be predicted.

In summary, the basic diffusive random walk method is not useful for treating dense systems of many particles which interact with harsh repulsive forces. Importance sampling methods can be used to alleviate the problems discussed above. The drift term included in the importance sampled random walk forces the important regions of configuration space to be sampled so smaller ensembles may be used. Further, as described in Chapter 2, the birth-death process in the importance sampled random walk is no longer governed by the rapidly varying potential function. Rather, the "local energy", $\hat{H}\psi_T/\psi_T$, now controls the population growth rate. If ψ_T approximates the actual wave function the ensemble growth rate will be a slowly varying function of position and the population fluctuations are substantially reduced. Consequently treating the birth-death process as independent of drift or diffusion for small time steps should be a good approximation. In Chapter 2 we also noted that since the drift velocities depend on position there will be an error introduced in the drift path by making the finite time step approximation but the consequences of this

error should be much less severe than the problems described above.

We have performed importance sampled diffusion Monte Carlo calculations for the liquid helium system using the variational Jastrow form given in equation (4.2) together with equation (4.4) as the trial function for guiding the drifting random walk. This trial function has been used by Whitlock et al. (1979) in their Green's function Monte Carlo studies of liquid helium.

First, several 32 particle simulations were conducted using different time steps in order to study the influence of the short time approximation on the importance sampled random walk calculation. A Monte Carlo run sampling the trial distribution ψ_T^2 was performed and after equilibration, every 5000^{th} Monte Carlo configuration was used as a member of the initial ensemble for the importance sampled random walks. Each iteration of the quantum Monte Carlo run involved first calculating the drift velocities, $\underline{v}_k$, of the particles and evaluating the local energy of each system. The particles in a system were moved with a Gaussian displacement in each direction and a drift displacement $\underline{v}_k \Delta\tau$. Finally the systems were allowed to replicate or die depending on their local energy. A V_{ref} adjusting procedure was used to keep the total number of ensemble members fixed at approximately 200 systems.

Time steps used in these calculations were $\Delta\tau = 0.1$, 0.05 and 0.02×10^{-15}s which correspond to standard deviations for the Gaussian distribution of displacements of $\Delta x = 0.013$, 0.0089 and 0.0056 Å respectively. These displacements are on the order of a half to a quarter the size of typical displacements used in molecular dynamics simulations at triple point densities in classical liquids (D.J. Evans (1985)). For each calculation the initial variational wave function distribution was relaxed

for 500×10^{-15}s. Following the equilibration, averages were accumulated for at least 600×10^{-15}s.

The eigenvalues calculated from the average local energy are presented as a function of time step size in Figure 4.2. The errors were estimated by breaking the averaging run into blocks of 100×10^{-15}s and evaluating the average for each block. The standard deviation from the mean of these averages has been used as the error. The fluctuations are substantially reduced by the use of the importance sampling algorithm. For comparison we have included the result obtained from the unbiased random walk calculation using an ensemble of 1000 systems.

We also see from the figure that the importance sampled energy estimates are reasonably independent of time step size. Reducing the time step by a factor of 5 causes the energy estimate to increase by only a few percent. The statistical fluctuations for runs of this duration are of a similar order to these systematic time step errors.

The values presented in this figure have been approximately corrected for long range interactions. In our calculations the potential discontinuously became zero at the cut off. With the classical molecular dynamics method this discontinuity introduces an impulsive force which perturbs the equations of motion. In the classical Monte Carlo method the discontinuity causes a "pile up" in the distribution in the region of the cut off. The wave function sampled by the basic quantum Monte Carlo method will be effected by the cut off in a similar fashion. The birth-death rate becomes discontinuous at the cut off. When importance sampling is used, however, these truncation problems may be more significant since the drift velocities and the local kinetic energy are dependent on the derivatives of the trial wave function. The boundary conditions require that the trial

fig. 4.2

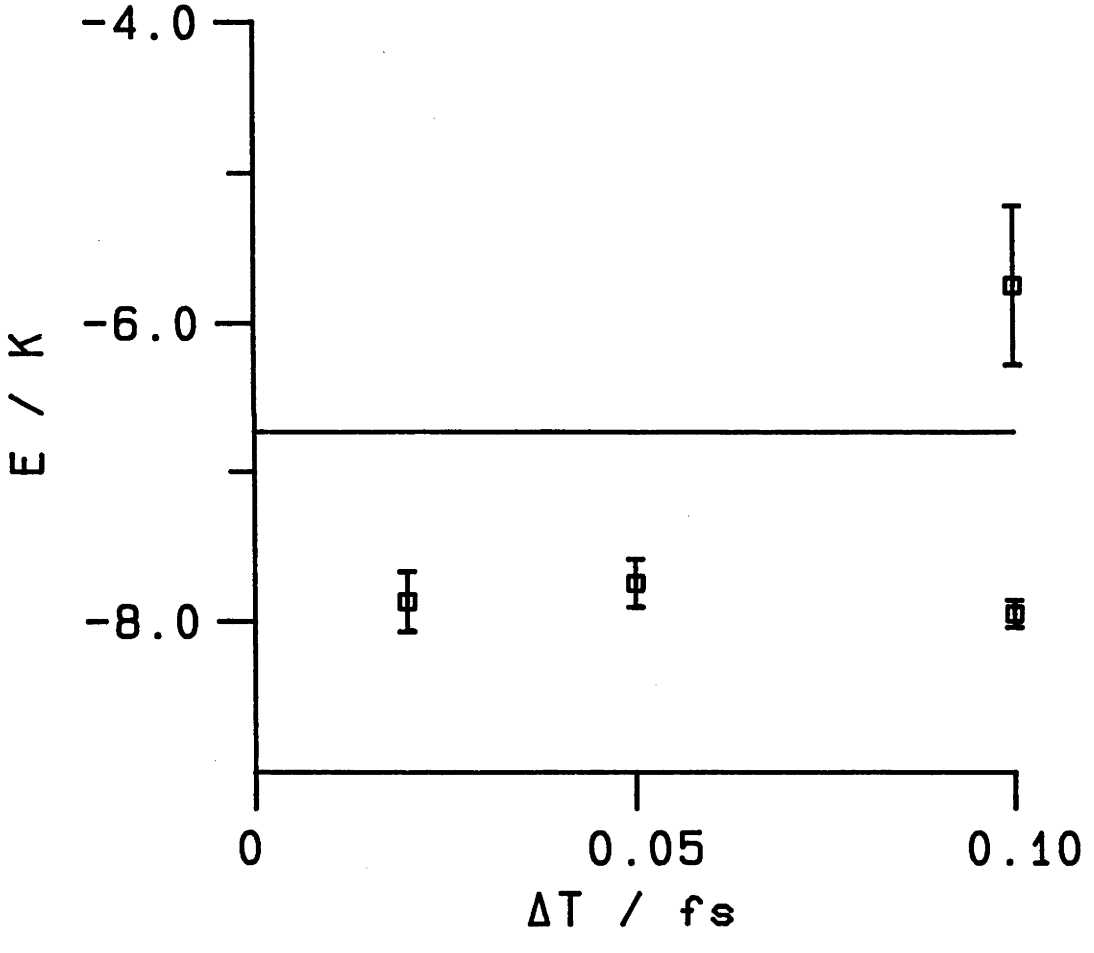

function goes to one discontinuously at r_c. Consequently the drift paths will be influenced by impulsive forces in a similar way to the classical trajectories in molecular dynamics. The effect is most significant with small systems where the discontinuity in the trial function is larger. Differences between the eigenvalues predicted by our importance sampled 32 particle simulations and the GFMC value which are apparent in Figure 4.2 are possibly due to the influences of these impulsive "quantum" forces. Wave function density will be "reflected off" the boundaries causing excessive sampling of lower energy configurations and the eigenvalue is underestimated.

In Chapter 2 we noted that averages of other quantities over the ψ^2 distribution could be obtained by extrapolating the results of importance sampling calculations by using variational results. Equation 2.34 gave an approximate means for performing this extrapolation. Figure 4.3 presents the extrapolated radial distribution functions obtained from our 32 particle calculations and compares them with similar results obtained with 108 particle GFMC calculations (Whitlock et al. (1979)). The radial distribution functions predicted by the shorter time step runs agree reasonably well with the GFMC results. However, the run which used a time step of $\Delta\tau = 0.1 \times 10^{-15}$s shows stronger structural features, the nearest neighbour peak is more pronounced and the portion of the second neighbour peak which is sampled by the calculation is shifted to smaller distances.

The most likely explaination for this behaviour is that with a longer time step the drift paths are more strongly perturbed by the discontinuity in the drift velocity caused by the boundary conditions. Consequently the effects of reflections off the boundaries are more pronounced with longer time steps. It is evident that the distributions obtained with the shorter

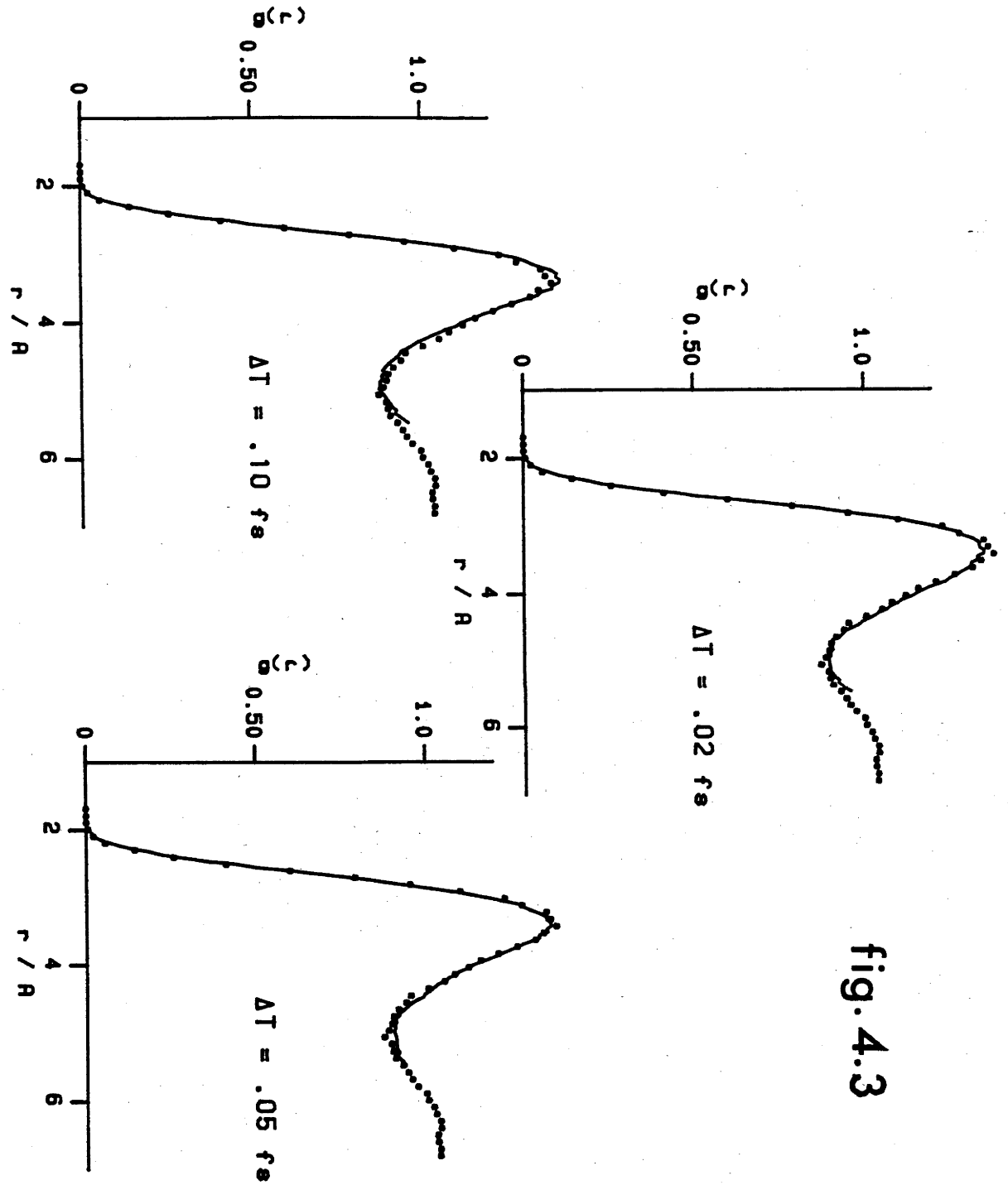

fig. 4.3

time steps ($\Delta\tau$ = 0.05 and 0.02 x 10^{-15}s) are also perturbed by the boundary conditions.

To examine the boundary condition problems discussed above we have performed importance sampled calculation with a system of 108 particles. A time step of $\Delta\tau$ = 0.05 x 10^{-15}s was used and the initial ensemble contained 100 systems distributed according to the variational wave function. In Figure 4.4 we show the effects of extrapolating the radial distribution function obtained from this run by using the variational distribution. Again the results are compared with GFMC values. Good agreement between the diffusion Monte Carlo and GFMC results is generally observed. The two simulations were performed at slightly different densities, ρ^*_{DMC} = 0.4 and ρ^*_{GFMC} = 0.401, so the small variations in the results are probably associated with this density difference. Agreement between the predicated eigenvalues (including only long range corrections) is also good, E_{DMC} = -6.78 ± 0.06 and E_{GFMC} = -6.743 ± 0.033 K/molecule. Whitlock et al. (1979) have obtained a perturbation estimate of the three body correction, and at this density they give $\langle V_{3B} \rangle$ = 0.206 ± 0.002 K/molecule or about 3% of the two body values given above. When the three body correction is made both the quantum Monte Carlo calculations give ground state energies which are approximately 0.5 K/molecule higher than the experimental value E_{exp} = -7.00 K/molecule (Roach, Ketterson and Woo (1970)). This discrepency is a result of the inadequacy of the Lennard-Jones potential (Whitlock et al. (1981)).

The total energy is obtained directly from the importance sampling calculation but the potential and kinetic components must be extrapolated from variational results. By taking the difference between the total and extrapolated potential energies, an estimate of the kinetic energy is

fig. 4.4

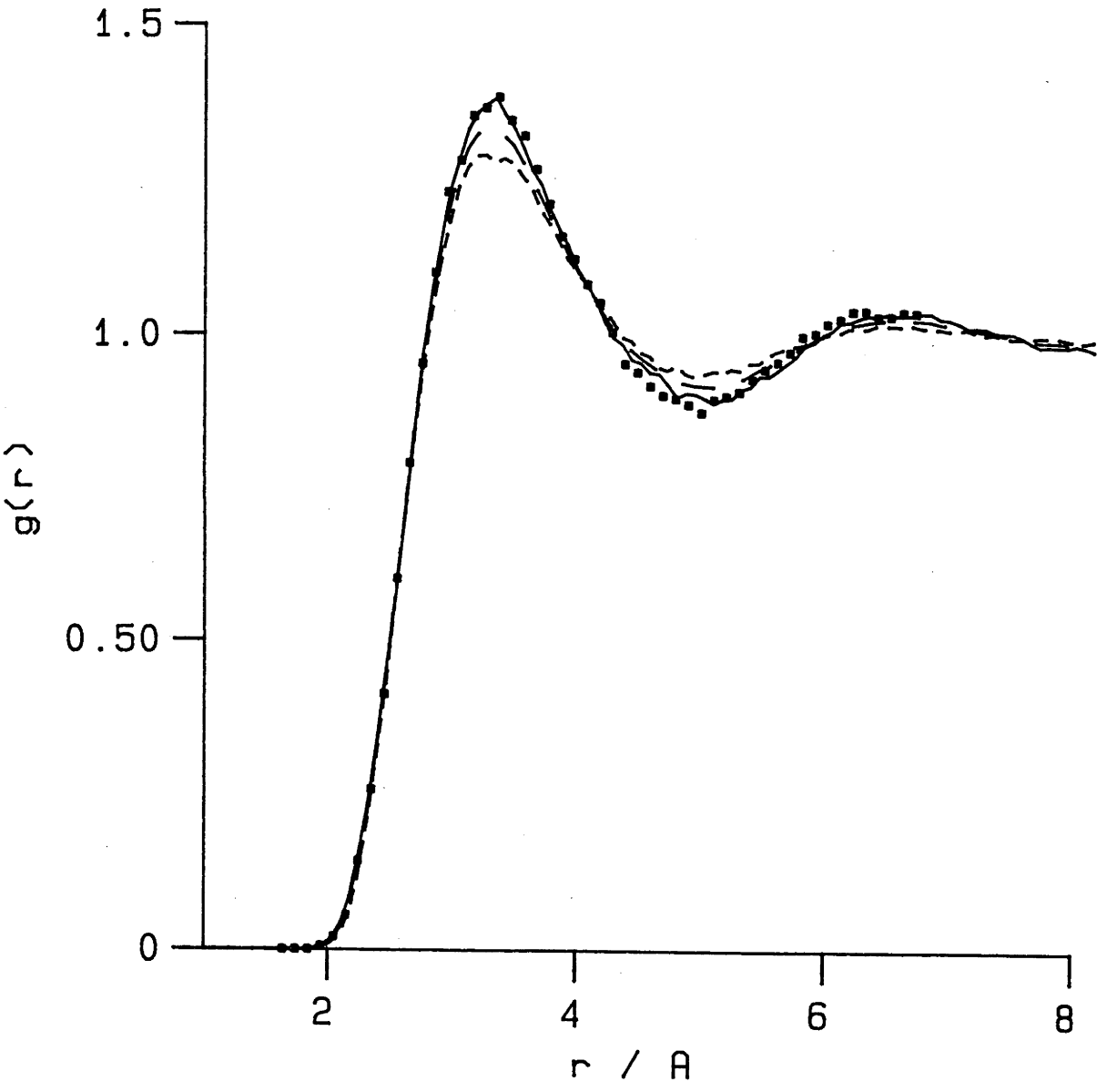

obtained. The potential and kinetic components calculated from our diffusion Monte Carlo run agree with the Green's function Monte Carlo values and $\langle V \rangle_{DMC} = -22.27 \pm 0.15$, $\langle V \rangle_{GFME} = -22.554 \pm 0.182$ and $\langle T \rangle_{DMC} = 15.51 \pm 0.15$, $\langle T \rangle_{GFMC} = 15.811 \pm 0.185$. The major difficulty with calculations on liquid helium is that the total energy is a small difference between two rather large numbers so in order to obtain reasonably accurate total energies very accurate values of the separate kinetic and potential components must be calculated.

The extrapolated full quantum radial distribution function presented in Figure 4.4 shows a more pronounced nearest neighbour peak than the variational result. Whitlock et al. (1979) have argued that this structural difference is a consequence of inadequacy of the variational Jastrow form which does not consider three body correlations. Many body correlations are included by the quantum Monte Carlo methods and these higher correlations should result in more pronounced structure. Chang and Campbell (1977) have performed variational calculations using integral equation methods together with a variational form which included three body correlations explicitly. They obtained ground state energy estimates for helium which are much lower than those predicted with the best Jastrow forms, and only slightly higher than the GFMC or our diffusion Monte Carlo results, indicating that these arguments about the importance of three body correlations in quantum liquids are quite reasonable.

We employed the virial theorem to calculate the pressure in our sample of liquid ^{4}He thus

$$\langle p \rangle = \rho \left[\tfrac{2}{3} \langle T \rangle - \tfrac{1}{3} \langle \Sigma \, \underline{r}_i \cdot \nabla_i V \rangle \right]$$

These values must again be extrapolated using the pressures obtained from

variational calculations. Variational energies are generally within 5 to 10% of the extrapolated full quantum values. Consequently the extrapolation of these quantities is reliable. The pressure obtained from the variational calculation using the virial theorem, $\langle p \rangle_{\psi_O^2} = 25.3 \pm 0.4$ atm, differs substantially from the result calculated from the importance sampled distribution $\langle p \rangle_{\psi\psi_O} = 18.8 \pm 3.$ atm. Thus the extrapolated value, $\langle p \rangle_{\psi^2} = 12.3 \pm 2.$ atm, is not a reliable estimate of the pressure. Whitlock et al. have reported similar difficulties when extrapolating their importance sampled Green's function Monte Carlo pressures. They find that better estimates of the pressure can be obtained by differentiating the energy v's density relation which was fitted to their results. For comparison the pressure they calculate using this procedure is $\langle p \rangle_{GFMC} = 10.388 \pm 1.22$ atm. Roach et al. (1970) have measured the pressure at this density and obtained 10.667 atm.

In the next section we discuss our diffusion Monte Carlo calculations on solid H_2. We will see that there are also significant differences between the variational description of this system and the true quantum solid.

4.) Diffusion Monte Carlo Study of the Ground State of Solid H_2

In this section we apply the importance sampled diffusion Monte Carlo method to study the ground state properties of solid molecular hydrogen. The basic algorithm is very similar to that used in the liquid ^{4}He studies discussed in the previous section. However the importance sampling trial function which guides the random walk is somewhat different for the quantum

solid. The trial function which we have used was proposed by Nosanow (1964) (1966) who performed variational calculations on solid ^{3}He and ^{4}He using cluster expansion methods. Each particle is associated with a lattice site at a position $\underline{R}_i$ and the variational wave function takes the form of a product of single particle functions which depend on the displacements of the particles from their lattice sites, together with a product of pair Jastrow functions which correlate the motions of different particles. Thus the trial function can be written as follows

$$\psi_T(\underline{r}) = \prod_i \phi(\underline{r}_i - \underline{R}_i) \prod_{i<j} f(r_{ij}) \qquad (4.17)$$

In this form the single particle functions model the long range order associated with phonons in the solid and the Jastrow functions take into account the short range correlations which result from the zero point motions together with the strongly repulsive interaction.

The pair function given in equatation (4.4) together with a Gaussian form for the single particle function has been employed by Krumhansl and Wu (1972) who studied solid H_2 using variational cluster expansion methods. Bruce (1972) and Pollock et al. (1972) performed Monte Carlo variational calculations on solid H_2 using the above trial form.

There have also been many variational studies on solid helium which have used this trial function. Hansen and Levesque (1968) considered ^{3}He and ^{4}He in a fcc geometry and Hansen (1969) (1970) studied the hcp and bcc lattices. Hansen and Pollock (1972) considered different single particle functions but no significant improvements over the Gaussian form

$$\phi = e^{-\beta(\underline{r}_i - \underline{R}_i)^2} \qquad (4.18)$$

could be found.

The trial function described above has also been incorporated in a useful, approximate expansion method known as the self consistent phonon theory which was developed and used in computations by Koehler (1966 a,b) (1967) (1968). Gillis et al. (1968 a,b) have discussed a variety of related theories and have used the approach to consider the crystalline rare gases including the hcp phase of ^{4}He. H_2 and D_2 have been studied using these methods by Klein and Koehler (1970 a,b).

Whitlock et al. (1979), (1980) have used the trial form discussed above in importance sampled GFMC calculations on the fcc and hcp crystal phases of ^{4}He. Comparisons between our studies and this work will highlight some interesting differences between solid H_2 and solid ^{4}He.

The major difference between the solid state importance sampled diffusion Monte Carlo algorithm and the method used in our liquid state calculations is that the phonon term in the trial function introduces both an extra kinetic term in the local energy and the drift velocity is modified. A drift component is introduced which pulls the particles towards their lattice sites. Thus if systems wander away from the crystalline structure they either die or drift back towards the lattice.

The hydrogen molecules in our calculations interacted through the spherical part of an effective pair potential presented by Buck et al. (1983) which was derived emperically from total differential scattering cross section measurements. Recently, the potential surface been recommended by Norman et al. (1984) who tested a variety of proposed spherical potentials for the H_2 interaction by comparing the results of both scattering calculations and solid state calculations, using the Monte Carlo variational method, with experimental data.

We have performed importance sampled diffusion Monte Carlo calculations

on solid H_2 at three different molar volumes: 23.08, 11.39 and 8.34 $cm^3\ mole^{-1}$. The system contained 108 particles in a periodic cube and an initial ensemble of 100 systems taken from a variational distribution was used. As the importance sampling function for our calculations we employed the solid state variational wave function described above together with the variational parameters determined by Bruce (1972) for the Lennard-Jones potential. These parameters are very similar to those used by Norman et al. (1984) in their variational studies on various interaction potentials for H_2.

A detailed study of the time step size dependence has not been conducted, rather, the time steps were chosen with two considerations in mind. First, we wanted the population fluctuations to have a maximum amplitude of one or two systems using a V_{ref} adjustment parameter, α (equation 2.15), which was of the order of 10% of the ground state energy per system. Secondly, for reasonable computation times, $\Delta\tau$ was chosen so that the relaxation from the initial variational distribution took several thousand time steps and quantities were averaged for a further few thousand steps. In order to meet these criteria we found that smaller time steps were necessary at higher densities. The steps which we used at the various densities were $\Delta\tau$ = 0.01, 0.005 and 0.002 x 10^{-15}s at molar volumes 23.08, 11.39 and 8.34 $cm^3\ mole^{-1}$ respectively. These time steps are smaller than those used in our helium studies due to the difference in density (the molar volume in our helium work, for comparison, was 25.144 $cm^3\ mole^{-1}$).

The ground state energies and the kinetic and potential components, are compared with the results of variational calculations in table 4.1

Table 4.1 Calculated Energies (in Kelvin/molecule) for Solid H_2 Obtained from Diffusion Monte Carlo and Variational Studies.

Vmol	$\langle H \rangle^1$	$\langle V_2 \rangle^2$	$\langle T \rangle$	$\langle H \rangle^1_\nu$	$\langle V_2 \rangle^2_\nu$	$\langle T \rangle_\nu$	$\langle V_{3B} \rangle_\nu$	$\rho\sigma^3$
23.08	-96.5±1.2	-162±1	65.5±1.5	-84.6	-168.	76.6	6.8	0.676
11.39	358±4	46.3±0.5	262±3	385.	4.4	331.	49.6	1.37
8.34	1445±15	849±4	469±4	1525.	787.	610.	127.	1.87

subscript ν indicates variational results.

[1]Total energy includes the variational estimate of the three body Axilrod-Teller interaction (Norman and Watts (1985)).

[2]Long range correction to the potential energy is included.

Dispersion terms were integrated beyond the cut off, as discussed earlier, to give an estimate of the long range correction to the potential. The three body energies given in Table 4.1 were taken from Norman and Watts (1985) who averaged the triple dipole term of Axilrod and Teller (1943) in a 500 particle Monte Carlo variational calculation. These values have been used to approximately correct the diffusion Monte Carlo results.

In Table 4.2 the total energies and pressures obtained from variational and diffusion Monte Carlo calculations on solid H_2, modelled using the Buck potential, are compared with experimental results.

Table 4.2 Comparison with experiment of Energies and pressures obtained from variational and diffusion Monte Carlo calculations.

Vmol	$\langle H \rangle^{1}_{exp}$	$\langle H \rangle$	$\langle H \rangle_{v}$	$\langle P \rangle^{1}_{exp}$	$\langle P \rangle$	$\langle P \rangle_{v}$
23.08	-93.5	-96.5	-84.6	1	10±5	5.2
11.39	3.19×10^{2}	3.58×10^{2}	3.85×10^{2}	1.30×10^{4}	1.36×10^{4}	1.47×10^{4}
8.34	1.29×10^{3}	1.45×10^{3}	1.53×10^{2}	4.78×10^{4}	5.12×10^{4}	5.30×10^{4}

[1]Experimental values are taken from the work of Norman et al. (1984)

At each density the total energy obtained from the diffusion Monte Carlo calculation is of the order of 5 to 10% lower than the variational energy. Lower pressures are also found when the diffusion Monte Carlo method is used. The differences for both the energy and pressure bring the results of our diffusion Monte Carlo calculations into closer agreement with experiment than the variational values. At the higher densities the extrapolation of the pressures is quite reliable. However, there are considerable fluctuations in the pressure at the lowest density and the variational and DMC results differ substantially.

The most significant difference between the variational and diffusion Monte Carlo results presented in Tables 4.1 and 4.2 is the change in the break up of the energy into its potential and kinetic components. In Figure 4.5 we plot the components of the total energy as a function time during the importance sampled random walks. The figure demonstrates how the energies change as the initial variational distributions are modified by the quantum Monte Carlo calculation. The potential energies presented in the figure were calculated by extrapolation and the kinetic component was obtained by difference.

Fig. 4.5

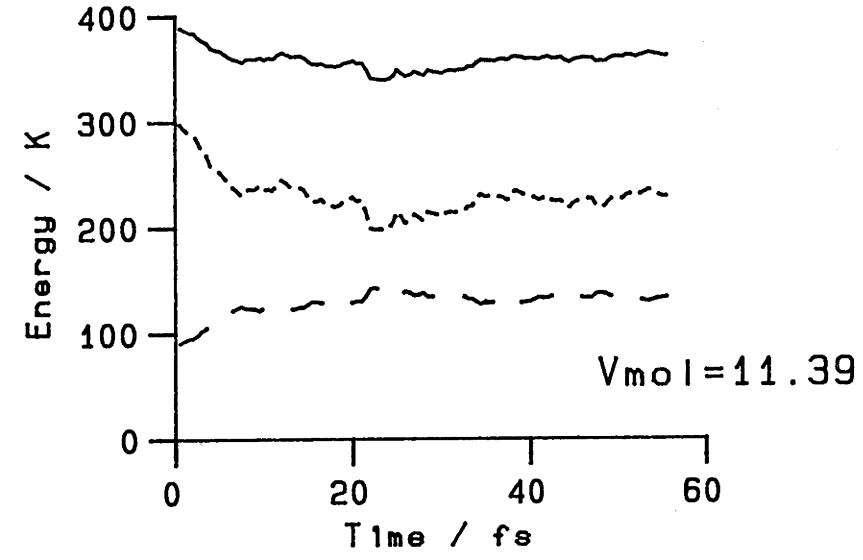
400
300
200
100
0
Energy / K
Vmol=11.39
0
20
40
60
Time / fs

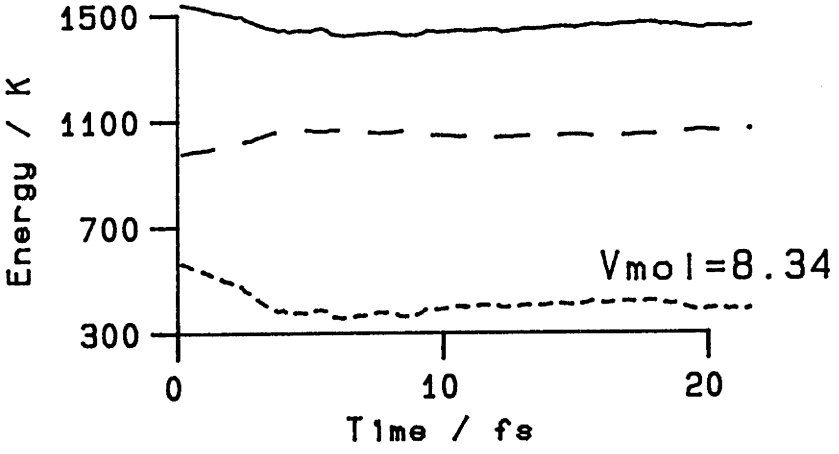
1500
1100
700
300
Energy / K
Vmol=8.34
0
10
20
Time / fs

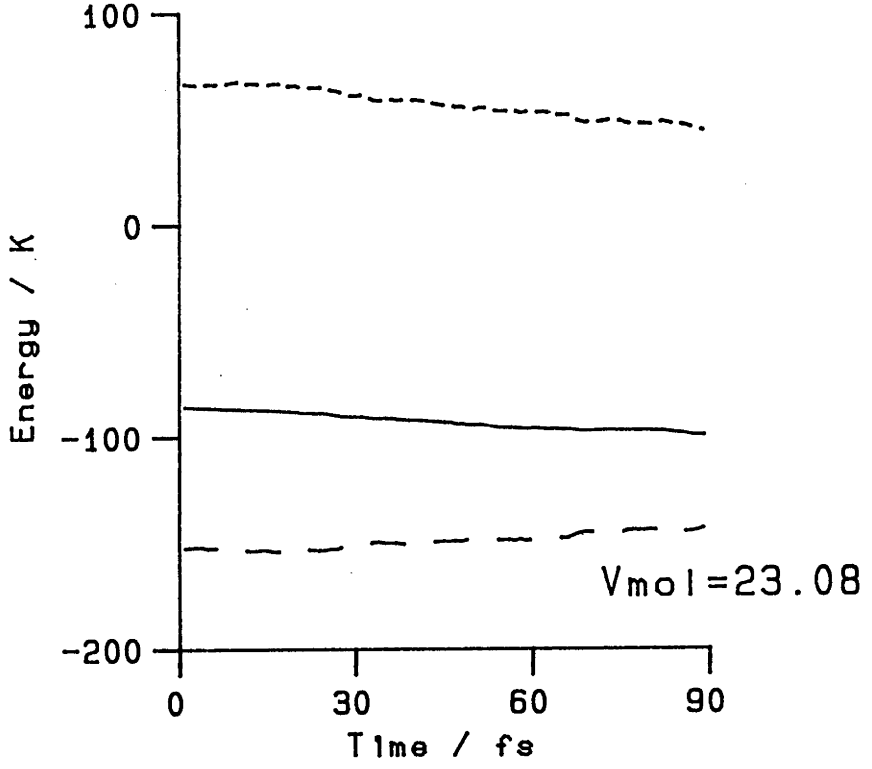
100
0
-100
-200
Energy / K
Vmol=23.08
0
30
60
90
Time / fs

Generally the potential energy increases as the variational distribution relaxes and the reduction in the total energies are the result of large decreases in the kinetic components. There is more than 20% reduction in the variational kinetic energy at the highest density. These energetic changes are the result of structural modifications in the crystal as demonstrated in Figure 4.6. In this figure we plot the radial distribution functions obtained from the ψ_T^2, $\psi_T\psi$ and extrapolated ψ^2 distributions. The changes in the potential energy can be understood in terms of the radial distribution functions. The pair potential used in our calculations is plotted in the figure to show the regions of the surface sampled at the different densities. For comparison, the Lennard-Jones potential for H_2 is also shown in this figure. All the peaks in the radial distribution functions are broader with the extrapolated wave function than with the variational form. The broadening of the nearest neighbour peak causes the repulsive wall of the potential to be more strongly sampled and a higher potential energy results.

The members of our ensemble which tunnel into the repulsive walls of the potential have negative kinetic energies. On average the kinetic energy can never be negative but components of the ensemble which sample "tunneling" configurations will make negative contributions to the kinetic energy as a result of the curvature of the trial function in this region. From the discussion in Chapter 2, the kinetic energy will depend on the quantity $-\hbar^2/2m\nabla^2\psi/\psi_T$. The ensemble describing the wave function in our solid state calculations is thus able to obtain a lower average total energy by allowing more systems to tunnel into the repulsive wall so that the decrease in the average kinetic energy of the ensemble distributions is larger than the resulting increase in the potential energy.

fig.4.6

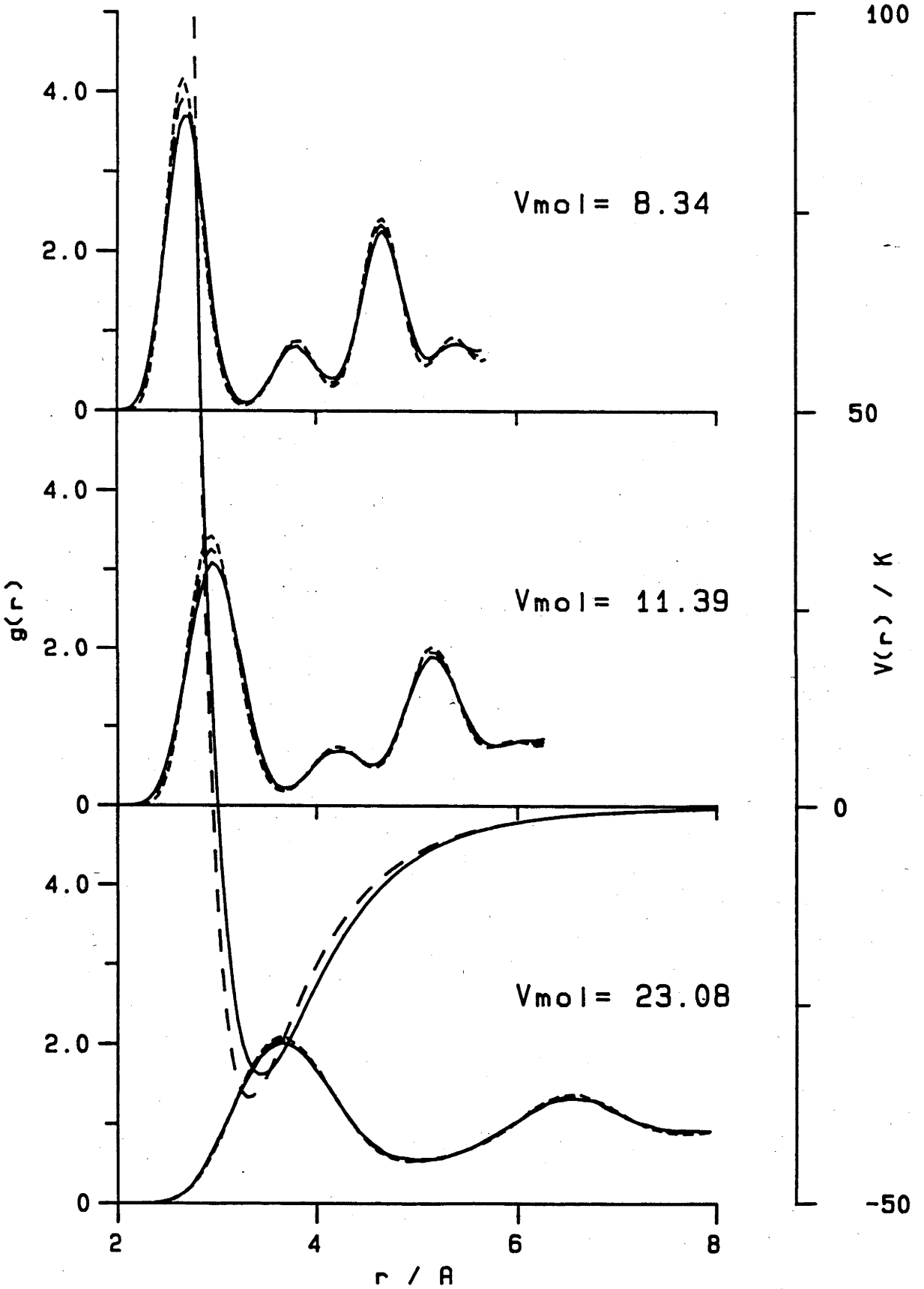

The inadequacies of the solid state variational wave function which we have used are different from those of the trial form for the liquid state. Earlier we saw that with liquid ^{4}He the Jastrow form gave a fluid which was not sufficiently structured, possibly due to the neglect of many body correlations. The trial form used in the variational calculations of Norman et al. (1984) and in our variational work gives a solid which is too strongly structured. A possible reason for this problem is that the pair form, $\tilde{u}(r) = (\alpha/r)^5$, used in the trial wave function does not allow sufficient penetration into the repulsive wall of the potential. As discussed in Section 1.), the pair function is based on the WKB approximate solution for the r^{-12} hard wall problem. In Figure 4.6 we also show the Lennard-Jones potential for H_2. It is apparent that the r^{-12} wall of this potential rises more steeply than the potential due to Buck et al. (1983). Hence, using the variational form based on the more rapidly rising potential does not seem to allow sufficient tunneling into the softer Buck potential. It would be useful to consider different variational forms based on softer analytic potentials. Use of such forms should give better variational results and provide more efficient importance sampling trial functions.

The differences between the diffusion Monte Carlo results and the experimental values apparent in Table 4.2 are most likely due to the inadequacies of the spherical pair potential which was used in the calculations. In general the energies calculated using this potential are on the order of only 10% too high so the form provides a better description of the interaction than the variational results would have us believe. The discrepancy may result in part due to the assumption of a spherical interaction. Hydrogen molecules deviate from a spherical shape by about 8%

(Kolos and Roothan (1960)) so their interaction should be anisotropic. The potential which we have used in our calculations is only the spherical part of the interaction given by Buck et al. who have presented a full anisotropic form written in terms of a spherical harmonic expansion (see also Norman et al.).

Explaination in terms of the neglect of anisotropy is consistent with the way the discrepancy between the experimental and calculated results changes with density. At the lowest density the difference is only 3%, whereas at higher densities the spherical potential gives energies which are about 12% too high. Large zero point motions which characterise the low density quantum solid will average out the effects of a weakly anisotropic potential but at high densities the anisotropy may have a significant effect.

An alternative explaination for the differences between the calculated and experimental results may be the use of the finite time step approximation. Since the rapidly varying parts of the potential are most often sampled at high densities, very small time steps are required for accurate results. As mentioned earlier we have used smaller time steps with the high density runs but it may be possible that the finite time step approximation is still inaccurate.

Conclusion

In this chapter we have seen that the diffusion Monte Carlo method may be applied successfully to study bulk phase quantum systems with harsh repulsive forces provided importance sampling methods are used. Without

importance sampling the diffusive random walk gives very large fluctuations and the method is not useful. When importance sampling is incorporated however, the procedure is able to give results which are sufficiently accurate to provide a sensitive test for intermolecular potentials. Since variational methods can only give an upper bound for the energy the results of these calculations can provide only a qualitative understanding of a quantum system.

The major problem with both the diffusion Monte Carlo and Green's function Monte Carlo methods is the enormous expense of the calculations. Typically these procedures require on the order of 50 to 100 times more computer resources than equivalent variational computations. Generally the improvements are significant, but on the order of only 10%. A profitable approach for future developments may be to use the results of full quantum calculations to study the performance of different variational forms. By monitoring the relaxation of the variational distribution as the full quantum calculation proceeds useful information about the inadequacies of the variational form can be obtained.

CHAPTER 5 QUANTUM MONTE CARLO AT NON-ZERO TEMPERATURES

1.) Formal Preliminaries

In this chapter we concern ourselves with extending the basic quantum Monte Carlo method described in Chapter 2 to treating systems in thermal equilibrium at non-zero temperatures. The quantum operator of interest for such systems is the density operator which, in the canonical ensemble takes the following form

$$\hat{\rho} = e^{-\beta\hat{H}} \tag{5.1}$$

Here $\beta = 1/k_B T$ and $\hat{H}$ is the Hamiltonian operator given by

$$\hat{H} = -\sum_{i=1}^{N} \frac{\hbar^2}{2m_i} \nabla_i^2 + V(\underline{r}) \tag{5.2}$$

for a system of N particles interacting with one another through a potential $V(\underline{r})$. We will restrict ourselves to dealing with the canonical ensemble. Only Boltzmann statistics is considered in our discussion.

In the coordinate representation the density operator becomes a continuous matrix whose elements are defined as

$$\rho(\underline{r},\underline{r}';\beta) = \sum_n \psi_n^*(\underline{r}') e^{-\beta\hat{H}} \psi_n(\underline{r}) \tag{5.3a}$$

$$= \sum_n e^{-\beta E_n} \psi_n^*(\underline{r}') \psi_n(\underline{r}) \tag{5.3b}$$

Here E_n and $\psi_n(\underline{r})$ are the energy eigenvalues and normalised position eigenfunctions of the Hamiltonian.

The diagonal elements of this matrix

$$P(\underline{r};\beta) = \rho(\underline{r},\underline{r};\beta) \tag{5.4}$$

represent the probability of finding a system which is in thermal equilibrium at a temperature β, at a point $\underline{r}$ in the configuration space.

In the momentum representation the density matrix takes a form analogous to equation (5.3)

$$\begin{aligned}\rho(\underline{p},\underline{p}';\beta) &= \sum_n e^{-\beta E_n}\Phi_n^*(\underline{p}')\,\Phi_n(\underline{p}) \\ &= \int \rho(\underline{r},\underline{r}';\beta)e^{-i/h(\underline{p}\cdot\underline{r}-\underline{p}'\cdot\underline{r}')}d\underline{r}\,d\underline{r}'\end{aligned} \tag{5.5}$$

$\rho(\underline{p},\underline{p}';\beta)$ is the complete Fourier transform of the density matrix in the coordinate representation.

In the above $\Phi_n(\underline{p})$ are the energy eigenfunctions in the momentum representation and $\Phi_n(\underline{p})$ and $\psi_n(\underline{r})$ are related by Fourier transformation.

$$\psi_n(\underline{r}) = \hbar^{-3N}\int \Phi_n(\underline{p}')\, e^{i/\hbar\ \underline{p}'\cdot\underline{r}}\, d\underline{p}' \tag{5.6}$$

$$\Phi_n(\underline{p}') = (2\pi)^{-3N}\int \psi_n(\underline{r}'')\, e^{-i/\hbar\ \underline{p}'\cdot\underline{r}''}d\underline{r}'' \tag{5.7}$$

The components, p_i of the vector $\underline{p}$ are the eigenvalues of the momentum operators $\hat{p}_i = i\hbar\ \partial/\partial r_i$ and satisfy the following

$$i\hbar\ \frac{\partial}{\partial r_i}\,|\underline{p}\rangle = p_i|\underline{p}\rangle$$

Here the momentum eigenfunctions are

$$|\underline{p}\rangle = e^{-i/\hbar\ \underline{p}\cdot\underline{r}}$$

The correspondence principle gives that in the high temperature limit the momentum eigenvalues become the classical momenta of the particles and

$$\lim_{\beta \to 0} p_i = m_i \dot{r}_i \tag{5.8}$$

The quantum mechanical probability of finding a system with a momentum vector $\underline{p}$ at a temperature β is related to the diagonal elements of the density operator in the momentum representation. Thus in a similar fashion to equation (5.4) we have that

$$P(\underline{p};\beta) = \rho(\underline{p},\underline{p};\beta) \tag{5.9}$$

If the functions $P(\underline{p};\beta)$ and $P(\underline{r};\beta)$ are known then integrations over $\underline{p}$ or $\underline{r}$ would yield average values of various quantities in the same way as classical averages are calculated from the Gibbs phase space distribution function. The position and momentum probability densities can be obtained from the function $F(\underline{p},\underline{r};\beta)$ which is defined as the partial Fourier transform of the density matrix

$$F(\underline{p},\underline{r};\beta) = \int e^{i/\hbar\, \underline{p}\cdot\underline{r}'} \rho(\underline{r},\underline{r}';\beta)\, d\underline{r}' \tag{5.10}$$

An alternative form for F can be obtained by the following manipulations. Substituting equation (5.3a) into (5.10) we find

$$F(\underline{p},\underline{r};\beta) = \int e^{i/\hbar\, \underline{p}\cdot\underline{r}'} \sum_n \psi_n^*(\underline{r}') e^{-\beta\hat{H}} \psi_n(\underline{r})\, d\underline{r}'$$

Now by using equation (5.6) the above expression is written as

$$F(\underline{p},\underline{r};\beta) = \iint e^{i/\hbar\, \underline{p}\cdot\underline{r}'} \sum_n \psi_n^*(\underline{r}')\, \Phi_n(\underline{p}') e^{-\beta\hat{H}}\, e^{i/\hbar\, \underline{p}'\cdot\underline{r}}\, d\underline{p}'d\underline{r}'$$

Employing equation (5.7) to eliminate the functions Φ_n we find

$$F(\underline{p},\underline{r};\beta) = \iiint e^{i/\hbar\, \underline{p}\cdot\underline{r}'} \sum_n \psi_n^*(\underline{r}')\, \psi_n(\underline{r}'') e^{-i/\hbar\, \underline{p}'\cdot\underline{r}''} e^{-\beta\hat{H}}\, e^{i/\hbar\, \underline{p}'\cdot\underline{r}}\, d\underline{p}'d\underline{r}'d\underline{r}''$$

Using the completeness relation

$$\sum_n \psi_n^*(\underline{r}') \, \psi_n(\underline{r}'') = \delta(\underline{r}'-\underline{r}'') \tag{5.11}$$

and the properties of integrals of $\delta(\underline{r}'-\underline{r}'')$, the integral over $\underline{r}''$ can be performed to give

$$F(\underline{p},\underline{r};\beta) = \iint e^{i/\hbar \, (\underline{p}-\underline{p}').\underline{r}'} \, e^{-\beta\hat{H}} \, e^{i/\hbar \, \underline{p}'.\underline{r}} \, d\underline{p}' d\underline{r}'$$

The $\underline{r}'$ integration can now be done using the relation

$$\int e^{i/\hbar \, (\underline{p}-\underline{p}').\underline{r}'} d\underline{r}' = \delta(\underline{p}-\underline{p}') \tag{5.12}$$

Finally by integrating over $\underline{p}'$ we obtain the following form for F

$$F(\underline{p},\underline{r};\beta) = e^{-\beta\hat{H}} \, e^{i/\hbar \, \underline{p}.\underline{r}} \tag{5.13}$$

The functions $P(\underline{r};\beta)$ and $P(\underline{p};\beta)$ are related to F by the following results which were first given by Kirkwood (1933)

$$P(\underline{r};\beta) = \int e^{-i/\hbar \, \underline{p}.\underline{r}} \, F(\underline{p},\underline{r};\beta) \, d\underline{p} \tag{5.14}$$

$$P(\underline{p};\beta) = \int e^{-i/\hbar \, \underline{p}.\underline{r}} \, F(\underline{p},\underline{r};\beta) \, d\underline{r} \tag{5.15}$$

Equation (5.14) is easily proved by substituting the definition for F given in equation (5.10)

$$P(\underline{r};\beta) = \iint e^{i/\hbar \, \underline{p}.(\underline{r}'-\underline{r})} \, \rho(\underline{r},\underline{r}';\beta) \, d\underline{r}' d\underline{p}$$

The $\underline{p}$ integral gives a $\delta(\underline{r}'-\underline{r})$ factor and performing the $\underline{r}'$ integration gives the required diagonal elements. (5.15) can be justified by again substituting (5.10), using (5.3b) and rearranging to obtain

$$P(\underline{p};\beta) = \sum_n e^{-\beta E_n} \int e^{i/\hbar \, \underline{p}.\underline{r}'} \psi_n^*(\underline{r}') \, d\underline{r}' \int e^{-i/\hbar \, \underline{p}.\underline{r}} \psi_n(\underline{r}) \, d\underline{r}$$

Using equation (5.7) in this result completes the proof of (5.15).

The function F satisfies the Bloch equation (Hill (1956))

$$\frac{\partial F(\underline{p},\underline{r};\beta)}{\partial \beta} = -\hat{H}\, F(\underline{p},\underline{r};\beta)$$
$$= \sum_{i=1}^{N} \frac{\hbar^2}{2m_i} \nabla_i^2 F - V(\underline{r})F \qquad (5.16)$$

This can be shown by differentiating (5.13) with respect to β. The initial condition for the solution of equation (5.16) is obtained from equation (5.13) as

$$F(\underline{p},\underline{r};\beta=0) = e^{i/\hbar\ \underline{p}.\underline{r}}$$

The Bloch equation is isomorphic with the time dependent Schrödinger equation, the reciprocal temperature, β, replacing the imaginary time, $it/\hbar$. By considering this isomorphism further it should be possible to extend the quantum random walk method, described in Chapter 2 and so solve (5.16) to obtain $F(\underline{p},\underline{r};\beta)$.

In this section then we have seen that there exists a function $F(\underline{p},\underline{r};\beta)$ whose spatial Fourier transform gives the momentum probability density and whose momentum Fourier transform gives the spatial probability density. The function can be obtained at different temperatures by solving the Bloch equation.

2.) The Non Zero Temperature Quantum Monte Carlo Method

At high temperatures, an approximation for F is

$$\lim_{\beta \to 0} F(\underline{p},\underline{r};\beta) = e^{-\beta H_{class}} e^{i/h\ \underline{p}\cdot\underline{r}} \tag{5.17a}$$

$$= e^{-\beta \sum_j p_j^2/2m_j} e^{-\beta V(\underline{r})} e^{i/\hbar\ \underline{p}\cdot\underline{r}} \tag{5.17b}$$

As discussed earlier, p_j are the components of the classical momenta.

Following Kirkwood (1933) the classical form given in 5.17 provides an initial condition for solution of the Bloch equation. In Chapter 2 we saw that the quantum Monte Carlo method may be used to propagate an ensemble from some initial distribution through imaginary time. The details of the motion were determined by the time dependent Schrödinger equation. In the non zero temperature quantum Monte Carlo method which we shall now describe, the random walk procedure is used to solve the Bloch equation to give a distribution which evolves as a function of the inverse temperature variable β.

At some high initial temperature, β_o, an ensemble distributed according to equation (5.17b) must first be established. We use the classical Monte Carlo method of Metropolis et al. (1953) to generate an ensemble distributed according to the $e^{-\beta V(\underline{r})}$ factor. In order to sample the initial distribution given in (5.17b), the ensemble must be modified to include the factors which contain momenta. A procedure for sampling the classical momentum distribution involves giving each particle a momentum chosen from a Gaussian density. In this way a classical distribution of points in phase space is produced. Weighting each system by a phase factor, $e^{i/\hbar\ \underline{p}\cdot\underline{r}}$, gives an ensemble distributed according to the high temperature

approximation for F which we use as the initial condition for our solution of the Bloch equation.

Momentum variables do not appear explicitly in the Bloch equation, consequently the particle momenta in a given ensemble member do not change as the Bloch equation is solved. Rather, the momenta can be considered as parameterising each random walker and determining its contribution to the ensemble. The procedure outlined above is used to average over the initial position and momentum distributions. We shall see shortly that due to the simple form of the classical momentum distribution the momentum average may be performed analytically. To proceed with our development, however, it is more convenient to consider propagating a set of systems which are weighted by the factors $e^{i/\hbar\ \underline{p}\cdot\underline{r}}$.

A diffusion and birth-death algorithm similar to that described in Chapter 2 is used to evolve the ensemble according to the Bloch equation. Briefly, as the reciprocal temperature is incremented by $\Delta\beta$, the particles in each system are moved through small displacements chosen from a normal distribution with variance $\Delta x = (\hbar^2\Delta\beta/m)^{\frac{1}{2}}$. Diffusion of the ensemble members models the effect of the kinetic operator on the distribution $F(\underline{p},\underline{r};\beta)$ and a birth-death procedure models the potential operator.

There are differences between the physical nature of the solutions of the Schrödinger and Bloch equations and special consideration must be given to the method for modelling the potential term. When solving the Schrödinger equation we have an additional requirement that the physical solutions should be time independent and an eigenvalue problem results. Consequently, the details of the transient behaviour of the ensemble are of no concern. The energy scale can be arbitarily adjusted to slow the population growth or decay and give a stable ensemble in the long time

limit. In Chapter 2 we saw that using a V_{ref} adjusting algorithm forces the ensemble distribution towards the ground state. With this procedure, information about the transient evolution is lost but a stable ensemble with the correct asymptotic distribution is obtained.

The Bloch equation has the same form as the time dependent Schrödinger equation but we are no longer interested in stationary solutions and the equation can not be written as an eigenvalue problem.Information about the system at different temperatures will be obtained by monitoring the transient behaviour of the ensemble. Consequently the V_{ref} adjusting method cannot be used in its current form since it perturbs the transient evolution.

If the V_{ref} adjustment procedure is removed from the birth-death algorithm, the growing or decaying ensemble which results will evolve as the solution of the Bloch equation but this method is unstable and has poor statistical properties. Equivalently, the influence of the potential term may be included as an accumulated weight which is the product of the birth-death probabilities. Thus, if a system samples a set of n points $(\underline{r}_1,\underline{r}_2,\ldots,\underline{r}_n)$ as it evolves through n steps in reciprocal temperature, it is given a weight

$$w = e^{-\sum_{i=1}^{n} \Delta\beta\, V(\underline{r}_i)} \qquad (5.18)$$

The approach outlined above gives the correct transient behaviour, but since the ensemble diffuses freely there is nothing to prevent systems from wandering into "unphysical" regions of the configuration space. The longer systems diffuse, the greater the chance of sampling a region of high potential energy which results either in death or equivalently, a zero weight according to equation (5.18). Consequently the statistics for

sampling low temperature distributions with the method discussed above are very poor.

There are two alternatives which may be used to improve the statistical properties of the algorithm. First an importance sampling scheme may be implemented. In this approach we use quantum Monte Carlo methods to solve the equation of motion for a function f related to $F(\underline{p},\underline{r};\beta)$ by the following expression

$$f = F(\underline{p},\underline{r};\beta)\ F_T(\underline{p},\underline{r};\beta)$$

The function F_T is some known analytic form which resembles F. Proceeding in the manner described in Chapter 2 the following equation of motion for f may be obtained

$$\frac{\partial f}{\partial \beta} = \sum_k \frac{\hbar^2}{2m_k} \nabla_k^2 f - \sum_k \frac{\hbar^2}{m_k} \nabla_k \cdot (f \nabla \ln F_T) - \frac{1}{F_T} \left(\hat{H}\ F_T - \frac{\partial F_T}{\partial \beta}\right) f$$

With a well chosen F_T, the drift term modifies the free diffusive motion so that the ensemble members are forced away from the unphysical regions of configuration space and into the more important regions. By choosing the β dependence of F_T appropriately, a slowly varying birth rate may be obtained and accurate calculations with larger β steps are possible.

As described in Chapter 2, when importance sampling is used to solve the Schrödinger equation an ensemble distributed according to $\psi\psi_T$ is generated. If ψ_T approximates ψ, the importance sampled ensemble distribution will approximate the probability density. Expectation values were evaluated by averaging quantities over the $\psi\psi_T$ distribution and extrapolating to give a ψ^2 distribution. The ensemble generated by importance sampling the Bloch equation, however, cannot be used directly since the importance sampling function must be divided out in order that

averages may be evaluated.

An alternative means of improving the statistical properties of the basic random walk procedure is to use a V_{ref} adjusting approach but to keep track of the values which V_{ref} takes as the ensemble evolves. If the p^{th} ensemble member samples the n points $(\underline{r}_1^p, \underline{r}_2^p, \ldots, \underline{r}_n^p)$ as it diffuses then, with a V_{ref} adjusting algorithm, the systems contributions are weighted by

$$W_n^p = e^{-\sum_{i=1}^{n} (V(\underline{r}_i^p) - V_{ref}^i)\Delta\beta} \tag{5.19a}$$

$$= e^{-\sum_{i=1}^{n} V(\underline{r}_i^p)\Delta\beta} \; e^{\sum_{i=1}^{n} V_{ref}^i \Delta\beta} \tag{5.19b}$$

Here V_{ref}^i is the value of the energy reference which is set by the V_{ref} adjustment mechanism at the i^{th} step in the trajectory. The value of V_{ref}^i is the same for all systems in the ensemble.

As outlined above, the correct transient behaviour may be obtained if a weight of the form given in equation (5.18) is used. Equation (5.19b) differs from (5.18) only in the term involving V_{ref}. Consequently a V_{ref} adjusting algorithm may be used to evolve an ensemble having the correct transient behaviour provided the contributions of the ensemble to various averages are weighted by the factor

$$e^{-\sum_{i=1}^{n} V_{ref}^i \Delta\beta}$$

We have chosen the V_{ref} adjustment scheme outlined above to improve the statistical properties of the random walk technique rather than use importance sampling methods. An importance sampling scheme has been employed by Pollock and Ceperly (1984) to calculate the pair density matrix for the Lennard Jones system.

The discussion so far in this section has described a stable quantum random walk method which can be used to evolve an initial ensemble sampled from a classical high temperature distribution. The motion of the distribution models the solution of the Bloch equation. To proceed, a method for using the evolving ensemble to obtain averages of various quantities at different temperatures must now be devised.

In Section 1.) it was shown that the position and momentum probability densities are related to the Fourier transforms of $F(\underline{p},\underline{r};\beta)$ by equations (5.14) and (5.15). Averages can be calculated by integrating over these probability density functions. Let us now consider using the evolving ensemble to obtain the position probability density at different temperatures.

With the approach we have described, each ensemble member has a weight $e^{i/\hbar\ \underline{p}\cdot\underline{r}}$ which depends on the point in the classical phase space where it commences its random walk. As β is incremented, the system diffuses away from the initial point, $\underline{r}$. After a number of increments, the reciprocal temperature has reached a value β' say, and the system may have diffused to a point $\underline{r}'$. As discussed earlier the particle momenta are unchanged during the random walk. Equation (5.14) gives that the position probability density at β' is obtained by multiplying the distribution $F(\underline{p},\underline{r}';\beta')$ by the factor $e^{-i/\hbar\ \underline{p}\cdot\underline{r}'}$ and integrating over $\underline{p}$. Thus the position probability density may be obtained from the ensemble by weighting each system with another phase factor which depends on the point in configuration space sampled by each system after it has been propagated. The random walkers carry their initial weights $e^{i/\hbar\ \underline{p}\cdot\underline{r}}$ until their trajectory termiantes. Consequently, a system having momentum $\underline{p}$ which diffuses from a point $\underline{r}$ at β_o to a point $\underline{r}'$ at β' shall receive a total weight

$$e^{i/\hbar\ \underline{p}.(\underline{r}-\underline{r}')}$$

The momenta which parameterise the random walkers are chosen from a classical distribution at the initial temperature β_o. The terms appearing in equation (5.14) containing momenta may thus be combined to give a multiplicative factor as follows

$$\int e^{i/\hbar\ \underline{p}.(\underline{r}-\underline{r}')}\ e^{-\beta_o \sum_j \underline{p}_j^2/2m_j}\ d\underline{p} \qquad (5.20)$$

Integrating equation (5.20) gives

$$\prod_{j=1}^{3N} \left(\frac{2\pi m_j}{\hbar^2 \beta_o}\right)^{\frac{1}{2}}\ e^{-m_j/2\beta_o\hbar^2\ (r_j-r_j')^2} \qquad (5.21)$$

An ensemble distributed according to the full quantum position distribution at different temperatures is obtained by weighting the contributions of the ensemble members by Gaussian factors which depend on the distance between the initial and final configurations in the random walk. Thus as a system diffuses away from its starting configuration, its contribution to the ensemble changes according to equation (5.21). The weight given in equation (5.21) is an approximation and its accuracy depends on how well the quantum position and momentum distributions are approximated by the classical results at the initial temperature. Using the classical position distribution, $e^{-\beta_o V(\underline{r})}$, is an approximation which becomes more accurate as the initial temperature is increased. The use of these approximations and more accurate results will be considered in detail in Chapter 6.

A summary of the method which we have used to calculate averages over the quantum position distribution can now be presented:

(1) A classical Monte Carlo method is used to sample configurations at some

high initial temperature. Several hundred systems selected from the Markov chain are used to construct an initial ensemble.

(2) The quantum Monte Carlo method is employed to propagate the ensemble along a "trajectory" in β. Systems are allowed to diffuse, replicate and die.

(3) V_{ref} is adjusted at the end of each β step so as to keep the ensemble population approximately constant. A similar stabilisation procedure to that described in Chapter 2 is used to adjust the energy reference at each time step.

(4) At particular temperatures various position dependent properties are evaluated and averages are accumulated. The contribution of each system is determined by the displacement from its initial configuration as described by equation (5.21).

(5) The contribution which each ensemble of systems makes to the final averages must be weighed by the factor

$$e^{-\sum_{i=1}^{n} V_{ref}^{i} \Delta\beta}$$

In this way the correct temperature evolution may be obtained together with a stable ensemble.

(6) Once the trajectory has reached its final temperature we return to step (1) to establish and propagate another ensemble.

With the algorithm outlined above, averages over a very large ensemble are constructed by accumulating properties from much smaller ensembles. The correct contributions from the smaller ensembles are ensured by using the weighting scheme outlined in step (5).

The statistical convergence of the algorithm will be influenced by the number of systems in the component ensembles. If relatively few systems are

propagated in each cycle, the statistical fluctuations will be large. The value of the energy reference at each β step is related to the average potential energy of the ensemble. Consequently, the set of V^i_{ref} values which is sampled as small ensembles are propagated may differ substantially from one ensemble to the next. Thus the exponential weights included in step (5) may be very different for each small ensemble. With a larger ensemble and a better sampling of the configuration space the values of V^i_{ref} will be similar for all the ensembles and better statistical properties will result. The fluctuations in the algorithm discussed above therefore depend on the exponential of the fluctuations in the quantity $\sum_i V^i_{ref}$.

Finally in this section we consider calculating properties which depend on the momenta. It can be shown (Feynman (1972)) that the average kinetic energy of a system at a temperature β may be calculated from the momentum probability density given in equation (5.15) using the following expression

$$\begin{aligned} \left\langle \sum_j^{3N} p_{j/2m_j}^2 \right\rangle_\beta &= \int \left(\sum_j^{3N} p_{j/2m_j}^2 \right) P(\underline{p};\beta)\, d\underline{p} \\ &= \iint \left(\sum_j^{3N} p_{j/2m_j}^2 \right) e^{-i/\hbar\, \underline{p}\cdot\underline{r}'} F(\underline{p},\underline{r}';\beta)\, d\underline{r}'\, d\underline{p} \end{aligned} \tag{5.22}$$

Here equation (5.15) has been substituted. Collecting factors containing the momenta we find that the momentum integrals in (5.22) can be written in a similar fashion to equation (5.20)

$$\int \left(\sum_j^{3N} p_{j/2m_j}^2 \right) e^{i/\hbar\, \underline{p}\cdot(\underline{r}-\underline{r}')}\, e^{-\beta_o \sum_j \underline{p}_{j/2m_j}^2}\, d\underline{p} \tag{5.23}$$

and this result reduces to the following form

$$\prod_{j=1}^{3N} \left(\frac{2\pi m_j}{\hbar^2 \beta_o}\right)^{\frac{1}{2}} \; e^{-m_j/2\beta_o\hbar^2 \, (r_j - r_j')^2}$$

$$\times \sum_{j=1}^{3N} {}^{1}/_{2\beta_o}\left[1 - m_j/\hbar^2\beta_o (r_j - r_j')^2\right] \tag{5.24}$$

The spatial integrations in (5.22) are performed as before by averaging over the ensemble and including the Gaussian weights. Thus to obtain the kinetic energy we average the summation appearing in (5.24) in the same way as averages of position dependent properties were calculated. Equation (5.24) is an approximation and again its accuracy depends on the assumed classical distributions at the initial temperature.

More detailed information about the quantum momentum distribution can be obtained from the non-zero temperature quantum Monte Carlo procedure. Consider the single particle momentum distribution, defined as follows

$$P(\underline{p}_1;\beta) = \int\!\!\ldots\!\int P(\underline{p}_1,\ldots,\underline{p}_N;\beta)\, d\underline{p}_2 \ldots d\underline{p}_N$$

Substituting (5.15) we find that this result may be written in the form

$$P(\underline{p}_1;\beta) = \int\!\!\ldots\!\int e^{-i/\hbar \; \underline{p}_1\cdot(\underline{r}_1 - \underline{r}_1')} \; e^{-i/\hbar \sum_{j=2}^{N} \underline{p}_j\cdot(\underline{r}_j - \underline{r}_j')}$$

$$\times \xi(\underline{r}\rightarrow\underline{r}';\beta_o\rightarrow\beta)\; e^{-\beta_o \underline{p}_1^{\,2}/2m_1} \; e^{-\beta_o \sum_{j=2}^{N} \underline{p}_j^{\,2}/2m_j}$$

$$\times \, d\underline{r}'\, d\underline{p}_2 \ldots d\underline{p}_N$$

Here the function $\xi(\underline{r}\rightarrow\underline{r}';\beta_o\rightarrow\beta)$ represents the position distribution propagated by the quantum Monte Carlo procedure. As discussed earlier, the integrations over the 3N-3 momentum variables reduce the above equation to the form

$$P(\underline{p}_1;\beta) = \int \prod_{j=4}^{3N} \left(\frac{2\pi m_j}{\hbar^2\beta_o}\right)^{\frac{1}{2}} e^{-m_j/2\beta_o\hbar^2\,(r_j-r_j')^2} \times \xi(\underline{r}\to\underline{r}';\beta_o\to\beta)\; e^{-i/\hbar\;\underline{p}_1\cdot(\underline{r}_1-\underline{r}_1')}\; e^{-\beta_o\underline{p}_1{}^2/2m_1}\; d\underline{r}' \tag{5.25}$$

The probability of finding a particle with vector momentum in a momentum space volume element $d\underline{p}_1$ about $\underline{p}_1$ is

$$P(\underline{p}_1;\beta)d\underline{p}_1 = P(\underline{p}_1;\beta)p_1{}^2\sin\theta dp_1 d\theta d\phi$$

For an isotropic system, all orientations of the momentum vector are equivalent so we can integrate over the angle variables to obtain a distribution of momentum magnitudes. Considering the terms in equation (5.25) which depend only on $\underline{p}_1$, transforming to spherical polar coordinates and letting the z-axis lie along the vector $\underline{r}_1-\underline{r}_1'$ we can write the integral over orientations as

$$\int_0^{2\pi} d\phi \int_{-1}^{1} e^{-i/\hbar\; p_1|\underline{r}_1-\underline{r}_1'|\cos\theta}\; e^{-\beta_o p_1{}^2/2m_1}\; d\cos\theta$$

$$= 2\pi\; e^{-\beta_o p_1{}^2/2m_1} \int_{-1}^{1} \left(\cos(p_1/\hbar\;|\underline{r}_1-\underline{r}_1'|\chi) + i\sin(p_1/\hbar\;|\underline{r}_1-\underline{r}_1'|\chi)\right) d\chi$$

$$= 4\pi\; e^{-\beta_o p_1{}^2/2m_1}\; \mathrm{sinc}(p_1/\hbar\;|\underline{r}_1-\underline{r}_1'|)$$

where $\mathrm{sinc}\; x = \sin x/x$.

Using this result in equation (5.25) we find that the orientation averaged single particle momentum distribution can be written as

$$P(p_1;\beta) = \int \prod_{j=4}^{3N} \left(\frac{2\pi m_j}{\hbar^2\beta_o}\right)^{\frac{1}{2}} e^{-m_j/2\beta_o\hbar^2\,(r_j-r_j')^2} \times \xi(\underline{r}\to\underline{r}';\beta_o\to\beta)\; e^{-\beta_o p_1{}^2/2m_1}\; \mathrm{sinc}(p_1/\hbar\;|\underline{r}_1-\underline{r}_1'|)\; d\underline{r}' \tag{5.26}$$

Equation (5.26) is used to obtain the momentum distribution from a quantum Monte Carlo calculation as follows: At certain points along the temperature trajectory a histogram of the sinc function in the displacement of the particle is accumulated. Each added function must be weighted by a product of Gaussians in the displacements of the other particles. Averaging over many trajectories performs the spatial integrations in equation (5.26). Finally, each histogram must be multiplied by the high temperature Gaussian momentum distribution to give the distribution at the different temperatures along the trajectory.

In this section we have described a random walk procedure which may be applied to calculate the properties of systems at non zero temperatures. The method involves propagating classical high temperature initial ensembles to lower temperatures by performing random walks which simulate the Bloch equation. Position and momentum dependent properties may be obtained from these calculations. The ensemble developed at each step in the random walk contains systems whose configurations are typical of the equilibrium at the temperature associated with the step. Averages at the various temperatures sampled during the random walk are obtained by accumulating the results of many random walks having different initial conditions sampled from the high temperature distribution.

In the next section we give a brief summary of some related methods which have been developed for performing quantum calculations at non-zero temperatures and compare these with the procedure described in this section.

3.) A review of other Quantum Methods for Treating Systems at Non-Zero Temperatures

Most of the methods which have been considered for performing quantum calculations at non-zero temperatures are based on the path integral formulation of quantum statistical mechanics due to Feynman (Feynman and Hibbs (1965)). With the path integral method the density operator is developed incrementally by dividing β up into M small segments of length ε so that $\beta = \varepsilon M$. Thus the density operator for some low temperature β may be written as a product of M high temperature factors

$$\rho(\beta) = \rho(\varepsilon)\rho(\varepsilon)\ldots\rho(\varepsilon)$$

In the coordinate representation the above expression gives the following form for the density matrix

$$\rho(\underline{r},\underline{r}';\beta) = \int\ldots\int \rho(\underline{r},\underline{r}_1;\varepsilon)\rho(\underline{r}_1;\underline{r}_2;\varepsilon)\ldots\rho(\underline{r}_{M-1},\underline{r}';\varepsilon)d\underline{r}_1 d\underline{r}_2\ldots d\underline{r}_{M-1} \qquad (5.27)$$

By considering the analogy between the solution of the Bloch equation and the idea of a "classical trajectory", a useful interpretation of equation (5.27) can be obtained. A series of intermediate configurations $\underline{r}_1,\underline{r}_2,\ldots,\underline{r}_{M-1}$ defines a path along which the system travels as it moves between $\underline{r}$ and $\underline{r}'$. Equation (5.27) thus states that the total amplitude $\rho(\underline{r},\underline{r}';\beta)$ for the system to begin at $\underline{r}$ and end at $\underline{r}'$ is obtained as the sum over all possible paths of M segments which connect the configurations $\underline{r}$ and $\underline{r}'$. In the limit as $\varepsilon\to 0$ the number of intermediate points in the paths becomes infinite and each path may be represented as a function $\underline{r}(t)$ where the variable t is defined on the interval $0 \leq t \leq \beta$. The multidimensional Riemann integral in equation (5.27) becomes a functional or Wiener integral

in the limit as $\varepsilon \to 0$ and, using the notation of Feynman, the density matrix is written as follows

$$\rho(\underline{r},\underline{r}';\beta) = \int\!\!\int \Phi[\underline{r}(t)]\, D\underline{r}(t) \tag{5.28}$$

Here the functional Φ is defined by

$$\Phi[\underline{r}(t)] = \lim_{\substack{\varepsilon\to 0 \\ :M\varepsilon=t}} \rho(\underline{r},\underline{r}_1;\varepsilon)\rho(\underline{r}_1,\underline{r}_2;\varepsilon)\ldots\rho(\underline{r}_{M-1},\underline{r}';\varepsilon) \tag{5.29}$$

and

$$D\underline{r}(t) = \lim_{M\to\infty} d\underline{r}_1 d\underline{r}_2 \ldots d\underline{r}_{M-1} \tag{5.30}$$

The random walk procedure for solving the Bloch equation described in the previous section assumes that in a small β interval we may model the kinetic and potential terms by seperate, independent processes. In the same way, Feynman assumes that for an infinitessimal increment, ε, the system may be considered as a collection of free particles with a small correction due to the potential. A perturbation approach is used to obtain the following high temperature approximation for the density matrix

$$\rho(\underline{r},\underline{r}';\varepsilon) = \left(\frac{2\pi\hbar^2}{m}\varepsilon\right)^{-3N/2} e^{-m/2\hbar^2\varepsilon\,(\underline{r}-\underline{r}')^2}\, e^{-\varepsilon V(\underline{r})} \tag{5.31}$$

The first exponential term, together with the normalization factor, gives the density matrix for a collection of N free particles at a temperature ε. The final exponential is the perturbation correction due to the influence of the potential.

Substituting the high temperature approximation for the density matrix given in equation (5.31) into (5.29), the following expression for the functional Φ is obtained

$$\Phi[\underline{r}(t)] = \lim_{\substack{\varepsilon\to 0 \\ :M\varepsilon=t}} \exp\{-\varepsilon([m/2\hbar^2(\frac{\underline{r}-\underline{r}_1}{\varepsilon})^2 + V(\underline{r})] + [m/2\hbar^2(\frac{\underline{r}_1-\underline{r}_2}{\varepsilon})^2 + V(\underline{r}_1)] + \ldots + [m/2\hbar^2(\frac{\underline{r}_{M-1}-\underline{r}'}{\varepsilon})^2 + V(\underline{r}_{M-1})])\} \tag{5.32}$$

Taking the indicated limit we find that the quantity $(\underline{r}_{j-1}-\underline{r}_j)/\varepsilon$ becomes the derivative $(d\underline{r}(s)/ds)_{s=j\varepsilon}$ and further that the sum of terms in the exponent can be written as an integral in the following manner

$$\int_o^t m/2\hbar^2\ \dot{\underline{r}}(s)^2\ ds + \int_o^t V(\underline{r}(s))\ ds \tag{5.33}$$

Thus the following functional integral expression for the density matrix is obtained

$$\rho(\underline{r},\underline{r}';\beta) = \int_{\underline{r}(0)=\underline{r}}^{\underline{r}(\beta)=\underline{r}'} \exp\{-\int_0^\beta (m/2\hbar^2\ \dot{\underline{r}}(s)^2 + V(\underline{r}(s)))ds\}\ D\underline{r}(s) \tag{5.34}$$

The exact multidimensional Riemann integral form for the density matrix ymgae in equation (5.27) together with the high temperature approximation presented in (5.31), or variations on this form, provide the basis of most of the path integral methods for evaluating the density matrix. Monte Carlo techniques are powerful methods for performing multidimensional Riemann integrals. The idea of using Monte Carlo methods to calculate the density matrix was suggested in the early 50's by Kac and Cohen (1952). An excellent review of the early ideas for evaluating functional integrals is presented by Brush (1961).

A number of different Monte Carlo calculations of density matrices and related quantities have been reported. An understanding of the path integral approach can be obtained by substituting the "primitive" high temperature approximation, (5.31), into equation (5.27). If the $\underline{r}$ vectors represent configurations of an N particle system, equation (5.27) involves

a 3N x (M-1) dimensional integral. The integrand in (5.27) is everywhere positive and is treated as a probability density which has the same form as the expression for the functional given in (5.32). The points $\underline{r}$ and $\underline{r}'$ are constants which parameterise the probability density and by using a Markov process to sample the points $(\underline{r}_1,\underline{r}_2,\ldots,\underline{r}_{M-1})$ from the 3N x (M-1) dimensional distribution, the off diagonal elements of the density matrix may be calculated. By equating the end points $\underline{r} = \underline{r}'$ and drawing points from the 3N x M dimensional probability density, configurations distributed according to the diagonal elements of the density matrix may be sampled and properties of the system are calculated as averages over this distribution. Thus the quantum partition function for N particles is mapped onto a classical partition function for N x M particles and the classical Monte Carlo method of Metropolis et al. is used.

There are a number of variations on the method described above. Fosdick and Jordan (1966) used a discrete path integral method to evaluate the two body Slater sum for Lennard-Jones ^{4}He over a range of temperatures between 2°K and 273°K. Rather than using a Markov chain for selecting points to construct their paths, they employed conditional Brownian motion paths using an interpolation formula due to Levy (1954). With this approach, the intermediate points are chosen according to the free particle Gaussian terms and the end points of the diffusing random walks are constrained. When the primitive high temperature approximation is used the potential integral in equation (5.33) may be evaluated using the trapezoidal rule and the values of the potential at the points along each Brownian motion path are summed. Averaging the exponential of this sum and related quantities over many Brownian paths provides a means for estimating the direct and exchange contributions to the density matrix. An identical approach has

been used by Jacucci and Omerti (1983) to test the usefulness of different high temperature approximations.

There are two major differences between the method used by Fosdick and Jordan and the approach we described in Section 2.). First, with their procedure the diagonal elements of the density matrix are calculated by considering paths which are constrained to start and finish at the same point in configuration space. The method described in Section 2.), however, uses diffusing paths with free end points. The contribution each path makes to the diagonal elements of the density matrix is determined by the Gaussian weight. Secondly, as discussed in Section 2.), the birth-death procedure has an implicit importance sampling character since systems give "birth" in the right regions of configuration space and die in the unfavourable regions.

The Markov chain Monte Carlo method outlined earlier is an alternative importance sampling method since the rapidly varying potential terms are included in the sampling probability density. Jordan and Fosdick (1968) recognised this and used Brownian motion paths in which the points were accepted or rejected on the basis of a transition probability chosen to include the parts of their integrands which varied rapidly. They used the first few terms in the Wigner-Kirkwood expansion to give a more accurate high temperature approximation for the density matrix and with this approach were able to explore in some detail the influence of three body effects on the pair distribution function for ^{4}He gas.

Barker (1979) showed that employing the Metropolis sampling method was not sufficient to give an efficient Monte Carlo scheme for studying many body systems with hard core interactions when the primitive high temperature approximation of equation (5.31) is used. More accurate high

temperature approximations must be considered. The reason for the problem is related to the difference in distance scale between the Gaussian (kinetic) term and the short range repulsive part of the potential. The primitive high temperature approximation given in equation (5.31) is only valid if $V(\underline{r})$ is slowly varying compared with the quadratic term arising from the free particle Gaussian. Increasing the number of intermediate points in the path reduces the width of the Gaussian factor. Thus in the limit as $M \to \infty$ the approximation in (5.31) becomes valid. Barker found that for systems with hard cores the convergence with increasing M was slow. The early ^{4}He calculations of Fosdick and Jordan in which a Lennard-Jones interaction was assumed indicated that reasonable accuracy could be obtained with the primitive approximation using on the order of $10^2 - 10^3$ intermediate points. The tests performed by Jacucci and Omerti (1983) showed that the convergence with the primitive high temperature approximation is even slower for a system of hard spheres.

Barker presented more accurate forms for the high temperature approximation. Using an "image approximation" for a system with infinite hard core repulsions, he obtained a dramatic improvement in the convergance of the discrete path integral Monte Carlo method. Jacucci and Omerti studied the radial distribution function for a system of quantum hard spheres over a wide range of temperatures. They found that with the image approximation well converged results could be obtained using as few as 20 path segments.

Barker also presented a more accurate high temperature approximation applicable to many body systems with pair additive potentials. His suggested approximation takes the following form

$$\rho(\underline{r},\underline{r}';\varepsilon) = \left(\frac{2\pi\hbar^2}{m}\varepsilon\right)^{-3N/2} e^{-m/2\hbar^2\varepsilon\,(\underline{r}-\underline{r}')^2} \tag{5.35}$$

$$\times \prod_{1<n}^{N} \left\{ \frac{\rho_2(\underline{r}_1,\underline{r}_n;\underline{r}_1',\underline{r}_n';\varepsilon)}{\left(\frac{2\pi\hbar^2}{m}\varepsilon\right)^{-3} e^{-m/2\hbar^2\varepsilon\left[(\underline{r}_1-\underline{r}_1')^2+(\underline{r}_n-\underline{r}_n')^2\right]}} \right\}$$

The factor $e^{-\varepsilon V(\underline{r})}$ in equation (5.31) is thus replaced by a product of pair density matrices ρ_2. The denominators in the product divide out the free particle contributions contained in ρ_2 which are already included in the first many body Gaussian factor.

Pollock and Ceperley (1984) used equation (5.35) to perform non-zero temperature quantum calculations on the bulk phases of ^{4}He. In their work the terms appearing in the pair product in equation (5.35) were approximated by the following form

$$e^{-\frac{1}{2}\left[P(r;\varepsilon)+P(r';\varepsilon)\right]} \tag{5.36}$$

Here the function $P(r;\varepsilon)$ is the logarithm of the diagonal elements of the pair density matrix and depends only on the distance $r = |\underline{r}_1-\underline{r}_n|$. Pollock and Ceperley have presented a summary of a number of different methods for calculating the pair density matrix. Some of these approaches will be considered in more detail shortly.

The connection between the various path integral Monte Carlo methods described above and the quantum random walk approach which was detailed in the previous section can be discussed in terms of the isomorphism between the path integral formulation of quantum statistical mechanics and the classical statistical mechanics of polyatomic fluids. The isomorphism has been considered by Chandler and Wolynes (1981), and with their coworkers (Schweizer et al. (1981)) they have applied the perturbation techniques of classical fluid theory to develop improved discrete path integral methods.

The isomorphism can be appreciated if one again considers substituting the primitive high temperature approximation presented in equation (5.31) into equation (5.27). We may write the result in a slightly different form

$$\rho(\underline{r},\underline{r};\beta) = \int\cdots\int \prod_{j=1}^{N} B(\underline{r}^j,\underline{r}_1{}^j,\underline{r}_2{}^j,\ldots,\underline{r}_{M-1}{}^j;\varepsilon) \tag{5.37}$$

$$\times\, e^{-\varepsilon \sum_{i<j}^{N} \left(V(|\underline{r}^i-\underline{r}^j|)+\sum_{t=1}^{M-1} V(|\underline{r}_t{}^i-\underline{r}_t{}^j|)\right)} d\underline{r}_1 d\underline{r}_2\ldots d\underline{r}_{M-1}$$

Here

$$B(\underline{r}^j,\underline{r}_1{}^j,\underline{r}_2{}^j,..,\underline{r}_{M-1}{}^j;\varepsilon) = e^{-m/2\hbar^2\varepsilon\left[(\underline{r}^j-\underline{r}_1{}^j)^2+\sum_{t=1}^{M-2}(\underline{r}_t{}^j-\underline{r}_{t+1}{}^j)^2+(\underline{r}_{M-1}{}^j-\underline{r}^j)^2\right]} \tag{5.38}$$

In the above the superscripted indices i and j label the particles in the system and the subscripted values of t specify the different configurations sampled as the system wanders along a path. The function B contains all the Gaussian factors which represent the free motion of particle j.

Chandler and Wolnyes noted that the factor B was isomorphic with the classical Boltzmann factor for a ring polymer molecule. Each "atom" in the ring molecule is connected to only two neighbours by a harmonic interaction potential. The constituent "atoms" of the polymer are actually the same particle, j, but sampled from different configurations of the path. Consequently, the product of B factors appearing in equation (5.37) is related to the partition function for a classical fluid of non-interacting polymer molecules. The term containing the potential in equation (5.37) describes how the polymers interact with one another. Due to the form of the potential term, two polymers interact through a site-site potential. Thus site t on polymer i interacts only with the sites labeled by t on the other polymers in the fluid.

From the isomorphism discussed above the diagonal elements of the

density matrix are proportional to the partition function of a particular classical fluid of polymers. For an N particle system there will be N polymers in the classical fluid and if the discrete path integral is written in terms of M high temperature factors, there will be M "atoms" in each polymer. The polymers must have closed ring structures since the path integral expression for the diagonal elements of the density matrix involves paths which start and finish at the same points.

With the quantum random walk method described in the previous section, the terms in the integrand of equation (5.27) are simulated by the random walk procedure rather than using a Metropolis Monte Carlo sampling scheme. Each system in the propagating ensemble is selected from the high temperature distribution

$$e^{-\beta_o V(\underline{r})}$$

The recriprocal temperature increment, $\Delta\beta$, is chosen so that there are M steps in the random walk which ends at a temperature β thus

$$\Delta\beta = \frac{\beta-\beta_o}{M}$$

As β is incremented, the systems diffuse according to the Gaussian distribution

$$e^{-m/2\hbar^2\Delta\beta(\underline{r}-\underline{r}_1)^2}$$

Births and deaths occur so that after k increments in β each system is effectively weighted by the factor

$$e^{-\sum_{i=1}^{k} V(\underline{r}_i)\Delta\beta}.$$

Finally to obtain the diagonal elements of the density matrix each path is

weighted by another Gaussian factor

$$e^{-m/2\hbar\beta_o(\underline{r}-\underline{r}_k)^2}$$

The total weight of a diffusing system after k increments in reciprocal temperature is thus

$$e^{-m/2\hbar^2\Delta\beta[(\underline{r}-\underline{r}_1)^2+(\underline{r}_1-\underline{r}_2)^2+\ldots+(\underline{r}_{k-1}-\underline{r}_k)^2]}\, e^{-m/2\hbar\beta_o(\underline{r}-\underline{r}_k)^2}$$

$$\times\, e^{-\sum_{i=1}^{k} V(\underline{r}i)\Delta\beta}\, e^{-\beta_o V(\underline{r})}$$

This form is an alternative way of splitting up the integrand when the primitive high temperature approximation is used in the discrete path integral expression for the density matrix.

The integration over the momentum variables which gives rise to the extra Gaussian factor in the displacement $\underline{r}-\underline{r}_k$ can thus be considered as a mechanism for closing each ring polymer at any temperature along the random walk trajectory. The method for closing the polymer rings is illustrated in Figure 5.1 where the 9 segment rings for a pair of interacting particles have been closed with Gaussian bonds at the 3^{rd}, 6^{th} and 9^{th} segments.

From the above discussion, the method discribed in Section 2.) presents an efficient means for extracting all the information from a path integral calculation. High and low temperature results are obtained from a single run by assuming that there is a linear relationship between β and the number of path segments needed to accurately evaluate the discrete path integral. Thus at higher temperatures we assume that similar accuracy can be obtained using fewer path segments. The accuracy will be determined by the high temperature approximation used. In Section 2.), the algorithm was developed using the primitive high temperature approximation. From the

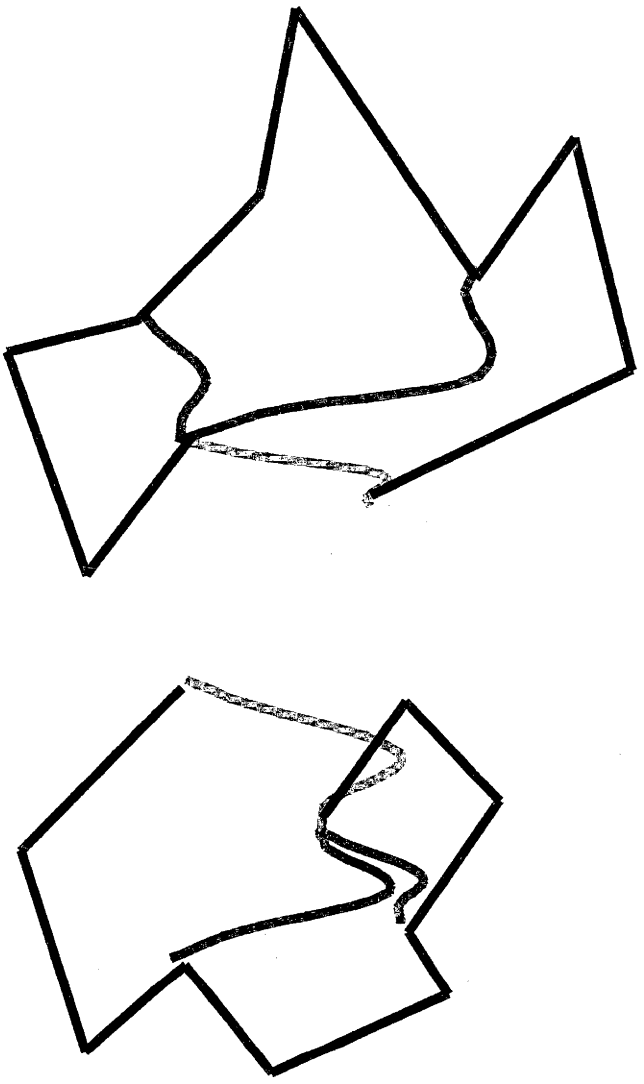

Fig. 5.1

discussion presented above, however, it is likely that the accuracy of the random walk approach will be improved by using high temperature approximations of the forms suggested by Barker and by Pollock and Ceperley to replace the potential in the birth-death step. We could also follow Jordan and Fosdick and use the Wigner-Kirwood quantum corrections.

The inefficiency of the conventional Metropolis Monte Carlo method for sampling the configuration space of polymer systems was noted by Pollock and Ceperley. Due to the strength of the high temperature intrapolymer interaction, very few moves are accepted. With the random walk approach, the diffusion process directly samples the intrapolymer geometries. The birth-death process should also provide an efficient means of sampling the interpolymer interaction.

The statistical methods for calculating the density matrix which have been discussed in this chapter are important for studying systems with many dimensions. For problems with few dimensions much more precise techniques are available. The partial wave expansion may be used to reduce the three dimensional two body problem to a single dimension. For a one dimensional problem standard numerical methods may be used to calculate the eigenvalues and eigenfunctions and the density matrix is obtained by directly summing over all the states as in equation (5.3). Larsen, Witte and Kilpatrick (1966) used this approach to calculate the direct and exchange contributions to the diagonal elements of the density matrix for a pair of helium atoms interacting with Lennard-Jones forces.

A powerful iterative procedure for evaluating path integrals in low dimensional problems was developed by Storer (1968). The method makes use of the following result

$$\rho(\underline{r},\underline{r}';2\varepsilon) = \int \rho(\underline{r},\underline{r}";\varepsilon)\rho(\underline{r}",\underline{r}';\varepsilon)d\underline{r}" \qquad (5.39)$$

which is a particular case of equation (5.27). A high temperature approximation for $\rho(\underline{r},\underline{r}';\varepsilon)$ is used to commence the iteration and when the integral in (5.39) is performed, the density matrix at half the temperature, 2ε, is obtained.

For problems which can be reduced to one dimension the high temperature density matrix is set up as a square grid in r and r'. Using numerical quadratures the integral in equation (5.39) is replaced by a matrix multiplication. Repeating the matrix multiplication procedure n times is equivalent to performing an $M = 2^n-1$ segment discrete path integral and the temperature obtained after these iterations corresponds to $\beta = 2^n\varepsilon$.

Storer first used the approach to determine the quantum radial distribution function for a plasma at small ion-electron separations. Later Klemm and Storer (1973) applied the procedure to evaluate the direct and exchange contributions to the pair correlation function for helium and neon over a range of temperatures.

Berne and his coworkers (Thirumalai and Berne (1983), Thirumalai, Bruskin and Berne (1983)) have used the iterative procedure to treat a number of chemical problems. Due to the speed and efficiency of the technique for low dimensional applications, many iterations could be performed and consequently they found that the primitive high temperature approximation was adequate.

All the path integral methods which have been discussed in this chapter involve representing the integration paths in terms of a set of discrete configurations. An alternative approach, however, is to represent the paths in terms of a complete set of orthogonal functions. By varying the coefficients of the functions in the expansion one runs through all the paths. The idea was used by a number of workers in the late 1950's when

analytic methods for evaluating functional integrals were being developed. The review article of Brush (1961) summarises much of this work.

Fosdick (1962) presented a Monte Carlo method for evaluating general Wiener integrals using paths which were represented in terms of an othogonal expansion. By truncating the infinite expansion at some finite value n the infinite dimensional Wiener integral was reduced to an n dimensional Riemann integral in a similar fashion to the discrete path integral methods. Now, however, the integration variables were the expansion coefficients rather than the intermediate configurations in the discrete path.

Recently Freeman and Doll (1984), (1985) have developed a quantum Monte Carlo method which is based on a Fourier series representation of the paths. Their approach is similar to the work of Fosdick. The path traced out by particle i as the system moves from $\underline{r}$ to $\underline{r}'$ is expanded about a fixed linear path connecting $\underline{r}$ and $\underline{r}'$. Thus as t is varied between 0 and β particle i moves along a path described as follows

$$\underline{r}_i(t) = \underline{r}_i + (\underline{r}_i' - \underline{r}_i)t/\beta + \sum_{k=1}^{\infty} \underline{a}_{ki} \sin(k\pi t/\beta) \qquad (5.40)$$

When the above result is introduced into the functional integral expression given in equation (5.34) a form for the density matrix involving integrals over the Fourier coefficients, $\underline{a}_k$, is obtained. Freeman and Doll used this form together with the following result

$$\langle \hat{o} \rangle = \frac{Tr\hat{\rho}\hat{o}}{Tr\hat{\rho}} \qquad (5.42)$$

to derive expressions for the average values of various operators. These results involve integrals over the particle coordinates and Fourier

coefficients and by truncating the Fourier series at some value k_{max} the finite dimensional integral obtained may be evaluated by the Metropolis Monte Carlo method.

The amount of computational effort involved in a Fourier path integral Monte Carlo calculation depends on k_{max} in much the same way as the computational effort in a discrete path integral calculation depends on the number of path segments M. From their studies using the Fourier path integral method Freeman and Doll have found that the convergence with increasing k_{max} is quite repid even at low temperatures. Further the convergence properties of the Fourier path integral method are not strongly dependent on the form of the potential and there seem to be no significant problems in applying the method to systems with harsh repulsive core interactions. The approach has so for been applied to some simple one dimensional oscillator problems and a rather extensive theoretical study of the properties of argon clusters has been conducted.

In the next chapter we present the results of some calculations which use the discrete path integral method described in Section 2.). First the properties of the method are exployed using some simple one dimensional problems and finally the method is used to study the properties of some atomic and molecular clusters.

CHAPTER 6 APPLICATION OF THE NON-ZERO TEMPERATURE QUANTUM MONTE CARLO METHOD

Introduction

In this chapter the methods described in Chapter 5 are applied to a variety of quantum problems. To study the behaviour of the algorithm we first calculate the properties of the one dimensional harmonic and Morse oscillators as functions of temperature. Analytic results for these oscillators are available so comparisons can be made and the algorithm tested.

To demonstrate its application to multidimensional problems we next use the non-zero temperature quantum Monte Carlo procedure to study the properties of a low density gas at low temperatures. We have simulated Neon gas using a Lennard-Jones potential. The results of this study are compared with classical theory and also with the earlier matrix squaring calculations performed by Klemm and Storer (1972). Excellent agreement between the two quantum methods is found.

Finally the results of some calculations on the water dimer are presented. The cluster has been modelled over a range of temperatures between 2000°K and 200°K. The aim of this study is to determine the significance of quantum behaviour in molecular clusters at finite temperatures. In Chapter 3 we saw that the classical description of the intermolecular degrees of freedom in this cluster at very low temperatures was rather poor. Here we shall study the differences between the classical and quantum descriptions of the motions of molecules at higher

temperatures. Many simulations of molecular liquids have been perfomed recently in which the validity of classical mechanics has been assumed. For systems of light molecules which interact with strong forces such as the hydrogen bonding interactions in water, the assumptions of classical theory are questionable. In the final section of this chapter we test these assumptions by comparing the results of classical and full quantum calculations over a range of temperatures.

1.) One Dimensional Oscillators

To study the general properties of the non-zero temperature quantum Monte Carlo algorithm we have used the method described in Chapter 5 to solve the Bloch equation for the one dimensional harmonic and Morse oscillators. The Hamiltonians for these problems can be summarised as follows

$$\hat{H} = \frac{-\hbar^2}{2\mu}\frac{d^2}{dx^2} + V(x)$$

where $$V_H(x) = \frac{1}{2}\mu\omega^2 x^2 \qquad (6.1)$$

and $$V_M(x) = D_e\left(1-e^{-\alpha x}\right)^2$$

We first consider a harmonic oscillator having the reduced mass of a neon atom and a frequency $\hbar\omega$ = 100 K. This problem models the intermolecular interactions of light molecules.

All the Bloch equation trajectories in our studies involved propagating ensembles with average populations of 5000 systems through 100 steps in reciprocal temperature. The behaviour of the oscillator was studied down to

a temperature of 10°K and time step size dependence was monitored by comparing with calculations which terminated at 30°K. Initial condition dependence has been considered by starting the trajectories at 100, 500 and 1000°K. The results of these studies are summarised in Figure 6.1 where we show the potential, kinetic and total energies of the oscillator at various temperatures along the random walk trajectory. The potential energy was obtained by averaging $V_H(x)$ over the ensemble distribution including the Gaussian weights which depend on the displacement from the initial configuration as given in equation (5.21). In a similar manner, equation (5.24) was used to calculate the kinetic energy and the total energy was obtained from the sum of the potential and kinetic components. The values presented in the figures are the results of averaging over more than 10 independent trajectories each having an average population of 5000 systems. The contribution of each trajectory must be weighted by the values of V_{ref} as discussed in Section 2.) of Chapter 5.

The Bloch equation for the harmonic oscillator can be solved analytically (Feynman (1972)) and the potential and kinetic energies are given by the following

$$\langle V \rangle = \langle T \rangle = \frac{\hbar\omega}{4} \left(\frac{1+\exp(-\hbar\omega\beta)}{1-\exp(-\hbar\omega\beta)} \right) \qquad (6.2)$$

Solid lines appearing in Figure 6.1 were obtained using this result while the dashed curves are the predictions of classical equipartition theory. In the figure we study the initial condition dependence of the random walk results. The lower group of curves give the potential and kinetic energies. When a classical initial distribution at 100°K is used the kinetic and potential energy curves obtained from the quantum random walk calculation differ significantly from the exact results. The kinetic energy is under

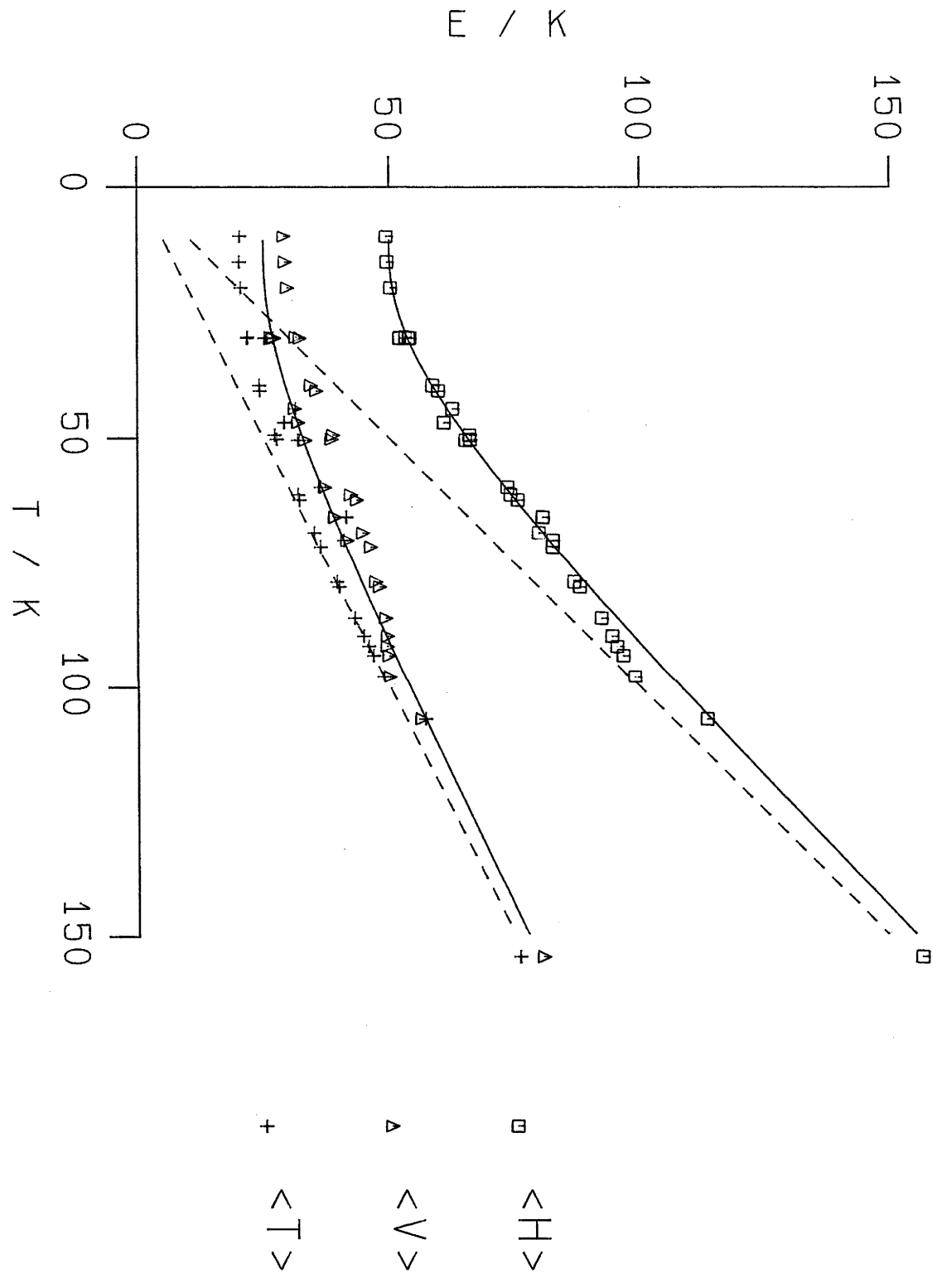

fig. 6.1

estimated along the length of the trajectory while the potential energy starts lower than the exact result and ends too high. Similar behaviour is observed to a lesser extent with higher temperature initial conditions. The points clustering around the exact potential-kinetic curve were obtained from calculations sampling classical initial distributions at 500 and 1000°K. The results seem independent of step size since the values obtained from calculations using final temperatures of 10°K and 30°K are identical. Despite the initial condition dependence of the breakup of the energy into potential and kinetic components, the total energies at the lower temperatures considered in our calculations are all within 1% of the exact result irrespective of the initial distribution.

The initial condition dependence which was described above can be understood by examining the expressions used to calculate the components of the energy. If we consider equation (5.24) for a single dimension, the kinetic energy is obtained by performing the following average over the weighted ensemble members

$$T(\beta) = \langle {}^{1}/_{2\beta_o}[1-{}^{\mu}/_{\hbar^2\beta_o}\,{}^{(x-x')^2}]\rangle_{\beta}$$

Initially $\beta = \beta_o$ and $x = x'$ so the kinetic energy in the initial distribution is the classical result ${}^{1}/_{2\beta_o}$. At a temperature of 100°K the exact kinetic energy of our oscillator is 54.1 K so the classical initial condition gives a kinetic energy which is about 4 K too low. From Figure 6.1 we see that this initial discrepancy is propagated along the trajectory.

The behaviour of the kinetic energy discussed above and differences between the potential energies obtained from the simulation and the exact values is due to assuming classical behaviour at the initial temperature.

When low initial temperatures are used the deviations are large because the classical results provide a poor approximation to the true quantum behaviour. With higher initial temperatures more accurate calculations can be performed. We shall see shortly that this initial condition dependence causes severe problems when the approach is applied to oscillators with widely spaced energy levels such as the Morse oscillator which describes the O-H stretching motion of a water molecule.

The energies obtained from simulations using the higher initial temperatures are in good agreement with the analytic results. Similar accuracy is found with the various distributions which were calculated during the simulation which used a classical initial distribution at 1000°K. The position distributions obtained from this calculation are compared with the exact quantum distributions in Figure 6.2a. Feynman (1972) gives that the diagonal elements of the harmonic oscillator density matrix take the following form

$$P(r;\beta) = \exp\left(-m\omega/\hbar \tanh(\hbar\omega\beta/2)r^2\right) \qquad (6.3)$$

Excellent agreement between the distributions obtained from the quantum simulation and the above analytic result is observed.

Figure 6.2b compares the calculated momentum distributions with classical results. The one dimensional case of equation (5.25), (5.26) was used to obtain these curves. As a self consistency check, we numerically integrated the momentum distributions presented in Figure 6.2b and averaged the kinetic operator $p^2/2m$. The kinetic energies obtained with this approach agreed with the results obtained by averaging equation (5.24) over the ensemble distribution.

The classical momentum distributions are sharper than the quantum

fig. 6.2 a

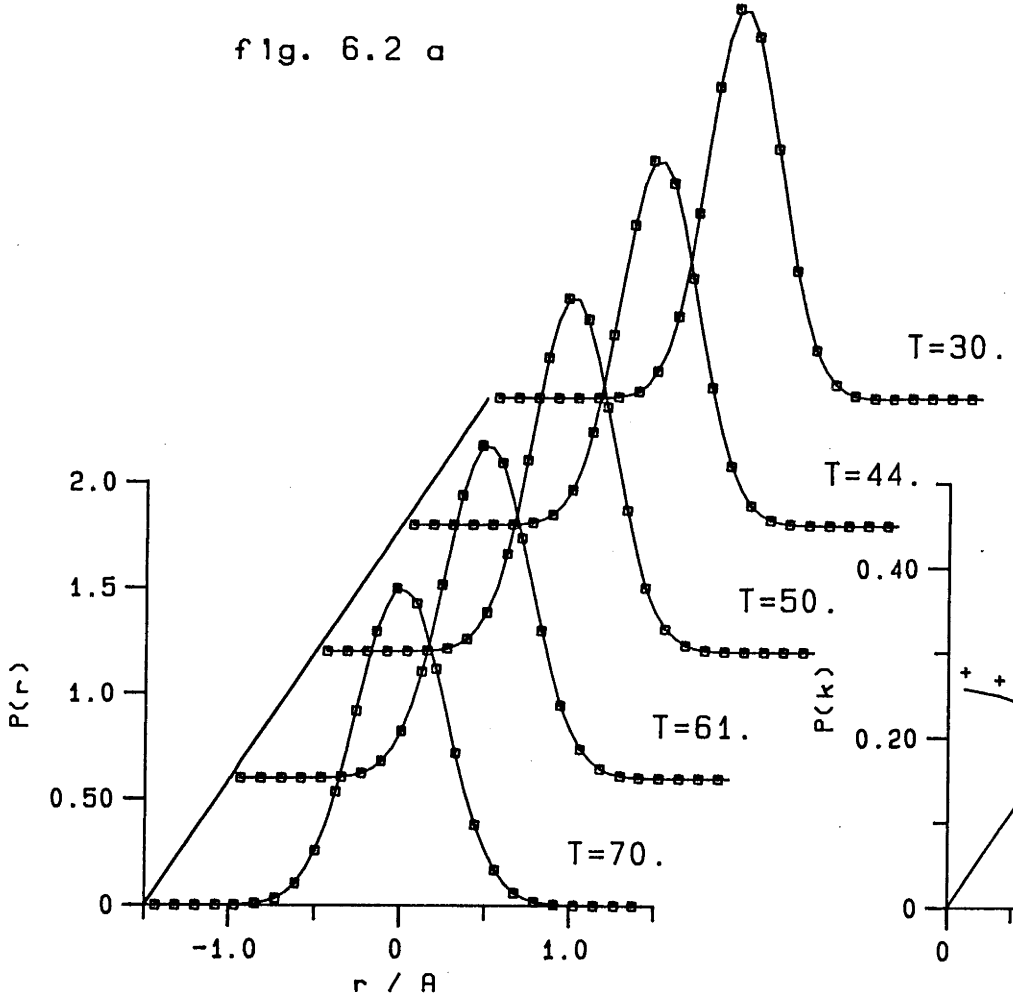

fig. 6.2 b

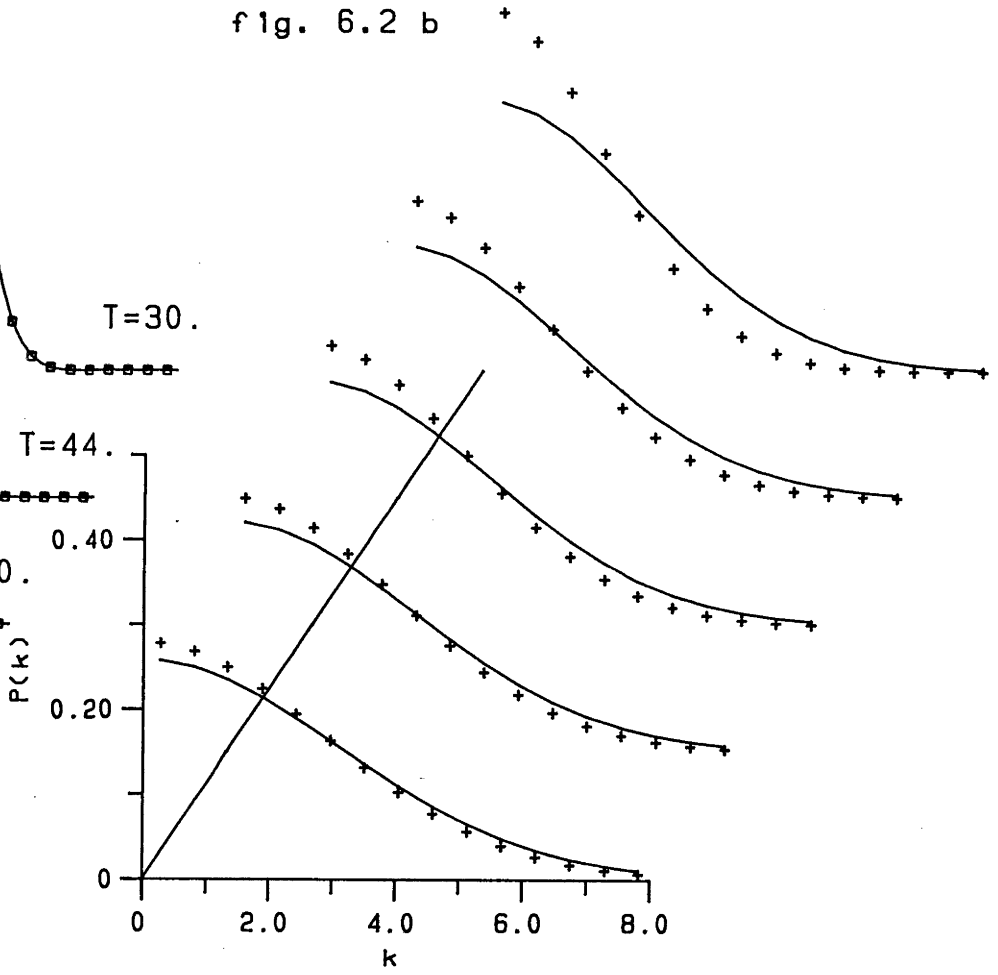

results. In the limit of zero temperature the classical oscillator is stationary so its momentum distribution will be a delta function at k = 0. Quantum mechanically, the zero point motion will give the zero temperature momentum distribution a finite width.

Later in this chapter we will use the non-zero temperature quantum Monte Carlo method to study the behaviour of a cluster of water molecules at elevated temperatures. The most quantum mechanical degrees of freedom in such a cluster are the intramolecular vibrations. We now consider application of our non-zero temperature quantum Monte Carlo method to the Morse oscillator describing the OH stretch motions in the water monomer. Our aim here is to explore the initial condition dependence of the random walk algorithm for this oscillator so as to determine the range of operating conditions for which reliable results can be obtained.

As discussed in Chapter 3 the bound state eigenfunctions of the Morse oscillator are analytic so the diagonal elements of the density matrix for temperatures well below dissociation can be obtained by performing a Boltzmann weighted sum over the bound eigenstates. For higher temperatures continuum states will also be important.

In Figure 6.3 we compare the energies calculated during a number of quantum Monte Carlo simulations of the Morse oscillator with the results obtained by explicitly summing over the states as outlined above. Classical distributions at initial temperatures of 5000, 7500 and 10,000°K were used. The dissociation energy of the OH Morse oscillator is about 66,000°K. As with the harmonic oscillator, the potential energy obtained from the quantum simulation is too high and the kinetic energy too low due to the assumed classical initial distributions. With higher initial temperatures the classical forms are more accurate approximations and the quantum Monte

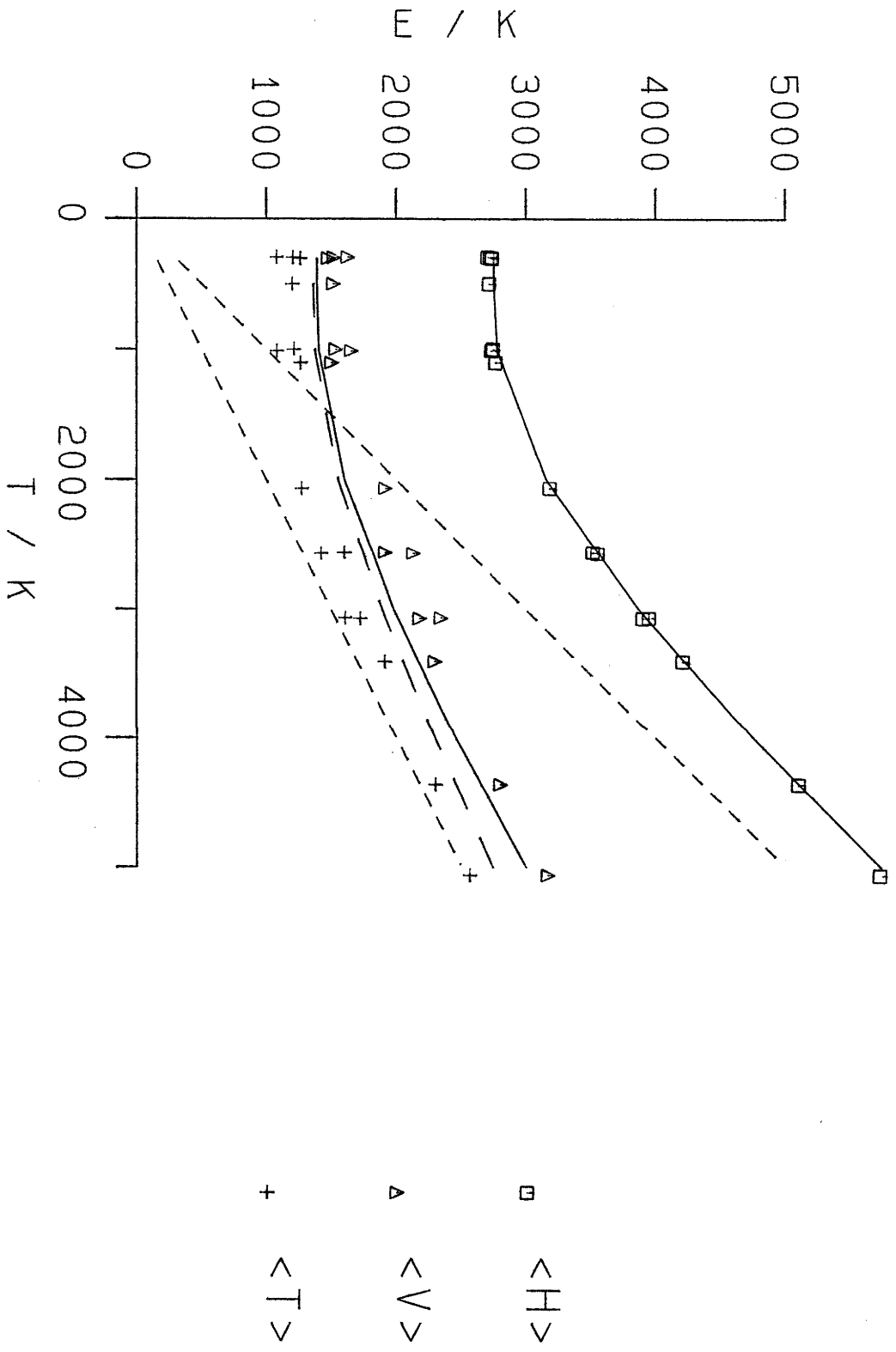

fig. 6.3

Carlo estimates of the potential and kinetic energies tend to the exact results as the initial temperature is increased. As with the harmonic oscillator we see that the offsets in the potential and kinetic components which occur due to the use of the classical initial distributions almost exactly cancel giving total energies which are in excellent agreement with the exact results. The reason for this behaviour is not fully understood.

We can conclude from our studies of the Morse oscillator that an accurate representation of the intramolecular vibrations in a water molecule can only be obtained if initial temperatures of the order of tens of thousands of degrees are employed. There are significant problems with using such high temperatures. The major difficulty is due to the form of the Gaussian weights which are used to obtain the diagonal elements of the density matrix. From equation (5.21) the width of the Gaussian weight distribution decreases as the initial temperature is increased. If high initial temperatures are necessary for the classical results to be accurate, very narrow Gaussian distributions result. As systems diffuse away from their initial geometries they recieve very small weights. Consequently the statistical properties of the algorithm deteriorate rapidly as the initial temperature is increased.

The problems with using the classical distributions as initial conditions for the Bloch equation simulation which were noted above can be overcome by starting at lower temperatures and employing more accurate high temperature approximations. This may be demonstrated for the harmonic oscillator by using exact results for the initial condition at some moderate temperature where employing the classical initial condition would otherwise give problems. Feynman (1972) shows that the off diagonal elements of the harmonic oscillator density matrix have the form

$$\rho(r,r';\beta) = e^{-a(r^2+r'^2) + brr'} \tag{6.4}$$

where $a = \frac{m\omega}{2\hbar} \coth(\beta\hbar\omega)$ and $b = \frac{m\omega}{\hbar \sinh(\beta\hbar\omega)}$

When equation (6.4) is used in equation (5.10) the following expression for $F(p,r;\beta)$ may be derived

$$F(p,r;\beta) = e^{\frac{-m\omega}{2h} \tanh(\beta\hbar\omega)\, r^2} \; e^{\frac{-\tanh(\beta\hbar\omega)}{2\hbar m\omega} p^2} \; e^{i/h \frac{pr}{\cosh(\beta\hbar\omega)}} \tag{6.5}$$

It is easily shown that this result reduces to the classical form given in equation (5.17b) in the limit as $\beta \to 0$. We may perform a non-zero temperature quantum Monte Carlo calculation using the result in equation (6.5) evaluated at some temperature β_o as the initial conditon. As with the case where a classical initial conditions is used, points (r,p) in phase space are sampled according to the first two terms in equation (6.5) and each ensemble member is weighted by the final term in the equation. The ensemble may be propagated to lower temperatures using the usual diffusion and birth-death processes. When a system diffuses from a point r at β_o to r' at β', we can use equation (5.14) to obtain weights which will give the full quantum position distribution in the same manner as equation (5.21) was derived. The following expression for the weight is found

$$w(r,r') = \exp\left[\frac{-m\omega(r'-r/\cosh(\beta_o\hbar\omega)}{2h \tanh(\beta_o\hbar\omega)}\right] \tag{6.6}$$

Proceding in the same way as equation (5.24) was obtained, the kinetic energy can be calculated by averaging over the weighted ensemble distribution as follows

$$\left\langle \frac{p^2}{2m} \right\rangle_{\beta'} = \left\langle \frac{\hbar\omega}{2 \tanh(\beta_o h\omega)} \left(1 - \frac{m\omega}{\hbar \tanh(\beta_o h\omega)} (r'-r/\cosh(\beta_o h\omega))^2\right)\right\rangle \tag{6.7}$$

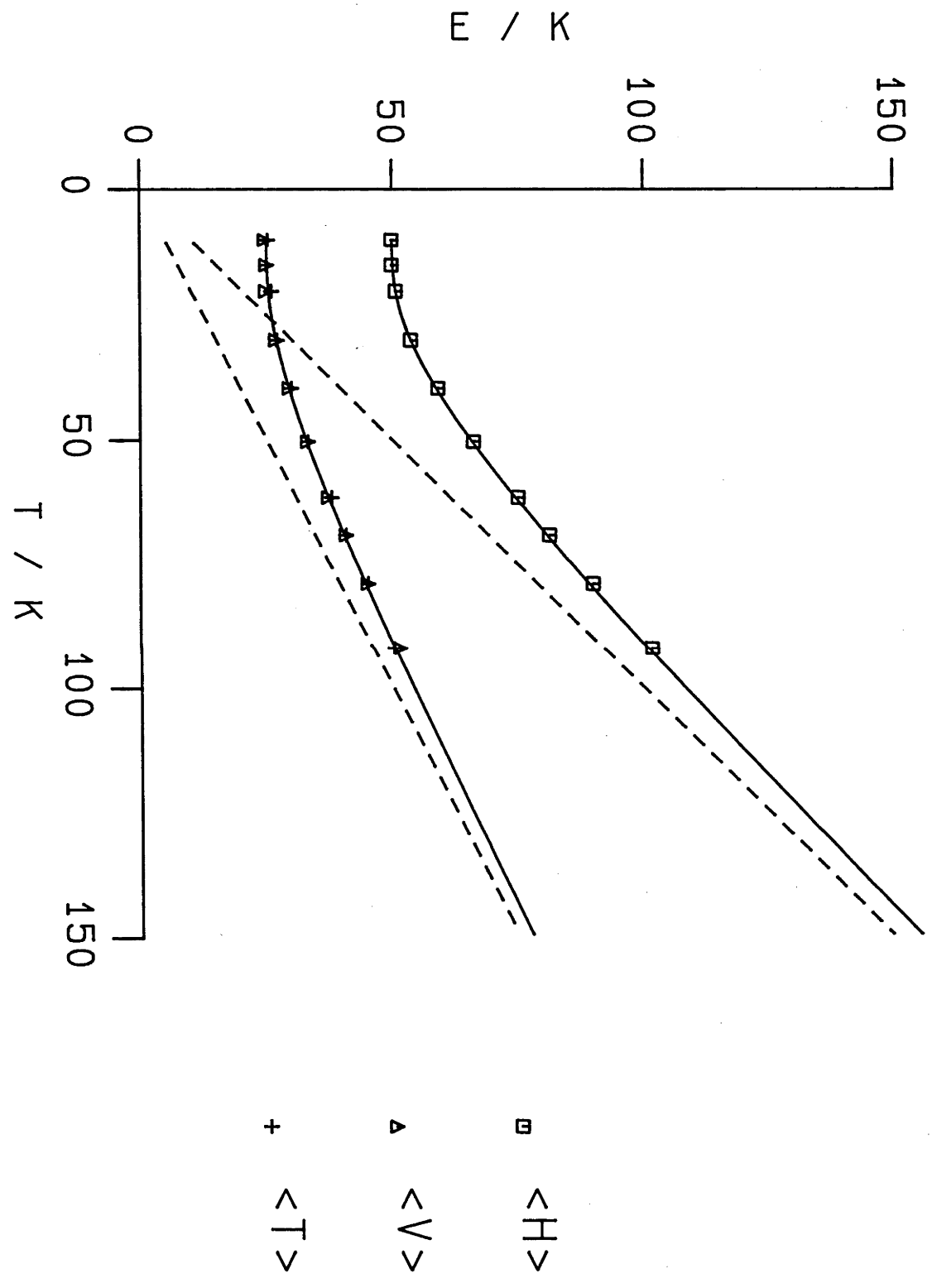

fig. 6.4

Equation (6.6) and (6.7) have been employed in a simulation of the harmonic oscillator using an initial temperature of 100°K. The results of this study are presented in Figure 6.4 and are found to be in excellent agreement with the exact values.

The approach used above to improve the accuracy of the harmonic oscillator calculation can be generalized to other problems. More accurate high temperature approximations for the density matrix are required. The development presented in Chapter 5 assumed the following high temperature form for the initial condition

$$\rho(\underline{r},\underline{r}';\beta_o) = e^{-\beta_o V(\underline{r})}\ e^{-\frac{m}{2\beta_o\hbar^2}(r'-r)^2}$$

In our applications, the classical Boltzmann factor is sampled with the Monte Carlo method and the Gaussian is included as a weight. As $\beta_o \to 0$ the Gaussian gives weight to systems which sample the near diagonal region so the above form is only useful in the high temperature limit. At lower temperatures a more accurate form

$$\rho(\underline{r},\underline{r}';\beta_o) = e^{-\beta_o/2 V(\underline{r})}\ e^{-\beta_o/2 V(\underline{r}')}\ e^{-m/2\beta_o\hbar^2(\underline{r}'-\underline{r})2} \qquad (6.8)$$

may be used.

When information about the diagonal elements of the density matrix, $\rho(\underline{r},\underline{r},\beta_o)$, is available an improved form, based on equation (6.8) can be considered.

$$\rho(\underline{r},\underline{r}';\beta_o) = [\rho(\underline{r},\underline{r};\beta_o)\ \rho(\underline{r}',\underline{r}';\beta_o)]^{\frac{1}{2}}\ e^{-m/2\beta_o\hbar^2(\underline{r}'-\underline{r})2} \qquad (6.9)$$

This result is the same as the "end point" approximation used by Pollock deh Ceperley (1984) and presented in equation (5.36).

Equation (6.9) has been used to perform more accurate calculations on

the Morse oscillator. The diagonal elements of the density matrix at the initial temperature were obtained by summing over the analytic bound state eigenfunctions as discussed earlier. A Monte Carlo calculation was used to sample configurations drawn from the distribution $\rho(\underline{r},\underline{r};\beta_o)^{\frac{1}{2}}$. These systems were propagated with the random walk method and at a temperature β' configurations r' were obtained. By weighting the contributions of these configurations with the factor

$$\rho(\underline{r}',\underline{r}';\beta_o)^{\frac{1}{2}}\ e^{-\frac{m}{2\beta_o\hbar^2}(\underline{r}'-\underline{r})^2} \tag{6.10}$$

the polymer rings are closed and averages of various quantities are evaluated.

An expression for the kinetic energy is obtained in the same way as equation (5.24) was derived. In the discussion above $F(p,r;\beta_o)$ was sampled by weighting the configurations generated by the Monte Carlo calculation with the momentum factor

$$\int e^{i/\hbar\ \underline{p}\cdot\underline{r}''}\ \rho(\underline{r}'',\underline{r}'';\beta_o)^{\frac{1}{2}}\ e^{-\frac{m}{2\beta_o\hbar^2}(\underline{r}''-\underline{r}'')^2}\ d\underline{r}''$$

After propagation, each system must be weighted by the final phase factor $e^{-i/\hbar\ \underline{p}\cdot\underline{r}'}$. As with equation (5.24), a function, $K(\underline{r},\underline{r}')$, which may be averaged over the spacial distribution of the ensemble to give the kinetic energy, may be obtained by integrating $p^2/2m$ over the momentum distribution

$$K(\underline{r},\underline{r}') = \int e^{-i/\hbar\ \underline{p}\cdot\underline{r}'}\ \underline{p}^2/2m \int e^{i/\hbar\ \underline{p}\cdot\underline{r}''}\ \rho(\underline{r}'',\underline{r}'';\beta_o)^{\frac{1}{2}}\ e^{-\frac{m}{2\beta_o\hbar^2}(\underline{r}''-\underline{r})^2}\ d\underline{r}''d\underline{p} \tag{6.11}$$

By making use of the following property of the Fourier transform

$$\underline{\kappa}^2 \int f(\underline{r})\ e^{i\underline{\kappa}\cdot\underline{r}}\ d\underline{r} = -\int \nabla^2 f(\underline{r})\ e^{i\underline{\kappa}\cdot\underline{r}}\ d\underline{r}$$

equation (6.11) is reduced to the form

$$K(\underline{r},\underline{r}') = \frac{-\hbar^2}{2m} \nabla^2_{\underline{r}'} \left[\rho(\underline{r}',\underline{r}';\beta_o)^{\frac{1}{2}} e^{-\frac{m}{2\beta_o\hbar^2}(\underline{r}'-\underline{r})^2}\right] \qquad (6.12)$$

Setting $g = \rho(\underline{r}',\underline{r}';\beta_o)^{\frac{1}{2}}$, we find after some algebra that the kinetic energy can be obtained from the following average over the ensemble which is weighted as in equation (6.10)

$$\left\langle \frac{p^2}{2m} \right\rangle = \left\langle {}^1/_2\beta_o\left[1 - \frac{m}{\beta_o\hbar^2}(\underline{r}'-\underline{r})^2 + 2(\underline{r}'-\underline{r}).\nabla \ln g - \frac{\hbar^2\beta_o}{m}\{\nabla^2 \ln g + (\nabla \ln g)^2\}\right]\right\rangle \qquad (6.13)$$

The more accurate high temperature results presented above were used to simulate the OH Morse oscillator. Energies obtained from these calculations are compared with the exact values in Figure 6.5. We see from this figure that there is a great improvement in the accuracy of the results obtained from our calculations. The most important feature evident in this figure is that the results are not strongly dependent on the initial temperature. Energies calculated using initial temperatures as low as 1000°K are within a few percent of the exact results. This is in marked contrast to the values obtained when classical initial distributions are used. In Figure 6.3 we observed differences between the exact and calculate potential and kinetic components on the order of 10-20% when the highest initial temperature of 10,000°K was used. At 5000°K discrepencies as large as 50% were found.

The substantial improvements in accuracy obtained when the high temperature approximation presented in equation (6.9) is employed make it possible to use our method to perform non-zero temperature quantum calculations on systems with mixed "quantum" and "classical" degrees of freedom. In Section 3.) the high temperature approximation of equation

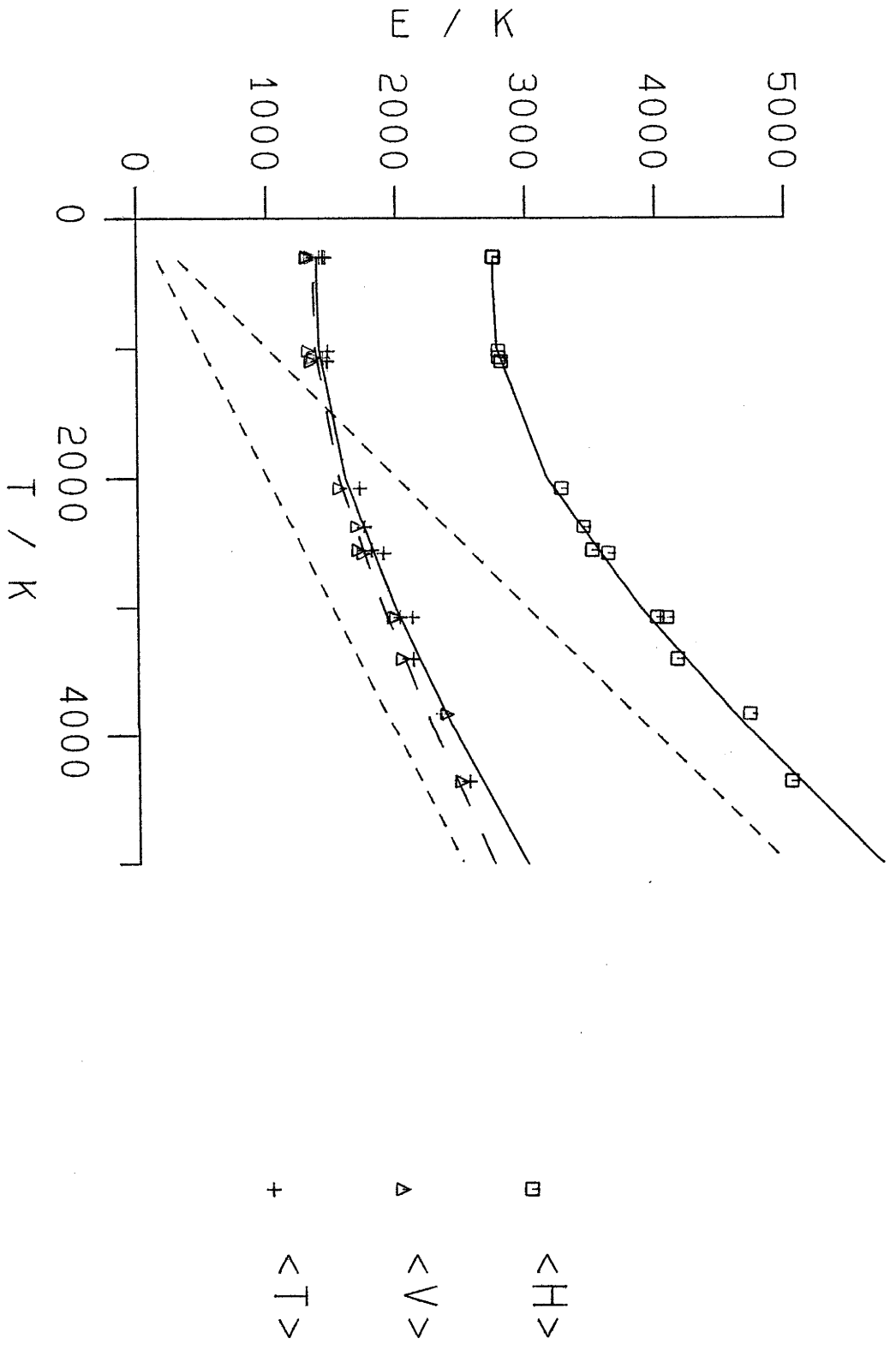

fig. 6.5

(6.9) is used to provide the initial condition for the intramolecular vibrations of the molecules in the water dimer. With this calculation the classical initial distribution in equation (6.8) will be used for the intermolecular motions of the cluster. In the next section we demonstrate that the primitive classical approximation is useful for performing calculations on systems with weak interactions such as the rare gases.

2.) Neon Gas at low temperatures

To test the non-zero temperature quantum Monte Carlo method on a more complicated problem we have calculated the pair distribution function for neon gas over a range of temperatures. Klemm and Storer (1972) used the matrix squaring method described in the previous chapter to calculate this function in helium and neon. As mentioned earlier their approach involved using a spherical harmonic expansion to reduce the three dimensional two body problem to a series of one dimensional equations. Each equation was solved using the numerical matrix multiplication method and by summing the truncated series to large ℓ a converged estimate of the pair distribution function was obtained.

The advantages of the method outlined above are that the nummerical matrix multiplication is very rapid (Thirumalai, Bruskin and Berne (1983)) and further the results obtained are free from the statistical noise which characterises Monte Carlo methods. A disadvantage of the procedure is that only problems with a few dimensions can be studied. The multichannel expansions employed in atom-molecule scattering theory could in principle be used to perform matrix squaring calculations on more complicated

systems. In most applications of scatting theory single energy calculations are performed and a thermal average of the results of calculations at different energies must be conducted. Using matrix squaring, the same information may in principle be obtained from a single calculation. It may prove useful to consider the matrix multiplication method or a related iterative scheme in future developments of scatting theory. However, for problems with more dimensions stochastic methods are essential.

To demonstrate the generality of the random walk method described in Chapter 5 we have considered the two body problem in terms of a system with 6 periodic dimensions. A pair of Lennard-Jones neon atoms were placed in a Monte Carlo cell with side length 3σ. Periodic boundary conditions and minimum imaging were employed so that the periodic system modelled a low density gas with a reduced density $\rho^* = 0.0093$. A classical Monte Carlo calculation at 100°K was used to provide configurations for the initial ensemble. Random walks with 100 steps were performed and the $\Delta\beta$ step was chosen so that the final temperature was 10°K. Ensembles containing 2500 systems were propagated along the trajectory using the diffusion and birth-death procedure and V_{ref} was adjusted to keep the average population approximately constant. At certain temperatures along the trajectory the values of various properties were calculated and averaged as described earlier. The results presented below were obtained by averaging over 500 trajectories each using a different initial ensemble sampled from the high temperature classical distribution.

In Figure 6.6 we present the components of the energy of the periodic, two particle system obtained from our calculations. The figure also gives the results of classical calculations. As expected, the classical and quantum results are in reasonable agreement at higher temperatures but as

fig. 6.6

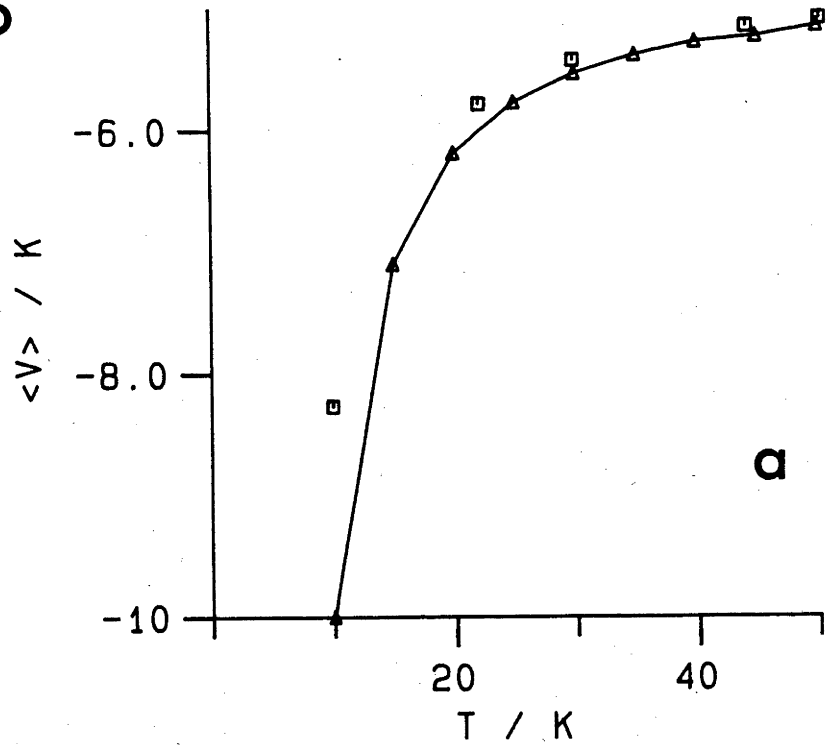

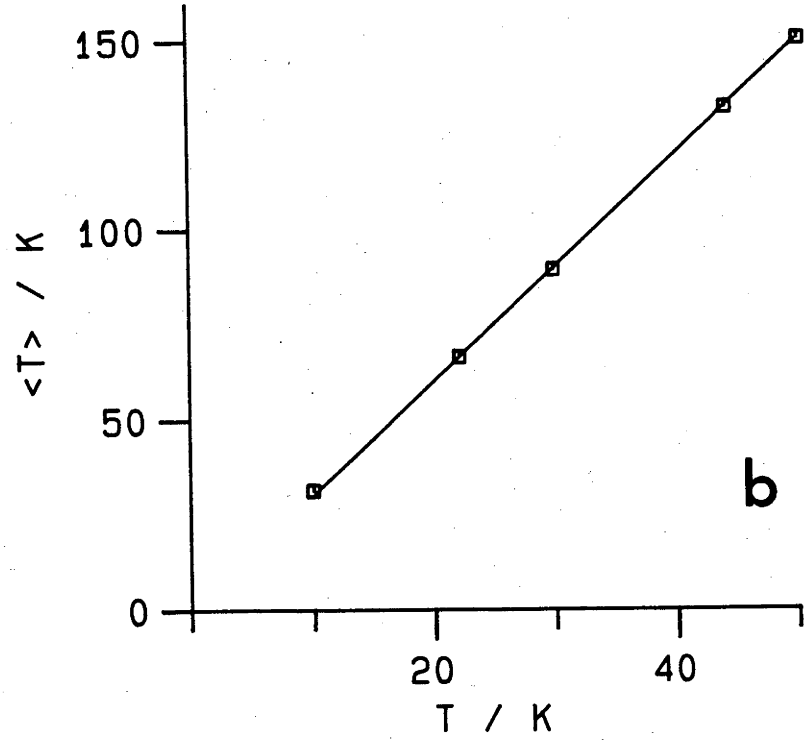

the temperature is reduced the true quantum behaviour of the gas gives results which deviate from the classical values. The potential component shows the most significant deviation of the classical from the quantum results while the value of the kinetic energy differs only slightly from the classical form, $3/2\ k_B T$ per particle.

Figures 6.7 and 6.8 show our calculations of the position and momentum distributions for the quantum gas at a variety of temperatures and compares these results with the predictions of classical theory. As expected from the discussion above our quantum postion distributions show large deviations from the classical results at lower temperatues while the quantum momentum distributions deviate only slightly from the classical form. At the lowest temperatures the classical position distribution functions are much more strongly peaked than the quantum distributions. The most important difference between the two distributions occurs in the region of the repulsive wall. Quantum tunnelling allows the particles to penetrate the classically forbidden hard core region of the potential. Slight changes to the distribution in this region substantially effect the average potential energy. Due to the increased sampling of the repulsive core with the quantum distribution, higher potential energies result. In the limit as $T \to 0$ the classical distribution should become infintely peaked in the minimum of the well so classically the asymptotic potential energy should be ε. Due to the zero point motion, however, the asymptotic energies trend to their ground state values.

Figure 6.7 also compares our quantum position distributions with the results obtained by Klemm and Storer who used the matrix squaring procedure described earlier. The agreement between the two sets of quantum results is very good and demonstrates that the diffusion Monte Carlo method is able to

fig. 6.7

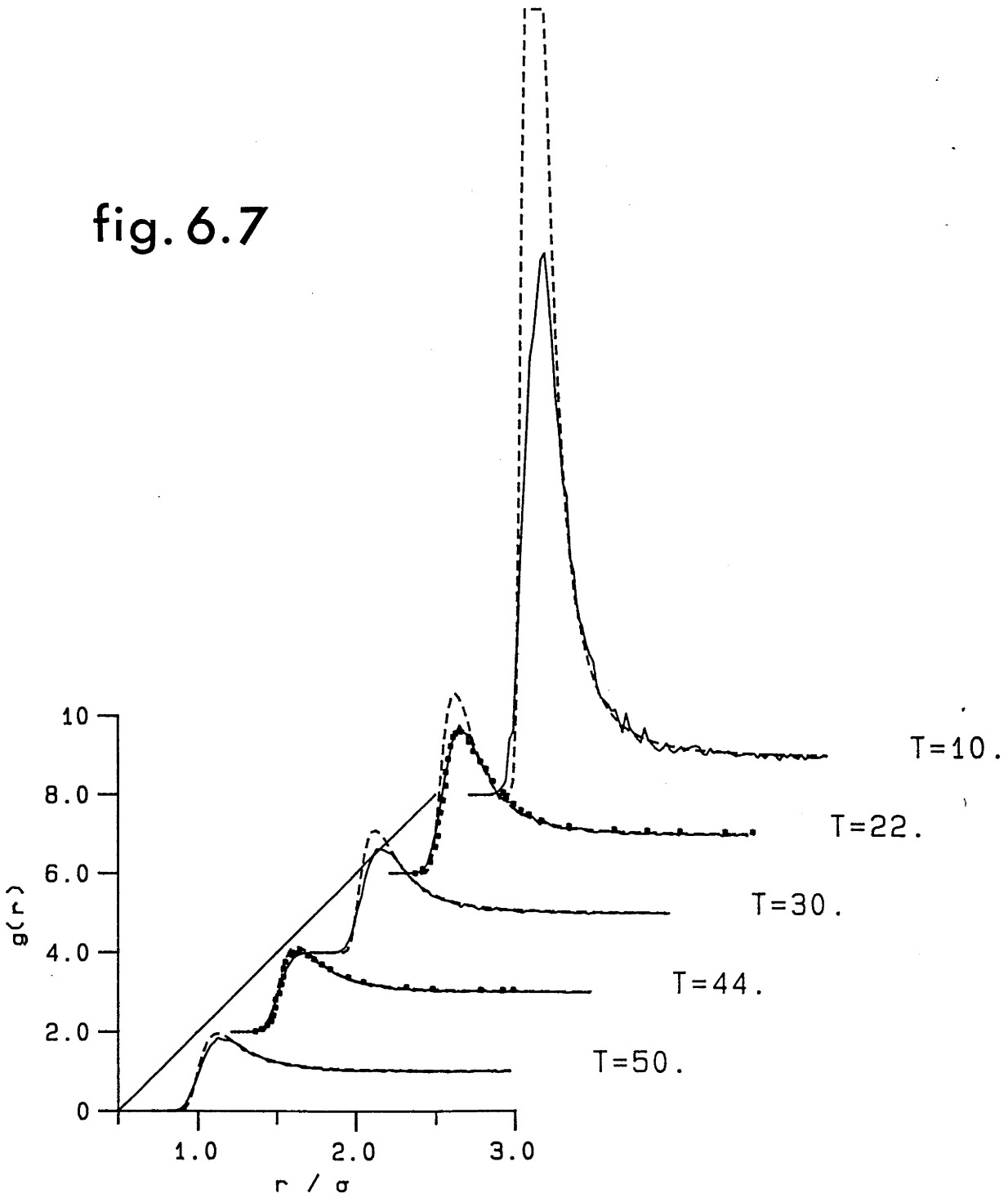

fig. 6.8

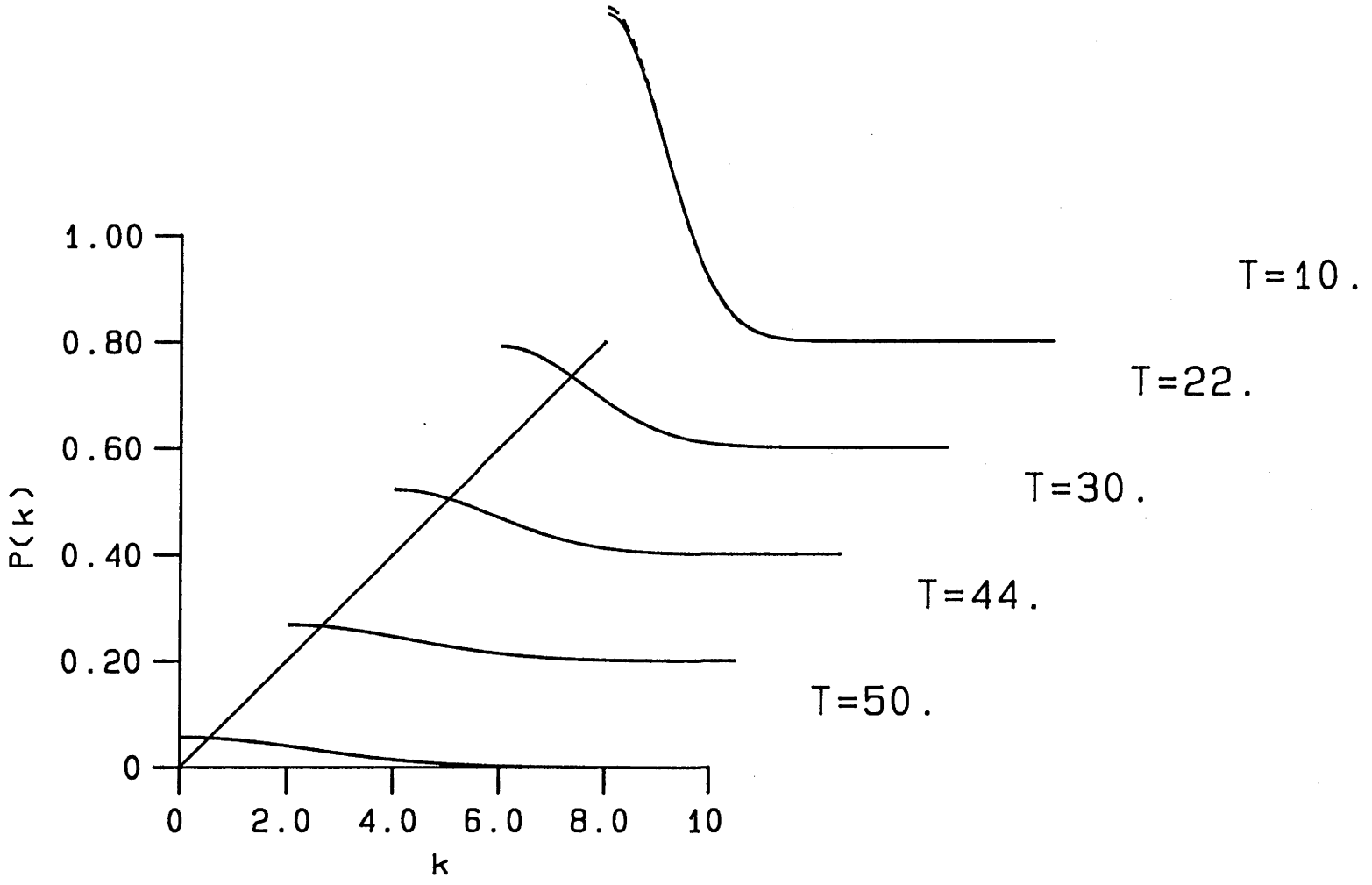

give accurate pair distribution functions for more complicated quantum systems.

The momentum distributions, P(k), are presented in Figure 6.8. The classical and quantum curves are very similar at all the temperatures considered in our calculations. Classically, in the limit as $T \to 0$ the particles will be stationary and a delta distribution at zero momentum will result. Quantum zero point motions, however, give a momentum distribution with non-zero width. The onset of these differences is observed in momentum distributions presented in Figure 6.8.

The random walk calculations described above use the primitive high temperature approximation as the basis of the diffusion and birth-death steps but since the "time" step used corresponds to a temperature in excess of 1000°K this primitive form is quite accurate. Thirumalai et al. (1983) have reported similar accuracy using the primitive high temperature form with the numerical matrix multiplication procedure. The most significant approximation in these studies is employing the classical distributions at 100°K as the initial condition for the quantum random walk. As discussed earlier more accurate approximations like equation (6.9) could have been employed but the agreement between the pair distributions obtained from matrix squaring and our results indicates that the classical approximation is reasonably accurate at 100°K in this system characterised by weak interactions.

In the next section we describe the results of non-zero temperature quantum Monte Carlo calculations on a higher dimensional problem. The onset of quantum behaviour as a function of temperature is explored for the water dimer.

3.) Quantum Behaviour of the Water Dimer at Non-Zero Temperatures

In Chapter 3 we investigated the properties of the water dimer in its ground state. It was noted that due to the neglect of zero point motions classical mechanics was not useful for studying this system at very low temperatures. The ground state of the molecular cluster is characterised by large amplitude zero point motions and the sharp intermolecular position distributions predicted by classical theory are unphysical. In this section we shall address the question of the importance of quantum behaviour in water at higher temperatures. The water molecule has a particularly small mass and it binds strongly to other molecules through hydrogen bonding. Thus quantum effects are expected to be important but how their significance changes with temperature is not fully understood. Many calculations using both the classical molecular dynamics and Monte Carlo methods have been performed on the different phases of water and aqueous solutions (Watts and McGee (1976), Reimers and Watts (1984)). The aim of this section is to employ the non-zero temperature quantum Monte Carlo method to consider the accuracy of the classical approximation for a system of water molecules and to obtain some information about the onset of quantum behaviour in such systems.

The problem which we shall study here is again the water dimer. Non-zero temperature quantum calculations on this 18 dimensional system are feasible given a few hours of CYBER 205 time. Due to the lower density of states, quantum behaviour is expected to be more important with this small system than for larger polymers. Further, the understanding of the ground state properties of the dimer which was obtained in Chapter 3 will be useful in interpreting our finite temperature results.

From the discussion of the Morse oscillator in Section 1.) the intramolecular vibrations of the cluster will be best represented if the high temperature approximation in equation (6.9) is used to describe these motions. The intermolecular degrees of freedom will probably be well represented by the classical form of equation (6.8) at a temperature of one or two thousand degrees. Thus we used the Monte Carlo method to sample configurations of the dimer drawn from the distribution

$$\prod_{i=1}^{6} \rho_i(s_i;\beta_o)^{\frac{1}{2}}\, e^{-\beta_o/2 V_{inter}(\underline{r})}$$

Here the functions $\rho_i(s_i;\beta_o)$ are the diagonal elements of the Morse oscillator density matrix in the local coordinates of the molecules. At the initial temperature, β_o, we constructed the intramolecular density matrix as a product of independent Morse oscillator factors. As in Section 1.) these functions were obtained by performing the Boltzmann weighted sum over the analytic eigenfunctions of the independent oscillators.

The initial distribution was propagated to lower temperatures with the diffusion and birth-death processes which were implemented in the same way as with our ground state calculations described in Chapter 3. At various temperatures along the trajectory averages were accumulated by weighting the contributions of each system in a similar fashion to equation (6.10)

$$w(r,r') = \prod_{i=1}^{6} \rho_i(s_i';\beta_o)\, e^{-\beta_o/2 V_{inter}(\underline{r}')} \prod_{j=1}^{6} e^{-\frac{m_j}{2\beta_o\hbar^2}(\underline{r}_j-\underline{r}_j')^2}$$

In our finite temperature water dimer calculations the cluster was prevented from dissociating by a rapidly rising potential wall positioned about its centre of mass. This idea has been employed by Lee, Barker and Abraham, (1973) and we have followed Freeman and Doll (1985) who used the

following constraining potental

$$V_c(\underline{r}) = (|\underline{r} - \underline{R}_{cm}|/R_c)^{20} \qquad (6.14)$$

together with the Fourier path integral Monte Carlo method to calculate the thermodynamic properties of argon clusters. Here the vector $\underline{r}$ describes the positions of the atoms in the cluster and $\underline{R}_{cm}$ is the position of its centre of mass. Confining the clusters in this way improves the sampling of configuration space. The diameter of the cluster R_c must be chosen sufficiently large so that the boundary conditions do not effect the final results. The calculations of Lee, Barker and Abraham indicated that the results were fairly insensitive to R_c except for small clusters at high temperatures. The systems they considered were weakly bound clusters of argon atoms. For a water cluster, where the binding is much stronger, the boundary which confines the cluster is expected to have less effect though at the highest temperatures we consider it may be significant.

Calculations using ensembles with 2500 systems and trajectories of 100 steps starting at both 1000 and 2000°K were performed. Final temperatures of 200 and 300°K were used. Averages of various energetic and structural properties were accumulated at different temperatures along the trajectories. As well as these quantum calculations we have also performed classical Monte Carlo calculations on the water dimer at different temperatures so that the results of classical and quantum theories may be compared.

The distributions of intramolecular local coordinates obtained from our quantum and classical calculations are presented in Figures 6.9 and 6.10 respectively. As expected the classical distributions are substantially narrower than the quantum results due to the neglect of zero point motions

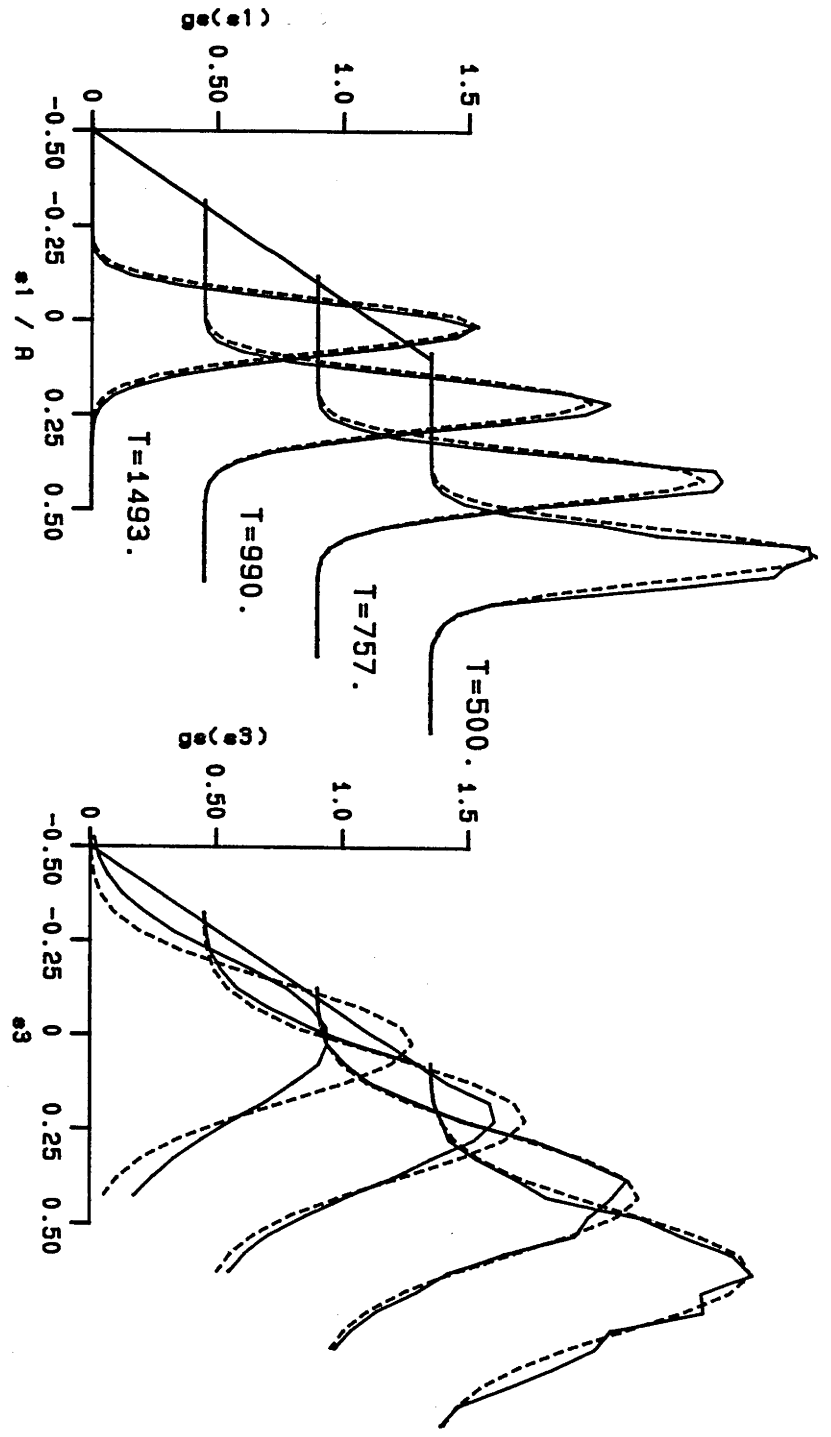
ge(e1)
0
0.50
1.0
1.5
-0.50
-0.25
0
0.25
0.50
e1 / A
T=1493.
T=990.
T=757.
T=500.
ge(e3)
0
0.50
1.0
1.5
-0.50
-0.25
0
0.25
0.50
e3

fig. 6.9

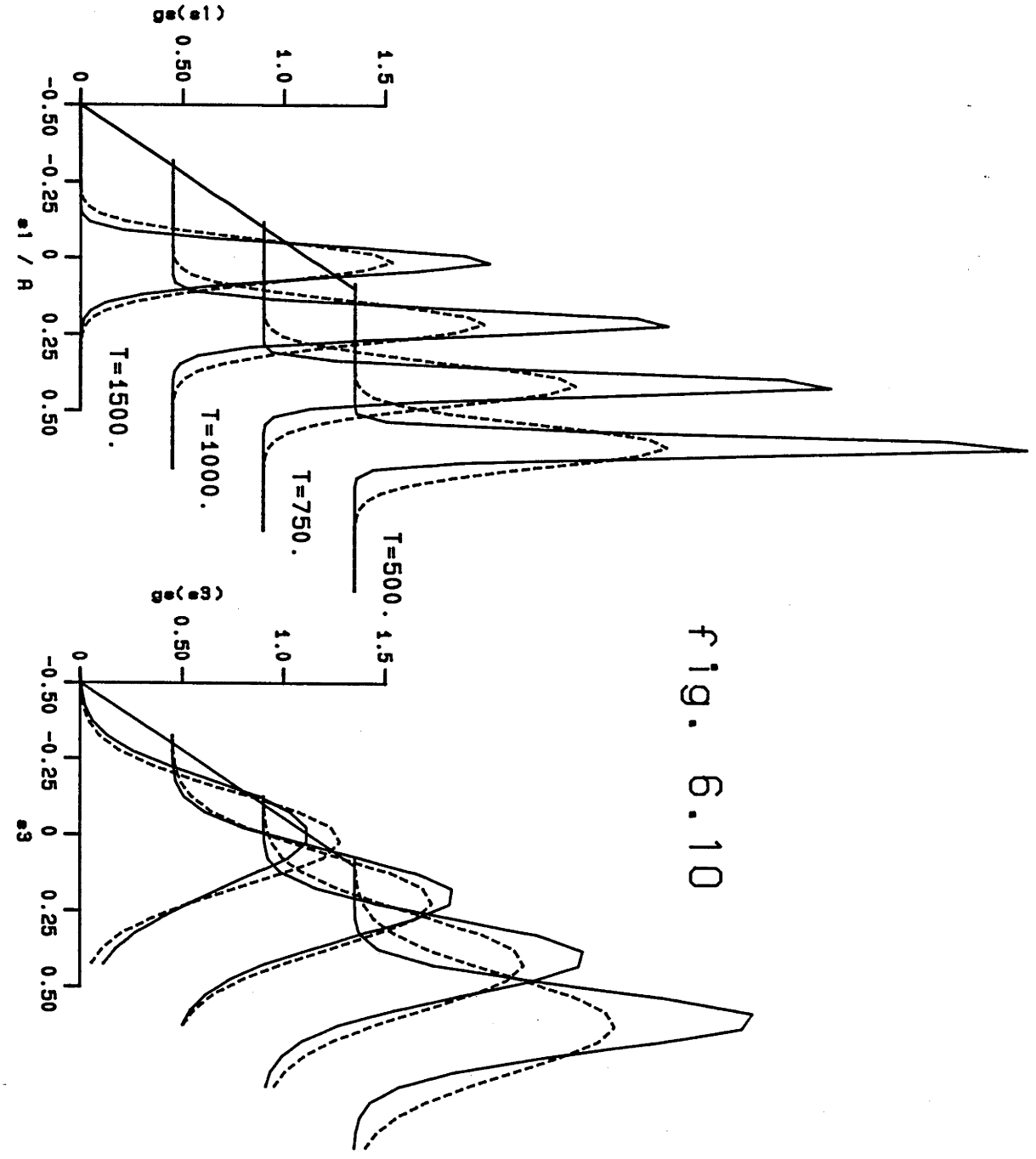
ge(e1)
0.50
1.0
1.5
0
-0.50 -0.25 0 0.25 0.50
e1 / A
T=1500.
T=1000.
T=750.
T=500.
ge(e3)
0.50
1.0
1.5
0
-0.50 -0.25 0 0.25 0.50
e3

fig. 6.10

and quantum tunnelling. Distributions for the various intramolecular local coordinates in the cluster were accumulated but all showed very similar forms within the statistical uncertainties. The bonded O-H stretch and bend coordinates for the donor are shown. In the figure we also present the square of ground state, independent Morse oscillator eigenfunctions of the monomer. The close agreement between the distributions of bond stretching coordinates obtained at the various temperatures and the ground state distribution indicates that over the temperature range considered, ground state behaviour dominates these motions. This is not the case, however, for the distribution of angle bending coordinates. Here the higher temperature distributions are significantly broader than the ground state result indicating that at these temperatures there is significant excitation of the bending vibration. At the lower temperatures, however, ground state behaviour dominates the bending vibrations.

The distributions of intermolecular distances obtained from our quantum simulations are compared with classical results in Figure 6.11. Here we observe close agreement between the classical and quantum pair distributions down to temperatures as low as 500°K. At 300 and 200°K we see evidence of the growing importance of quantum effects. Again tunneling and zero point motions make the quantum distributions broader and more diffuse than the classical results.

Above about 750°K both the classical and quantum g_{HH} and g_{OH} distributions show broad, structurless features as though hydrogen bonding is not important at these elevated temperatures. By about 500°K, however, the double peaked g_{OH} and g_{HH} distributions which characterise the hydrogen bonded structure become evident. The final box in the histograms which were used to accumulate the intermolecular distributions recorded the number of

fig. 6.11
$g_{oo}(r)$

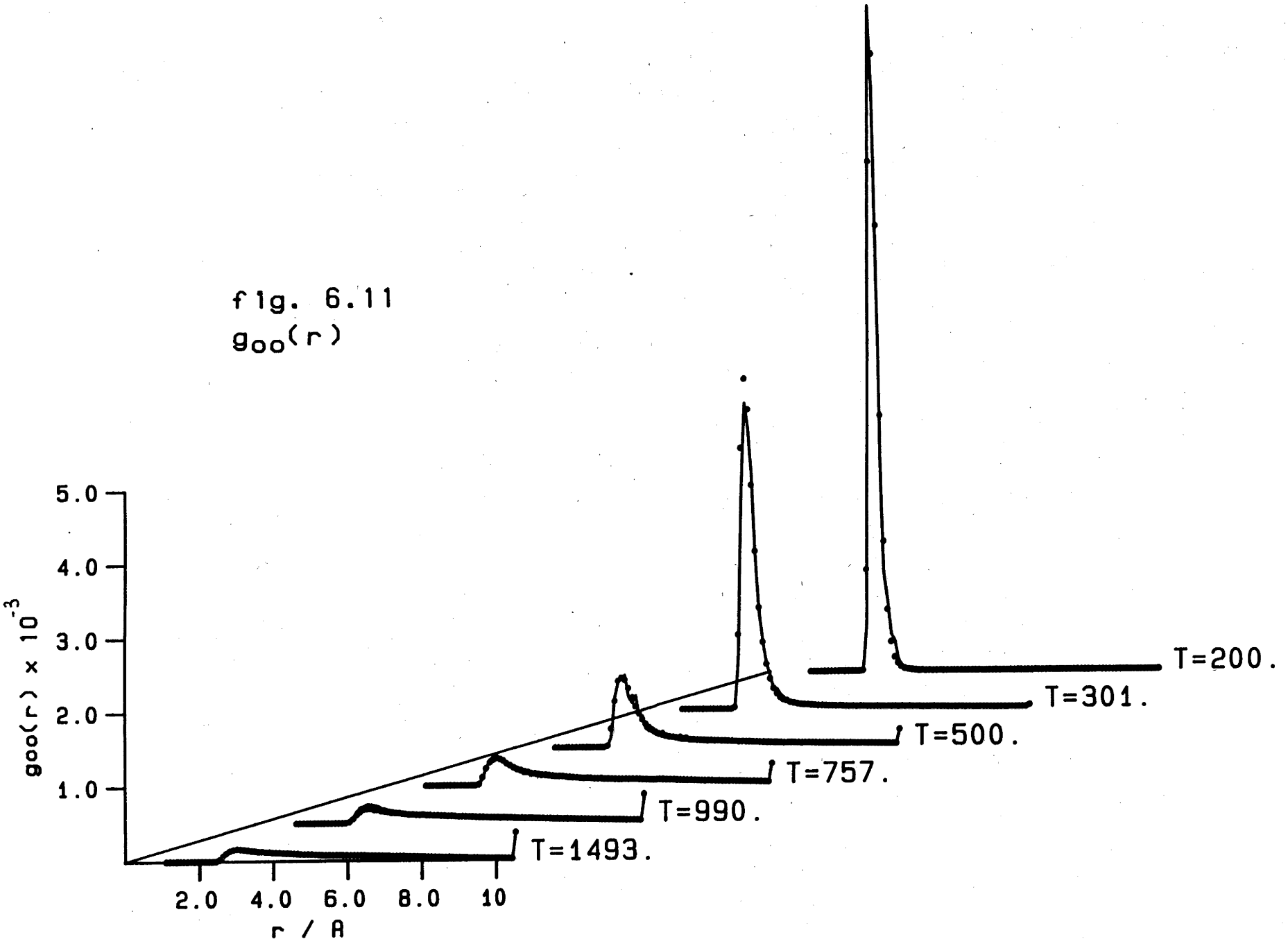
5.0
4.0
3.0
2.0
1.0
goo(r) x 10^-3
2.0
4.0
6.0
8.0
10
r / A
T=200.
T=301.
T=500.
T=757.
T=990.
T=1493.

fig. 6.11
$g_{oh}(r)$

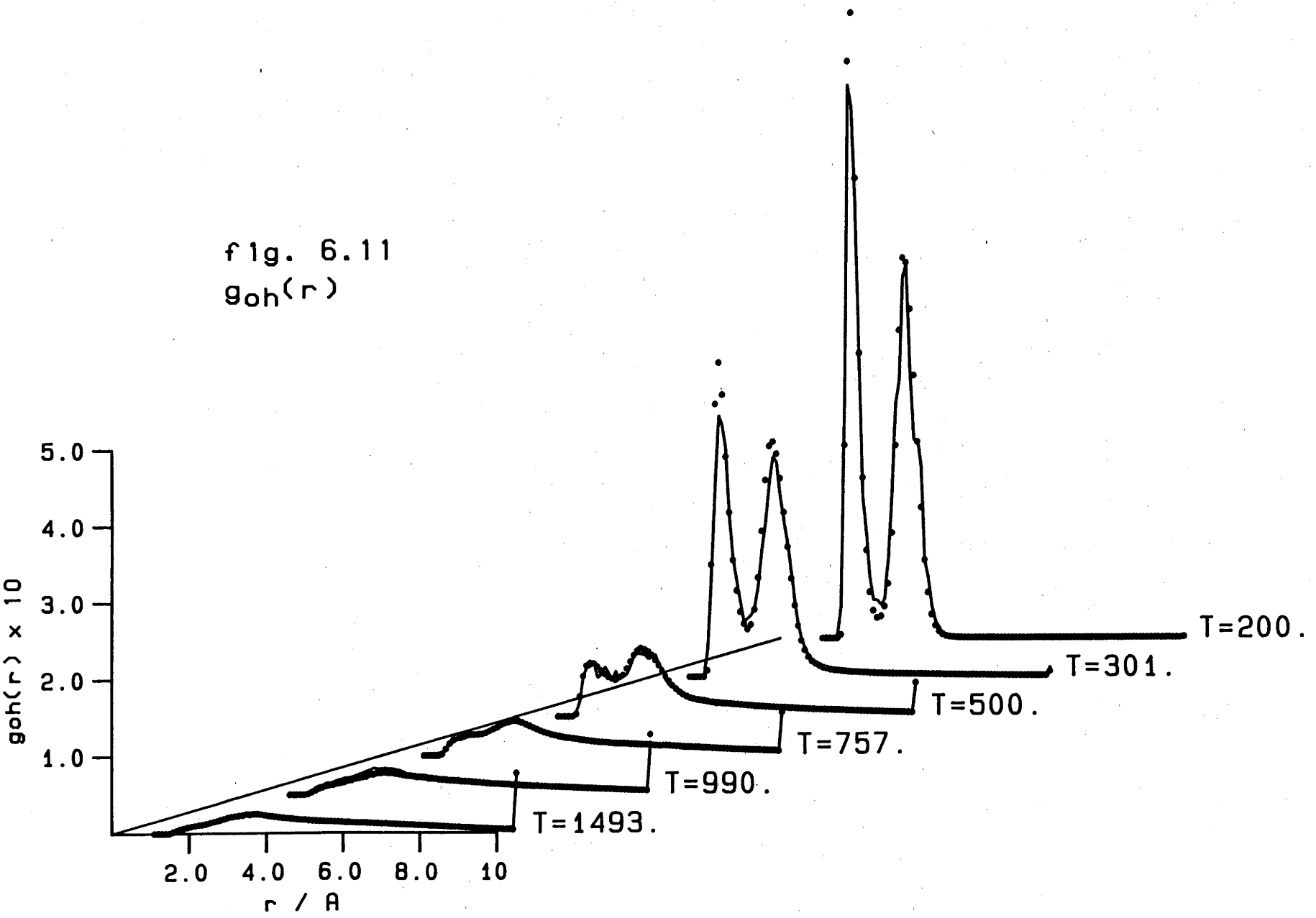
5.0
4.0
3.0
2.0
1.0
goh(r) x 10^-3
2.0
4.0
6.0
8.0
10
r / A
T=200.
T=301.
T=500.
T=757.
T=990.
T=1493.

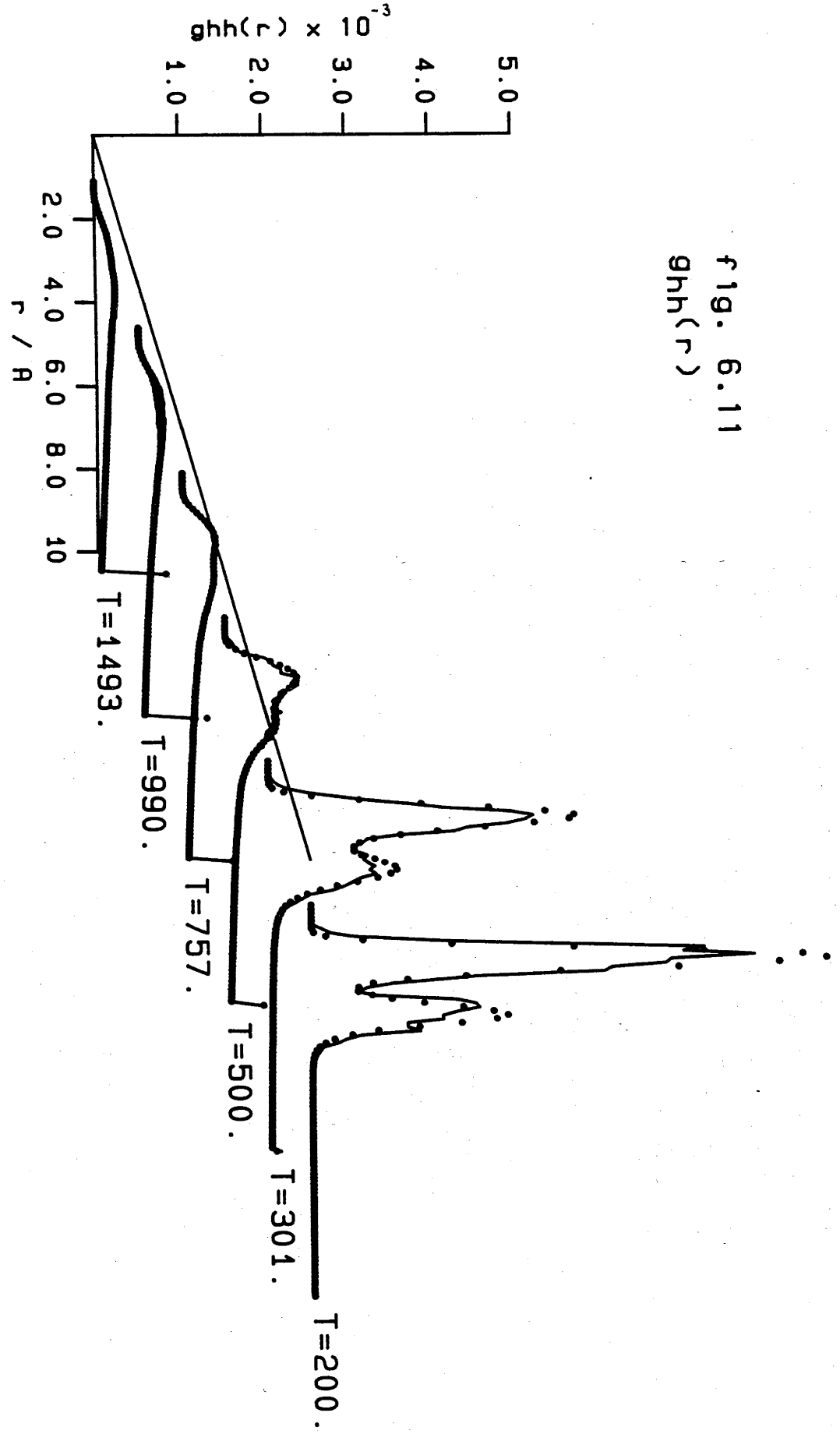
ghh(r) x 10^-3
1.0
2.0
3.0
4.0
5.0
2.0
4.0
6.0
8.0
10
r / A
T=1493.
T=990.
T=757.
T=500.
T=301.
T=200.

fig. 6.11
ghh(r)

systems which moved beyond the cluster confining radius. We note that at the higher temperatures studied a significant number of systems are able to reach the barrier so that the boundary conditions may influence the solutions at these higher temperatures. The energy associated with the barrier does not contribute to the total energy of the cluster; rather it only effects the birth-death process in the random walk. Further, since the intermolecular interaction is very small at the barrier radius used in our calculations (R_c = 20 a.u.) these dissociating clusters are expected to have little influence on our final results.

The fact that the intermolecular motions of a pair of water molecules are well approximated by classical mechanics at temperatures as low as 500°K is an important result which is not necessarily expected. Reimers and Watts (1984) have reported the results of normal mode calculations on the water dimer. The 6 lowest frequency modes are associated with intermolecular vibrations and they range in frequency between 115 cm^{-1} and 782 cm^{-1} (165-1125°K). Thus at 500°K it is expected that relatively few vibrational levels of these oscillators will be populated. Consequently at this temperature quantum behaviour should in principle be important for these modes. The fact that our full quantum distributions do not show significant deviation from classical behaviour at 500°K highlights the inadequacy of normal mode theory for treating anharmonic motions such as the intermolecular vibrations of the water dimer. In Chapter 3 we found that quantum simulation gave a frequency of 150 cm^{-1} for the O...O stretch intermolecular vibration, in agreement with experimental results. Normal mode analysis gives almost double this frequency (272 cm^{-1}). The large anharmonicity of the intermolecular potential causes serious convergence problems for normal mode analysis and the frequencies predicted for this

system are unreliable. The anharmonicity also gives a high density of intermolecular vibrational states and this is probably why classical theory provides a reasonable description of the intermolecular modes at moderate temperatures.

We have also calculated the inter- and intramolecular components of the potential energy of the dimer as a function of temperature. Classical and quantum results are compared in Figures 6.12 and 6.13. As expected, in Figure 6.12 we see very significant differences between the classical and quantum intramolecular potential energies. The values obtained from classical Monte Carlo calculations are in close agreement with the predictions of classical equipartition theory ($^1/_2\ k_BT$ per intramolecular oscillator). On the other hand, the intramolecular energies obtained from the quantum calculations are nearly independent of temperature. The dashed line in this figure is the intramolecular potential energy of a pair of monomers in their ground states. Agreement between this value and the full quantum results for the dimer is consistent with our discussion of the intramolecular distributions and indicates that at the lowest temperatures the intramolecular motions are dominated by the ground state behaviour. The deviation between the ground state value and the non-zero temperature quantum results at the higher temperatures is also consistent with the excitation of the bending modes as discussed earlier.

The classical and quantum intermolecular potential energies presented in Figure 6.13 show close agreement down to a temperature of about 500°K and below this temperature quantum effects become important as expected from the discussion of the intermolecular distributions presented earlier. At 200°K there is a deviation between the classical and quantum intermolecular energies of about 5%.

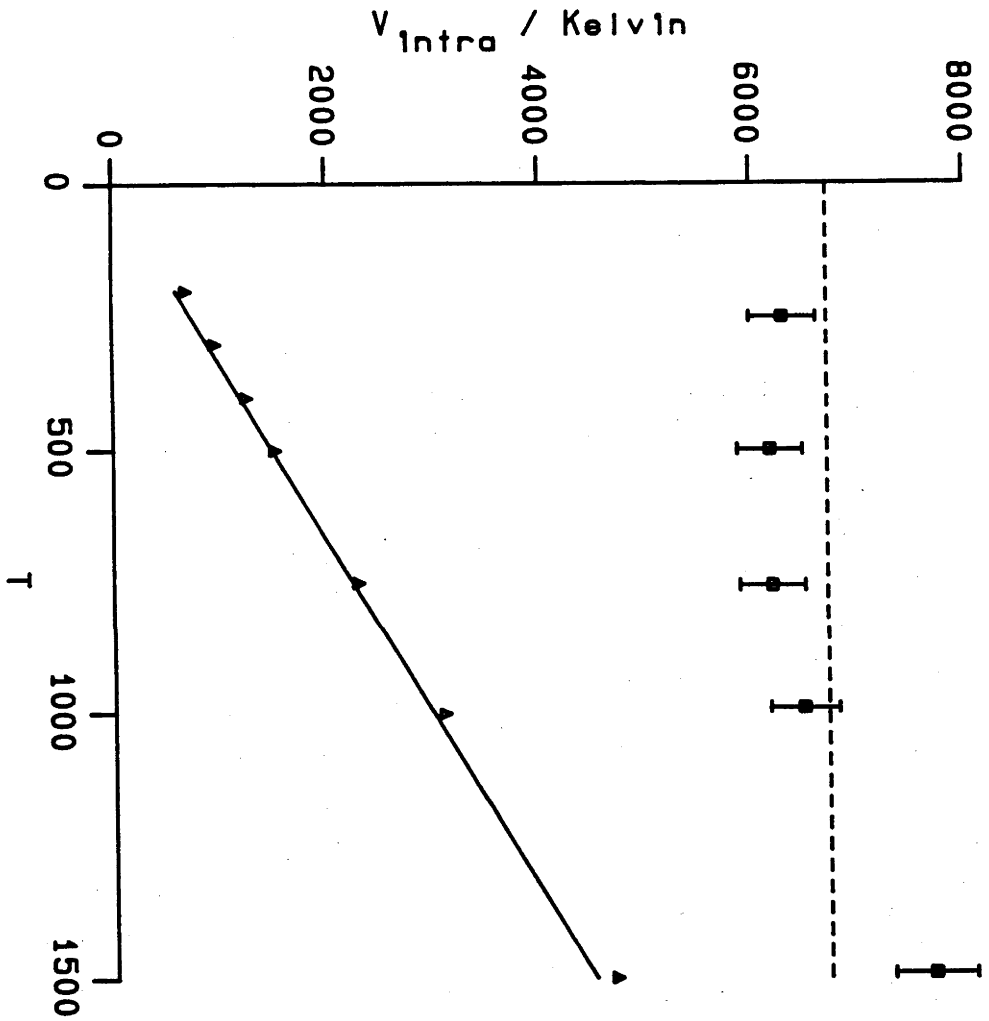

fig. 6.12

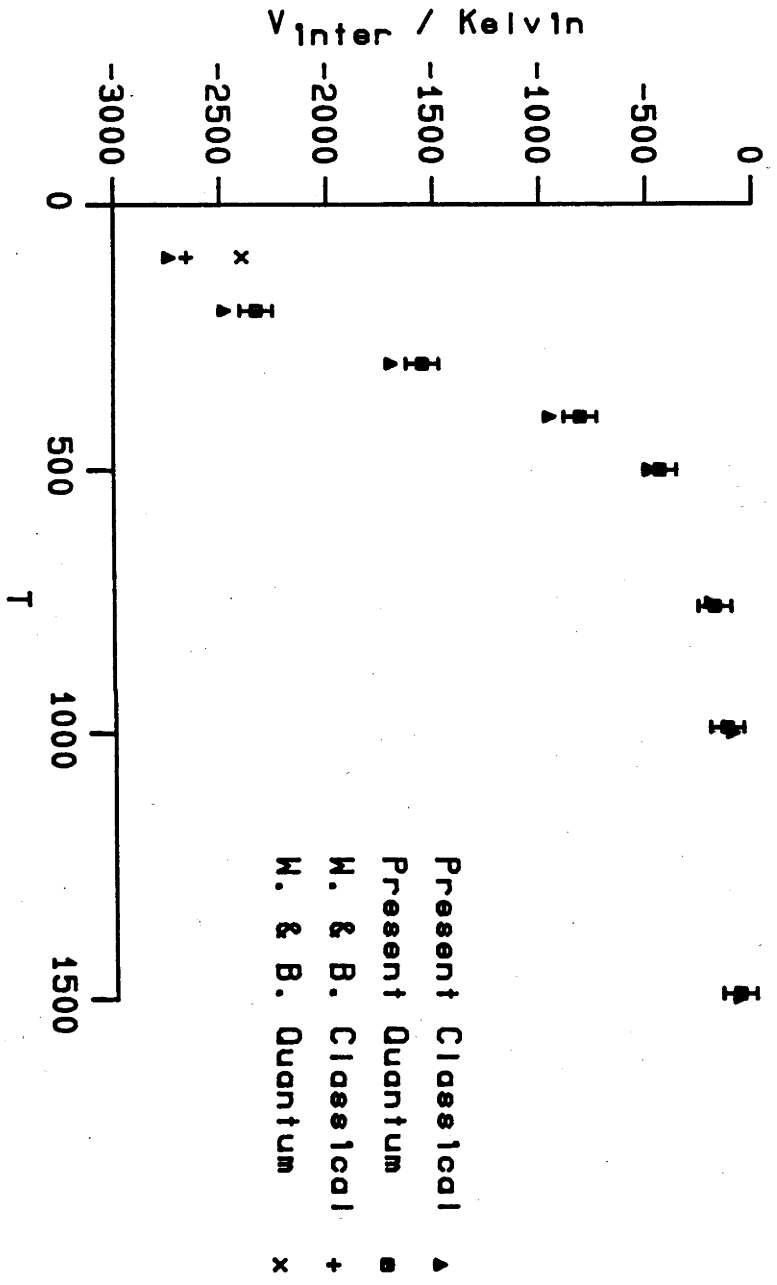
V inter / Kelvin
-3000
-2500
-2000
-1500
-1000
-500
0
0
500
1000
1500
T
Present Classical ▶
Present Quantum ■
W. & B. Classical +
W. & B. Quantum ×

fig. 6.13

Recently Wallquist and Berne (1985) have reported the results of path integral Monte Carlo and molecular dynamics calculations on the water dimer and trimer at 100°K and liquid water at 300°K. Their classical and quantum values for the intermolecular potential energy of the water dimer are also presented in Figure 6.13. We have extended our classical calculations down to 100°K and the differences between the classical results of Wallquist and Berne and our value result from the differences in the intermolecular potentials used in these calculations. Wallquist and Berne observe differences between the classical and quantum intermolecular energy on the order of 10% at 100 K and their values are consistent with the 5% differences which we see at 200°K.

Conclusion

In this chapter we have seen that the primitive high temperature approximation used in the development of our non-zero temperature quantum Monte Carlo algorithm in Chapter 5 can be useful provided the system considered is well described by classical theory at moderate temperatures. Thus we have been able to successfully simulate low density neon gas and observe the onset of quantum behaviour at low temperatures using this approximation.

For systems with degrees of freedom which are dominated by quantum behaviour there are problems with using the classical distributions as initial conditions. The difficulty arises because the Gaussian weight distribution is very narrow when high initial temperatures are employed and the statistics of the calculations become poor.

Lower initial temperatures can be used, giving improved statistics, if more accurate initial distributions are employed. It has been shown that the end point approximation presented in equation (6.9) can be used to give accurate high temperature initial distributions for the Morse oscillator. We have constructed the high temperature density matrix for a molecular cluster using the above form to describe the intramolecular motions of the molecules together with classical distributions to describe the intermolecular modes. When this initial distribution is employed in a quantum simulation of the water dimer we find that the intramolecular vibrations are dominated by ground state behaviour over a range of temperatures between 1500°K and 200°K. Excitation of the bending vibrations have been observed at the higher temperatures. On the other hand the intermolecular motions of the water dimer are well represented by classical theory at temperatures as low as 500°K but we find that quantum behaviour is reasonably important for intermolecular motions at temperatures around 300°K.

The diffusing random walk method which we have used to solve the Bloch equation provides an alternative to the path integral Monte Carlo methods which recently become important in statistical physics. The major problem with the algorithm which has been used in our work is the need to include weights in order to sample the diagonal elements of the density matrix. It may be possible in future developments to include these weights in the equation of motion of the distribution. Importance sampling methods may be useful for this purpose (Whitlock and Kalos (1979), Pollock and Ceperley (1984)).

CHAPTER 7 CONCLUSIONS

The diffusion Monte Carlo method has been extended in a variety of ways in this thesis. With zero temperature applications we have demonstrated that a simple scheme employing an ensemble consisting of opposite signed systems which are capable of annihilation can be used to model excited quantum states as well as antisymmetrized states of Fermion systems. The method can be used to perform completely ab initio calculations on systems of a few fermions and reasonably accurate results are obtained. There are difficulties in extending the method to problems with more dimensions which have yet to be resolved. The annihilation step requires a discrete representation of the multidimensional configuration space. For problems in which the wave function density changes sign rapidly in regions of high potential energy, using a discrete representation of the configuration space may cause errors. Nodal surfaces in ground state fermion wave functions which result from antisymmetry do not seem to have these problems and reasonably accurate results can be obtained using the discrete space. The accuracy of the technique improves when systems occupying smaller regions of configuration space are used. Larger ensembles are necessary and excessive amounts of computer time are required for very accurate calculations using this method. Fermion systems with more particles require consideration of many permutations and a Monte Carlo procedure may be useful for sampling the possible operators.

The diffusion Monte Carlo method has been applied to study the ground state of some interesting Boson problems. We have calculated the ground state properties of the water dimer and trimer using effective pair

potentials. A method for calculating the intramolecular vibrational spectrum of a molecular cluster from the ground state wave function generated by a diffusion Monte Carlo calculation has been presented. The technique provides an accurate means of including the couplings between the inter and intramolecular zero point motions. For hydrogen bonded systems these couplings have significant effects on the intramolecular vibrational spectrum of the cluster. We have shown that comparing the intramolecular vibrational spectra obtained using this method with the results of molecular beam experiments provides a sensitive test of the effective potential surface used in the calculations. When the intermolecular potential surface presented by Reimer, Watts and Klein (1981) is combined with a slightly modified version of the monomer potential reported by Reimers and Watts (1984), almost quantitative agreement betweeen calculated and experimental spectra is obtained. This approach provides valuable information which has been used in the assignment of vibrational bands in the cluster spectrum.

The procedure for performing cluster vibrational analysis relies on the assumption that the excited intramolecular vibrational states of the molecules can be well represented in terms of a Morse oscillator basis set obtained by fitting to the numerically exact ground state wave function. An alternative approach, which does not require this assumption, would be to employ the excited state methods developed in Chapter 2 to directly simulate the excited intramolecular vibrational states of the cluster. Such a calculation is feasible and would require a random walk in which the ensemble distribution was held orthogonal to the intramolecular projections of the ground state wave function.

The basic diffusion Monte Carlo algorithm, which includes both simple

diffusion and birth-death steps, can be used to simulate bulk phase systems with strongly repulsive interactions. However, small time steps and large ensembles are required. The method is prone to substantial fluctuations and is generally inefficient. Importance sampling procedures give great enhancements in the efficiency and accuracy of the algorithm but care must be taken with effects that depend strongly on the size of the system. If small systems with periodic boundaries are used, discontinuities in the drift velocity at the cut off in the potential surface may cause problems. In helium these boundary condition effects seem to be reasonably large when a 32 particle system is employed. With 108 particles, however, the effects are much reduced. Good agreement between the results of importance sampled diffusion Monte Carlo calculations and Green's function Monte Carlo results is observed. When importance sampled methods are used the finite time step approximation seems reasonably unimportant with the step sizes considered in our studies.

Diffusion Monte Carlo can be used to accurately calculate the thermodynamic and structural properties of solid molecular hydrogen over a range of densities. When the spherical part of the potential due to Buck et al. (1983) is used, the calculated ground state energy of the zero pressure solid is within 3% of the experimental value while at higher pressures agreement to within 10% is obtained. The ground state energies calculated using the diffusion Monte Carlo method are generally about 10% lower than the results of variational calculations performed using a Jastrow trial function together with a Gaussian single particle correlation function. The Jastrow part of this wave function, which is based on an r^{-12} repulsion, does not seem to allow sufficient penetration into the softer repulsive wall of the Buck potential. Consequently the kinetic energy is

overestimated when this variational form is used.

The differences between the experimental thermodynamic properties and the diffusion Monte Carlo results obtained using the spherical part of the Buck potential are possibly due to the neglect of anisotropy. It may be possible to perfom diffusion Monte Carlo calculations using angle dependent potentials. The kinetic term becomes complicated when angular coordinates are introduced and the operator can no longer be modelled using a simple Gaussian diffusion process. The rotational diffusion equation has analytic solutions (Carrington and McLachlan (1979)). Using these results it may be possible to perform random walk simulations with angle dependent potentials such as the full anisotropic interaction for H_2 which has been presented by Buck et al. (1983).

We have successfully applied the diffusion Monte Carlo method to solve the Bloch equation. An initial distribution may be propagated in β using this approach and temperature dependent properties of quantum systems calculated. Initial conditions for these calculations must be carefully chosen. For systems of heavier particles with weak interactions classical results may be employed at fairly low initial temperatures with reasonable accuracy. When considering degrees of freedom for which quantum effects dominate, however, more accurate high temperature approximations must be used as initial conditions if efficient calculations are to be performed.

The method described here is equivalent to the discrete path integral Monte Carlo procedure. By assuming that at higher temperatures fewer path segments are required to obtain accurate results, the non-zero temperature diffusion Monte Carlo method may be used to calculate properties at many different temperatures during a single calculation. The method has been

used to study the onset of quantum behaviour in neon gas and the temperature dependence of quantum effects for the water dimer have been considered. Quantum behaviour does not seem to be important for the intermolecular motions of the water dimer at 500°K but by about 200°K the intermolecular energy obtained from our quantum calculations differ from the results of classical calculations by about 5%. The pair distribution functions obtained from quantum simulation are broader than the results of classical calculations. At these temperatures the most significant differences occur with the intramolecular degrees of freedom. Quantum calculations show intramolecular distributions which are dominated by the zero point motions and the classical distributions are much sharper.

Anderson J.B. (1975) J. Chem. Phys. 63, 1499.

Anderson J.B. (1976) J. Chem. Phys. 65, 4121.

Anderson J.B. (1979) Int. J. Quant. Chem. 15, 109.

Anderson J.B. (1980) J. Chem. Phys. 73, 3897.

Anderson J.B. (1985) J. Chem. Phys. 82, 2662.

Anderson J.B. and Freihaut B.H. (1979) J. Comp. Phys. 31, 425.

Arnow D.W., Kalos M.H., Lee M.A. and Schmidt K.E. (1982) J. Chem. Phys. 77, 5562.

Aviles Jr J.B. (1958) Ann. Phys. 5, 251.

Axilrod B.M. and Teller E. (1943) J. Chem. Phys. 11, 293.

Barker J.A. (1979) J. Chem. Phys. 70, 2914.

Barker J.A., Fisher R.A. and Watts R.O. (1971) Molec. Phys. 21, 657.

Ben-Naim A. and Stillinger F.H. (1972) in "Structure and Transport Processes in Water and Aqueous Solutions". Ed. Horne R.A. (Interscience, New York).

Bentwood R.M., Barnes A.J. and Orville-Thomas W.J. (1980) J. Mol. Spectrosc. 84, 391.

Bruce T.A. (1972) Phys. Rev. B 5, 4170.

Brush S.G. (1961) Revs. Modern Phys. 33, 79.

Buck U., Huisken F., Kohlhase A., Otten D., Schaefer J. (1983) J. Chem. Phys. 78, 4439.

Carrington A. and McLachlan A.D. (1979) "Introduction to Magnetic Resonance" (Chapman and Hall, London).

Ceperley D.M. (1978) Phys. Rev. B 18, 3126.

Ceperley D.M. (1981) in "Recent Progress in Many-Body Theories". Ed. Zabolitzky J.G., deLlano M., Fortes M. and Clark J.W. Lecture Notes in Physics No. 142 (Springer, Berlin) 262.

Ceperley D.M. and Alder B.J. (1980) Phys. Rev. Letts. 45, 566.

Ceperley D.M. and Alder B.J. (1981) Physica 108B, 875.

Ceperley D.M. and Alder B.J. (1984) J. Chem. Phys. 81, 5833.

Ceperley D.M. and Kalos M.H. (1979) in "Monte Carlo Methods in Statistical Physics". Ed. Binder K. (Springer, Berlin) 145.

Chandler D. and Wolynes P.G. (1981) J. Chem. Phys. 74, 4078.

Chang C.C. and Campbell C.E. (1977) Phys. Rev. B 15,4238.

Coker D.F., Miller R.E. and Watts R.O. (1985) J. Chem. Phys. 82, 3554.

Coker D.F., Reimers J.R. and Watts R.O. (1982) Aust. J. Phys. 35, 623.

Coulson C.A. and Robertson G.N. (1974) Proc. R. Soc. Lond. A 337, 167.

Coulson C.A. and Robertson G.N. (1975) Proc. R. Soc. Lond. A 342, 289.

Curtiss L.A. and Pople J.A. (1975) J. Mol. Spectrosc. 55, 1.

Darling B.T. and Dennison D.M. (1940) Phys. Rev. 57, 128.

de Boer J. and Michels A. (1938) Physica 5, 945.

De Michelis C. and Reatto L. (1974) Phys. Letts. 50A, 275.

De Raedt B., Sprik M. and Klein M.L. (1984) J. Chem. Phys. 80, 5719.

Dingle R.B. (1949) Phil. Mag. 40, 573.

Doll J.D. and Freeman D.L. (1984) J. Chem. Phys. 80, 2239.

Donsker M..D. and Kac M. (1950) J. Res. Natl. Bur. Std. B 44, 551.

Dyke T.R., Mack K.M. and Muenter J.S. (1977) J. Chem. Phys. 66, 498.

Eckart C. (1935) Phys. Rev. 47, 552.

Eisenberg D. and Kauzmann W. (1969) "The Structure and Properties of Water" (Oxford Univ. Press, Oxford).

Evans D.J. (1985) private communication.

Feynman R.P. (1972) "Statistical Mechanics" (Benjamin, New York).

Feynman R.P. and Hibbs R.H. (1965) "Quantum Mechanics and Bath Integrals" (McGraw-Hill, New York).

Fosdick L.D. (1962) J. Math. Phys. 3, 1251.

Fosdick L.D. and Jordan H.F. (1966) Phys. Rev. 143, 58.

Freeman D.L. and Doll J.D. (1984) J. Chem. Phys. 80, 5079.

Freeman D.L. and Doll J.D. (1985) J. Chem. Phys. 82, 462.

Gillis N.S., Koehler T.R. and Werthamer N.R. (1968a) Phys. Rev. 175, 1110.

Gillis N.S., Werthamer N.R. and Koehler T.R. (1968b) Phys. Rev. 165, 951.

Grimm R. and Storer R.G. (1969) J. Comput. Phys. 4, 230.

Hansen J.P. (1969) Phys. Letts. 30A, 214.

Hansen J.P. (1970) J. Phys. (Paris) 31, Suppl. (3, 67).

Hansen J.P. and Levesque D. (1968) Phys. Rev. 165, 293.

Hansen J.P. and Pollock E.L. (1972) Phys. Rev. A 5, 2651.

Heaps H.S. and Herzberg G. (1952) Z. Physik 133, 48.

Hill T.L. (1956) "Statistical Mechanics; Principles and Selected Applications" (McGraw-Hill, New York).

Hirschfelder J.O., Curtiss C.F. and Bird R.B. (1964) "Molecular Theory of Gases and Liquids" (Wiley, New York).

Jacucci G. and Omerti E. (1983) J. Chem. Phys. 79, 3051.

Jastrow R. (1955) Phys. Rev. 98, 1479.

Jordan H.F. and Fosdick L.D. (1968) Phys. Rev. 171, 128.

Kac M. and Cohen M. (1952) Natl. Bur. Standards (U.S.) Rept.No. 1553.

Kalos M.H. (1962) Phys. Rev. 128, 1791.

Kalos M.H. (1967) J. Comp. Phys. 2, 1967.

Kalos M.H. (1970) Phys. Rev. A 2, 250.

Kalos M.H. (1981) in "Recent Progress in Many-Body Theories". Ed. Zabolitzky J.G., deLlano M., Fortes M. and Clark J.W. Lecture Notes in Physics No. 142 (Springer, Berlin) 252.

Kalos M.H. (1984) in "Monte Carlo Methods in Quantum Problems". Ed. Kalos M.H. (D. Reidel, Dordrecht) 19.

Kalos M.H., Lee M.A., Whitlock P.A. and Chester G.V. (1981) Phys. Rev. B 24, 115.

Kalos M.H., Levesque D. and Verlet L. (1974) Phys. Rev. A 9, 2178.

Kirkwood J.G. (1933) Phys. Rev. 44, 31.

Klein M.L. and Koehler T.R. (1970a) J. Phys. C 3, L102.

Klein M.L. and Koehler (1970b) Phys. Letts. 33A, 253.

Klemm A.D. and Storer R.G. (1973) Aust. J. Phys. 26, 43.

Koehler T.R. (1966b) Phys. Rev. 144, 789.

Koehler T.R. (1966a) Phys. Rev. Letts. 17, 89.

Koehler T.R. (1967) Phys. Rev. Letts. 18, 654.

Kolos W. and Roothaan C.J.J. (1960) Rev. Mod. Phys. 32, 219.

Kolos W. and Wolniewicz L. (1975) J. Mol. Spectrosc. 54, 303.

Krumhansl J.A. and Wu S.Y. (1972) Phys. Rev. B 5, 4155.

Kuchitsu K. and Morino Y. (1965) J. Chem. Soc. (Japan) 38, 814.

Kuchitsu K. and Morino Y. (1966) Spectrochem. Acta 22, 33.

Larsen S.Y., Witte K. and Kilpatrick J.E. (1966) J. Chem. Phys. 44, 213.

Lee J.K., Barker J.A. and Abraham F.F. (1973) J. Chem. Phys. 58, 3166.

Lee M.A., Schmidt K.E., Kalos M.H. and Chester G.V. (1981) Phys. Rev. Letts. 46, 728.

Levy P. (1954) Memor. Sci. Math. Fasc. 126 (Gauthier-Villas, Paris, 1954).

Lowe J.P. (1978) "Quantum Chemistry" (Academic Press, New York).

Matsuoka O., Clementi E. and Yoshimine M. (1976) J. Chem. Phys. 64, 1351.

McGee I.J. and Murphy R.D. (1972) J. Phys. C 5, L311.

McMillan W.L. (1965) Phys. Rev. A 138, 442.

Mentch F. and Anderson J.B. (1981) J. Chem. Phys. 74, 6307.

Merzbacher E. (1970) "Quantum Mechanics", 2nd Ed. (Wiley, New York).

Metropolis N., Rosenbluth A.W., Rosenbluth M.N., Teller M. and Teller E. (1953) J. Chem. Phys. 21, 1087.

Metropolis N. and Ulam S. (1949) J. Am. Stat. Assoc. 44, 335.

Miller R.E., Watts R.O. and Ding A. (1984) Chem. Phys. 83, 155.

Morse P.M. (1929) Phys. Rev. 34, 57.

Moskowitz J.W., Schmidt K.E., Lee M.A. and Kalos M.H. (1982) J. Chem. Phys. 77, 349.

Mott N.F. (1949) Phil. Mag. 40, 61.

Murphy R.D. (1972) Phys. Rev. A 5, 331.

Murphy R.D. and Watts R.O. (1970) J. Low Temp. Phys. 2, 507.

Norman M.J., Watts R.O. and Buck U. (1984) J. Chem. Phys. 81, 3500.

Norman M.J. and Watts R.O. (1985) private communication.

Nosanow L.H. (1964) Phys. Rev. Letts. 13, 270.

Nosanow L.H. (1966) Phys. Rev. 146, 120.

Öksüz I. (1984) J. Chem. Phys. 81, 5005.

Page R.H., Frey J.G., Shen Y.R. and Lee Y.T. (1984) Chem. Phys. Lett. 106, 373.

Parrinello M. and Rahman A. (1984) J. Chem. Phys. 80, 860.

Pekeris C.L. (1959) Phys. Rev. 115, 1216.

Pollock E.L., Bruce T.A., Chester G.V. and Krumhansl J.A. (1972) Phys. Rev. B 5, 4180.

Pollock E.L. and Ceperley D.M. (1984) Phys. Rev. B 30, 2555.

Reatto L. (1984) in "Monte Carlo Methods in Quantum Problems" Ed. Kalos M.H. (D. Reidel, Dordrecht) 13.

Reatto L. and Chester G.V. (1966) Phys. Letts. 22, 276.

Reimers J.R. (1982) Ph.D. Thesis, Australian National University, Canberra.

Reimers J.R. and Watts R.O (1984a) Molec. Phys. 52, 357.

Reimers J.R. and Watts R.O (1984b) Chem. Phys. 85, 83.

Reimers J.R., Watts R.O. and Klein M.L. (1981) Chem. Phys. 64, 95.

Reynolds P.J., Ceperley D.M., Alder B.J. and Lester Jr. W.A. (1982) J. Chem. Phys. 77, 5593.

Roach P.R., Ketterson J.B. and Woo C.W. (1970) Phys. Rev. A 2, 543.

Robertson C.W. and Williams D. (1971) J. Opt. Soc. Am. 61, 1316.

Schiff D. and Verlet L. (1967) Phys. Rev. 160, 208.

Schmidt K.E. and Kalos M.H. (1984) in "Applications of Monte Carlo Method in Statistical Physics". Ed. K. Binder (Springer, Berlin), 125.

Schweizer K.S., Stratt R.M., Chandler D. and Wolynes P.G. (1981) J. Chem. Phys. 75, 1347.

Siegel A. and Burke T. (1972) J. Math. Phys. 13, 1681.

Slania Z. (1981) Adv. Mol. Relxn. Interact. Processes 19, 117.

Storer R.G. (1968) J. Math. Phys. 9, 964.

Storer R.G. (1968) Phys. Rev. 176, 326.

ter Haar D. (1946) Phys. Rev. 70, 222.

Thirumalai D. and Berne B.J. (1983) J. Chem. Phys. 79, 5029.

Thirumalai D. and Berne B.J. (1984) J. Chem. Phys. 81, 2512.

Thirumalai D., Bruskin E.J. and Berne B.J. (1983) J. Chem. Phys. 79, 5063.

Thirumalai D., Hall R.W. and Berne B.J. (1984) J. Chem. Phys. 81, 2523.

Vernon M.F., Krajnovich D.J., Kwok H.S., Lisy J.M., Shen Y.R. and Lee Y.T. (1982) J. Chem. Phys. 77, 47.

Wallace R. (1975) Chem. Phys. 11, 189.

Wallqvist A. and Berne B.J. (1985) Chem. Phys. Letts. 117, 214.

Watson I.A., Henry B.R. and Ross I.G. (1981) Spectrochem. Acta A, 37, 857.

Watts R.O. (1977) Chem. Phys. 26, 367.

Watts R.O. and McGee I.J. (1976) "Liquid State Chemical Physics" (Wiley, New York).

Weast R.C. (1983) "CRC Handbook of Chemistry and Physics" (CRC Press, Florida).

Whitehead R.J. and Handy N.C. (1975) J. Molec. Spectrosc. 55, 356

Whitlock P.A., Ceperley D.M., Chester G.V. and Kalos M.H. (1979) Phys. Rev. B. 19, 5598.

Whitlock P.A. and Kalos M.H. (1979) J. Comput. Phys. 30, 361.

Whitlock P.A., Kalos M.H., Chester G.V. and Ceperley D.M. (1980) Phys. Rev. B 21, 999.

Wigner E. (1932) Phys. Rev. 40, 749.

Wilson E.B. (1939) J. Chem. Phys. 7, 1047.

Wilson E.B. Decius J.C. and Cross P.C. (1955) "Molecular Vibrations" (Dover, New York).